Visualizing synapses during sleep and wake states in zebrafish larvae

Anya Suppermpool

A dissertation submitted in partial fulfilment
of the requirements for the degree of
Doctor of Philosophy
in Neuroscience

PhD Supervisor: Prof Jason Rihel

Department of Cell and Developmental Biology
University College London

June 2021

I, Anya Suppermpool, confirm that the work presented in this thesis is my own. Where information has been derived from other sources, I confirm that this has been indicated in the thesis

Abstract

Sleep is a behavioural state that is conserved throughout the animal kingdom. However, the function of sleep is still unknown. The Synaptic Homeostasis Hypothesis (SHY) proposes that the increased synaptic strength during wakefulness must be renormalized by sleep. Some evidence from both rodents and Drosophila in favour of SHY include observed increases in synaptic protein levels during waking and a population-wide reduction of synapse size during sleep. However, the most powerful test for SHY—directly observing synapse dynamics in the same neuron across sleep/wake states—has not been performed to date.

In this project, we modified a genetic marker for synapses, Fibronectin Intrabodies Generated with mRNA display (FingRs), to visualize both excitatory and inhibitory synapses in vivo in the optically translucent zebrafish. We demonstrated that FingRs label bona fide synapses with high fidelity and dynamically change over time in vivo. Using FingRs to image synapse dynamics across multiple day/night cycles, we found that at the populational level, net excitatory synapse number of optic tectal neurons increased during the day phase and decreased over night, consistent with the predictions of SHY. However, individual neuron synapse trajectories are diverse, such that only certain subtypes of tectal cells are strongly rhythmic across the day. While synapse dynamics in tectal cells do not correlate with prior total sleep duration or waking activity, extended wakefulness acutely increases synapse number, with a reduction in synapses in the subsequent sleep period. Together, these data indicate that day-night rhythms in synapse number are influenced by the sleep-wake cycle, but this is not observed universally in all neurons.

Impact statement

Why do we sleep? We spend a third of our lives sleeping. Animals from jellyfish to humans undergo this period where they go offline from the outside world, when they cannot protect themselves from predators, hunt for food, or mate. Sleep is clearly evolutionary important, yet we do not understand the function of sleep. 1) This thesis developed a method to observe changes in the tiny structures involved in neuronal communication—the synapse—over sleep and wake states repeatedly in the same animal. 2) The manipulation of duration and strength of sleep revealed that synapses are modulated by the sleep-wake cycle, by lighting conditions, and by time-of-day. 3) This thesis therefore is an important direct test of a major theory for why we sleep, namely to regulate our synapses. 4) The tools developed here are of wide utility in a variety of neuroscience fields, including development, circuit function, behaviour, and disease. 5) Finally, since this work uncovers an important function of sleep, the thesis may have an impact on our understanding how sleep disorders affect cognitive abilities.

Acknowledgements

It would not have been possible to undertake this PhD journey without the help and support of the truly outstanding human beings around me. Here is my small tribute to all those people:

Firstly, this thesis would have not been possible without the guidance and tremendous patience of my supervisor Prof Jason Rihel, always the were the kindest and most enthusiastic scientist in the room. You taught me to admire the beauty of the natural world, I cannot thank you enough. I would also like to thank my: secondary supervisor, Tom Hawkins, for his encouragement, worldly knowledge, and constant supplies of puzzles; my graduate tutor, Yama, for always being there to give personal advice whenever and for believing in me.

The proverb 'it takes a village to raise a child', could not be more accurate. I wholeheartedly say that I am the person I am today because of the nurturing of the Rihel lab and the wider First Floor family. I would like to thank the past and current members of the Rihel lab for daily advices on the project, to only some of whom it is possible to give particular mentions here: Sabine, for putting up with my questions and negativity. You are an inspiration to what a good scientist should be. Declan, for his astounding knowledge of the literature and his lovable wit. Sumi, for knowing my fish better than myself and for having the kindest soul and the ability to listen to everything I spit out.

The members of Wilson, Bianco, Tada, and Dreosti lab, all had a hand in shaping this project and me as a scientist. In particular, Masa who taught everything I know about cloning. I will always be in awe of your ingenious genetic trick, impeccable discipline, and kindness. I would like to give special thanks to: Gaia and Steve, for always looking out for me and their tremendous efforts in fostering a sense of family on the floor. Kate Turner, for her impeccable knowledge of teleost neuroanatomy and love for Korean chicken. Gareth, for his wise words and heroic efforts in dealing with Imaris niggles. Pedro, my desk neighbour, you have taught me more than I want to admit. Diz and Claudia, floor experts, who taught me to navigate the lab. Members of the Fish Facility, especially Jenna and Heather for going above and beyond just taking care of my lines through the years and throughout the pandemic. Confocal facility boys, specifically Alan, Chris, and Mike for your insights and introducing me to the AiryScan. Departmental administrators, Debbie and Marilyn for making the navigation of

bureaucracy maze enjoyable. Members of offices (old and new) namely Ana, Asaph, Charlie, Chintan, Françios, Ingrid, MK, and Paride who have made daily PhD obstacles more tolerable.

If I remember anything from this period of my life, it is that the PhD has given me life-long friends. I would like to thank the following people for being a part of my life: Nico for his love of boardgames and influx of happiness. Renato for being the best co-PhD student representatives anyone could ask for and his infectious laughter. Candela and Rawan in their words: “you guys keep me living”. Mandy and Aggie for always being there for me no matter what. Beth, Bing, Eilidh, Lucy, Vera, and Xenia for keeping my work/life balance in check. Joanna and Lisa for the most caring PhD and life sisters and for always having my back. Words cannot describe how lucky I am to be able to call you, my friends.

To James for giving me unequivocal support throughout, particularly in the last stretch of my PhD. You were my personal cheerleader, postdoc, chef, carpenter, cleaner, and my best friend for which my mere expression of thanks does not suffice.

และสำหรับคนที่สำคัญที่สุด ปริญญานี้ และ ปริญญาอื่นๆ จะหาไม่หากไม่มี แม่และป๊า คำว่าขอบคุณ จะไม่มีวัน เพียงพอ รักเสมอ

วิทยานิพนธ์ฉบับนี้สำหรับพวกเขาทั้งสอง

To all the fishes,

Table of Contents

List of Figures

List of Tables

Abbreviations

AMPA	a-Amino-3-Hydroxy-5-Methyl-4- Isoxazolepropionic Acid
ANOVA	Analysis of variance
EEG	electroencephalogram
FingR	Fibronectin intrabodies generated with mRNA display
FR	Free-running
FWHM	full width half max
GFP	green fluorescent protein
GPHN	gephyrin
Hcrt	Hypocretin
LC	Locus coeruleus
LD	Light:dark
LHA	Lateral hypothalamic area
LL	Light:light
LTD	long-term depression
LTP	long-term potentiation
MAGUK	membrane-associated guanylate kinase
NMDA	N-methyl-D-aspartate
NREM	non-rapid eye movement
OT	Optic tectum
PSD	postsynaptic density
PSD95	Postsynaptic density protein 95
REM	rapid eye movement
RFP	red fluorescent protein
RGCs	Retinal ganglion cells
RoC	Rate of Change
SHY	Synaptic Homeostasis Hypothesis
UAS	upstream activation sequence

Chapter 1 Introduction

1.1 SLEEP AND SYNAPSES

Sleep is a behavioural state that takes up a large fraction of the day and occurs throughout an animal's life. Sleep is also conserved throughout the animal kingdom from the early branching lineage such as jellyfish *Cassiopea* to arthropods and nematodes to vertebrates (Hendricks *et al.*, 2000; Trojanowski and Raizen, 2016; Nath *et al.*, 2017). This reversible disconnect from the environment, usually along with immobility, not only risks the animal losing vigilance against danger, but also represents time not participating in productive behaviours such as feeding or mating. This suggests that sleep serve some important function. Furthermore, the lack of sleep disrupts cognitive, metabolic, and immune functions (Joiner, 2016), indicating that sleep is essential. Short-term sleep deprivation results in deficits in performance on memory, attention, and perceptual tasks in human subjects (Van Dongen *et al.*, 2003). This has led to the hypothesis that some forms of synaptic plasticity associated with cognitive processes like learning occur preferentially during sleep.

1.1.1 Synaptic Homeostasis Hypothesis (SHY)

One of the most influential theories of sleep in recent years, the Synaptic Homeostasis Hypothesis (SHY) proposes that sleep is 'the price the brain pays for plasticity' (Tononi and Cirelli, 2014). SHY assumes that through learning and adapting to the ever-changing environment, wakefulness brings about a net increase in synaptic strength and number. Such an increase is unsustainable, as stronger synapses consume more energy and require more cellular supplies within the neuron and from supporting cells such as glia. Importantly, potentiated synapses cannot be further potentiated, thereby saturating the animal's ability to learn (Tononi and Cirelli, 2006). According to SHY, renormalization of synaptic strength is required to reduce the burden of plasticity on neurons and restore the ability to learn (Figure 1.1). Such processes could also enhance signal-to-noise ratios at synapses, leading to the consolidation of memories.

SHY proposes that renormalization of synaptic strength should happen primarily during sleep. The basic outline of SHY's argument goes as follows. While the brain is disconnected from the outside world, there is no incoming stimuli, sensory or motor, from the environment that can

bias neuronal activity one way or another. Neurons can then comprehensively sample the brain's overall environment and memories without outside interference (Tononi and Cirelli, 2014). During certain stages of sleep (slow-wave sleep), many neurons exhibit synchronized depolarized and hyperpolarized firing patterns. These firing patterns occur during non-rapid eye movement (NREM) sleep and are conducive to synaptic renormalization (Tononi and Cirelli, 2014). Furthermore, during this sleep phase, changes in the neuromodulatory milieu, such as low levels of noradrenaline, ensure that synaptic activity is not followed by synaptic potentiation (Walling and Harley, 2004; Tononi and Cirelli, 2006). SHY argues that low levels of neuromodulator combined with spontaneous slow oscillatory activity permit comprehensive sampling of the brain's overall state, which would then allow synaptic renormalization to occur.

In the early form of SHY, the repeated sequences of depolarization—hyperpolarization were proposed to cause the homeostatic downscaling in all synapses of every neuron throughout the brain proportionally (Tononi and Cirelli, 2006). According to this model, all synapses decrease in strength proportionally, for example by 20%. In this case, smaller synapses prior to downscaling would end up below a minimal threshold and become eliminated. This attractive idea that neurons globally downscale together raises multiple questions: How do neurons communicate to each other to downscale proportionally throughout the brain? What is the baseline level of synaptic strength? Is this baseline the same throughout all neurons and circuits?

More recent version of SHY proposes that synapses undergo competitive 'down-selection', where after sleep, some synapses become less effective than others (Tononi and Cirelli, 2016). It is unclear whether down-selection implies a scenario where stronger synapses undergo less depression in strength than weaker ones or stronger synapses are spared from depression all together. In the latter scenario, the highly activated synapses during the day are protected and become consolidated, while synapses that are comparatively less activated during the day are depressed. Either scenario of down-selection would result in an enhanced signal-to-noise ratio. Both the early and the more recent down-selection versions of SHY propose that sleep will result in 'net' weakening of synapses which is termed 'downscaling' (Tononi and Cirelli, 2014).

Overall, SHY proposes that wakefulness brings about a net increase in synaptic strength that is needed to be downscaled during sleep. According to the theory, this increase in neuronal-signal-to-noise ratio through homeostatic synaptic downscaling is the reason *why* the nervous system evolved sleep. However, it is still unclear whether downscaling, as proposed by SHY, occurs globally throughout the brain or only in some neurons. It is also unknown whether other synapse types such as inhibitory synapses also need to be renormalized after wake. Critically, whether sleep itself is enough to drive synaptic downscaling is still unclear. We will explore the various evidences for and against SHY in the next sections.

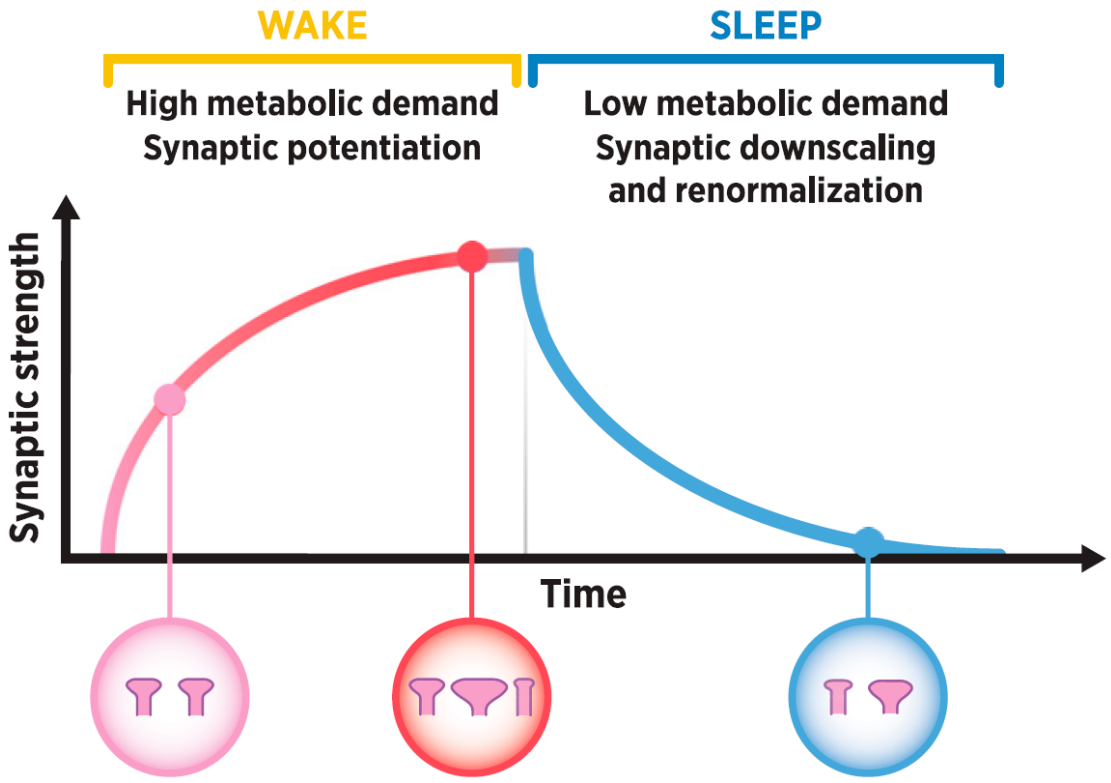

Figure 1.1: Synaptic Homeostasis Hypothesis (SHY). Through learning and interacting with the environment, wakefulness brings about a net increase in synaptic strength and number (indicate by the illustration of increase in spine size and number). Such an increase is unsustainable due to high metabolic demands and excessive potentiation and excitability. The sleep period serves to promote systematic renormalization of synaptic strength throughout the brain, with the relative strength of synapses preserved. SHY proposes that this mechanism allows for further strengthening, thereby learning, to take place during the next wakefulness period. Taken from (Rantamäki and Kohtala, 2020).

1.1.2 Evidence for Wake-Dependent Strengthening and Sleep-Dependent Synaptic Weakening

Synaptic Protein Expression

The first experiments to test the core ideas of SHY examined how genes and proteins associated with synaptic plasticity changed during extended wakefulness and sleep. Early studies found that gene expression of components of synapses change during periods of sleep, wake, and sleep deprivation. Sleep decreases and wake increases expression of a subset of long term potentiation (LTP)-related genes such as *arc*, *cfos*, *bdnf*, *narp*, and *homer1a* in different parts of the brain (Mackiewicz *et al.*, 2007; Abel *et al.*, 2012). These gene expression data are consistent with SHY and support the idea that widespread activity-mediated synaptic plasticity occurs mostly during wake compared to sleep. However, changes in gene expression does not always mirror protein levels at the same timeframe. Therefore, a critical question is whether the rate of synaptic protein translation is dependent on sleep/wake states.

Using a combination of single-molecule fluorescence in situ hybridization and mass spectrometry-based methods, Noya et al. found that nearly all synaptic mRNAs and proteins showed circadian clock-controlled oscillations in synaptoneurosomes under natural sleep/wake cycles (2019). However, under high sleep pressure, the daily oscillations in mRNA expression were unaffected, while the diurnal rhythms of synaptic proteins were completely abolished, suggesting sleep/wake states had driven regulation that is independent of time of day. Transcriptomic and proteomic studies such as Noya et al. revealed the synaptic protein levels are dependent on sleep/wake states. Other studies also found changes in synaptic protein levels during sleep and wake. In Drosophila, the level of Bruchpilot protein, a protein essential to the active zone of all synapses, was higher in flies that were awake compared to those that were asleep (Gilestro *et al.*, 2009). Moreover, flies that had been sleep deprived produced even higher signals of Bruchpilot immunofluorescence than controls. In rodents, AMPAR expression level in cortex and hippocampus, as well as from postsynaptic densities (PSDs) taken from the whole forebrain, are high during the circadian wake phase compared to the sleep phase (Vyazovskiy *et al.s*, 2008; Diering *et al.*, 2017). These findings indicate that there are more AMPAR at the synapse during wake than sleep, which is consistent with SHY's view that synapses are strengthened during wake and not in sleep. However, there are also

contradictory data from these studies. While Vyazovskiy et al. found that AMPAR subunits levels increased after sleep deprivation compared to sleep, Diering et al. found that AMPAR subunits remained constant across sleep, sleep deprivation, and sleep deprivation with recovery sleep in mouse forebrain synaptosomes (Vyazovskiy *et al.*, 2008; Diering *et al.*, 2017). Overall, in both Drosophila and rodents, the global levels of proteins associated with synaptic strengthening are consistent with the predictions of SHY, but not all of the data are wholly consistent.

Despite having levels that follow sleep and wake cycles predicted by SHY, these gene and protein expression studies must be taken with reservations. Firstly, genes-related to synaptic strengthening that were found at higher levels after wakefulness relative to sleep are also involved in synaptic weakening. For example, *Arc* mediates not only synaptic strengthening mechanism like LTP, but also weakening mechanism such as LTD (Shepherd and Bear, 2011). It also is not clear whether changing levels of *Bdnf* in relation to sleep and wake is caused by changes in excitatory synaptic strength. *Bdnf* promotes glutamatergic synaptic potentiation as well as synthesis of GABA in inhibitory neurons (Gottmann, Mittmann and Lessmann, 2009).

Secondly, while these protein dynamics studies have suggested subtle decreases in synaptic strength across the brain after a period of sleep when compared to wake, consistent with SHY, they lack spatial clarity of the underlying mechanisms. Furthermore, they give snapshots of whole-brain or region-wide synapse profiles between animals in different behavioural states. These studies accrue different types of neurons, excitatory and inhibitory, into one story. For example, Vyazovskiy et al. (2008), using Western blot, measured the levels of AMPAR subunit in synaptosomes from the entire cortical and hippocampal homogenate. To overcome some of these issues, more recent studies have attempted to tease apart the synapse dynamics of different types of neurons by investigating synapse morphology.

Synaptic Morphology

Additional evidence consistent with SHY comes from the examination of synaptic morphology. It has long been observed that synaptic strength is associated with changes in dendritic spine size (Matsuzaki *et al.*, 2004; Holler *et al.*, 2021). To see if synaptic strength change as a function of sleep state, various studies have used different techniques such as electron microscopy and in vivo imaging to study changes in spine size.

Using serial block-face scanning electron microscopy, De Vivo et al. (2017) found that the axon-spine interface decreased approximately 18% in mice that slept compared to mice that were awake. Unexpectedly, this sleep-dependent decrease in spine size was not uniform across all synapses. Sleep-dependent synaptic scaling is found in small and medium size synapses (constituting about 80% of total synapses) and not in the largest synapses. These findings indicate downscaling may not be uniformly experienced across all synapses and thus is not a 'global' phenomenon, as suggested by SHY. While inconsistent with the early form of SHY, this is consistent with the idea that down-selection occurs in some synapses and not others, as more recent iterations of SHY predict.

Diering et al., using two-photon imaging of super- ecliptic pHluorin-tagged GluA1 in dendritic spines in the primary motor cortex, found that on average the spine AMPAR subunit signal was reduced during the sleep phase compared to wake. However, they found that big synapses have a disproportionate loss of GluA1 and reduced spine size during sleep, while small synapses showed no change in GluA1 or size. It must be noted that mice were not implanted for EEG recordings, the gold standard for identifying sleep/wake states, but rather these measurements were taken during the light or dark phase when mice are most likely to be asleep or awake, respectively. This study and De Vivo et al (2017) contradict on whether sleep-dependent synaptic downscaling preferentially targets small or larger synapses. It is possible that sleep-dependent synaptic renormalization in different circuits: layer V pyramidal neurons on the primary motor cortex in Diering et al. (2017) and layer 2 of primary motor and sensory cortices in de Vivo et al's (2017) study. Nonetheless, in line with SHY, these studies both found that in mouse motor and sensory cortices most, but not all, synapses reduced in size with sleep.

In vivo imaging studies also found that spine number changes with sleep and wake. Imaging in somatosensory cortex of juvenile and adolescent mice showed that the elimination rate of dendritic spines in layer 5 pyramidal neurons is higher during sleep than wake and formation rates are higher in wake than in sleep, while spine formation occurred at a higher rate during wake than sleep (Maret *et al.*, 2011; Yang and Gan, 2012). This results in a net increase in cortical spines during wake and net spine loss during sleep (Maret *et al.*, 2011). These studies

looking at spines suggest that the number of spines changes with sleep and wake cycles as SHY predicts.

Another way to examine synapse dynamics is to express exogenous synaptic proteins tagged with fluorescent proteins such as GFP and visualize them in freely behaving animals across periods of sleep, wake, and circadian time. Appelbaum et al. (2010) first tracked the presynaptic marker, synaptophysin, in a single population of wake-promoting Hypocretin (Hcrt) neurons, throughout day and night. Using overexpression of exogenous synaptophysin-tagged with GFP, they found that there is a rhythmicity of fluorescence puncta that rises during the day that dissipates during the night when examining synapses along a small section of axon. These findings show that the readout of presynaptic proteins associated with synaptic strength increases during the day and decrease over night, which is consistent with SHY. Nonetheless, overexpression of fluorescence-tagged synaptic proteins has been found to cause unwanted effects, making it difficult to interpret these results (El-Husseini *et al.*, 2000; Zhang and Lisman, 2012) (see 1.3 Methods to visualize synapses).

Electrophysiological Changes

So far, we have discussed physical changes in synapse size as a proxy for synaptic strength. Direct measurements of synaptic strength with electrophysiology such as field recordings, miniature excitatory post-synaptic currents (mEPSCs), and neuronal firing rates have also been used to study SHY.

First, studies have used neuronal firing rates as an indirect readout of synaptic strength. In rat barrel cortex, neuronal firing rates are low at the end of the day, when sleep pressure is low, compared to the beginning of the day, when sleep pressure is high (Vyazovskiy *et al.*, 2009). Assuming that firing rate was proportional to synaptic strength in excitatory synapses, the authors argued that the increased in synaptic strength is associated with high sleep pressure and that sleep reduces synaptic strength, which is consistent with SHY.

More recently, Torrado Pacheco et al. showed that downregulation of firing rate to an individual neuron's set point after sensory perturbation only occurs during sleep, while upregulation only occurs during wake (2021). They recorded firing rates of rats' primary visual

cortex after monocular deprivation (suturing one eye shut) and reopening the sutured eye after 4 days. The authors observed that homeostatic increases in firing rates induced by monocular deprivation occurs during wake-dense periods. These activity changes were shown to be associated with synaptic scaling, with both an increase of mEPSCs in vitro and an increase in spine size in vivo (Keck *et al.*, 2013). Conversely, a decrease in firing rate down to baseline level post eye reopening was due to synaptic downscaling that only occurred during sleep (Torrado Pacheco *et al.*, 2021). This suggests that synaptic down - and up-scaling are gated by sleep and wake states, respectively, and is in line with SHY. However, the control hemispheres, which were recorded for 4-5 days and nights, did not exhibit changes in firing rate rhythmicity linked to sleep and wake states. This study indicates that sleep/wake gated strengthening and weakening of synapses occurs during salient experiences such as sensory deprivation. However, in healthy animals, sleep itself may not be sufficient to drive widespread changes in synaptic strength which is inconsistent with SHY.

In contrast, other studies have observed synaptic strengthening during sleep. In visual learning and contextual fear conditioning paradigms, sleep is required for task-related neurons to undergo LTP, which resulted in increases in the firing of in task-related neurons. However, interference with cellular pathways required for LTP during sleep hindered learning and disrupted the increase in task-related neuronal firing (Vecsey *et al.*, 2009; Ognjanovski *et al.*, 2014; Durkin and Aton, 2016). Together, these studies using neuronal firing rates point to the possibility that different forms of synaptic plasticity, not only synaptic weakening alone, may be promoted during sleep, depending on the animal's prior waking experience. This paints a more complex picture of sleep and synaptic plasticity and is inconsistent with SHY. Nevertheless, direct measurements of neuronal firing rate are influenced by the output of a combination of various mechanisms within the neuron: synaptic, cellular, and neuronal network homeostatic modulation (Cirelli, 2017). Therefore, neuronal firing rate may not be directly addressing SHY.

Unlike neuronal firing rates, which only measures the neuronal output, mEPSCs provide more direct measurements of excitatory synaptic strength from a single neuron. An mEPSC is the postsynaptic response to the release of a single neurotransmitter vesicle, so changes in mEPSC amplitudes are directly correlated to changes in AMPA receptor number (Turrigiano

and Nelson, 2004). Several groups have examined how mEPSCs change during sleep and wake states. Liu et al. recorded mEPSCs of 2/3 pyramidal neurons in the frontal cortex of mice and rats that had been awake or asleep and found that the frequency and amplitude of mEPSCs increased after waking and decreased after sleep (2010). Moreover, mEPSCs were significantly increased in sleep deprived rats than controls at the same circadian time. These findings showed direct evidence for SHY as postsynaptic strength were higher in waking than sleep. Conversely, Cary and Turrigiano measured mEPSC amplitudes and frequencies from the same neurons (and also in other areas of the brain) and found that they were stable across sleep and wake dense periods (2021). This is directly contradictory to Liu et al. and inconsistent with SHY.

While measuring the same 2/3 pyramidal neurons, Liu et al. and Cary and Turrigiano found contradicting results. This could be due differences in methodology, particularly how these authors kept track of prior sleep/wake history of the animals. As animals must be sacrificed for ex vivo recording of mEPSCs, Liu et al. sacrificed animals at certain circadian times where rats had been spontaneously awake or asleep. However, different animals at the same circadian time showed drastically different amounts of consolidated sleep/wake (Cary and Turrigiano, 2021). Cary and Turrigiano, on the other hand, elegantly tracked individual animal's sleep/wake history and were able to compare mEPSCs of animals that had experienced sleep dense and wake dense phase at the same circadian time. Their findings showed that natural periods of sleep/wake do not affect postsynaptic strength. This direct opposition of SHY shows that the effect of sleep and wake on synapse are far from monolithic and cannot be parsimoniously explained by SHY.

1.1.3 Key unanswered questions

While there are numerous studies with data consistent with SHY's predictions, there are also various ones that are not wholly consistent with SHY. These conflicting accounts of synapse dynamics through sleep and wake could be due to the variable effects among brain regions and neuronal populations. Some discrepancies between studies are likely due to methodological differences; for example, not all studies separate the effects of sleep and circadian cycle, carefully consider the sleep/wake history of the animal, or measure synaptic strength directly.

Sleep/wake vs circadian cycle

Most of the evidences for and against SHY have been 'snapshot' studies where different animals in different states, prior sleep/wake experience, and/or circadian cycle are compared to one another (Gilestro *et al.*, 2009; Liu *et al.*, 2010; de Vivo *et al.*, 2017).

For example, De Vivo et al. (2017) compared the axon-spine interface of mice that were asleep to other mice that were awake but sacrificed these two groups of mice at different circadian times, although circadian rhythms and sleep/wake states are distinct processes. The circadian clock has also been shown to alter synapse number and strength independently from its effects on sleep (Frank and Cantera, 2014). For example, in Drosophila the number of synaptic bouton in flight motor neurons are high during the subjective night and low during the subjective day (Mehnert *et al.*, 2007). This pattern persists under constant dark but is abolished in clock mutants, suggesting circadian regulation. While careful examination of circadian and sleep/wake cycle influences is vital in addressing SHY, 'snapshot' studies sample synaptic dynamics at different circadian times and therefore cannot separate circadian effects on synapse dynamics. In order to carefully examine SHY, it is vital to compare synaptic changes within the same animal, to disentangle circadian and sleep/wake influences, and to track animals' sleep/wake behaviour prior to synaptic measurements.

Inextricably linked with the sleep/wake vs circadian problem is the nature by which studies have looked at synapse dynamics. The major studies that have observed synaptic changes during sleep and wake cycles are 'snapshots' studies, which often compare the synaptic properties of different animals in different states. These types of methods often compare whole-brain or region-wide synapse profiles, which lumped together both excitatory and inhibitory neurons. Vyazovskiy et al. (2008), Gilestro et al. (2009), and Diering et al. (2017) compared entire brains or brain regions of different animals in different behavioral states together. While these studies lack spatial clarity, they also do not allow direct examinations of sleep/wake and circadian influences.

SHY and Inhibitory Synapses

SHY is unclear about whether inhibitory synapses also need to be renormalized after wake. How Inhibitory synapses are regulated through sleep and wake cycles in accordance to SHY have thus far been understudied.

Although not addressing SHY per se, in vivo imaging studies in rodents have shown that sensory deprivation via monocular deprivation induce loss of inhibitory synapses in layer 2/3 pyramidal neurons (Chen *et al.*, 2012; van Versendaal *et al.*, 2012). Inhibitory neuron presynaptic output also have been shown to decrease after focal retinal lesions in adult visual cortex (Keck *et al.*, 2011). These studies pointed to the importance of inhibitory synapses and circuits in maintaining circuit stability during sensory deprivation. Recording miniature inhibitory postsynaptic currents (mIPSCs) from pyramidal cells in slices showed that mIPSCs frequency is higher at ZT12 (end of light phase) than at ZT0, which is the opposite to mEPSCs dynamics (Liu *et al.*, 2010; Bridi *et al.*, 2020), suggesting the possibility that inhibitory synapses can change at timescales associated with changes in sleep/wake state and/or circadian time. How inhibitory synapse dynamics integrate with excitatory ones over the course of sleep/wake states is currently unknown.

Key unanswered questions of SHY are:

1. Is there increase and decrease in synapse strength and/or number of excitatory and inhibitory synapses associated with wake and sleep, respectively?
2. If so, do all neurons exhibit this state-related synaptic change, or is it a property of specific neurons?
3. What controls these synaptic changes: the state of sleep itself or the circadian clock?

To address these questions, sleep/wake and circadian influences on synapses must be carefully examined in various types of neurons during natural sleep and wake cycles. What is needed is a method to track synapse dynamics in living animal transitioning through sleep and wake states. To achieve this, we can utilise an emergent neuroscience animal model for live imaging, the zebrafish.

1.2 ZEBRAFISH AS A SLEEP-SYNAPTIC MODEL

Zebrafish (*Danio rerio*) is rapidly becoming a popular model organism in neuroscience. Their genetic toolbox, unique physical characteristic, quantifiable behaviours, and conserved neurochemistry make zebrafish a potent model for studying sleep and synapse.

Due to their small size, external development, and optical translucence, zebrafish embryos provide an unparalleled utility for non-invasive functional and whole-brain imaging over time in vivo (Ahrens *et al.*, 2013). These properties, together with the availability of various transgenic lines in which subsets of neurons are labelled by reporters, make zebrafish a powerful model for neurocircuitry and synaptic studies. One such well-established system in zebrafish is the Gal4/UAS system, which allows for the expression of any reporter gene in spatially and temporally restricted fashions (Kawakami *et al.*, 2016). The plethora of published Gal4 and UAS database allows for targeting of numerous neuronal populations and using various labelling and manipulation tools (Marquart *et al.*, 2015). For instance, genetically-encoded calcium indicators or optogenetic actuators such as channel-rhodopsins, can be inducibly expressed under the control of UAS promoters to label virtually any neuronal population allowing for tracking and manipulations of those neurons (Ahrens *et al.*, 2013; Antinucci *et al.*, 2020).

Various established genetic methods to visualize synapse dynamics and synaptic activity also exist in zebrafish. Many types of synaptic markers are available for both pre- and post-synaptic labelling. For instance, fusion of synaptic vesicle protein synaptophysin with GFP labels presynaptic boutons, and the postsynaptic scaffolding protein, PSD95, tagged with GFP labels postsynaptic density (Niell, Meyer and Smith, 2004; Meyer and Smith, 2006). While expression of exogenous synaptic protein can cause undesirable effects, other live synaptic markers that avoid overexpression are also available, such as the live intrabody labelling (Gross *et al.*, 2013; Son *et al.*, 2016) (further discussed in 1.3). Synapse activity can also be observed live and non-invasively in zebrafish. Tools such as the glutamate reporter molecule, iGluSnFR, allows the recording of glutamate release as a readout of individual synapse activity (Marvin *et al.*, 2013). The optical translucency of zebrafish larvae combined with well-established genetic reporters and tools could allow for the monitoring of synapse dynamics in any neuronal population in a freely behaving vertebrate.

Apart from various tools to label synapses, zebrafish larvae also exhibit numerous quantifiable behavioural repertoires from reflexive responses such as escape swimming and optic flow responses to more complex ones such as hunting and social behaviours (Kimmel, Patterson and Kimmel, 1974; Easter and Nicola, 1997; Bianco, Kampff and Engert, 2011; Dreosti *et al.*, 2015). More importantly, zebrafish larvae exhibit established and quantifiable sleep-wake patterns (Figure 1.2). A set of behavioural parameters such as rest-wake duration, sleep latency, and arousal sensitivity can be measured and altered using pharmacological agents in a high-throughput manner (Rihel *et al.*, 2010). With advances in functional neuroimaging and the availability of transgenic reporters, zebrafish offer a special opportunity among vertebrate model systems to link neural population and synapses activity with behaviour such as sleep.

To address questions of SHY and examine the effects of sleep on synapse strength, we need to disentangle sleep/wake states from the circadian clock. Zebrafish provide an attractive model in separating these two processes. Environmental signals such as the light/dark cycle reset the clock on a daily basis to ensure it remains synchronized with the environmental cycle of 24 h. As zebrafish larvae are optically translucent, direct exposure of both central and peripheral tissues to light entrains the cellular clock (Whitmore *et al.*, 2000). For instance, when raised on a 14:10 hour light/dark cycle, the larval zebrafish circadian clock is phase locked with the light/dark cycle (Figure 1.2) (Kaneko and Cahill, 2005). This light entrainment is also reflected in their sleep/wake behaviour, where zebrafish larvae have more swim bouts during the lights-on phase and more inactive sleep states, during lights-off (Figure 1.2) (Prober *et al.*, 2006). In contrast, when reared in constant conditions, zebrafish have an unsynchronized circadian clock and do not exhibit oscillations in locomotor activity levels like in light/dark rearing fish (Prober *et al.*, 2006). When maintained on a light/dark cycle and then transferred to constant dark or light conditions, the spontaneous locomotor activity of larvae and adults continues to cycle with a circadian rhythm set by the prior entraining light/dark cycle but eventually dampens and becomes arrhythmic (Figure 1.2) (Kaneko and Cahill, 2005; Gandhi *et al.*, 2015). Thus, the zebrafish represents an attractive model to tease apart circadian and sleep/wake effects using rearing conditions.

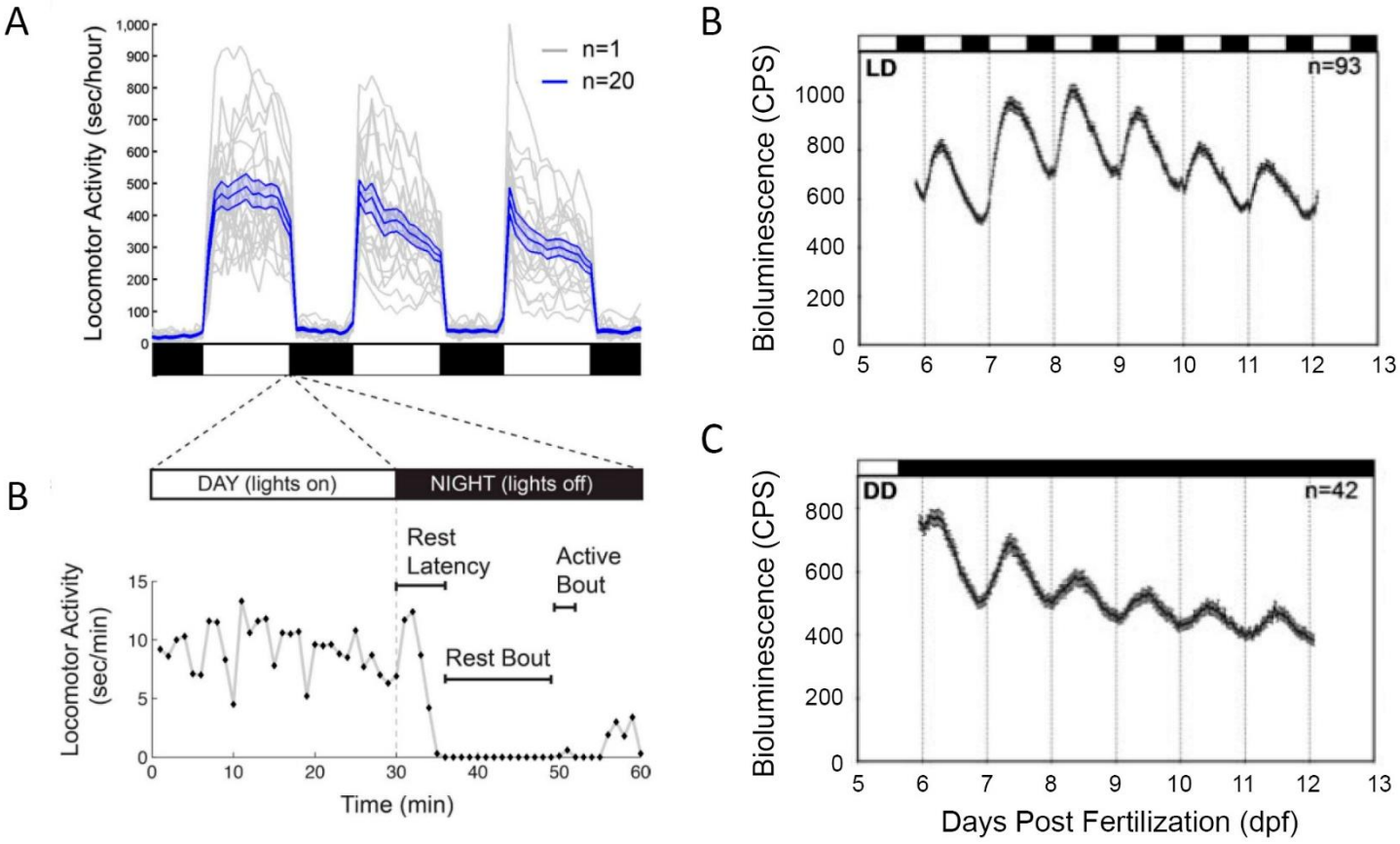

Figure 1.2: Monitoring sleep and wake behaviours and circadian rhythm in zebrafish larvae. A-B) Representative traces of zebrafish larval locomotor activity assay. Modified from (Chiu et al., 2013). A) Example of locomotor activity data for 20 wild-type larvae (grey traces) and their mean locomotor activity (blue trace). C) An example of typical larval zebrafish behaviour at the end of the day. A rest bout is defined as a period of inactivity of at least 1 minute, which is associated with an increase in arousal threshold (Prober et al., 2006). B-C) Representative traces of bioluminescence rhythms mediated by per3-luc used as a circadian clock output readout. Bioluminescence levels measured in counts per second (CPS). Modified from (Kaneko and Cahill, 2005). B) Average plot of bioluminescence rhythms in 14hr:10hr light:dark (LD) cycles. Zebrafish larvae were entrained in 6 LD cycles prior to monitoring. C) Average plot of bioluminescence rhythms in 'free-running' zebrafish larvae, in which larvae were entrained in 14hr:10hr LD cycles for 6 days and transferred into constant dark. Error bars represent ± standard error of the mean.

In contrast to invertebrates, zebrafish share conserved central nervous system organization, sleep-wake circuits and neurochemistry, and synaptic structure with mammals. It has been shown that core sleep-wake regulators in mammals are largely conserved in zebrafish, including monoaminergic, norepinephrine, and hypocretinergic system (Kaslin, 2004; McLean and Fetcho, 2004; Prober *et al.*, 2006; Yokogawa *et al.*, 2007; Singh, Oikonomou and Prober, 2015). Moreover, responses to many hypnotic and wake-promoting drugs such as melatonin

agonists, alpha-2 adrenergic agonists, and others are also conserved in the zebrafish (Zhdanova *et al.*, 2001; Rihel *et al.*, 2010).

Despite the teolost-specific genome duplication, which expanded synapse protein families, zebrafish postsynaptic density ultrastructure is conserved. For example, while zebrafish contain more NMDAR and AMPAR subunits, the core vertebrate post synaptic density is conserved, with approximately 1,000 synaptic proteins shared between mouse and zebrafish (Bayés *et al.*, 2017). These include major cytoskeletal proteins, ribosomal proteins, kinases, phosphatases, and adenylate cyclase. Furthermore, the synapses ultrastructural features are conserved between zebrafish and mammals. For example, synapses in the telencephalon show spine-like characteristics of mammalian synapses (Bayés *et al.*, 2017). With largely conserved synapses, core sleep-wake regulators, and unique ability to monitor sleep/wake behaviour and synapse dynamics in freely behaving vertebrate, zebrafish is a potent model to study synaptic changes during sleep-wake states.

Overall, features such as established synaptic genetic tools, quantifiable sleep/wake behaviour, and the ease in which circadian and sleep/wake cycle can be separate make zebrafish a potent model to study synaptic changes during sleep-wake states and address SHY.

1.3 METHODS TO VISUALIZE SYNAPSES

Given the limitations of previous studies addressing SHY, we asked whether there is a method to observe the same synapses of the same neurons through sleep and wake and circadian time without disrupting its functions. Following synapse dynamics of the same neurons would allow for comparison within neuron as an internal control and circumvents animal-to-animal and circadian differences.

Therefore, to tackle SHY systematically, we need reliable tools that 1) label excitatory and inhibitory synapses, and 2) allow long-term tracking of the same neurons in living animal. Only by tracking synapse dynamics in live animals can we answer critical questions about SHY. Firstly, do synapse strength and density change in temporal relationship with sleep and wake cycle? Secondly, do these changes occur globally or only in certain neurons? Thirdly, is this process occurring during periods that coincide with sleep or is sleep itself driving these synaptic changes?

1.3.1 Existing methods to observe synapses

Traditional electron microscopy and the more recent super resolution array tomography allow precise super-resolution observation of endogenous synaptic proteins and large volumetric tissue coverage (Wang and Smith, 2012). However, these methods are incompatible with continuous synapse dynamics tracking we want to achieve due to the necessity of fixation, permeabilization, and physical sectioning of the sample. Studies that used these methods such as De Vivo et al. (2017) were limited to comparing synaptic properties of different neurons from different animals in different states, which does not fulfil our criteria.

The primary approach for tracking synapse dynamics in vivo has been to tag synaptically-localized proteins with fluorescent proteins (FPs). However, FPs are generally overexpressed, which is known to cause unwanted effects in localization, maturation, and function of synaptic proteins (El-Husseini *et al.*, 2000; Zhang and Lisman, 2012; Taft and Turrigiano, 2014). Overexpression of FP-tagged PSD95 can drive maturation of synapses by driving pre-synaptic development and increase spine size and density postsynaptically (El-Husseini *et al.*, 2000).

Additionally, it also decreased the turnover rates of pre- and postsynaptic structures, thus promoting the stabilization of synaptic contacts (Taft and Turrigiano, 2014). Critically, overexpression of postsynaptic proteins such as CaMKII and PSD95 can drastically increase synaptic strength and saturate long-term potentiation (Zhang and Lisman, 2012). Although, knock-in of FP-tags may circumvent the confounding effects of overexpression, knock-in strategies lead to global expression of FP, resulting in the lack of cell-type-specific labelling.

Studies addressing SHY that used overexpression of FP-tagged synaptic markers could alter properties and functions in both pre- and post-synaptic structures that they were investigating (Appelbaum *et al.*, 2010; Elbaz *et al.*, 2016). Therefore, currently, there has not yet been a study addressing SHY by tracking changes in endogenous synaptic proteins in vivo with conclusive verification of synaptic markers labelling bona fide synapses.

Various studies addressing SHY have taken the approach of looking at dendritic spines as a proxy for excitatory synapses in fluorophore-filled neurons (Maret *et al.*, 2011; Yang and Gan, 2012; Li *et al.*, 2017), as the head sizes of dendritic spines are linearly correlated with synaptic strength (Holler *et al.*, 2021). However, using dendritic spines as a proxy of synapses has limitations, as this method does not label all types of synapses. Although the majority of excitatory inputs synapse onto dendritic spine protrusions, some excitatory synapses are not located on spines (Peters, 2002). For example, non-spine synapses were observed on dendritic shafts and soma of cortical layer 6 pyramidal neurons (Colonnier, 1968). Therefore, using dendritic spines as proxy might not be an accurate readout of whole cell synapse dynamics. Moreover, measuring dendritic spines does not consider inhibitory synapses. Inhibitory input synapses onto neurons at a variety of locations, including dendritic spines, dendritic shafts, axon initial segments, and cell bodies (Markram *et al.*, 2004). Unlike excitatory synapses, there is no morphological surrogate for the visualization of inhibitory synapses. Additionally, monitoring dendritic spines requires imaging through transcranial windows. In non-mammalian animal models, where synapses can be imaged non-invasively, dendritic spines associated with excitatory synapses are not ubiquitously found. Apart from some spine-like structures, dendritic spines are not found in zebrafish (Jontes, Buchanan and Smith, 2000). In the Xenopus, the only reported spiny neurons are Granule cells in the olfactory bulb (Huang *et al.*, 2015).

Is there an approach that would allow the visualization of both excitatory and inhibitory synapses without interfering with their functions over time? One promising tool, Fibronectin intrabodies generated with mRNA display (FingRs), has recently been developed to allow for the visualization of synapses without overexpression artefacts (Gross *et al.*, 2013). FingRs are antibody-like proteins that can target endogenous excitatory and inhibitory synaptic proteins, PSD95 and Gephyrin, respectively. PSD95 (also known as DLG4), a member of Membrane-Associated Guanylate Kinase (MAGUK) family, is a scaffolding protein that assembles glutamate receptors, ion channel complexes and signalling proteins (Chen *et al.*, 2015). PSD95 complexes are vital in controlling synaptic strength and plasticity (Taft and Turrigiano, 2014). On the other hand, Gephyrin is the core scaffolding protein for inhibitory post synaptic densities. Gephyrin self-assembles into a scaffold, interacts with the cytoskeleton, and anchors ligand-gated chloride channels such as $GABA_A$ and glycine receptors (Tyagarajan and Fritschy, 2014). Gephyrin's clustering properties are essential in the structural and functional regulation of inhibitory neurotransmission in response to patterns of neural activity. FingRs binds to these endogenous synaptic targets, and, as FingRs are tagged with FPs, this allows the visualization of endogenous synaptic target in vivo.

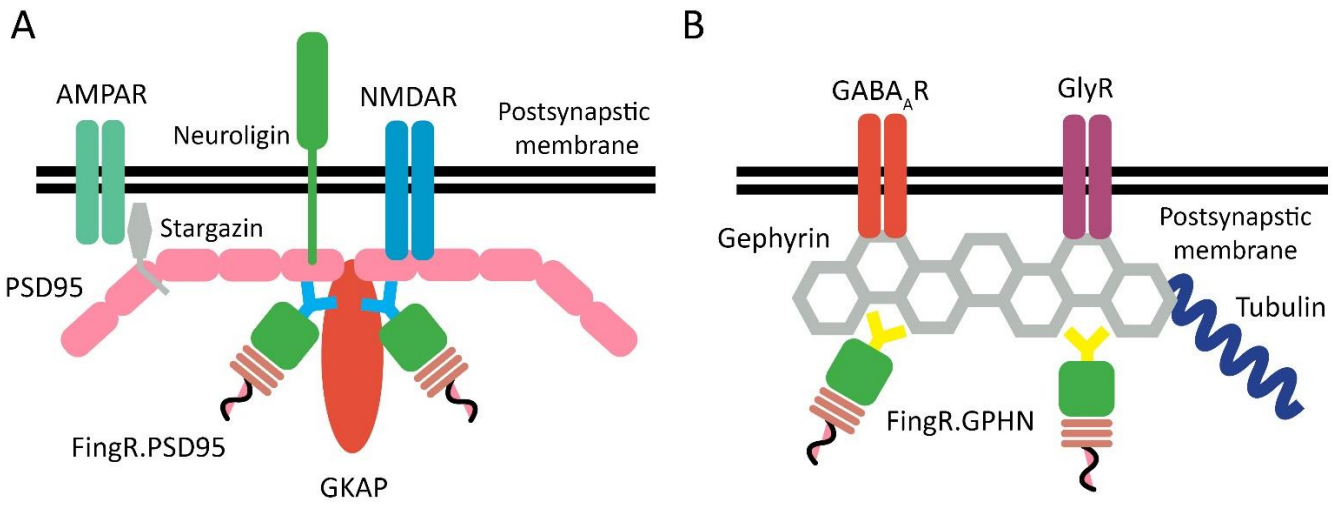

Figure 1.3: Illustration of where FingR binds to their target synaptic protein within the postsynaptic density. A) FingR.PSD95 binds to the scaffolding PSD95/GKAP complex in excitatory synapses. B) FingR.GPHN binds to the trimerized state of endogenous gephyrin within inhibitory synapses.

Moreover, FingRs binds to these endogenous synaptic targets without disrupting their functions (Figure 1.3). PSD95.FingR binds to PSD95 at the SH3-GK domain, which mediates intra- and intermolecular interactions, while GPHN.FingR binds the G domain of endogenous Gephyrin, which mediates trimerization (Gross *et al.*, 2013). In the case of Gephyrin, FingR will only bind the protein in a trimerized state.

Gross et al. (2013) showed that FingRs do not have off-target effects, do not affect electrophysiological properties of neurons, and bind to functional synapses in dissociated neurons and brain slices. For example, FingRs expression does not change the size of gephyrin or PSD95 puncta. The presence of FingRs does not change the morphology or electrophysiological properties of synapses of neurons in hippocampal slices (Gross *et al.*, 2013). Therefore, FingRs allow for the visualization of endogenous synaptic proteins without disturbing their function.

Furthermore, unlike conventional overexpression techniques, FingRs utilize a transcriptional control system designed to closely match the expression level of a FingR with that of its endogenous target. Such a system not only allows FingRs to accurately report the localization of their endogenous targets but also circumvents the confounding effects of overexpression. Thus, FingRs are attractive tools to address SHY systematically.

Although FingRs have the potential to visualize synaptic dynamics, more extensive testing is needed to ensure that synapses are not affected in vivo. For instance, the regulatory domains and the FP add a significant size to the intrabody, which may reduce its accessibility to the target protein in densely packed structure such as the PSD in vivo and particularly in developing neurons. Although Gross et al. (2013) and Son et al. (2016) have shown FingR labels endogenous PSD95 and Gephyrin via immunohistochemistry, they did not quantify this in vivo. Moreover, it is unknown how well this type of transcriptional regulation matches with acute local translation of pre-existing mRNAs at dendritic sites. While this can be a major drawback in acute short-term studies, it may not pose substantial complication as this project's aim is to visualize synaptic changes over extended period such as days.

1.4 POTENTIAL NEURONAL POPULATION TO STUDY SHY

Tracking a single neuron's synapse dynamics through multiple timepoints is a considerable technical challenge. Neurons that are suitable for multi-day tracking will have the following characteristics: 1) The neurons must be easily accessible for imaging small structures such as synapses so that they do not photo-bleach after multiple rounds of imaging; 2) They must be imaged as a whole cell (i.e. have self-contained processes) so that the synaptic dynamics of whole neurons can be examined; and 3) They must have known and predictable functional identities so their function can be retrospectively mapped to their synapse dynamics. We found a group of neurons which is a good candidate for testing SHY - the optic tectum (OT) neurons of zebrafish larvae.

1.4.1 The Larval Zebrafish Optic Tectum

The OT and its mammalian homologue, the superior colliculus, is a centre for visual processing involved in behaviours such as prey capture and predator avoidance (Bollmann, 2019). The OT is the main retinorecipient brain region and makes bilateral connections with the pretectum, dorsal thalamus, dorsal tegmentum, nucleus isthmi, reticular formation and contralateral tectum. Through connections with these several other brain regions, the OT integrates visually acquired information with motor inputs and outputs to initiate appropriate behavioural responses (Bollmann, 2019).

Retinotopic Organization

Tectal neurons, also called periventricular neurons, sit within the OT, receive input from retinal ganglion cells (RGCs), and relay information to downstream neural systems to produce visually-guided behaviours such as prey capture and avoidance (Bianco and Engert, 2015).

The main areas of the tectum can be easily demarcated. The stratum periventriculare (SPV) contains the cell bodies of most tectal neurons whereas the neuropil region contains tectal cells neurites and terminating axons of RGCs as well as other neurons involved in visually guided behaviour (Henriques *et al.*, 2019). The tectal neuropil is a highly laminated structure, which makes imaging straightforward. OT neuropil layers are, starting from the most superficial: the stratum opticum (SO), the stratum fibrosum et griseum superficiale (SFGS), the stratum griseum centrale (SGC), and the stratum album centrale (SAC), which sits on the border with the SPV (Gebhardt, Baier and Del Bene, 2013). RGC axons responding to a specific

cue in the visual scene project to a specific axis and layer within the OT neuropil (Figure 1.4A). The temporonasal and dorsoventral axes of the retina are mapped onto the rostrocaudal and lateromedial axes of the tectum, respectively (Stuermer, 1988). Moreover, a single RGC axon will only innervate a single sublaminar layer, which means that RGCs relaying different types of visual properties terminate in a lamina-specific manner (Xiao and Baier, 2007). Consequently, functional studies have confirmed that RGCs encoding specific visual features such as direction- and orientation-selectivity, topographically target a distinct OT sublaminar layer. For example, the superficial sublaminae of SFGS receive input from upward-, downward-, and forward-directed motion selective RGCs (Gabriel *et al.*, 2012; Nikolaou *et al.*, 2012). This means that each lamina within the OT is highly predictive of input types, giving us prior knowledge of the type of synaptic inputs we are imaging when addressing SHY.

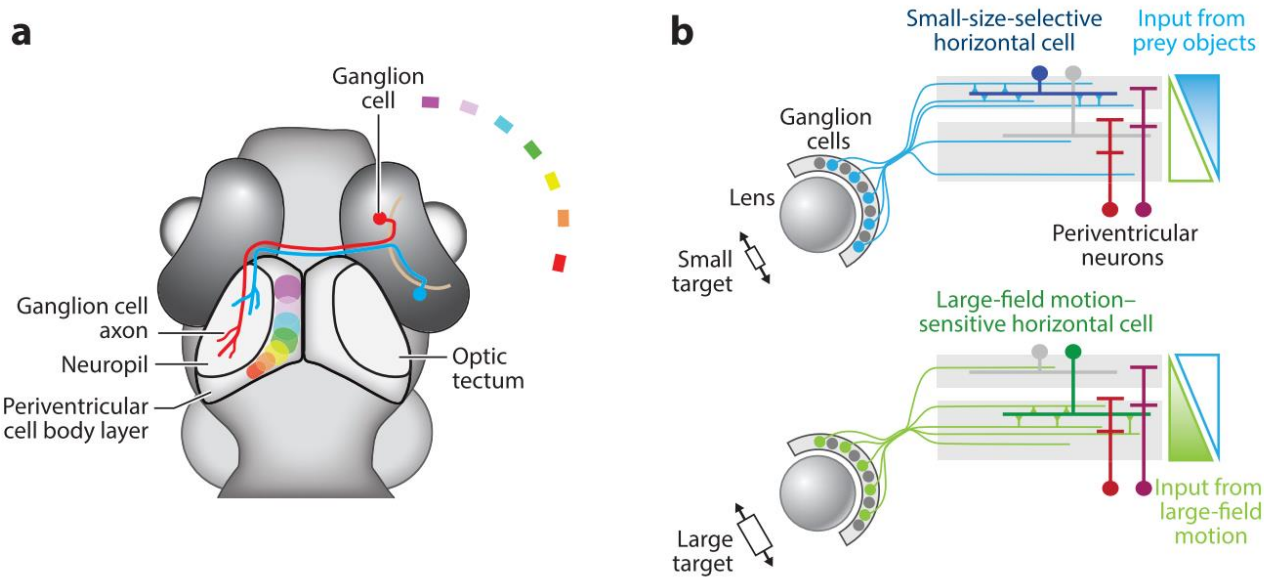

Figure 1.4: Retinotopic layer and maps of the optic tectum (taken from Bollmann, 2019). A) Schematic of retinotopic maps showing the temporonasal axis of the retina is mapped onto the rostrocaudal axis of the tectal neuropil. B) Examples of visual feature selective tectal neurons arborizing in a layer-specific manner. Superficial interneurons (SINs), also known as horizontal cells, that respond to small-field motion exhibit dendritic branching in the superficial layer while large-field motion responsive SINs branches in deep tectal layers.

Functional and morphological identities of tectal neurons

Like the RGCs that innervate the OT, tectal periventricular neurons have functional subtypes that are selective for up, down, forward, and backward motion (Gebhardt, Baier and Del Bene, 2013). The specific sublayer where tectal neurons laminar arborizes correlates to their visual-

selective features (Del Bene *et al.*, 2010; Gabriel *et al.*, 2012; Preuss *et al.*, 2014). For example, direction-selective neurons with different tuning preferences arborize in distinct layers of the superficial, retinorecipient layers of the neuropil. Gabriel et al. (2012) found two types of motion-active neurons: rostrocaudal- and caudorostral-direction selective. Both display bistratified morphology with their proximal branch deep within the neuropil layer. However, their distal arborizations target the superficial neuropil at different levels. The rostrocaudal-tuned neurons have a thinner and flatter arborization and target a more superficial layer than that of the caudorostral-tuned neurons. Moreover, excitatory synaptic inputs from the RGCs are directionally tuned and match the preferred direction of spike output in these cells, while inhibitory inputs are selective for nonpreferred directions. Another example of layer specific arborization correlating with function is the superficial interneurons (SINs). SINs are monostratified and target a single retinorecipient layer (Del Bene *et al.*, 2010). Subpopulations of SINs with distinct size-tuning properties are dependent on their target layer. SINs that stratify in the superficial OT layer at the SO are tuned to small-size-selectivity, while SINs that arborize deeper in the SFGS are large-size-selective (Figure 3.1B) (Preuss *et al.*, 2014). These examples show that where tectal neurons arborize matches with their functional identity and incoming excitatory inputs from the RGCs. Such anatomical and functional predictivity gives us a priori knowledge of the neuron's functional identity based on their location when imaging synapses to address SHY.

Apart from matching lamination layer to tuning properties, the morphology of tectal neurons is related to their functional identity. The dendrites of SINs cover a large extent of the neuropil in both the rostrocaudual and mediolateral directions and filter spot size information to different layers of the tectal neuropil (Del Bene *et al.*, 2010; Preuss *et al.*, 2014) (Table 1.1). In another study, Nikolaou et al. found that tectal neurons labelled with a FoxP2.A transgenic reporter can be grouped into four subtypes according to their morphology (2015). Each of the morphological types shows a high probability of having similar functional properties. For example, cell classified as Morphological Type 3 (Mt3) are only vertically tuned and Mt2 contain two functional subtypes with approximately half the population horizontally tuned and the other half vertically tuned. Furthermore, the tuning curves of direction-selective tectal neurons do not change between 4-7dpf, suggesting that the functional specification is

fixed within these cells and stable throughout early development of the tectum (Nikolaou *et al.*, 2015).

These predictive properties of tectal neurons are highly desirable as we can map functional and morphological identities to their synapse dynamics. The correlation between at least some morphologies and functional properties will allow us to test whether SHY holds universally in all neurons or whether SHY is only detectable in functionally distinct subtypes of neurons.

Table 1.1: Examples of Tectal neurons types and functional identity. Italics indicate our own interpretation from published works. * indicates genetically undefined transgenic line or enhancer trap line.

Name	Type	Distal Arbour Layer (µm)	Proximal Arbour Layer (µm)	AP Span (µm)	Arbour Thickness (µm)	Soma location	Neurotransmitter	Presynapse	Functional Identity	Gene Reporter	Age	Citation
nsPVINs	non-stratified periventricular interneurons	deeper layer of the SFGS and the SGC	N/A	30.48±1.66	28.87±1.58	deep in the SPV layer	GABAergic	Separate branch with postsynaptic but not stratified	Unknown	dg4ii dlx5/4	5dpf	(Robles, Smith and Baier, 2011)
bsPVINs	bistratified periventricular interneurons	13.0 ± 1.5 most superficial layer of the SFGS	39.2 ± 2.3 stratum griseum centrale (SGC	41.29±2.14 µm proximal, 22.4±1.5 distal	6.8 ± 0.7 (Proximal) 5.5 ± 0.4 (Distal)	deeper/intermediate SPV	GABA ⊖ Glutamatergic ?	Proximal not distal via SypGFP + array tomography	Unknown	dg4ii or dlx5/4	5dpf	(Robles, Smith and Baier, 2011)
PVPN	periventricular projection neuron	deep SGC and SAC	N/A	22.01±1.7	25.55±1.14	superficial 25 µm of SPV and SAC	GABAergic	Projects to Hb. Syp GFP in Hb + neuropul	Unknown	dg4ii or dlx5/5	5dpf	(Robles, Smith and Baier, 2011)
Type 1 RC	bistratified	SO (6.1±1.5)	SFGS/ SGC	38.7±6.9	10.0±2.2		GABAergic	Unknown	Direction selective RC	Oh:G-3	6-8dpf	(Gabriel *et al.*, 2012)
Type 2CR	bistratified	SFGSB,D (13.6±3.9)	SFGS /SGC	24.4±3.3	16.3±5.8		GABAergic	Unknown	Direction selectiveCR	Oh:G-4	6-8dpf	(Gabriel *et al.*, 2012)
Glut nsPVINs	non-stratified	SFGS/SGC	N/A	Unknown	Bushy/Unknown	Unknown	Glutamatergic >GABAergic	Unknown	Small size tuning	*Gal4mpn354	*7dpf*	(Barker and Baier, 2015)
Mt1	*bistratified*	Unknown	Unknown	Unknown	Unknown	Unknown	Unknown	Unknown	OS Vertical>DS Fw > DS backward	FoxP2.A	7dpf	(Nikolaou *et al.*, 2015)
Mt2	*nonstratified*	Unknown	Unknown	Unknown	Unknown	Unknown	Unknown	Unknown	Osvertical>OS Horizontal	FoxP2.A	7dpf	(Nikolaou *et al.*, 2015)
Mt3	*multi-stratified*	Unknown	Unknown	Unknown	Unknown	Unknown	Unknown	Unknown	Orientation selective Vertical	FoxP2.A	7dpf	(Nikolaou *et al.*, 2015)
Mt4	*monostratified*	Unknown	Unknown	Unknown	Unknown	Unknown	Unknown	Unknown	OS Vertical> DS Fw> DS Backward	FoxP2.A	7dpf	(Nikolaou *et al.*, 2015)
SINs	*monostratified*	SFGS	N/A	Broad	Unknown	SO	GABAergic	Monostratified layer	Large stimuli	*Gal4s1156t-	5dpf	(Del Bene *et al.*, 2010)
SINs	*monostratified*	SO	N/A	Broad	Unknow	SO	GABAergic	Unknown	Small stimuli	*Oh:GCaMP6s	5-8dpf	(Preuss *et al.*, 2014)

1.4.2 The Larval Zebrafish Hypocretin neurons

To comprehensively understand SHY, we must thoroughly examine synapse dynamics at the single-cell level during sleep/wake states in various neuronal populations throughout the brain. Another set of neurons that would be interesting to investigate are neurons of the sleep/wake regulatory circuits, where sleep pressure (i.e. effects of prior duration of wakefulness on sleep need) and circadian clock regulation are tightly linked to sleep effector neurons. One such neuronal type is the Hypocertin (Hcrt, also known as Orexin) neurons within the hypothalamus. To investigate whether SHY exists in these neurons, we need to better characterize the Hcrt circuit in larval zebrafish.

Hypocretin neurons

The hypothalamus plays a critical role in body homeostasis and regulates various behaviours such as feeding, thermogenesis, and sleeping (Inutsuka and Yamanaka, 2013). Hcrt are neuropeptides expressed exclusively by a small subset of neurons in the lateral hypothalamic area, approximately up to 70,000 cells in humans, 30,000 in dogs, and 3,400 in rodents (Siegel *et al.*, 2001). They were initially discovered as regulators of feeding behaviour, but they are now also recognized as key modulators of the sleep/wakefulness cycle (De Lecea *et al.*, 1998; Sakurai *et al.*, 1998). They have since been studied in many other different areas of neuroscience research, including addiction, reward and motivation, anxiety and depression, cardiovascular regulation, pain, migraine, and neuroendocrine regulation (Peyron and Kilduff, 2017).

The importance of Hcrt neurons for sleep regulation is made most clear by their role in the human sleep disorder, narcolepsy. A dysfunctional Hcrt system in both humans and dogs leads to narcolepsy, which is characterized by excessive daytime sleepiness, cataplexy, and alterations in the timing of rapid eye movement (REM) sleep (Beuckmann and Yanagisawa, 2002). Narcoleptic humans have been shown to have lower numbers of Hcrt neurons and reduced Hcrt concentration in the cerebrospinal fluid (Nishino *et al.*, 2000). Mice mutant lacking Hcrt neuropeptide production or Hcrt Receptor display frequent episodes of sudden cataplexy-like behavioural arrest, reduced average duration of wake periods, and direct transitions from wakefulness to REM sleep, which strongly resembles human narcolepsy (Chemelli *et al.*, 1999; Willie *et al.*, 2003). As in rodents, elimination of Hcrt activity (via receptor or ablation of the neurons) results in sleep and fragmented wake periods in both

adult and larval zebrafish (Yokogawa *et al.*, 2007; Elbaz *et al.*, 2012). Conversely, overexpression of Hcrt in zebrafish promotes wakefulness and reduces their ability to initiate and maintain rest at night (Prober *et al.*, 2006). Activation of Hcrt via optogenetic or chemogenetic methods is sufficient to induce wakefulness and reduce sleep (Singh *et al.*, 2015; Chen *et al.*, 2016).

The role of Hcrt in feeding is also important, as Hcrt-ablated transgenic mice exhibit profound hypophgia and late-onset diabetes (Hara *et al.*, 2001). Finally, in terms of reward behaviour, infusion of Hcrt into local ventral tegmental in rodents drives behaviour motivated by either food or drug rewards. Conversely, intra-tegmental microinjection of an Hcrt receptor (HcrtR) antagonist abolished a conditioned place preference for morphine and locomotor sensitization to cocaine (Inutsuka and Yamanaka, 2013). Thus, Hcrt performs multiple functions regulating not only sleep, but other important behaviours.

Hypocretin system input and output

Hcrt in the zebrafish larvae is expressed by approximately 10 pairs of bilateral, glutamatergic neurons of the anterior hypothalamus by 5dpf and up to 60 neurons in adult. As in mammals, zebrafish Hcrt neurons were also found to innervate widespread areas of the brain. Hcrt have conserved innervation to the telencephalon, diencephalon, mesencephalon, rhombencephalon, and the pineal gland, innervating various nuclei such as noradrenergic, dopaminergic, serotonergic, cholinergic, histaminergic, and melatonin producing nuclei (Kaslin, 2004; Prober *et al.*, 2006). For example, in adult zebrafish, Hcrt neurons project to hypothalamic nuclei, the locus coeruleus, ventrolateral preoptic nucleus (VLPO), posterior tuberal nucleus, raphe area, pretectal nuclei, the optic tectum, dorsal tegmentum, and spinal cord (Kaslin, 2004; Panula, 2010) (Figure 1.5). Unlike mammals, zebrafish have one Hcrt Receptor that is most similar to mammalian HcrtR1 (Faraco *et al.*, 2006). Expression of the zebrafish HcrtR has been reported in several areas matching with Hcrt projection sites including clusters in the telencephalon, diencephalon, hindbrain, and rows of neurons along the spinal cord (Prober *et al.*, 2006). The widespread and conserved projection sites and receptor distribution in humans, rodents, and zebrafish indicate Hcrt's roles in regulation of various behaviours.

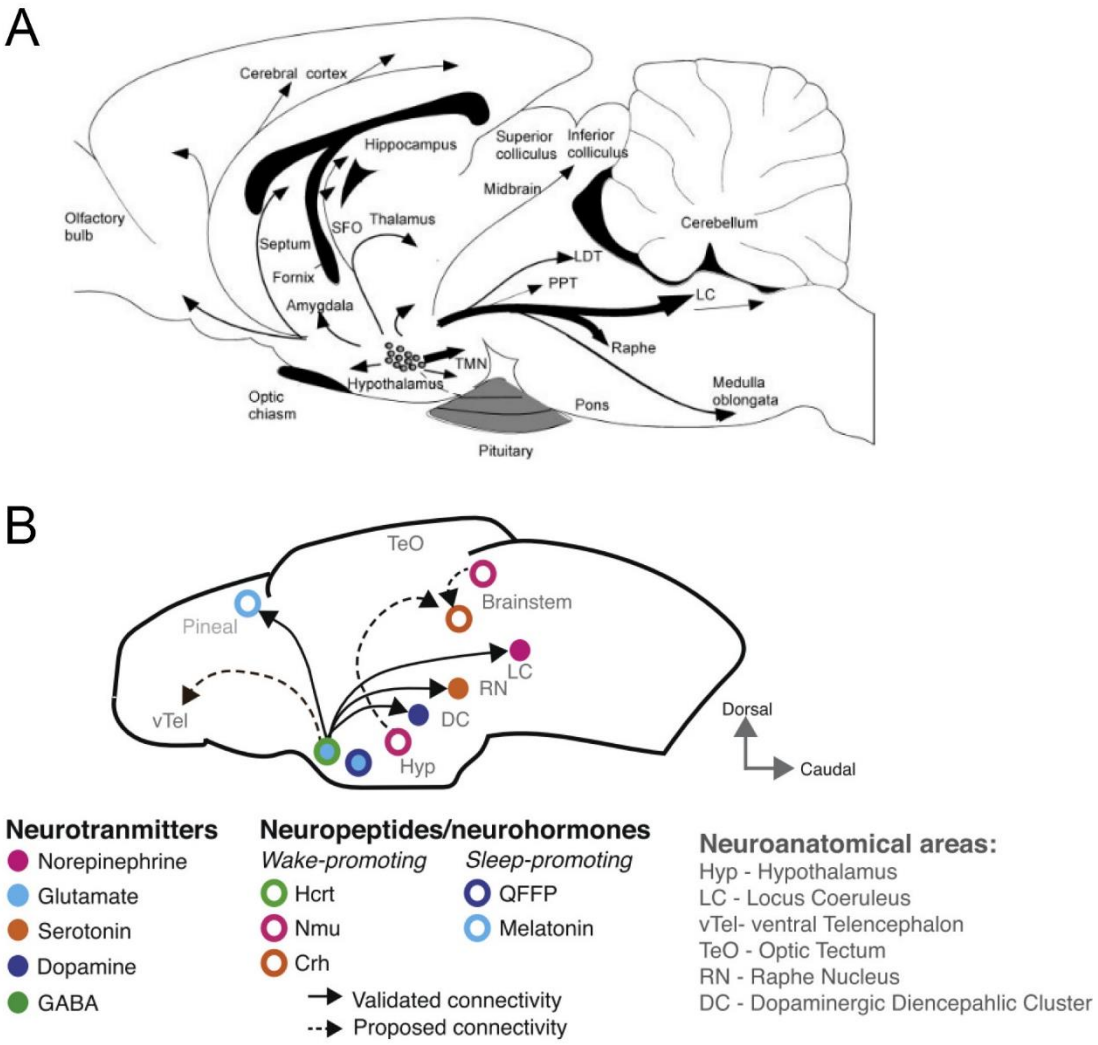

Figure 1.5: Hypocretin (Hcrt) neurons projection maps in the rodent and zebrafish brain. A) Diagram of a sagittal section through the rat brain. Hcrt neurons reside in the lateral hypothalamus and project to the entire central nervous system. The thickness of arrows represents the relative abundance of projection fibres. LC, Locus coeruleus; LDT, laterodorsal tegmental nucleus; PPT, pedunculopontine tegmental nucleus; TMN, tuberomammillary nucleus; and SFO, subfornical organ. B) Diagram of sagittal section through larval zebrafish brain showing known Hcrt connections to neuronal nuclei promoting sleep/wake behaviour. Modified from (Tsujino and Sakurai, 2009; Barlow and Rihel, 2017).

Heterogeneity of Hcrt system

It is evident that Hcrt neurons are involved in various circuits and behaviours. An unanswered question is whether distinct Hcrt neuron subtypes exist and mediate specific behaviours. Are all Hcrt neurons homogenously involved in these processes? Alternatively, are there subsets of functionally distinct Hcrt neuron pools that are involved in different aspects of behaviour – arousal, feeding, reward and motivation? Importantly, are functionally distinct Hcrt neuron pools synapse dynamics differentially altered across sleep/wake cycles?

Several studies have shown that Hcrt neurons can be grouped into subtypes. Works in rodents have shown that Hcrt neurons within the preifornical and dorsomedial hypothalamic areas (PFA-DMH) and within the lateral hypothalamic area (LHA) may be involved in different functions. Estabrooke et al. found that expression of the immediate early gene Fos (a marker for neuronal activation) in Hcrt neurons of the PFA-DMH shows diurnal changes consistent with Hcrt's role in sleep/wake regulation. However, LHA Hcrt neurons did not show such diurnal changes in activation (2001). This suggests that Hcrt neurons of PFA-DMH are involved in sleep/wake behaviour but not Hcrt neurons within the LHA. Conversely, during a reward behaviour paradigm, Harris et al. showed that conditioned cues associated with food/drug reward increased activity (measured by Fos) of the LHA Hcrt neurons but not PFA-DMH Hcrt neurons (Harris *et al.*, 2005). This indicates that LHA Hcrt neurons may be involved with feeding and addition behaviour. These two potential subpopulations of Hcrt neurons have also been shown to respond differently to different drugs. For example, amphetamine increased Fos expression in Hcrt neurons of the DMH but not the LHA (Fadel *et al.*, 2002), while weight gain associated with anti-psychotic drugs preferentially activate LHA rather than the DMH Hcrt neurons. The amount of LHA activation also correlates with weight gain. These data suggested that PFA-DMH Hcrt neurons are involved with sleep/wake regulation, whereas LHA Hcrt neurons play a role in feeding and addition behaviour.

In contrast, anatomical studies examining downstream projections of Hcrt neurons contradict with this functional dichotomy. Using dual retrograde tracer strategy, Iyer et al. found that individual neurons were more likely to project to both LC and TMN or to both the VTA and nucleus accumbens; however, these neurons are intermingled and do not show PFA-DMH or LHA topographic location within the hypothalamus (2018). Together, these findings suggest that there are projectome-specific subpopulations that are involved in distinct functions

within the Hcrt-expressing population. However, they cannot be grouped topographically by their soma location. Nonetheless, these studies using behavior-induced Fos mapping and retrograde tracer labelling in rodents can only tell us about certain potential functional and anatomical groups. Moreover, retrograde tracer labelling could cause spill over into neighbouring brain regions as the LC and TMN are compact structures. This method could also underestimate the number of Hcrt neurons labelled as tracer penetrance may not be 100% (Iyer *et al.*, 2018).

To examine whether there are subpopulations of Hcrt neurons, we need a more holistic approach that allows observation of Hcrt projections throughout the nervous system at a single-cell level. This would not only allow mapping of soma topography but also all the projection sites of a single Hcrt neuron. Similar single-cell approaches have been used in zebrafish to examine the heterogeneity of oxytocin neurons (Herget *et al.*, 2016). By targeting different colour fluorophore combinations to each oxytocin neurons within the population (i.e. the Brainbow method), Herget et al. found that there are two main subpopulations of oxytocin cells: one that innervates the pituitary and one that innervates diverse brain regions (2016). Mapping the single-cell projectome will help us systematically dissect Hcrt neurons' synapse dynamics. For example, if functionally distinct pools of Hcrt neurons exist, one could hypothesize that pools involved in the integration of circadian rhythm and sleep/wake behaviour may have different synapse dynamics compared to pools that are involved in reward and motivation behaviours.

1.5 AIMS AND APPROACHES

In its simplest form, SHY proposes that during wakefulness synapses are strengthened, and during sleep synapses are weakened. The decrease in synaptic strength throughout the brain is the function of sleep (Tononi and Cirelli, 2006). As discussed previously, various studies have been consistent with SHY, while others have equally contradicted it. We believe that the best way to investigate SHY is to track the same synapses through different behavioural sleep and wake states and circadian time. Our aim is to make use of the ease of imaging, rich genetic toolbox, and predictable behaviour of zebrafish larvae to investigate SHY.

Therefore, the aims of the project are as follows:

1) Develop tools to label both excitatory and inhibitory synapses in living zebrafish. Such tools should give us information about the strength and location of each synapse.
2) Identify whether sleep-dependent synaptic changes occur globally by tracking synapse dynamics of single neurons.
3) Disentangle sleep/wake and circadian cycle influences on synapse dynamics by tracking synapses in animals reared under different conditions such as:
    i. Constant conditions where synchronized circadian clocks are abolished.
    ii. Free-running conditions where sleep pattern is not entrained to a light/dark cycle
    iii. Sleep deprivation, where sleep homeostasis and the circadian clock are disentangled
4) Characterize the hypocretin neuronal population using single-cell reconstruction methods to provide a platform to address SHY in other neuronal types, especially sub-cortical circuits directly involved in sleep/wake regulation.

Chapter 2 Materials and Methods

2.1 ANIMALS

Adult zebrafish were maintained, mated, and raised at 28.5°C on a 14h light /10h dark cycle. All fish were maintained in the Fish Facility at University College London, according to the Animal Experimental Procedure Act (1986) under license from the United Kingdom Home Office (PIL number I07CABC30 and Project license PA8D4D0E5 awarded to Jason Rihel). Wildtype strains used were TL and AB/Tuebingen. Embryos were kept in fish water (5mM NaCl, 0.17mM KCl, 0.33mM $CaCl_2$, 0.33 mM $MgSO_4$ and 0.1% Methylene blue). The sex of the larvae is not defined at the early stages of development used for these studies. For live neuroanatomy experiments conducted in Chapter 3 and 5, 24hour post fertilization (hpf) were treated with 0.002% 1-phenyl-2-thiourea (PTU) until 3 days post-fertilization (dpf) to improves transparency of the larvae (Table 2.1). All larvae were fed with Paramecia from 7 dpf onward. For synapse tracking experiments larvae were placed into individual well in a 6-well plate (Thermo Fisher Scientific). Larvae fish were reared at 28.5°C on a 14/10 light/dark cycle unless stated otherwise.

Table 2.1: Fish line used in different types of experiments.

CHAPTER	EXPERIMENT	FISH USED	REASONING
3,5	Hcrt anatomy, synapse colocalization, and drug treatment	Larvae were treated with PTU at 24hpf-3dpf	improves transparency of the larvae
4	Synapse tracking	Tg(UAS: FingR(PSD95)-GFP-ZFC(CCR5TC)-KRAB(A)-P2A-mKate2f; Nacre$^{-/-}$)	Transparency of larvae improves imaging
4	Synapse and behavioral tracking	Tg(UAS: FingR(PSD95)-GFP-ZFC(CCR5TC)-KRAB(A)-P2A-mKate2f; Nacre$^{+/+}$ or $^{+/-}$)	Pigmented fish were required for behavioral tracking of the fish

2.1.1 Animal Rearing Conditions

For synapse tracking experiments larvae were placed into individual well in a 6-well plate (Thermo Fisher Scientific). All larvae were fed Paramecia from 7 dpf onward. Larvae were reared at 28.5°C with differing light:dark cycles (Table 2.2) For further details of animal use and maintenance see Chapter 6 Materials and Methods.

Table 2.2: Variants of rearing light conditions

Name	Property	Rearing light conditions (light:dark)
LD	Intact synchronized clock	14hr:10hr
LL	Clock break	Constant light (24hr:0hr)
FR	Free-running	14hr:10hr up to 6dpf transferred to constant light

2.2 CLONING

All DNA construct generated during this project has been performed using In-Fusion HD Cloning System (Clontech). Briefly, desired plasmid fragments were linearized and/or amplified using PCR and were fused together using the In-Fusion HD Enzyme (Clontech). Primers were designed to share an overlap of 15 homologous bases between the end of the linearized vector and/or the chosen PCR fragments (Table 2.3-4). The linearized or desired fragments were fused and transformed into Stellar Competent Cells according the In-Fusion Kit protocol. Successful infusion products were then miniprepped (QAIGEN, UK); screened using appropriate restriction digests with (New England Biolabs, UK); and sent for Sanger sequencing (Source Bioscience, UK) to confirm the correct inserts.

Plasmid templates used were pTol2-zcUAS:PSD95.FingR-EGFP-CCR5TC-KRAB(A) (from Bonkowsky lab, University of Utah, Addgene:72638); p5UAS-GPHN-FingR-eGFP-ZFC(CCR5TC)-KRAB(A) (gift from Meyer Lab, King's College London); pGP-CMV-jGCaMP7b (Dana *et al.*, 2019 Addgene: 104484); Hcrt:GFP (gift from Mourrain lab, Stanford); and KalTA4 (gift from Tada lab, UCL).

It must be noted that UAS:FingR(GPHN)-GFP cassette (from Meyer Lab, King's College London) were modified instead of Son et al.'s UAS:FingR(GPHN)-mCherry (2016) (Addgene:72639), despite ideally having a different fluorescent protein fusion, higher copy of UAS, and different regulatory elements were found to have a stop codon in the middle of the open reading frame for the FingR cassette (after mCherry but before KRAB(A) domain). This produce FingR(GPHN) protein without its essential regulatory system.

Table 2.3: Constructs made using In-Fusion Kit.

Construct Generated	Properties
pBR-Tol2-Hcrt:KalTA4	Hypocretin promoter driving Gal4 with Tol2 arms
pBR-Hcrt:Gap43-GFP	Hypocretin promoter driving membrane-bound GFP
pCS2-P2A-mKate2-farnesylation-GI	Self-cleavage site with membrane-bound mKate2
pBR-Tol2-UAS:myrCherry,UAS: FingR.PSD95-GFP-ZFC(CCR5TC)	FingR-GFP for PSD95 with separate UAS for membrane-bound Cherry flanked by Tol2 arms
pBR-Tol2-pUAS:FingR(GPHN)-GFP-ZFC(CCR5TC)-KRAB(A)-P2A-mKate2-F	FingR-GFP for Gephyrin and self-cleavage peptide with membrane-bound mKate2 flanked by Tol2 arms
pBR-Tol2-UAS:FingR(PSD95)-GFP-ZFC(CCR5TC)-KRAB(A)-P2A-mKate2-f	FingR-GFP for PSD95 and self-cleavage peptide with membrane-bound mKate2 flanked by Tol2 arms
pBR-Tol2-UAS:FingR(PSD95)-GCaMP7b-ZFC(CCR5TC)-KRAB(A)-P2A-mKate2-f	FingR for PSD95 labelled by calcium indicator and self-cleavage peptide with membrane-bound mKate2 flanked by Tol2 arms

Table 2.4: Primers used in generating DNA construct using the In-Fusion Kit.

Plasmid made	Primer Name	Sequence (5'-3')	Notes
pBR-Tol2-Hcrt:KalTA4 NcoI digest on Tol2 plasmid	HCRT-F1	TCACTAGTTGATCACGAAAATGAATGAATGAATGAA	PCR out Hypocretin promoter overlap with Tol2 plasmid
	HCRT-B1	CCGCTACGTACCATGGAGTTTAGCTTCTGTCCCCTG	
	KalTA4-F1	ACAGAAGCTAAACTCATGAAACTGCTCTCATCCATC	Infusion with Hcrt promoter fragment and Tol2 plasmid
	KalTA4-pA-B1	GCGGCCGCTACGTACCCGCGAATTAAAAAACCTCCC	
pBR-Tol2-pUAS:FingR.GPHN-GFP-ZFC(CCR5TC)-KRAB(A)-P2A-mKate2-F NcoI digest on Tol2 plasmid	PaulGPHN-Fw-InF-Tol2	TCACTAGTTGATCACATTGTCTCATGAGCGGATACA	PCR out FingR.GPHN-GFP with Tol2 and P2A-mKate2f overlap
	PaulGPHN-rv-InF-P2A	AGAGAAGTTCGTGGCAGCCATAGAAGCAAGATTAGA	
	P2AKate_rv_InF_tol2	CCGCTACGTACCATGGAATGCAATTGTTGTTGTTAAC	PCR out P2A-mKate2f with Tol2 overlap
	PSD_InF_PKate_Fw2	CTTGCTTCTATGGCTGCCACGAACTTCTCTCTGTTA	
pCS2-P2A-mKate2f-GI	P2A_InV_Rv	GGATCTAGGACCGGGGTTTTC	Inverse PCR (to linearize) pCS2-P2A-GFP-CAAX
	P2A InV_Fw	GTGCTCTCCTGACCTCTAGAA	
	P2A_InF_mKate_Fw	CCCGGTCCTAGATCCATGGTGAGCGAGCTGATTAAG	PCR out mKate2f with overhangs with linearized pCS2-P2A vector
	P2A_InF_mKate_Rv	AGGTCAGGAGAGCACTCAGGAGAGCACACAGCAGCT	
pBR-Tol2-UAS:FingR.PSD95-GFP-ZFC(CCR5TC)-KRAB(A)-P2A-mKate2-f	PSD_InF_PKate_Fw2	CTTGCTTCTATGGCTGCCACGAACTTCTCTCTGTTA	PCR out P2A-mKate2f fragment from pCS2-P2A-mKate2f-GI
	PSD_InF_PKate_Rv	ACCTCCCACACCTCCTCAGGAGAGCACACAGCAGCT	

	PSD_InV_P2A_Rv 2	AGCCATAGAAGCAAGATTAGA	Inverse PCR (to linearize) FingR.PSD95-GFP
	PSD_InV_P2A_fw	GGAGGTGTGGGAGGTTTTTTC	
pBR-Tol2-UAS:myrCherry,UAS: FingR.PSD95-GFP-ZFC(CCR5TC)	1D_PSD_myrRFP_Fw	CCCGGTCCTAGATCCATGGTGAGCGAGCTGATTAAG	PCR out FingR.PSD95 with overhangs. Digest pBR-Tol2-myrCherry with NotI.
	1D_PSD_myrRFP_Rv	TCCGCGGTGGCGGCCAAACCTCCCACACCTCCCCCT	
pBR-Tol2-UAS:FingR.PSD95-GCaMP7b-ZFC(CCR5TC)-KRAB(A)-P2A-mKate2-f	InF_PSD_Gcamp_Fw	AGTAGATCTGGGGTGATGGGTTCTCATCATCATCAT	PCR out GCaMP7b with overhangs to FingR.PSD95-GFP
	InF_PSD_GCamp_Rv	TCCAGCGCCAGCTCCCCTAGACTTCGCTGTCATCAT	
	InV_PSD95_Fw	CACCCCAGATCTACTGGAGCC	Inverse PCR (to linearize) FingR.PSD95-GFP
	Inv_PSD95_rv	TCTAGGGGAGCTGGCGCTGGA	

2.3 DNA CONSTRUCT EXPRESSIONS

2.3.1 DNA Construct Injections

To transiently and mosaically express DNA constructs such as Hcrt:GFP, constructs were injected into the cell of AB/Tub or TL strain wild-type embryos at the one-cell stage. Injection mix were diluted to total concentration of 10ng/*µL for each DNA construct in RNAse-free water.* Microinjection setup were as described in (Godinho, 2011) Briefly, backfill micropipette (1.2mmx0.69mm pulled glass capillaries, Harvard Apparatus, UK) with injection mix, mount micropipette to the micromanipulator (MN-153, Narishige, Japan). Through the stereomicroscope (Nikon SMZ1500) trim the micropipette tip using forceps and calibrate injection volume to ~1nL using micrometer (Pyser SGI). Microinjector (Picospritzer III, Parker Instrumentation, USA) were set to 40-50ms. Embryos were aligned using a glass slide instead of agarose chamber. Uninjected siblings from the same clutch were kept as controls.

2.3.2 Transgenic fish lines

Injection of DNA constructs and generation of stable transgenic lines was performed as described (Burket *et al.*, 2008). For the ease of screening, UAS constructs generated were injected into available Gal4 lines, and vice versa for Gal4 construct generated. DNA construct (10ng*/µL) and Tol2 transposase mRNA (100 ng/µL)* were microinjected *into the cell at one-cell stage* as described above. Tol2 transposase mRNA was in vitro transcribed from the pCS-TP6287 plasmid (gift from Wilson lab, UCL) using an SP6 mMESSAGE mMACHINE Kit (Ambion, USA). Positive embryos, mosaic expression of construct injected, at 3dpf were raised to adulthood and crossed with AB/Tub or TL strain wild-type fish to identify founder fish. The founder fish were outcrossed with wildtype and the F1 fish were selected on the basis of their fluorescent signal. Transgenic lines were maintained by outcrossing to Nacre fish (pigmentation mutant) for ease of imaging. Transgenic line made during this project and their properties can be found at Table 2.5.

Table 2.5: Transgenic line generated and their properties

Transgenic line generated	Properties
Tg(Hcrt:KaLTA4; cry:GFP,UAS:RFP)	Hcrt cells labelled with RFP; GFP marker in lens
Tg(UAS:myrCherry,UAS:PSD95.FingR-GFP-ZFC(CCR5TC)-KRAB(A);Hcrt:KalTA4)	Hcrt cells PSD95 labels with FingR-GFP; cell membrane in Cherry.
Tg(UAS:PSD95.FingR-GFP-ZFC(CCR5TC)-KRAB(A)-P2A-mKate2f)	PSD95 labels with FingR-GFP; cell membrane in mKate2.
Tg(UAS:GPHN.FingR-GFP-ZFC(CCR5TC)-KRAB(A)-P2A-mKate2f)	Gephyrin labels with FingR-GFP; cell membrane in mKate2.
Tg(UAS:FingR.PSD95-ZFC(CCR5TC)-KRAB(A)-GCaMP7b-P2A-mKate2-f)	PSD95 labels with calcium indicator, GCaMP7b; cell membrane in mKate2.

2.3.3 Single-cell FingR expression using electroporation

To label single tectal cells for repeated imaging, FoxP2.A tectal cells were mosaically labelled by electroporating linearized FoxP2.A: Gal4FF activator plasmid (construct was a gift of Martin Meyer, King's College London) into Tg(UAS:FingR(PSD95)-GFP-ZFC(CCR5TC)-KRAB(A)-P2A-mKate2-f)-positive larvae at 3dpf. Electroporation were adapted from (Nikolaou *et al.*, 2015). Anaesthetized 3 dpf zebrafish larvae were mounted in 1% low-melting point agarose (Sigma) perpendicular to a glass slide in a petri dish. Electroporation buffer (180 mM NaCl, 5 mM KCl, 1.8 mM CaCl2, 5 mM HEPES, pH 7.2) with Tricaine was used as fish medium. Excess agarose along the larval body was removed to allow access for the electroporation electrodes. Plasmid DNA was prepared using midi-prep kits (Qiagen) and ventricularly injected at a concentration of 500 ng/µl together with Tol2 mRNA (20ng/µl) and Phenol-red using a micro glass needle. Co-injection with Tol2 mRNA was found to improve efficiency of expression. The electroporation electrodes were positioned such that the positive electrode was lateral and slightly dorsal to the hemisphere of the optic tectum to be targeted and the negative electrode lateral and ventral to the opposite eye of the larva. DNA plasmids were electroporated by delivering 1 second trains of 5 ms, 85 V voltage pulses at 200 Hz using an SD9 stimulator (Grass Instruments). A total of five trains per larva were delivered. Electroporated larvae were screened for single-cell expression of FingR using a 10x water-immersion (0.5NA) objective and a Lightsheet Z1 microscope (Zeiss) at 6dpf. The Lightsheet was used over confocal microscopy as fish can be quickly mounted using a capillary and large number of animals can be screened in a short period of time.

2.3.4 Hcrt single cell expression by DNA Injections

To transiently express in a single Hcrt positive cell, 5ng/µL of a Hcrt:GFP DNA construct were injected into Tg(Hcrt:KalTA4;UAS:RFP;Cry:GFP) embryos at the one-cell stage. The microinjection setup was as described in the 6.3 DNA Construct Injection in Chapter 6 Materials and Methods. Injected embryos were first screened for the expression of GFP in single Hcrt cells using a Zeiss Z1 Lightsheet with a 10x/0.5 W Plan Apochromat water-immersion objective (Zeiss).

2.4 IMMUNOHISTOCHEMISTRY

2.4.1 Whole-mount Immunohistochemistry for Hcrt anatomy

Whole mount antibody staining of dissected embryos was performed as previously described (Wilson et al., 1990), with the following modifications. Fixed (and if applicable, dissected) embryos were rehydrated sequentially, washed in PBT (Phosphate Buffered Saline /0.5% Triton X-100), digested with proteinase K (for 2-3dpf; 10ug/mL for 20 minutes; for 4-5dpf; 30ug/mL for 20 minutes; for 6-10dpf, 40 ug/ml for 40 minutes), and post-fixed in 4% sucrose/4% paraformaldehyde (PFA) for 20 minutes at room temperature (RT). Embryos were blocked for at least 1 h at RT in PBT with 10% normal goat serum and 1% Dimethyl sulfoxide (DMSO), and then incubated in primary antibodies in PBT + serum overnight at 4°C. Embryos were washed 4-6 times in PBT for at least 30 minutes at RT and then incubated in secondary antibodies overnight at 4°C. Embryos were washed 4-6 times for at least 30 minutes at RT in PBT and mounted for imaging in 1% low melt agarose.

The following primary antibodies were used: anti-RFP (rabbit polyclonal, PM005, MBL, 1:1000); dsRed (rabbit polyclonal, #632496, Clonetech, 1:300); anti-GFP (chicken polyclonal, ab13970, Abcam, 1:500); and rabbit anti-orexin A (AB3704, 1:500; Chemicon, Temecula, CA). The following Alexa Fluor secondary antibodies were used with the appropriate primary 488 goat anti-chicken IgG; 568 goat anti-rabbit IgG; and 633 goat anti-rabbit IgG (H+L) (Life Technologies, 1:200). All samples were counterstained with DAPI (Molecular Probes, 1:1000) to label nuclei.

2.4.2 Whole-mount Synaptic Immunohistochemistry

Staining for MAGUK and Synapsin expressions were done by whole-mount immunohistochemistry adapted from (Sheets *et al.*, 2011). Zebrafish larvae at 2dpf were dechorionated and fixed with 4% formaldehyde methanol-free (Pierce™ Thermofisher, #28906) in BT buffer (1.0g sucrose, 18.75ul 0.2M CaCl2, topped up with PO_4 buffer to 15 ml). To increase signal-to-noise ratio, fixing time was decreased to 1.5-2hours at 4°C but this reduction also lead sample to softened. PO_4 buffer consists of 8 parts 0.1M NaH_2PO_4 and 2 parts 0.1M Na_2HPO_4. Samples were washed with PO_4 buffer and dH_2O for 5 minutes at room temperature (RT), and permeabilized with ice-cold acetone for 5 minutes in -20°C. After washing with dH_2O and PO_4 buffer for 5 minutes each, specimens were blocked with buffer containing 2% goat serum, 1% bovine serum albumin (BSA) and 1% dimethyl sulfoxide (DMSO) in 0.1 M Phosphate buffered saline (PBS) pH 7.4 for at least 2 hours. They were then incubated with primary antibodies diluted in PBS/BSA/DMSO at 4°C overnight. Embryos were washed 4-6 times for at least 20 minutes in PBS/BSA/DMSO at RT and incubated in secondary antibodies overnight at 4°C. It is critical that embryos were washed again and transferred to glycerol in a stepwise manner up to 80% glycerol in PBS to clear out unbound secondary antibodies.

To visualize GPHN and SV2, immunohistochemistry staining was adapted from (Hunter *et al.*, 2011). Larvae at 2dpf were dechorionated and fixed using freshly thawed 4% paraformaldehyde in PBS for 1.5hours at RT. After washing with PBS 3 times for 5 minutes each, larvae were permeabilized using 0.25% Trypsin (Gibco, ThermoFisher) for 15 minutes at RT. A small drop of 10% Heat-inactivated Normal Goat Serum (NGS) (Sigma, UK) was added to stop the reaction, the samples were blocked using 10% NGS in PBS for at least 1 hour at RT. Primary antibodies (concentration and suppliers listed below) incubation were done in 10% NGS and 2mM Sodium Azide in 1% PBS Triton (PBSTr) over 2days and nights at 4°C. Specimens were washed using PBSTr and incubate with secondary antibodies overnight. Embryos were washed again and transferred to glycerol in a stepwise manner up to 80% glycerol in PBS.

Primary antibodies to detect MAGUKs, GPHN, SV2, and cell morphology were anti-MAGUK (Anti-pan-MAGUK mouse monoclonal, clone K28/86, Millipore, 1:500), anti-GPHN (mouse monoclonal, #147111, Synaptic Systems, 1:1000) and tRFP (Anti-tRFP Rabbit Polyclonal, AB233, Evrogen, 1:500), respectively. FingR-GFP puncta were visualized using its own live

fluorescents. Antibodies against GFP (for FingR puncta) were not used as to avoid overamplifying FingR signals and retain puncta-like characteristics. The following Alexa Flour secondary antibodies were used (Life Technologies, 1:200); 568 goat anti-rabbit IgG; and 633 goat anti-mouse IgG monoclonal (H+L).

2.5 IMAGING

2.5.1 Imaging fixed sample for synaptic colocalization

Confocal images were obtained using a Leica TCS SP8 system with HC PL APO 20x/0.75 IMM CS2 multi-immersion objective set to glycerol (Leica Systems). Z stacks were obtained at 1.0µm depth intervals with sequential acquisition settings of 1024 x 1024 pixels. The raw images were compiled using NIH Image J software (http://imagej.nih.gov/ij/). To analyse the colocalization of the puncta, maximum projection of about 5-10µm were taken for each cell. Grey values were taken from cross-section of the puncta using the plot-profile tool from ImageJ. Puncta grey values were normalized against the whole stack grey value of their respective channels.

The colocalization and relationships between FingRs and antibodies staining (and vice versa) were analysed using custom written scripts on Python (available at https://github.com/anyasupp/thesis_21). For colocalization of FingR to corresponding antibody puncta (and vice versa), the presence of puncta (maximum normalized grey value should be at least 50% higher than the baseline) is used. It was found that overlapping of area under the curve of grey value for each channel did not work well as the normalized baseline in antibody channel is typically higher than FingR's, resulting in false positive overlap. For proxy of diameter of the puncta, normalized grey values were fitted with a non-gaussian prior to finding full width half maximum (FWHM).

2.5.2 Drug exposure for live imaging

Tg(FingR.PSD95-GFP-P2A-mKate2f; emx3:Gal4) larvae were treated with MK801. Larvae were screened and selected for sporadic single tectal neuron expression at 5dpf using Zeiss Z1 Lightsheet with 10x/0.5 W Plan Apochromat water-immersion objective (Zeiss). Fish were anaesthetized and immobilized in 1.5% agarose in fish water in a capillary glass tube (size 2/~1mm or 3/~1.5mm). At 7dpf, pre-drug exposure z-stacks were taken of positive larvae at 1.0µm depth intervals with sequential acquisition settings of 1024 x 1024 pixels. Larvae were transferred to induvial wells of a 6-well plate with fish water. After 1-hour rest post first

imaging, DMSO or 30 μM MK801 (Sigma) were added to each well, with the experimenter blinded to the drug condition. Larvae were placed in a 28.5°C L:D incubator for 2 hours, after which drugs were washed out by replacing drugs solutions with fish water carefully 2-3 times and larvae transferred to a new 6-well plate with fresh water. After 1 hour of recovery period, larvae were re-imaged using Lightsheet and once more at 18-20hours post drug exposure.

2.5.3 Imaging FingR during day/night

For FingR tracking experiments, FingR single-cell-positive larvae were anaesthetized for 5-10 minutes and immobilized in 1.5% low-melting point agarose (Sigma) in fish water. During imaging tail-free tethered larvae were unanaesthetised. Each larva was imaged at approximately 0-1 and 9-11 Zeitgeber Time (ZT, where ZT= lights ON) on 7dpf, 8dpf, and 9dpf at 28.5°C with chamber lights on. FingR-positive cell image stacks were acquired using a 20x water-immersion objective and an LSM 980 confocal microscope with Airyscan 2 (Zeiss). GFP and mKate2f were excited at 488nm and 594nm, respectively. Z stacks were obtained at 0.34µm voxel depth with sequential acquisition settings of 2024 x 2024 pixels (0.0595376x 0.0595376µm pixel width x height) and 16-bit using SR4 mode (imaging 4 pixel simultaneously). Pixel alignment and processing of the raw AiryScan stack were performed using ZEN software (Zeiss).

2.5.4 Imaging Hcrt neurons in fixed and live samples

Single-cell Hcrt neuron cell body and anatomical projection experiments were imaged on a Zeiss Z1 Lightsheet microscope with a 10x water objective (Zeiss Systems) using the tiling program. Z stacks were obtained at 1.0 - 2.0µm intervals with sequential acquisition settings of 1024 x 1024 pixels. The total final scan depths were between 300 – 400µm. Multiview stacks and tiles were fused using Arivis Vision4D. The raw images were adjusted for brightness and contrast, stacks were compiled, and depth-colour coded using NIH Image J software (http://imagej.nih.gov/ij/). As Lightsheet microscopy illuminates focused laser sheets from the lateral side of the fish, pigmentation and thickness of eye tissues obscure and reduce the visibility of small, fine Hcrt processes within the hypothalamic neuropil. Therefore, for single Hcrt cell imaging, Tungsten needles were used to remove the eyes from 7dpf larvae after being euthanized by an overdose of tricaine methane sulfonate (MS222, 200-300 mg/L) and imaged straight away. Despite this drawback, Lightsheet microscopy was preferred as pilot

imaging found it best detected the often lowly expressed fine processes of Hcrt neurons at lower laser power and the faster imaging allowed for quick image tiling across the whole larva.

2.5.5 Locomotor activity assay

The behavioural tracking of larval zebrafish was performed as previously described (Rihel, Prober and Schier, 2010). Zebrafish larvae were raised at 28.5°C on 14hr:10hr light:dark cycle. At 6dpf each larva was placed into individual wells of a 6-well plate (Thermo Fisher Scientific) containing approximately 4mL of fish water (half of each well). At 7dpf 1-1.5mL of filtered paramecia solution was added. Locomotor activity was monitored using an automated video tracking system (Zebrabox, Viewpoin LifeSciences) in a temperature-regulated room (26.5°C) and exposed to a 14hr:10hr white light:dark schedule unless stated otherwise with constant infrared illumination (Viewpoint Life Sciences). The larval movement was recorded using the Videotrack quantization mode with the following detection parameters: detection threshold, 12; burst, 100; freeze, 3; bin size, 60s. The locomotor assay data were analyzed using custom MATLAB (MathWorks) scripts. Any one-minute period of inactivity was defined as one minute of sleep, according to established convention (Prober et al., 2006).

2.5.6 Sleep Deprivation Assay

Zebrafish larvae raised at 28.5°C on 14hr:10hr light:dark cycle. At 6dpf larval sleep/wake behaviour were tracked as described above (see 2.5.5). Randomly selected larvae were then sleep deprived for 4 hours from ZT14-18 at 7dpf. Larvae subjected to sleep deprivation were individually housed in six-well plates and gentle stimulation was performed using a No. 1-2 paintbrush (Daler-Rowney Graduate Brush, UK) to prevent larvae from being immobilized for longer than 1 minute, which is the behavioural definition of sleep in zebrafish larvae (Rihel, Prober and Schier, 2010). All larvae were imaged at ~ZT14 and ZT18 on 7dpf and again at ZT0 on 8dpf. Sleep deprivation and larvae immobilization in agarose for imaging during lights OFF (ZT14-24) were conducted under dim red light (Blackburn Local Bike Rear Light 15 Lumen, UK) to prevent exposure to blue light that may cause shift in circadian rhythms (Steindal and Whitmore, 2020).

2.6 POST-HOC ANALYSIS

2.6.1 3D Image Registration for Hcrt population

Registration of image stacks was performed using the ANTs toolbox version 2.1.0 (Avants et al., 2011). Similar to Henriques et al., (2019), image stacks were converted to the NIfTi format using the ImageJ NIfTI Input/Output plugin. Each larval specimen 3D image stack (e.g. fishA) was registered using the DAPI channel and the following parameters performed on UCLs Legion cluster:

{antsRegistration -d 3 –float 1 -o [fishA_, fishA_Warped.nii.gz] –n WelchWindowedSinc - r [ref.nii, fishA–01.nii.gz,1] -t Rigid[0.1] -m MI[ref.nii, fishA–01.nii.gz,1,32, Regular,0.25] - c [200×200×200×0,1e-8,10] –f 12×8×4×2 –s 4×3×2×1-t Affine[0.1] - m MI[ref.nii, fishA–01.nii.gz,1,32, Regular,0.25] -c [200×200×200×0,1e8,10] –f 12×8×4×2 –s 4×3×2×1-t SyN[0.1,6,0] -m CC[ref.nii, fishA–01.nii.gz,1,2] - c [200×200×200×200×10,1e-7,10] –f 12×8×4×2×1 –s 4×3×2×1×0}

The deformation matrices output from above were then applied to the Hcrt:RFP channel using:

{antsApplyTransforms -d 3 -v 0 –float -n WelchWindowedSinc -i fishA–0N.nii.gz - r ref.nii -o fishA–0N_Warped.nii -t fishA_1Warp.nii.gz -t fishA_0GenericAffine.mat}

Each larval specimen was imaged twice: one from dorsal to ventral and another from ventral to dorsal. This is to circumvent the decrease in resolution as we imaged deeper into the sample. The 3D volumes imaged from each side were registered separately to the ZBB brain atlas (Marquart et al., 2015).

2.6.2 Synapse dynamics subtrends

To find whether subtrends of synapse number dynamics exists in LD rearing larvae, we used each RoC time point for each fish as features and hierarchical clustering with Euclidean distance to group synapse dynamics. We found that average linkage produced the highest Cophenetic correlation coefficient, suggesting that this method preserves the pairwise distance between raw data and the clustered data. By observing the dendrogram, we selected an optimal cluster of two. Clustering was performed using custom written scripts on Python (available at https://github.comanyasupp/thesis_21).

2.6.3 Tectal cell segmentation for tracking synapses

The morphology of tectal neurons was segmented using the Filament function in Imaris 8.0.2 software (Bitplane).

Various morphological features of the FoxP2.A tectal cells of 7dpf larvae were obtained using Imaris and ImageJ (NIH) softwares. FoxP2.A cell morphologies at 7dpf (ZT0) was chosen to age-match with the observations in Nikolaou et al. (2015). The total filament length for each neuron was obtained using the Filament function on Imaris. The anterior-posterior (AP) span of the distal arbour was obtain using the Measurement function on Imaris at an orthogonal view in 3D. The distance from the skin, distal arbour thickness, and distal arbour to skin distance were obtained using the rectangle Plot_Profile tool on ImageJ at an orthogonal view of the neuron to calculate the fluorescence intensity across the tectal depth. The intensity profiles were then analysed using custom Python scripts to obtained the maximum width using area under the curve functions – a similar method previously used to characterize tectal arbor morphology (Robles, Smith and Baier, 2011; Nikolaou *et al.*, 2015). Proximal arbour locations were calculated by dividing the proximal arbour distance from the nucleus by the total length of the neuron obtained using Filament function on Imaris.

Further analyses, such as clustering and statistics, were performed using custom written scripts on Python (available at https://github.com/anyasupp/thesis_21). For segmentation clustering, six morphological features of FoxP2.A cells were standardized and reduced in dimensionality by projecting into principal component analysis (PCA) space. The first 4 components, which explained 89% of the variance, were selected to use for clustering. These components were then clustered using K-means with K ranging from 1 to 11. Using the elbow method, Calinski Harabasz coefficient, and silhouette coefficient, we found that k = 4 was the most optimal number of k clusters.

2.6.4 Puncta quantification and statistics

All image files of synapse tracking experiments in Chapter 2 and 3 were blinded prior to segmentation and puncta quantifications. To count number of FingR(PSD95)-GFP puncta, first the neurons morphology were segmented using the Filament function in Imaris 8.0.2 software (Bitplane). FingR(PSD95)-GFP puncta were labelled using the Spots function, thresholded using the Quality classification at approximately 130-200 depending on the image file. Number and location of GFP puncta were also manually checked. Then the FingR(PSD95)-GFP

puncta that lie on the FingR+ neuron (mKate2f channel) were extracted using the Find Spots Close to Filament XTension (Ratio of Distance to Filament Radius of 0.5 were found to best separate puncta present on the cell of interest). Average 3D nuclear intensity per neuron per time point were obtained using Spots function on Imaris.

Rate of change (%) was calculated by the following formula:

$$RoC = \left(\frac{no.puncta - no.puncta\ of\ previous\ time\ point}{no.\ puncta\ of\ previous\ time\ point}\right) \times 100\%$$

Absolute puncta changes were calculated using the following formula:

$$\Delta Puncta = no.puncta - no.puncta\ of\ previos\ time\ point$$

Mixed-designed ANOVA (mixed-measure ANOVA) and post-hoc pairwise t-test were used for most comparisons. In longer synapse-tracking experiments where independent groups were more unbalanced and contain higher missing datapoints, another type of mixed-effects model, mixed linear were used. Values in figures represent mean 68 confidence interval, unless stated otherwise.

2.6.5 Hcrt single cell segmentation and clustering

The tracing of neuronal morphology and Sholl analyses were performed using the Simple Neurite Tracer plugin on ImageJ. Clustering was performed using K-means clustering in Python. Briefly, Sholl analysis for each single-cell Hcrt neuron were Z-scored. The Z-score values were then transformed into PCA space. The first 11 components explained 91.9% of the variance and were selected to use for clustering. These components were then clustered using K-means with K ranging from 1 to 11. The elbow method was then applied to the Within Cluster Sum of Squares from all clustering procedures, which resulted in K = 3 being selected.

Chapter 3 Generation and Evaluation of Synaptic Labelling Tools

Sleep is important for cognitive functions, but its function remains unclear. Aimed at explaining the cognitive benefits of sleep, Synaptic Homeostasis Hypothesis (SHY) proposes that the function of sleep is to drive global down scaling of synaptic strength (Tononi and Cirelli, 2003).

Given the limitations of previous studies addressing SHY, we asked whether there is a method to observe the same synapses of the same neurons through sleep and wake and circadian time without disrupting its functions. Following synapse dynamics of the same neurons would allow for comparison within neuron as an internal control and circumvents animal-to-animal and circadian differences.

Therefore, to tackle SHY systematically, we need reliable tools that 1) label excitatory and inhibitory synapses, and 2) allow long-term tracking of the same neurons in living animal. Only by tracking synapse dynamics in live animals can we answer critical questions about SHY. Firstly, do synapse strength and density change in temporal relationship with sleep and wake cycle? Secondly, do these changes occur globally or only in certain neurons? Thirdly, is this process occurring during periods that coincide with sleep or is sleep itself driving these synaptic changes?

In this Chapter, we utilized the FingR system, which unlike the more conventional overexpression techniques, labels endogenous excitatory and inhibitory synaptic proteins, PSD95 and Gephyrin, respectively. Firstly, we developed the FingR system to label synapses in zebrafish. Next, we enhanced the FingR system to allow for single cell labelling. This is important for distinguishing which synapses belong to which cell, as the traditional FingR tools label only synaptic puncta and the cell's nucleus. Therefore, we also modified the FingR system to allow for cell morphology visualization. Lastly, we tested the reliability of these constructs to label bona fide synapses using immunohistochemistry and confirmed that FingR labelled synapses show the expected dynamic changes in response to pharmacological agents.

3.1 NEW FINGR(PSD95) TRANSGENES FOR SIMULTANEOUS IMAGING OF SYNAPSES AND CELL MORPHOLOGY

Genetic constructs for expressing FingRs in zebrafish had previously been built and described (Son et al., 2016). The original constructs zcUAS:PSD95.FingR-GPF-ZFC(CCR5TC)-KRAB(A) consists of an artificial promotor (UAS) that can be activated by Gal4 driver lines and bound by specific zinc finger sequences (zc); and a FingR that binds to PSD95 fused to GFP, zinc finger DNA binding element (ZF(CCR5TC)) as well as a KRAB(A) domain capable of repressing transcription. Thus, once all available endogenous PSD95 molecules in the cell have been bound by FingR(PSD95)-GFP-ZF-KRAB(A) (hereafter abbreviated FingR(PSD95)), the remaining unbound FingR(PSD95) proteins will shuttle to the nucleus, bind to the zc domain in the promotor, and inhibit further transcription via repression of KRAB(A). Thus, neurons that express Gal4 and contain the UAS:FingR(PSD95)) constructs will have both the synapses and nuclei labelled green. Since the nuclei of neurons can be physically far removed from the synapse, it is difficult or impossible to accurately assign GFP-positive synapses to a single cell. This would not allow us to systematically track synapse dynamics of the same cell through time. Since we want to be able to unambiguously assign synapses to each expressing neuron, we needed a way to visualize both synapses and neuronal morphology.

To label both synapses and neuronal morphology, we wanted to co-express the FingR-GFP with a red fluorescent protein that labels cell membranes. In zebrafish, a classical way to do this is via a bidirectional UAS construct (Paquet *et al.*, 2009); however, given the need to regulate transcription with a zinc-finger binding domain in the promoter, bidirectional UAS cassettes are unsuitable for FingRs. To overcome this, I first generated FingR construct with a standalone UAS:myrCherry (Figure 3.1). However, transient expressions of FingR(PSD95)-GFP;UAS;myrCherry indicated competition between the two UAS elements where each UAS elements were expressed mosiacally and in non-overlapping patterns (Figure 3.1). Therefore, the construct was not used. Next, I introduced a self-cleaving peptide (P2A) between the FingR-fusion protein and a membrane-bound red fluorescent protein (mKate2f) (Kim *et al.*, 2011; Cai *et al.*, 2013) (Figure 3.2A). This construct is abbreviated as FingR(PSD95)-GFP-P2A-mKatef. The P2A elements are small viral elements that cleave post-translationally, allowing for the co-expression of two or more separate proteins from a single open reading frame

(ORF) (Kim *et al.*, 2011). Since only a single UAS promoter element is needed, the negative feedback loop of FingR system will not be interrupted. This also avoids UAS site competition for available Gal4 or KalTA4. This results in transcriptionally regulated FingR targeting PSD95 labelling synapses and nucleus in green with cell morphology visualization in far red (Figure 3.2B and 3.3).

However, we observed that transient expression of the modified FingR sometimes leads to overexpression of the cassette. This is highlighted by green signal diffused throughout the neurite and not in a punctate manner. We found that, due to FingR negative feedback mechanism, FingR works best when the whole of the FingR cassette is integrated into the genome. Transient injections of FingR (i.e. non-genome integration) likely disrupts the negative feedback system and yields variably expression and overexpression of FingRs. Therefore, to control the expression of KalTA4 and FingR and to allow quantification, stable transgenic line of FingR(PSD95)-GFP-P2A-mKate2f was made.

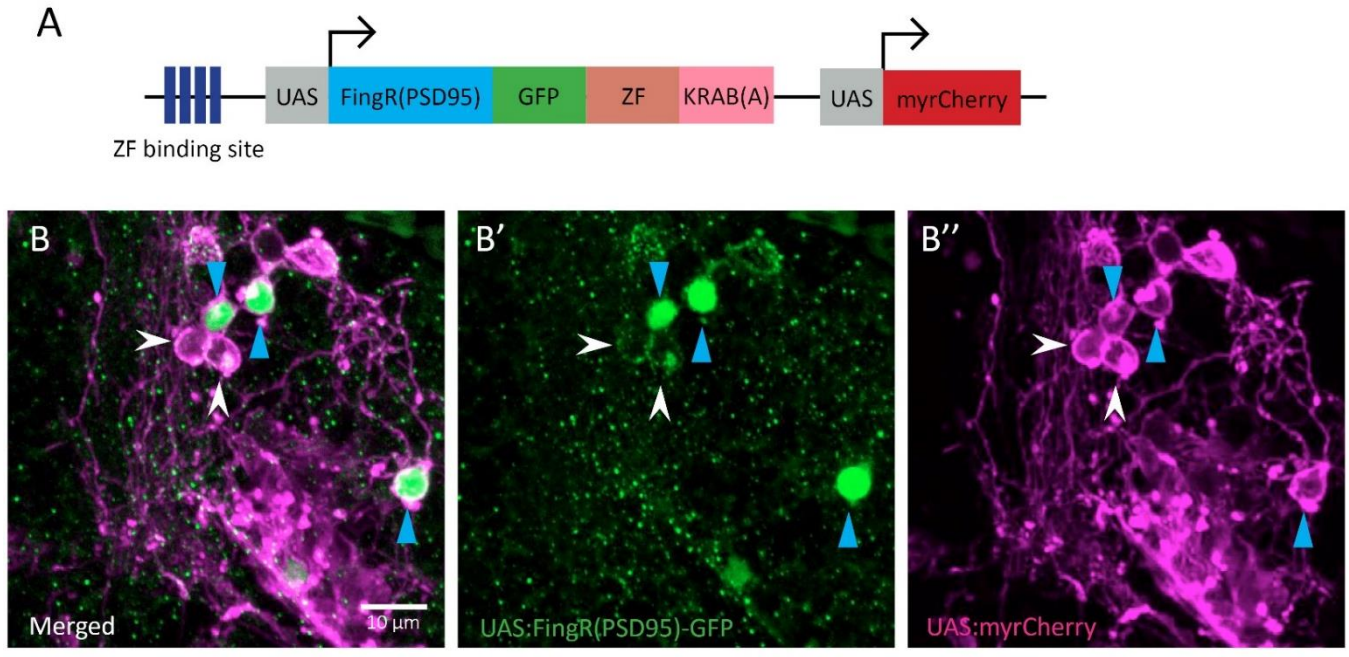

Figure 3.1: FingR(PSD95)-GFP;UAS;myrCherry construct. A) Schematic of construct with two UAS's. B) Competition of the two UAS elements on FingR(PSD95)-GFP;UAS;myrCherry. Some cells express only FingR (blue arrow) while some only myrCherry (filled white arrow), only a few express both. Transient expression of construct under the control of emx3:Gal4 at 6dpf

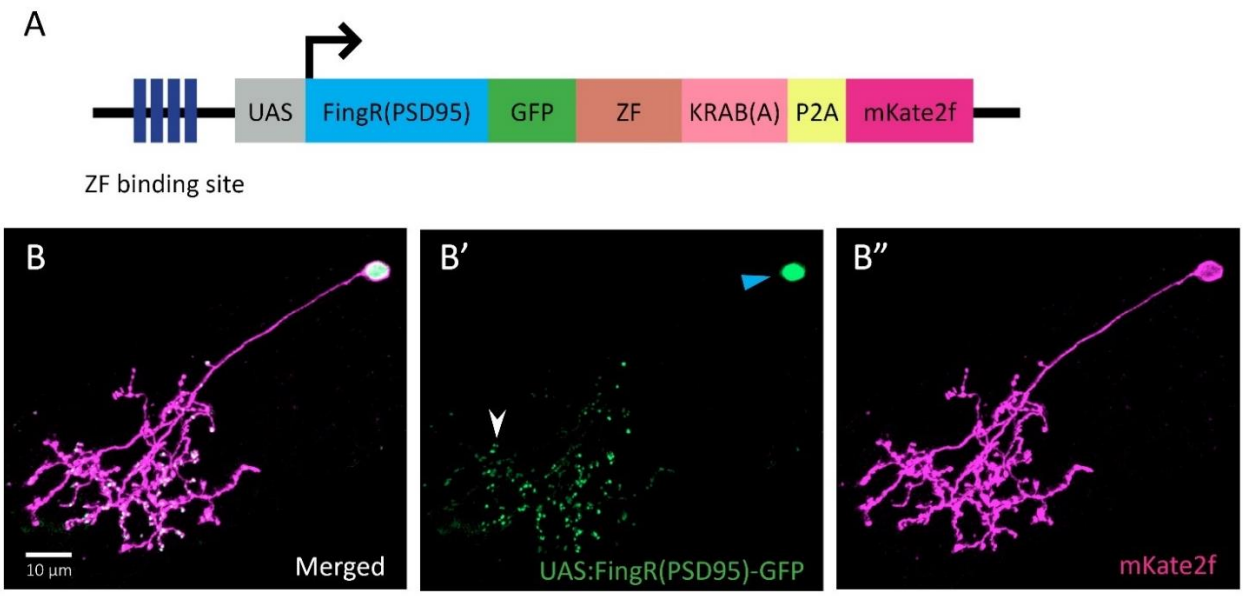

Figure 3.2: FingR(PSD95)-GFP-P2A-mKatef labels synapses and cell morphology. A) Schematic of construct allowing cell morphology visualization using P2A self-cleaving peptide and mKate2f fluorophore. B-B") Modified FingR(PSD95)-GFP labelling a single periventricular cell of zebrafish tectum at 8 days post fertilization (dpf). Expression of FingR(PSD95)-GFP under the control FoxP2:Gal4 labelling nucleus (green, blue arrow), synapses (green, white arrow indicating a single example), and cell morphology (magenta).

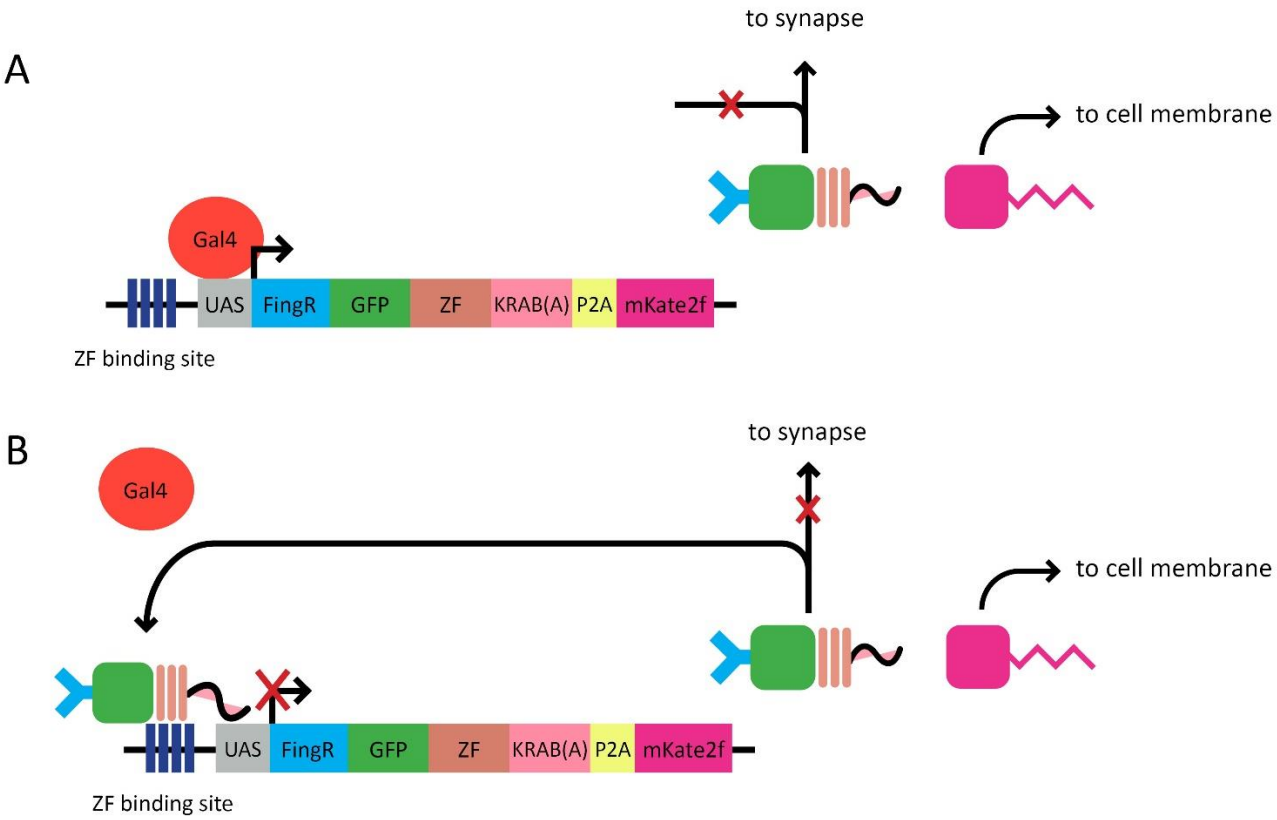

Figure 3.3: Schematic of modified FingR system that allows cell morphology visualization. A) When Gal4/KalTA4 is present, Gal4 (orange) binds to the UAS resulting in transcription and translation of our modified FingR cassette. Once translated, P2A (yellow) self-cleaved, releasing FingR protein and mKate2f. FingR binds to its endogenous synaptic target and is prevented from moving to the nucleus. mKate2f gets trafficked to cell-membrane; thereby labelling membrane morphology. B) When endogenous synaptic targets are all bound, then newly translated FingR no longer have free synaptic target to bind and, instead, moves to the nucleus due to the nuclear localization signal within the ZF. Once in the nucleus zinc finger domain (brown) binds to the ZF binding site (dark blue) 3' of the UAS. KRAB(A) domain (pink tail) prevents Gal4 to bind to the UAS and represses transcription. This light the nucleus in GFP. Thus, the level of FingR is matched to the level of the endogenous target protein.

3.2 FINGR GEPHYRIN CONSTRUCT WERE MODIFIED FOR CELL MORPHOLOGY VISUALIZATION

FingR that targets Gephyrin, (UAS:FingR.GPHN-GFP-ZFC(CCR5TC)-KRAB(A)), was also modified to fused with P2A-mKate2f. This construct is abbreviated as FingR(GPHN)-GFP-P2A-mKate2f. Transiently expressed, FingR(GPHN)-GFP-P2A-mKate2f exhibit GFP positive nucleus and puncta and far-red cell morphology (Figure 3.4). Similar to FingR that targets PSD95, our modified FingR(GPHN)-GFP-P2A-mKate2f produced uncontrolled expression when expression is not integrated within the genome (i.e. transient expression). To control the expression of FingR and to allow quantification, stable transgenic line of FingR(GPHN)-GFP-P2A-mKate2f is made.

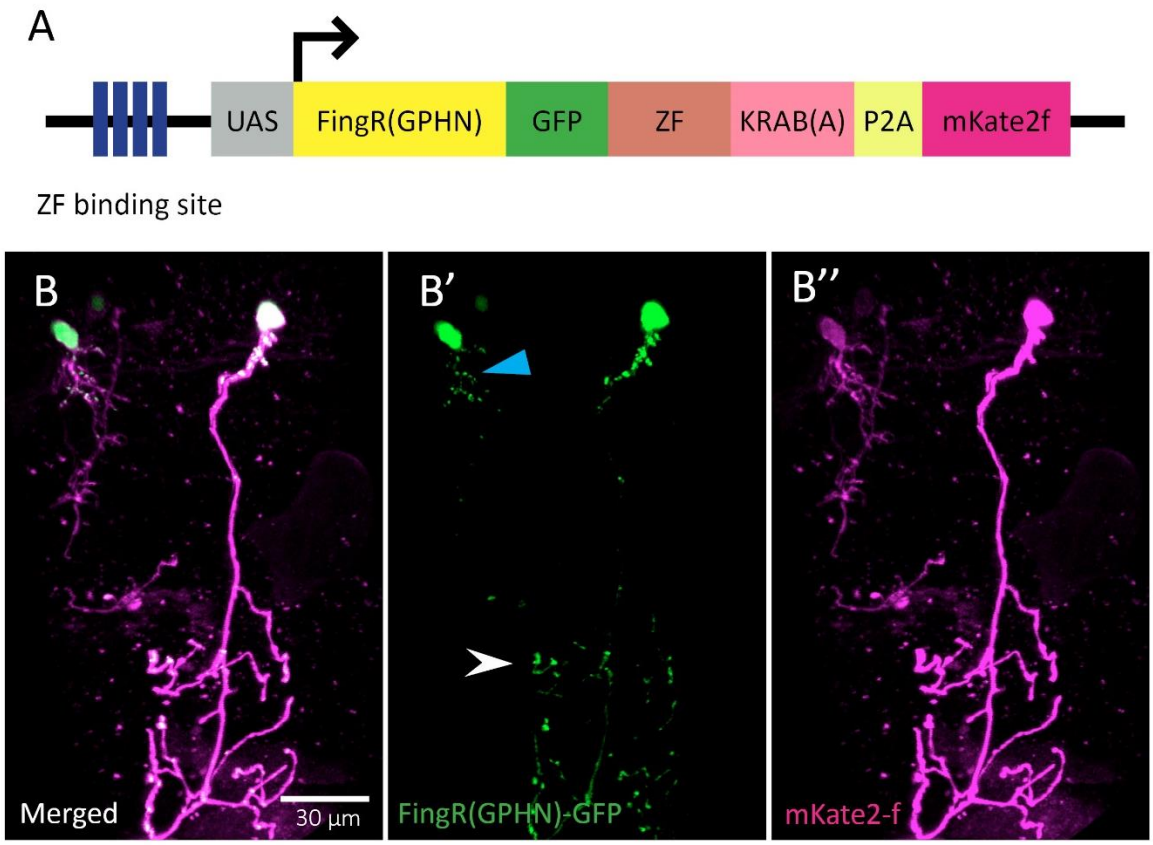

Figure 3.4:FingR(GPHN)-GFP-P2A-mKate2f labels inhibitory synapses and cell morphology. A) Schematic of construct allowing cell morphology visualization using P2A self-cleaving peptide and mKate2f fluorophore. B-B") Expression of modified FingR(GPHN)-GFP under the control of emx3:Gal4 in the spinal cord at 6dpf. Nuclei (green) and FingR.GPHN puncta on the cell (green, white arrow indicate an example of puncta). Example of FingR.GPHN puncta on another cell (blue arrow). Cell morphology (magenta).

3.3 FINGR PSD95 CONSTRUCT WERE MODIFIED FOR CALCIUM ACTIVITY RECORDING AT SYNAPSES

FingR can labels synapses with GFP, giving the ability to visualize the number and location of synapses within the cell. Despite showing synaptic properties such as strength, it does not convey any activity information about the cell or the synapses. We asked whether we can modify the FingR system in a way that allows for monitoring neural activity of the cell as a whole and of subcellular compartments. We introduced calcium indicator GCaMP7b into the construct in place of GFP. This modified FingR version, pBR-Tol2-UAS:FingR.PSD95-GCaMP7b-ZFC(CCR5TC)-KRAB(A)-P2A-mKate2-f (Figure 3.5), would potentially allow for calcium dynamics recording at the synapses and in the nucleus as well as the morphology of FingR-positive cells. jGCaMP7b was chosen for its brighter baseline fluorescence and high sensitivity, which allows better detection of small neuronal structures and facilitates detection of calcium activity in these structures (Dana *et al.*, 2019). This version of modified FingR could potentially give readout of activity-induced intracellular calcium changes at the synapses as well as the neuron neural activity output. As with the modified FingR with GFP versions, stable transgenic line FingR(PSD95)-GCaMP7b is made.

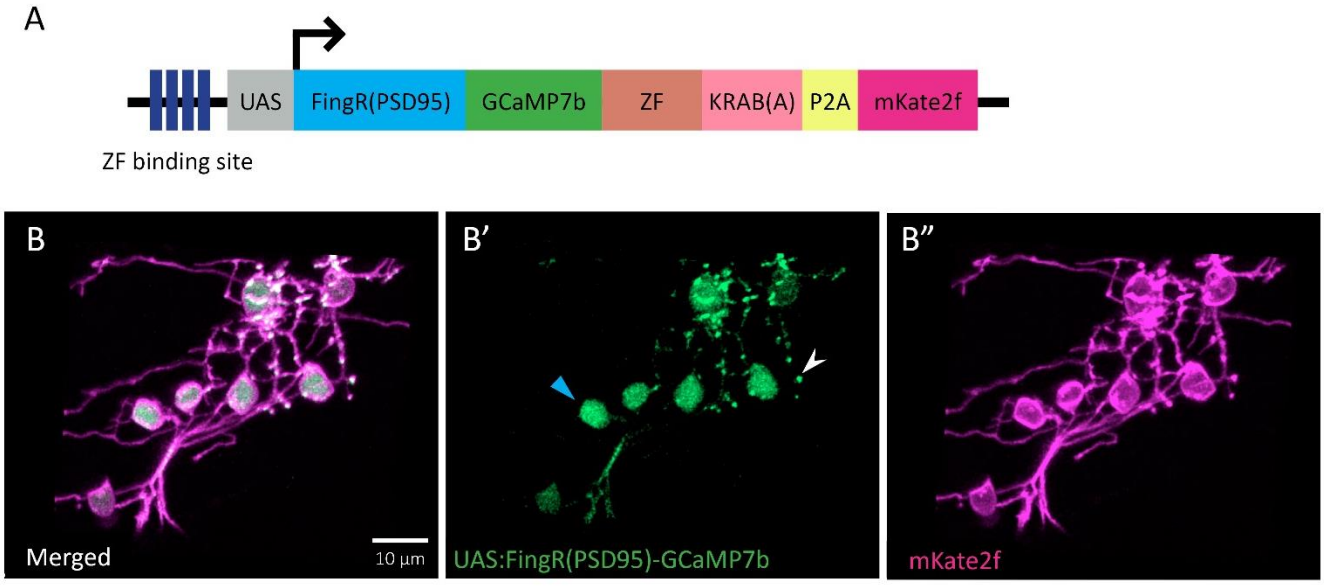

Figure 3.5:FingR(PSD95)-GCaMP7b-P2A-mKate2f labels excitatory synapses and nuclei with calcium indicator and cell morphology. A) Schematic of modified FingR construct swapping GFP to GCaMP7b with P2A self-cleavage peptide and mKate2f. B-B") Expression FingR(PSD95)-GCaMP7b under the control of mnx1:Gal4 labelling a group of motor neurons expressing in 3dpf larva. B') GCaMP7b can be seen in the neurons nuclei (green) and

excitatory synapses (green puncta). Blue arrow indicates an example of FingR+ nucleus. White arrow indicates a single GCaMP7b puncta. B") Cell morphology of FingR+ neurons in magenta.

3.4 FINGR(PSD95) COLOCALIZE WITH ANTI-MAGUK

Previous work in hippocampal cell culture and in vivo zebrafish had shown that FingR intrabodies that binds to PSD95 localizes to synapses with high fidelity (Son *et al.*, 2016; Cook *et al.*, 2019). Both found that FingR colocalizes with about 90% and 95% with anti-PSD95 antibody, respectively. Moreover, Cook et al found that the PSD95 antibody colocalizes approximately 80% of the time with FingR (2019); suggesting that FingR false negative rate is ~20% in hippocampal cell culture. Because of the transcription regulation feedback loop, FingR have been shown to report the abundance of endogenous synaptic proteins present in the cell (Gross *et al.*, 2013). However, Son et al. (2016) did not evaluate this relationship or the false negative rates in vivo. Furthermore, we also wanted to ascertain that the addition of P2A self-cleavage peptide and mKatef2 fluorophore in our modified system did not interfere with FingR labelling of synapses.

To verify that our modified FingR(PSD95)-GFP labels bona fide synapses in vivo, we performed immunohistochemistry labelling FingR(PSD95)-GFP and antibodies to synaptic proteins and quantified the co-localization and relationship between the two. Modified FingR(PSD95)-GFP were expressed in mnx1+ motorneurons by crossing Tg(FingR(PSD95)-GFP-P2A-mKate2f) to Tg(mnx1:GalTA4) obtained from (Böhm *et al.*, 2016). This population was selected as its synapses are sparse at 2dpf and the ease of doing whole-mount synaptic immunohistochemistry. After various unsuccessful immunohistochemistry protocols have been attempted, we found that anti-MAGUK antibody and acetone permeabilization improved signal-to-noise ratio for synapses labelling in whole-mount 2dpf zebrafish (See 2.4.2 Methods). MAGUK is family of scaffolding proteins which PSD95 is the most abundant (Zhu, Shang and Zhang, 2016). Cross-sectional grey values of each FingR puncta were collected and normalized (Figure 3.5B-C). We defined colocalization as the overlap of a peak in grey value of both channels. Peak in grey value was defined as being at least 50% higher than the baseline. This is confirmed by observation. For instance, Figure 3.5B-C shows puncta number 1-3 to be colocalized while puncta number 4 has no anti-MAGUK puncta. 540 FingR(PSD95)-GFP puncta were analysed in total from 5 larvae. We found that 90.19% FingR puncta

colocalized with anti-MAGUK puncta, while the colocalization of FingR puncta to a 90°-rotated anti-MAGUK image results in only 2.68% ($p<0.0001$, Chi-square corrected using Benjamini-Hochberg; Figure 3.5D). This suggests that the high degree of colocalization of FingR to MAGUK is unlikely due to chance. Moreover, this colocalized population were found to have inter-peak distance of approximately 0.1μm, which is in good agreement with electron microscope measurements of postsynaptic density sizes (Petersen *et al.*, 2003) (Figure 3.6E).

Although 90% of FingR(PSD95) puncta were co-localized with bona fide synapses as detected by anti-MAGUK antibodies, we also wanted to know if any MAGUK-positive puncta are not labelled with FingR(PSD95)-GFP. To examine the false negative rate, we measured the grey values of anti-MAGUK puncta (magenta) and observed whether they colocalize to FingR(PSD95) puncta. We used anti-MAGUK puncta that were on the cell membrane of the FingR-positive cell (cyan) only. This is to ensure that anti-MAGUK puncta observed are on FingR-positive mnx1 neurons. 100% anti-MAGUK puncta identified were colocalized with FingR(PSD95)-GFP puncta; indicating 0% false negative labelling, while the colocalization of anti-MAGUK puncta to a 90°-rotated FingR image results in only 6.06% ($p<0.0001$, Chi-square corrected using Benjamini-Hochberg; Figure 3.6A). This suggests that the high degree of colocalization of anti-MAGUK to FingR is unlikely due to chance. The inter-peak distance of colocalized puncta in the overlaid images are also within synaptic distance (Figure 3.6).

It has been observed that FingRs expression levels can match that of the endogenous targets (Gross *et al.*, 2013), suggesting readout of synaptic strength. We asked whether this relationship can be detected in vivo. To do this, we examined at the relationship between FingR(PSD95)-GFP and anti-MAGUK staining intensities and puncta size using whole-mount zebrafish immunohistochemistry. The GFP delta intensity against anti-MAGUK puncta delta intensity of observed colocalized puncta is a positive linear slope ($r = 0.364$, $r^2=0.1322$, $P>|t|=0.000$). Despite the low coefficient of determination, a significant p value for t-statistics suggests there is relationship between delta intensity of FingR(PSD95)-GFP and anti-MAGUK, albeit not a strong one.

To understand the size relationship between FingR(PSD95)-GFP and anti-MAGUK puncta, the full-width half maximum (FWHM) of the normalized grey value curve for each puncta was

used as a proxy for the diameter of each puncta. The relationship of the FWHM between the FingR(PSD95)-GFP and anti-MAGUK channels suggests there is a significant but a very weak positive correlation ($r=0.208$, $r^2=0.043$, $P>|t|=0.000$). On the other hand, non-colocalized puncta do not seem to have specific delta intensity and FWHM for FingR(PSD95). This suggests that we cannot predict false positive FingR labelling by specific intensity or size of puncta.

The correlations between FingR(PSD95) and anti-MAGUK were positive for intensity and puncta size but were not reliably strong. This weak relationship was more evident in puncta size than intensity; suggesting that as a tool FingR(PSD95)-GFP puncta size and intensity cannot reliably predict the amount of MAGUK during live imaging of FingR dynamics during sleep and wake. On the other hand, the FingR(PSD95)-GFP construct will label all MAGUK positive synapses, and over 90% of detected GFP puncta will be associated unambiguously with a MAGUK positive synapse. This should allow for reliable counting and tracking of synapse formation/elimination dynamics.

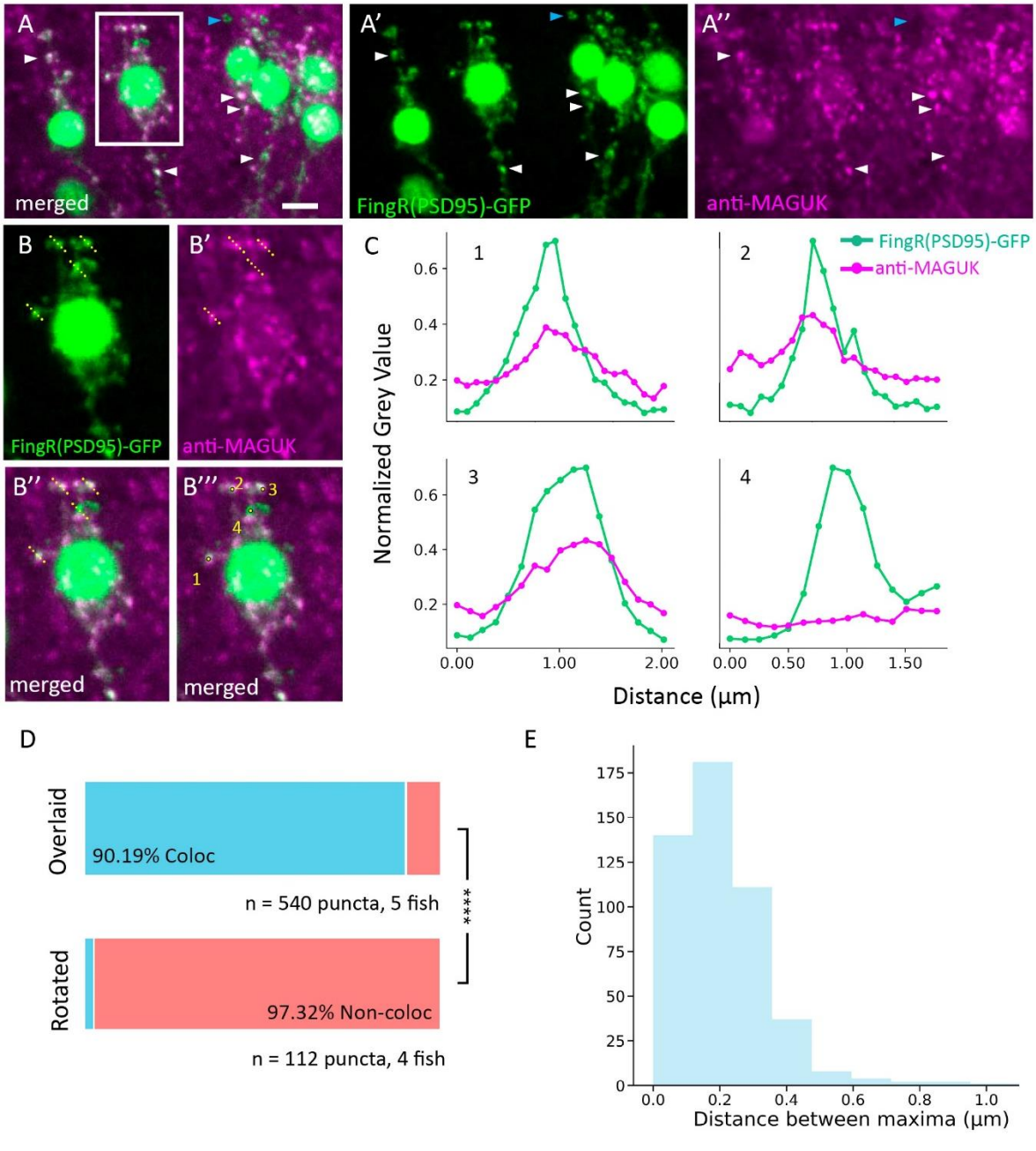
A
merged
A'
FingR(PSD95)-GFP
A''
anti-MAGUK
B
FingR(PSD95)-GFP
B'
anti-MAGUK
B''
merged
B'''
merged
C
Normalized Grey Value
FingR(PSD95)-GFP
anti-MAGUK
Distance (µm)
D
Overlaid
90.19% Coloc
n = 540 puncta, 5 fish
****
Rotated
97.32% Non-coloc
n = 112 puncta, 4 fish
E
Count
Distance between maxima (µm)
F
Colocalized: R²= 0.132, p<0.0001
Non colocalized: R²=0.000, ns
anti-MAGUK intensity
FingR(PSD95)-GFP intensity
G
Colocalized: R²= 0.043, p<0.0001
Non colocalized: R²=0.001, ns
anti-MAGUK FWHM (µm)
FingR(PSD95)-GFP FWHM (µm)

Figure 3.6 FingR(PSD95)-GFP puncta labels anti-MAGUK puncta in vivo. A) Maximum projection (~10 µm) of immunohistochemistry of anti-MAGUK and endogenous fluorescence of FingR(PSD95)-GFP on 2dpf larvae at the spinal cord. FingR+ puncta labelled by anti-MAGUK+ puncta (white arrowheads), FingR+ not labelled by anti-MAGUK- puncta (blue arrowhead). B-B''') Zoomed in area within the white box from A, depicting how sectional grey value were obtained. B) FingR(PSD95)-GFP channel showing part of a neuron with its nucleus and puncta (green). B') Anti-MAGUK puncta of the same neuron in B. B") Merged of the two channels B and B' with cross-section of grey values taken of puncta (yellow line). B''') Example of puncta that grey values have been measured numbering 1-4. C) Normalized grey value example of anti-MAGUK on FingR(PSD95)-GFP puncta number 1-4 form B. Puncta number 1-3 FingR signals colocalized with anti-MAGUK signals. Puncta number 4 showing false positive FingR labelling. D) Percentage FingR+ labelled by anti-MAGUK+ puncta. Colocalized puncta (blue) show FingR+ labelled by anti-MAGUK+ puncta. Non Colocalized puncta (red) show FingR+ not labelled by anti-MAGUK+ puncta. 'Rotated' indicates that the anti-MAGUK image was rotated by 90°. ****p < 0.0001 Chi-square with multiple comparison corrected using Benjamini-Hochberg. E) Distance between the peaks of normalized grey value between FingR(PSD95)-GFP and anti-MAGUK. F-G) Relationship between FingR(PSD95)-GFP and anti-MAGUK puncta in puncta intensity and puncta size, respectively. F) There is a weak linear relationship between intensity of FingR(PSD95)-GFP and anti-MAGUK puncta detected in vivo. G) The Full Width Half Max (FWHM) of normalized grey value curve were used as proxy for puncta size. There is an even weaker linear correlation between FingR(PSD95)-GFP and anti-MAGUK puncta size. Blue and red line depicted linear regression curve for colocalized and non-colocalized population, respectively. Ribbon represent ± standard deviation. Scale bar 5 µm. n= 540 puncta, 5 fish.

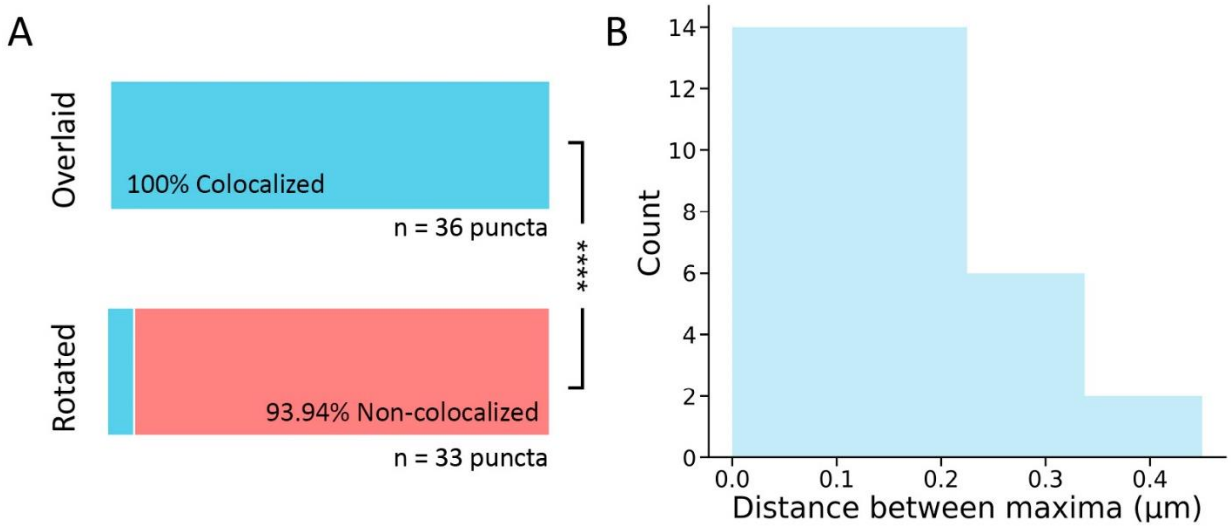

Figure 3.7: Anti-MAGUK puncta labelled by FingR(PSD95)-GFP in motorneurons of 2dpf larvae. A) Percentage anti-MAGUK+ labelled by FingR+ puncta. Colocalized puncta (blue) show anti-MAGUK+ labelled by FingR+ puncta. Non Colocalized puncta (red) show anti-MAGUK+ not labelled by FingR+ puncta. 'Rotated' indicates that the FingR image was rotated by 90°. ****p < 0.0001 Chi-square with multiple comparison corrected using Benjamini-Hochberg Percentage colocalization of synapses identified by anti-MAGUK that is also FingR(PSD95)-GFP positive. 100% were colocalized B) Inter-peak distance grey value of two channels of colocalized puncta (overlaid).

3.5 FINGR(GPHN) COLOCALIZE WITH ANTI-GPHN

Previous works have found that 90% FingR(GPHN) intrabodies colocalized with anti-$GABA_AR$ in hippocampal neuron cultures (Cook *et al.*, 2019). Conversely, anti-$GABA_AR$ antibody labelled ~75% of the time with FingR(GPHN) intrabodies; suggesting that FingR(GPHN) intrabodies false negative rate is ~25% in hippocampal cell culture. Son et al. (2016) also found that FingR(GPHN)-mCherry colocalized with anti-GPHN in zebrafish primary cell culture albeit without any quantification. There have yet been reports on how reliable FingR(GPHN) label inhibitory synapses in living zebrafish. Therefore, we sought to examine whether our modified FingR(GPHN)-GFP can reliably labels inhibitory synapses in vivo in zebrafish.

To achieve this, we performed double immunohistochemistry labelling FingR(GPHN)-GFP and antibodies against GPHN proteins and quantified the co-localization and relationship between the two. Similar to FingR(PSD95) colocalized experiments discussed above, we chose to investigate this in motor neurons of zebrafish larvae at 2dpf. Modified FingR(GPHN)-GFP were expressed in mnx1+ motorneurons by crossing Tg(FingR(GPHN)-GFP-P2A-mKate2f) to Tg(mnx1:GalTA4). Whole-mount immunohistochemistry were performed on these larvae and it was found that trypsin permeabilization improved signal-to-noise ratio for anti-GPHN labelling (see 2.4.2 Methods).

Cross-sectional grey values of each puncta from FingR(GPHN)-GFP and anti-GPHN channels were extracted and normalized to their respective channels (Figure 3.8A-C). 450 FingR(GPHN)-GFP puncta from 4 larvae showed that 90.44% were colocalized with anti-GPHN puncta, while the colocalization of FingR puncta to a 90°-rotated anti-GPHN image results in only 4.71% ($p<0.0001$, Chi-square corrected using Benjamini-Hochberg; Figure 3.8D). This suggests that the high degree of colocalization of FingR to GPHN is unlikely due to chance. Moreover, this colocalized population were found to have inter-peak distance within synaptic distance (Figure 3.8E) (Rizzoli and Betz, 2005). The reverse colocalization, anti-GPHN puncta labelled by FingR(GPHN)-GFP, could not be performed on this dataset due to the high density of anti-GPHN puncta from nearby mnx1-negative neurons present in the spinal cord of the larvae. Therefore, we cannot determine the false negative rate of FingR(GPHN)-GFP.

It has been observed intrabodies labelling GPHN expressed in rat hippocampus shows correlation between FingR intensity and abundant endogenous GPHN proteins (personal communications, Burrone lab). We asked whether this relationship can be detected in vivo of zebrafish larvae. To do this, we examined at the relationship between FingR(GPHN)-GFP and anti-GPHN staining intensities and puncta size using whole-mount zebrafish immunohistochemistry. The delta intensity of FingR(GPHN)-GFP and anti-GPHN puncta within the colocalized population shows no correlation (r^2=0.00, P>|t|=0.64). The FWHM between the two channels has a weak positive correlation of (r=0.229, r^2=0.052, P>|t|=0.000). Furthermore, non-colocalized puncta do not seem to have specific delta intensity and FWHM for FingR(GPHN). This suggests that we cannot predict false positive FingR labelling by specific intensity or size of puncta.

It must be noted that whole-mount zebrafish synaptic antibody labelling are difficult to perform. Despite being the gold-standard way to verify genetic labelling tools, the high background noises from synaptic antibody labelling could render it not reliable. For example, we often observed anti-GPHN in undistinguishable clusters while FingR(GPHN)-GFP clearly shows separate puncta within one large anti-GPHN blot (Figure 3.9). Therefore, quantifications obtained these images must be taken with some reservations.

Nonetheless, it can be seen that neither puncta intensity nor size of FingR(GPHN)-GFP can reliably extrapolate amount of GPHN as a tool during synaptic investigation during sleep and wake in vivo. On the other hand, over 90% of detected FingR(GPHN)-GFP puncta will be associated unambiguously with inhibitory synapse. This should allow for reliable counting and tracking of synapse formation/elimination dynamics during sleep/wake.

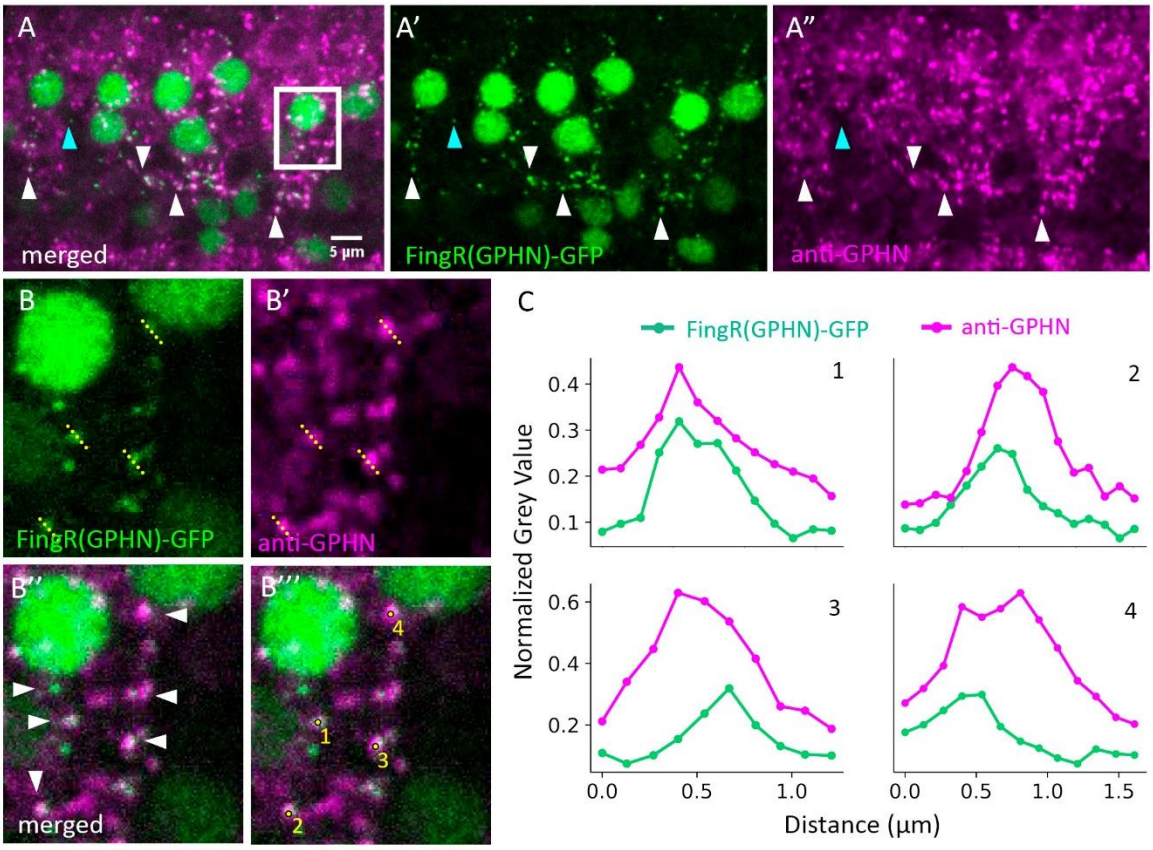
A
A'
A"
merged
5 µm
FingR(GPHN)-GFP
anti-GPHN
B
B'
B''
B'''
FingR(GPHN)-GFP
anti-GPHN
merged
1
2
3
4
C
FingR(GPHN)-GFP
anti-GPHN
Normalized Grey Value
Distance (µm)
1
2
3
4

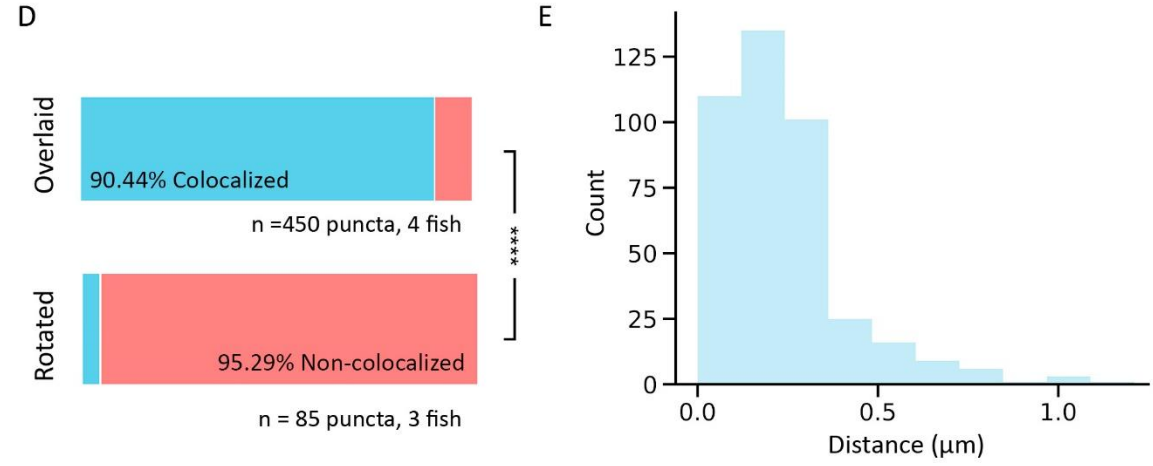
D
Overlaid
90.44% Colocalized
n =450 puncta, 4 fish
Rotated
95.29% Non-colocalized
n = 85 puncta, 3 fish
****
E
Count
Distance (µm)

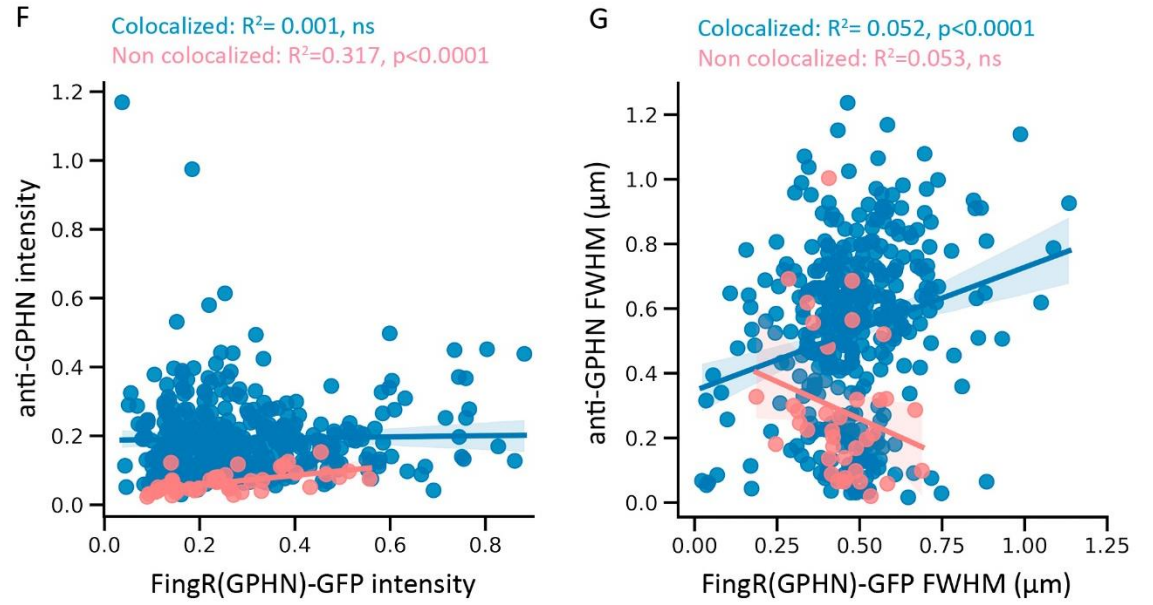
F
Colocalized: R²= 0.001, ns
Non colocalized: R²=0.317, p<0.0001
anti-GPHN intensity
FingR(GPHN)-GFP intensity
G
Colocalized: R²= 0.052, p<0.0001
Non colocalized: R²=0.053, ns
anti-GPHN FWHM (µm)
FingR(GPHN)-GFP FWHM (µm)

Figure 3.8: FingR(GPHN)-GFP puncta labels anti-GPHN puncta in vivo. A) Maximum projection (~10 µm) of immunohistochemistry of anti-GPHN and endogenous fluorescence of FingR(GPHN)-GFP on 2dpf larvae at the spinal cord. FingR+ puncta labelled by anti-GPHN+ puncta (white arrowhead), FingR+ not labelled by anti-GPHN puncta (blue arrowhead). B-B''') Zoomed in area within the white box from A, depicting how sectional grey value were obtained. B) FingR(GPHN)-GFP channel showing part of neurons with their nuclei and puncta (green). B') Anti-GPHN puncta of the same neuron in B. B") Merged of the two channels B and B' with cross-section of grey values taken of puncta (yellow line). B''') Example of puncta that grey values have been measured numbering 1-4. C) Normalized grey value example of anti-GPHN on FingR(GPHN)-GFP puncta number 1-4 from B, all colocalized. D) Percentage FingR+ labelled by anti-GPHN+ puncta. Colocalized puncta (blue) show FingR+ labelled by anti-GPHN+ puncta. Non Colocalized puncta (red) show FingR+ not labelled by anti-GPHN+ puncta. 'Rotated' indicates that the anti-GPHN image was rotated by 90°. ****$p < 0.0001$ Chi-square with multiple comparison corrected using Benjamini-Hochberg. E) Distance between the peaks of normalized grey value between FingR(GPHN)-GFP and anti-GPHN. F-G) Relationship between FingR(GPHN)-GFP and anti-GPHN puncta in puncta intensity and puncta size, respectively. F) No relationship between intensity of FingR(GPHN)-GFP and anti-GPHN puncta were detected in vivo. G) The Full Width Half Max (FWHM) of normalized grey value curve were used as proxy for puncta size. There was a very weaker linear correlation between FingR(GPHN)-GFP and anti-GPHN puncta size. Blue and red line depicted linear regression curve for colocalized and non-colocalized population, respectively. Ribbon represent ± standard deviation. n= 450 puncta, 4 fish.

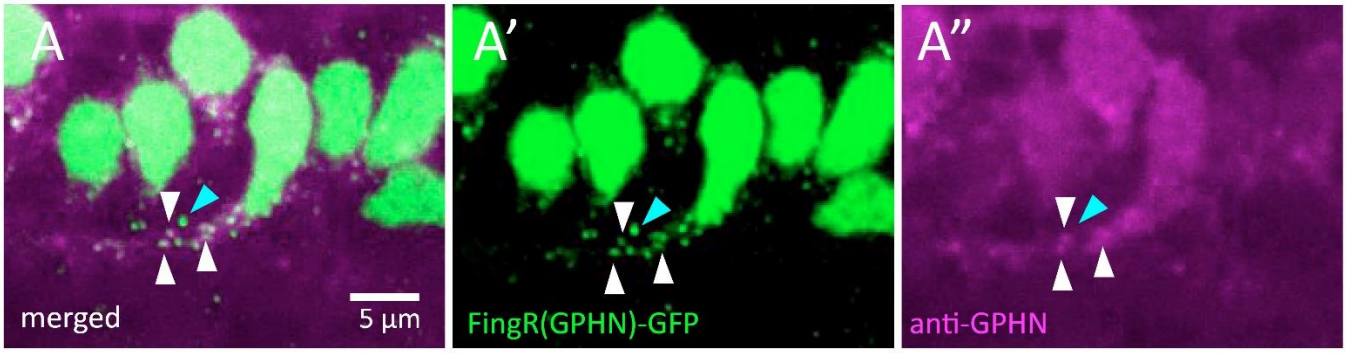

Figure 3.9: Example of undistinguishable anti-GPHN puncta. A) Whole-mount immunohistorchemistry of motorneurons in 2dpf of endogenous FingR(GPHN)-GFP and anti-GPHN. A') Endogenous FingR signals showing clearly distinguishable puncta (white arrowheads). A") anti-GPHN. channel showing GPHN puncta cluster that could not be distinguished from each other (white arrowheads). FingR(GPHN)-GFP puncta without anti-GPHN puncta (blue arrowhead).

3.6 FINGR(PSD95)-GCAMP7B LABELLED ANTI-MAGUK IN VIVO IN ZEBRAFISH

We have verified that our modified FingR constructs with GFP labelled bona fide synapses. Next, we asked whether the replacement of GFP with GCaMP7b still labels endogenous targets in vivo in zebrafish. To achieve this, we performed immunohistochemistry labelling FingR(PSD95)-GCaMP7b and ant-MAGUK and quantified the co-localization and relationship between the two. From 167 puncta of 8 different larvae, we found that 97.01% of FingR(PSD95)-GCaMP7b were labelled by anti-MAGUK puncta in mnx1 motorneurons, while the colocalization of FingR puncta to a 90°-rotated anti-MAGUK image results in only 6.25% ($p<0.0001$, Chi-square corrected using Benjamini-Hochberg; Figure 3.10). This suggests that the high degree of colocalization of FingR to MAGUK is unlikely due to chance. Moreover, this colocalized population were found to have average inter-peak distance of 0.1μm which is in agreement with electron microscope measurements of PSDs (Petersen *et al.*, 2003) (Figure 3.10E). The percentage of synapses identified by anti-MAGUK staining that was also positive for FingR(PSD95)-GCaMP7b was 96.83% (Figure 3.11A). In contrast, this colocalization dropped to 3.70% when FingR(PSD95)-GCaMP7b image were rotated 90°, suggesting that the high percentage of localization is unlikely due to chance ($p<0.0001$, Chi-square corrected using Benjamini-Hochberg; Figure 3.11).

These findings suggested that our modification to the FingR system to report calcium dynamics can label bona fide excitatory synapses. Next, we asked whether these modifications affect FingRs ability to infer synaptic protein abundance. To do this, we examined at the relationship between FingR(PSD95)-GCaMP7b and anti-MAGUK staining intensities and puncta size using whole-mount zebrafish immunohistochemistry. As GCaMP7b fluorescence level increases in the presence of calcium influx (Dana *et al.*, 2019), looking at FingR(PSD95)-GCaMP7b intensity, we assumed that the neurons were not receiving input that could cause calcium influx within the PSD during scarification. We anesthetized our larvae using tricaine mesylate (MS-222), which is a voltage-gated sodium channels blocker, prior to fixation and immunohistochemistry. This, therefore, should resulted in blockade of excitatory input into our neuron of interest and allowing us to examine the baseline fluorescence of GCaMP7b at the synapse.

The delta intensity of puncta from FingR(PSD95)-GCaMP7b and anti-MAGUK channels revealed that FingR(PSD95)-GCaMP7b has a weak positive linear relationship with anti-MAGUK puncta delta intensity (r=0.535, r^2=0.287, P>|t|= 0.000). Despite the low coefficient of determination, a significant p value for t-statistics suggests there is relationship between delta intensity of FingR(PSD95)-GCaMP7b and anti-MAGUK. Using FWHM as a readout for puncta size, the relationship of FWHM between GCaMP7b and anti-MAGUK puncta showed a weak positive correlation (r=0.206, r^2= 0.0423, P>|t| = 0.00932). Like FingR(PSD95)-GFP, the very weak relationship suggested that puncta size of FingR(PSD95)-GCaMP7b cannot reliably predict amount of MAGUK during live imaging. Moreover, non-colocalized puncta do not seem to have specific delta intensity and FWHM for FingR(PSD95). This suggests that we cannot predict false positive FingR labelling by specific intensity or size of puncta.

The correlations between FingR(PSD95)-GCaMP7b and anti-MAGUK were positive for intensity and puncta size but were very weak. Similar to FingR(PSD95)-GFP, these weak relationships was more evident in puncta size than intensity; suggesting that as a tool FingR(PSD95)-GCaMP7b puncta size and intensity cannot reliably predict the amount of MAGUK during live imaging of FingR dynamics during sleep and wake. On the other hand, the FingR(PSD95)-GCaMP7b construct will label all MAGUK positive synapses, and over 90% of detected GCaMP7b puncta will be associated unambiguously with a MAGUK positive synapse (Figure 3.11). This should allow for reliable counting and tracking of synapse formation/elimination dynamics.

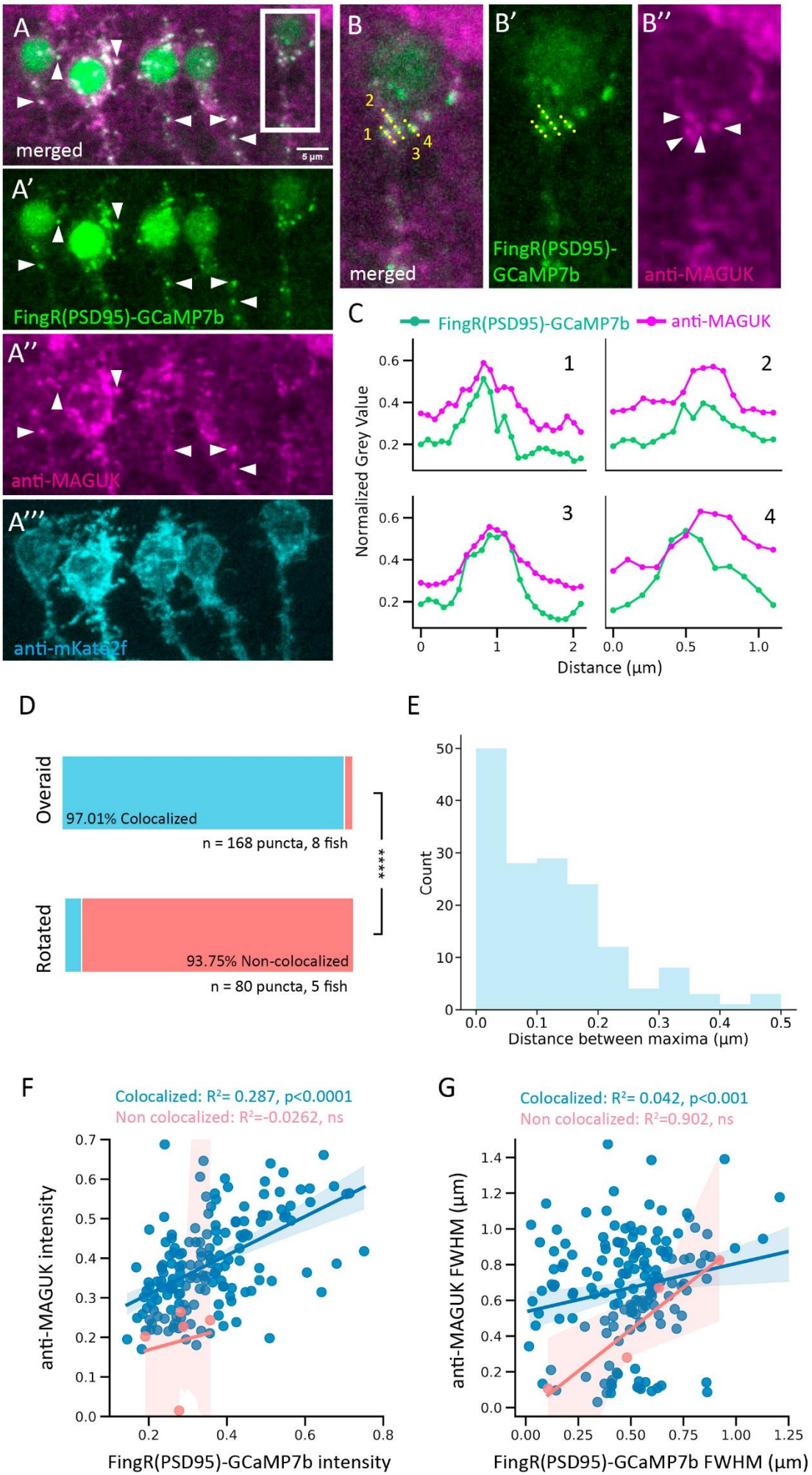
A
merged
5 µm
A'
FingR(PSD95)-GCaMP7b
A''
anti-MAGUK
A'''
anti-mKate2f
B
merged
2
1
4
3
B'
FingR(PSD95)-GCaMP7b
B''
anti-MAGUK
C
FingR(PSD95)-GCaMP7b
anti-MAGUK
Normalized Grey Value
Distance (µm)
D
Overaid
97.01% Colocalized
n = 168 puncta, 8 fish
****
Rotated
93.75% Non-colocalized
n = 80 puncta, 5 fish
E
Count
Distance between maxima (µm)
F
Colocalized: R²= 0.287, p<0.0001
Non colocalized: R²=-0.0262, ns
anti-MAGUK intensity
FingR(PSD95)-GCaMP7b intensity
G
Colocalized: R²= 0.042, p<0.001
Non colocalized: R²=0.902, ns
anti-MAGUK FWHM (µm)
FingR(PSD95)-GCaMP7b FWHM (µm)

Figure 3.10: FingR(PSD95)-GCaMP7b colocalized with anti-MAGUK puncta in vivo. A-A''') Maximum projection (~10 µm) of immunohistochemistry of anti-MAGUK and endogenous fluorescence of FingR(PSD95)-GCaMP7b on mnx1 motorneurons of 2dpf larvae. FingR+ puncta labelled by anti-MAGUK+ puncta (white arrowheads). B-B''') Zoomed in area within the white box from A, depicting how sectional grey value were obtained. B) Examples of puncta that grey values have been measured numbering 1-4, using cross-section drawn over each punctum (yellow line). B') FingR(PSD95)-GCaMP7b channel showing part of a neuron with its nucleus and puncta (green). B") Anti-MAGUK puncta of the same neuron in B. C) Normalized grey value example of anti-MAGUK on FingR(PSD95)-GCaMP7 puncta number 1-4 from B. All were colocalized. D) Percentage FingR+ labelled by anti-MAGUK+ puncta. Colocalized puncta (blue) show FingR+ labelled by anti-MAGUK+ puncta. Non Colocalized puncta (red) show FingR+ not labelled by anti-MAGUK+ puncta. 'Rotated' indicates that the anti-MAGUK image was rotated by 90°. ****p < 0.0001 Chi-square with multiple comparison corrected using Benjamini-Hochberg. E) Distance between the peaks of normalized grey value between FingR(PSD95)-GCaMP7b and anti-MAGUK. F-G) Relationship between FingR(PSD95)-GCaMP7b and anti-MAGUK puncta in puncta intensity and puncta size, respectively. F) There is a weak linear relationship between intensity of FingR(PSD95)- GCaMP7b and anti-MAGUK puncta detected in vivo. G) The Full Width Half Max (FWHM) of normalized grey value curve were used as proxy for puncta size. There is an even weaker linear correlation between FingR(PSD95)-GFP and anti-MAGUK puncta size. Blue and red line depicted linear regression curve for colocalized and non-colocalized population, respectively. Ribbon represent ± standard deviation. n=168 puncta, 8 fish.

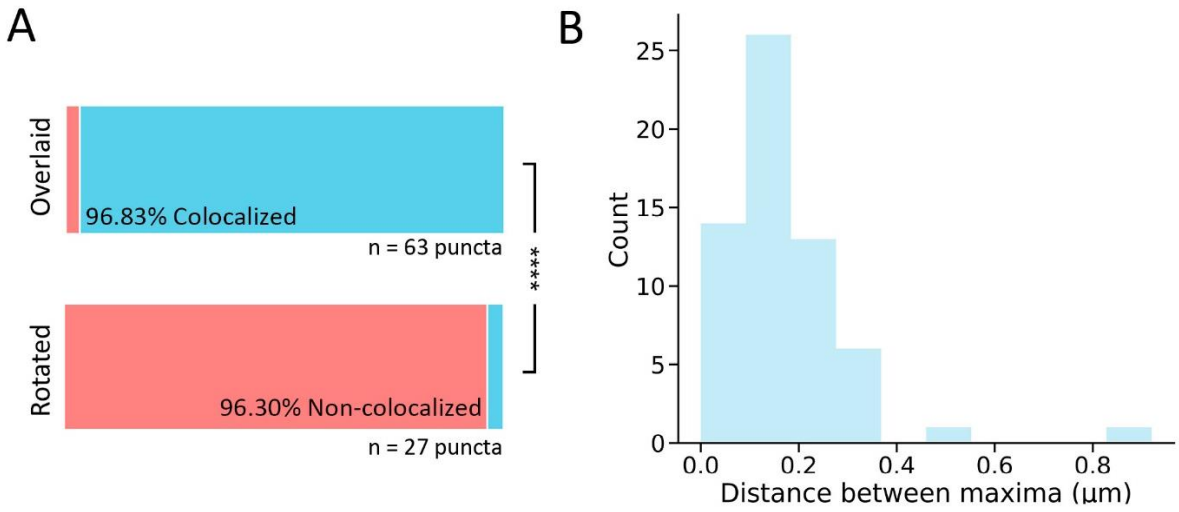

Figure 3.11: Colocalization of FingR.PSD95-GCaMP7b on anti-MAGUK puncta. A) Percentage anti-MAGUK+ labelled by FingR+ puncta. Colocalized puncta (blue) show anti-MAGUK+ labelled by FingR+ puncta. Non Colocalized puncta (red) show anti-MAGUK+ not labelled by FingR+ puncta. 'Rotated' indicates that he FingR image was rotated by 90°. ****p < 0.0001 Chi-square with multiple comparison corrected using Benjamini-Hochberg B) Distance between maxima grey value of FingR.PSD95-GCaMP7b and anti-MAGUK channels in colocalized population in overlaid images.

3.7 FINGR(PSD95)-GFP IS RESPONSIVE TO DRUGS AT 7DPF

Although we found FingR(PSD95)-GFP puncta accurately labelled synapses, we wanted to test whether changes in synapse formation or elimination could be reliably detected with this tool over timescales that are appropriate for sleep/wake dynamics. We took advantage of the ease by which zebrafish larvae can be pharmacologically manipulated (Rihel *et al.*, 2010).

Previous work in rats had found that a low dose of the nonselective NMDAR antagonist, ketamine, increased levels of PSD95 and spine number in prefrontal cortex of rats after 2 hours of treatment. This increase is sustained up to at least 72hours post-treatment (Li *et al.*, 2010). To test whether FingR(PSD95)-GFP can detect a similar NMDA antagonist response in zebrafish, 30μM of MK801, a non-competitive NMDAR antagonist, was given to 7dpf larvae for 2 hours. Larvae were imaged before blinded MK801 or DMSO treatment, imaged again 1-hour post-drug wash out, and imaged once more approximately 20 hours after drug treatment (Figure 3.12A). We looked at neurons in the zebrafish optic tectum which is mammal's equivalent of superior colliculi. We found that the absolute number of FingR(PSD95)-GFP was not different from DMSO- and MK801-treated fish (Figure 3.12B). We then looked at individual neuron synapse dynamics. The rate of change (RoC) shows changes in number of puncta of individual neuron from their own previous time point. The average RoC shows a significant increase at 1-day post drug treatment compare to DMSO-treated controls fish (p-value=0.015, mixed-design ANOVA with post-hoc pairwise t-test). Interestingly, the RoC is not significant at 1-hour post drug treatment. This is in concordant with Li et al. (2010) where they observed that ketamine, NMDA antagonist, administration increased levels of PSD95, GluR1, and synapsin I from 2 hour and remained elevated until 72 hours in rats. Moreover, ketamine administration increased spine density 24 hours post drug injection in layer V medial prefrontal cortex pyramidal neurons. This finding suggested that synapses of zebrafish tectal neurons responded to NMDAR antagonist similar to what was observed in the rat's prefrontal cortex. Importantly, this showed that our modified FingR system can detect changes in synapse number.

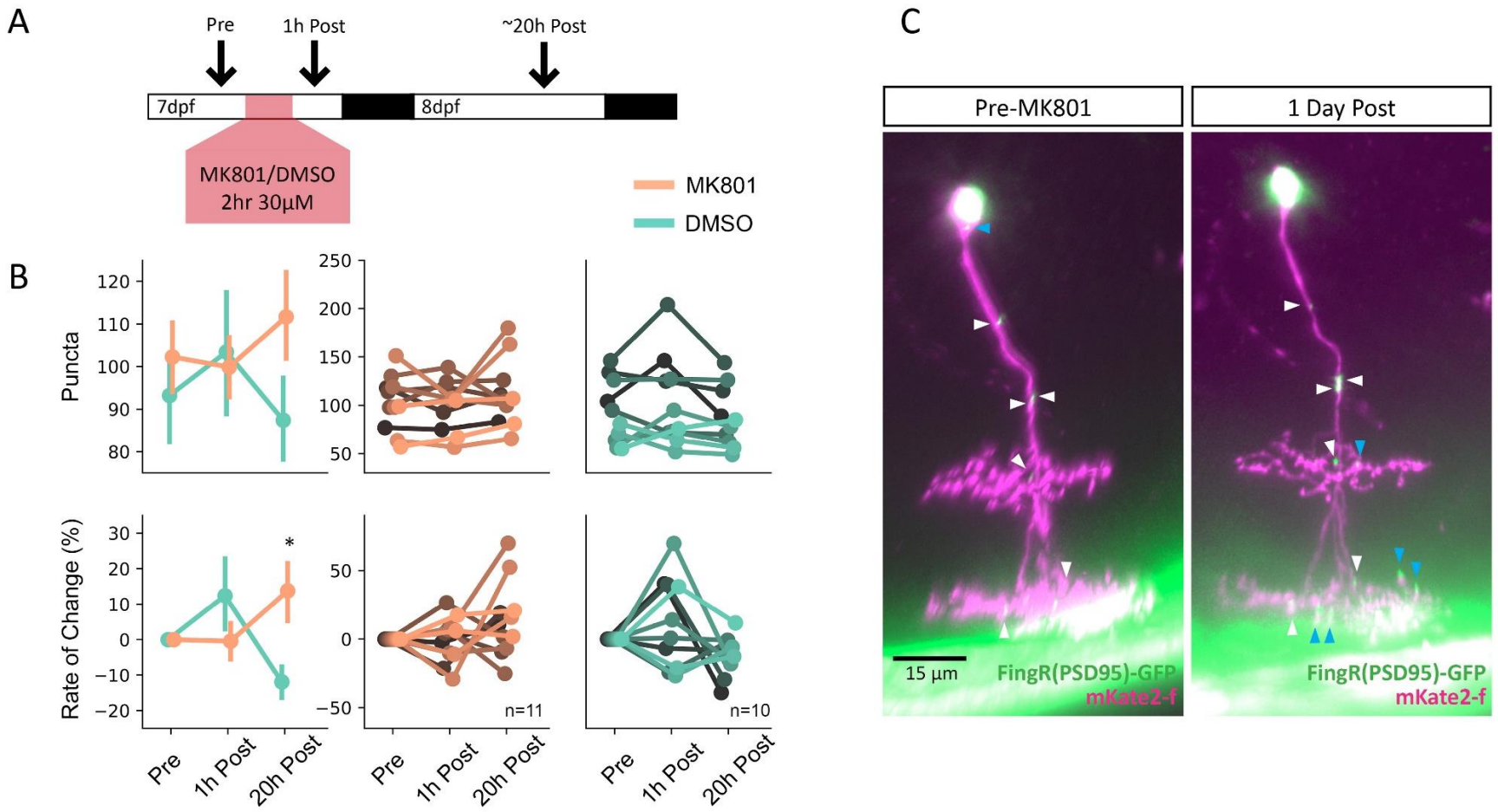

Figure 3.12:FingR(PSD95)-GFP is responsive to MK801 at 7dpf. A) Schematic of the drug exposure and image paradigm. Arrow heads show imaging times. B) Synapse dynamics in response of MK801 administration. Top row shows net FingR(PSD95)-GFP puncta present for during pre, post, and 20 hours post MK801 or DMSA administration. Bottom row shows rate of change of synapse number per cell between neurons that has been treated with MK801 or DMSO. Left column shows average populational values, while the other two columns show individual neurons dynamics. *p<0.05, Mixed-design ANOVA with post-hoc pairwise t-test. C) An example neuron pre and 1day post MK801 treatment. FingR(PSD95) puncta that persists through two time points (white arrowhead) and ones that disappear or appear (blue arrowhead).

Chapter 4 : Synaptic Dynamics during Sleep

In the previous chapter, we have established synaptic tools that allow tracking of the same neurons and their synapses over time. This tool allows for the observation of synapse dynamics of the same neuron through different sleep/wake states and across the circadian cycle. Moreover, by expressing this tool in multiple neuronal types, we will be able to test whether sleep-dependent synaptic weakening is a global process, as predicted by SHY, or whether synapse dynamics are different across neuronal type.

Tracking a single neuron's synapse dynamics through multiple timepoints is a considerable technical challenge. Neurons that are suitable for multi-day tracking will have the following characteristics: 1) The neurons must be easily accessible for imaging small structures such as synapses so that they do not photo-bleach after multiple rounds of imaging; 2) They must be imaged as a whole cell (i.e. have self-contained processes) so that the synaptic dynamics of whole neurons can be examined; and 3) They must have known and predictable functional identities so their function can be retrospectively mapped to their synapse dynamics. We found a group of neurons that satisfy all these properties, making them a good candidate for testing SHY - the optic tectum (OT) neurons of zebrafish larvae. In this chapter, we will monitor synapse dynamics of tectal neurons through multiple days and nights in different rearing conditions and examine whether sleep-dependent synaptic weakening occurs as predicted by SHY within these neurons.

4.1 FOXP2+ NEURON SYNAPSE NUMBER ARE DEVELOPMENTALLY STABLE AT 6-9DPF

To study synapse dynamics across multiple sleep-wake cycles, we identified FoxP2.A-labelled tectal cells as having the best combination of accessibility and well-defined morphology and functional identities (Nikolaou *et al.*, 2015). I first developed a method to express the FingR-PSD95 system in single FoxP2.A positive tectal neurons per larva by co-electroporating a FoxP2.A:Gal4FF plasmid and Tol2 mRNA into the tectum of Tg(UAS:FingR(PSD95)-GFP) larvae at 3dpf. This allowed for the simultaneous visualization of the morphology and synapses of single isolated tectal cells (hereafter referred to as FoxP2:FingR(PSD95) neurons) through repeated rounds of imaging.

Before investigating synapse dynamics associated with the sleep/wake cycle, we first examined synapse dynamics during development in these tectal neurons. To that end, we repeatedly imaged the same FoxP2:FingR(PSD95) neurons through multiple developmental days (4-10dpf) at a similar circadian time of approximately Zeitgeber Time (ZT) 3-4hr (n=5, 5 fish; ZT0 = lights ON). Within FoxP2+ neurons, there is a large increase in the average total synapse number from 4dpf to 5dpf from approximately 110 to 140 with an average rate of change (RoC, calculated as the percentage change from the previous time point) of 30% (Figure 4.1).

From 5dpf – 9dpf the rate of change oscillates around zero, indicating that, on average, the total synapse number is relatively stable during this period. Within this stable period, on average the RoC decreases at 5-6dpf and slightly increases on 6-8dpf. By 10dpf, the average RoC increased in variability, indicating a diverging developmental path among individual tectal neurons. This is consistent with studies using overexpression of PSD95, a postsynaptic marker, in genetically unidentified tectal cells, where PSD95 puncta increased dramatically from 3-7dpf and stabilized in both puncta number and arborization from 7-10dpf (Niell, Meyer and Smith, 2004). Such stabilization around 6-7dpf onwards is also reflected in the development of tectal presynaptic sites and RGC axons' innervation (Meyer and Smith, 2006; Gebhardt, Baier and Del Bene, 2013), suggesting that retinotectal circuits are relatively stable during this developmental phase.

These 3 days of relatively stable synapse numbers from 6 to 9dpf give us a time window to study synapse dynamics with minimal interference from developmental processes such as synapse maturation and pruning. Moreover, during this developmental time window, zebrafish larvae have an inflated swim bladder, which allows them to swim and hunt, and importantly allow us to track their sleep/wake behaviour (Winata *et al.*, 2009; Rihel, Prober and Schier, 2010; Bianco, Kampff and Engert, 2011).

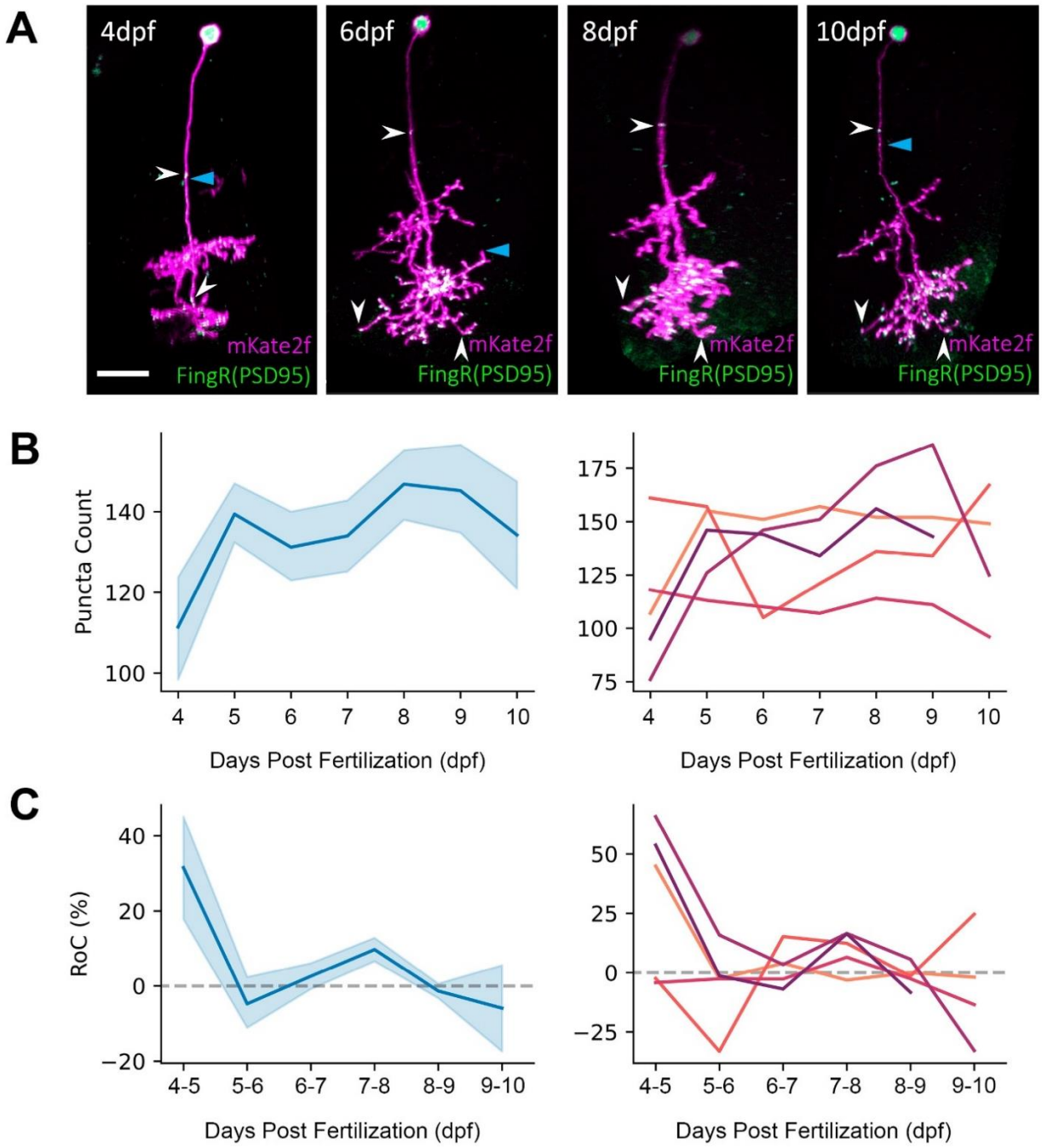

Figure 4.1: The synapse number of tectal neurons is developmentally stable at 6-9dpf. A) Example of the same FoxP2:FingR(PSD95) neuron through development from 4-10dpf. Nuclei and puncta are FingR(PSD95)- GFP positive (green). Cell morphology is labelled by mKate2f (magenta). White arrows indicate examples of puncta that persisted through time. Blue arrows indicate examples of puncta gained/lost through time. Scale bar = 15µm. B) FingR(PSD95) puncta numbers are developmentally stable from 6-9dpf. Left panel: average FingR(PSD95) puncta count through 4-10dpf.Right panel: individual FingR(PSD95) puncta count per neuron through time (n=5 cells, 5 fish). C) Rate of change (RoC) of FingR(PSD95) dynamics is close to zero around 6-9dpf. Left panel: average RoC calculated as a percentage change of FingR(PSD95) puncta in B from the previous time point. Right panel: individual neuron RoC trajectories through developmental time. The ribbon of each average trace depicts ± 68% confidence interval.

4.2 TECTAL NEURON SYNAPSE NUMBER CHANGES WITH THE LIGHT:DARK CYCLE

SHY predicts that the synapse number and/or strength should increase during wakefulness and decrease with sleep (Tononi and Cirelli, 2006). We asked whether there are changes in the synapse number of FoxP2.A tectal neurons as predicted by SHY. To answer this, we reared larvae in a normal 14:10hour light:dark cycle (LD) to fully entrain their circadian clock and sparsely expressed FingR(PSD95) in single FoxP2.A neurons by electroporation (see Methods). We then repeatedly imaged the same FoxP2:FingR(PSD95)+ neuron over three timepoints: early morning when the lights comes on (ZT0) on 7dpf, later in the evening (ZT10) on 7dpf, and again the next morning (ZT0) on 8dpf (Figure 4.2A). As zebrafish are diurnal, this paradigm allowed us to look at synapse dynamics during the day phase (ZT0-10) when fish are awake and more active and the night phase (ZT10-0), when larvae spend the majority of their time sleeping (Prober *et al.*, 2006).

Repeatedly imaging the same neurons through one day and one night showed that FoxP2.A neurons synapse number in LD animals on average increase from approximately 137 synapses in the morning to 153 synapses in the evening, while after the dark phase, the average synapse number mildly decrease to around 146 synapses (Figure 4.2B, blue. $p=0.021$, repeated measures ANOVA with Greenhouse-Geisser correction. Post hoc pairwise-Student's t-tests find statistically significant $p=0.019$ values between ZT0 and ZT10 on 7dpf). This corresponds to the RoC during the day (from ZT0-10, day dynamics) of a 14.4% increase and RoC overnight (ZT10-0, night dynamics) of -1.90% ($p=0.042$, repeated measures ANOVA). Because the RoC measurement gives more weight to neurons with fewer number of synapses at baseline and may miss dynamics in neurons with a high synapse count, we also examined the absolute synapse number change (Δ Puncta). The Δ Puncta measurements also follows the trajectories observed by the RoC analysis on average; tectal neurons gained a net of 16.5 synapses on average during the day and lost a net of 6.8 synapses on average during the night (Figure 4.2D). These analyses demonstrated that under LD conditions, which preserves the circadian structure of sleep/wake behaviour, tectal neurons, as a population, show an increase during the day (wakefulness) and a smaller but measurable average net decrease during the night (sleep phase). These observations are consistent with the predictions of SHY; however, not all individual neurons have this daytime net increase and night time net

decrease trajectory (Figure 4.2C-D, second panel), suggesting that synaptic homeostasis as envisioned by SHY is not present in all tectal neurons.

The synapse rhythmicity observed could be due to the sleep/wake cycle, the endogenous circadian clock, or even the physical light/dark exposure the larvae were reared in. To determine whether this rhythmicity requires an intact circadian clock, we reared the zebrafish larvae in constant light (LL, Figure 4.2A, annotated in pink) from fertilization, which results in unsynchronized circadian clock components and an arrhythmic sleep/wake pattern characterized by high levels of locomotor activity (Prober *et al.*, 2006). Although dark rearing during development can also remove coherent circadian clocks from zebrafish larvae, constant light was chosen because constant dark conditions during handling and especially imaging would be difficult to maintain, if not impossible.

Under constant LL conditions, FoxP2.A neurons had on average a similar number of synapses across all three measured timepoints: 121, 118, and 116 synapses at ZT0 7dpf, ZT10 7dpf, and ZT0 8dpf, respectively (Figure 4.2B, pink. p=0.4 ns, repeated measures ANOVA). The average synapse numbers through the three time point in LL are lower compared to LD's (average of 118 and 145 synapses, respectively), suggesting that either prolonged light exposure or the lack of a synchronized circadian clock reduces the initial development of tectal cell synapses. Constant light conditions also eliminated the statistically significant day-increases and, night reductions in synapse numbers observed in LD conditions, with the average percentage change during the subjective day at -1.52% and the subjective night of -0.20% (p= 0.796, repeated measures ANOVA, Figure 4.2C). The average absolute synapse number also did not change across the subjective day (a net loss of 3.48 synapses) or subjective night (-1.60 synapses). The arrhythmicity in synapse number in larvae reared in constant light shows that either a presence of synchronized circadian clock network or alternating light/dark cues are vital to have SHY-like synapse dynamics in FoxP2.A tectal neurons.

The elimination of synapse number dynamics in constant light could be due to the loss of synchronized circadian clocks; alternatively, physical light/dark itself could be driving changes in synapse number. To distinguish between these two alternatives, we raised larvae on a normal light dark cycle and then switched to constant LL conditions on 6dpf (Figure 4.2A). In contrast to the clock-breaking experiment, this paradigm creates a "free-running" clock (FR), in which the larval circadian clock rhythm will remain intact (Kaneko and Cahill, 2005). Thus,

if synapse dynamics remain intact in free running conditions, these dynamics are under the control of the endogenous circadian pacemaker. However, if synapse dynamics are eliminated, then a light/dark-driven cue underlies synapse rhythms

Under FR conditions, we observed several effects on synapse dynamics of tectal neurons. After one night of constant light, the average number of synapses is decreased relative to LD and to a similar level as observed in the LL clock-break experiment (123 and 118 synapses, respectively) (Figure 4.2B, green traces). However, in FR conditions, during the synapse tracking period, the synapses of tectal neurons increased in the subjective day period and decreased in the subjective night period, more similar to larvae reared in LD conditions. In FR, synapse dynamics during the subjective day increased by 5.2%, gaining an average of 6.53 synapse, and decreased by 3.8%, losing an average 5.60 synapses over the subjective night (Figure 4.2C-D, p= 0.26, ns, repeated measures ANOVA). Synapse dynamics between the three lighting conditions showed that only LD and LL are different from one another at 7dpf ZT10 (RoC: p=0.008 and Δ Puncta: p=0.014, Mixed ANOVA with posthoc pairwise t-tests). Together these data revealed that the endogenous circadian clock does contribute to synapse rhythms, but alternative light/dark cues are also needed to have full SHY-like rhythmicity.

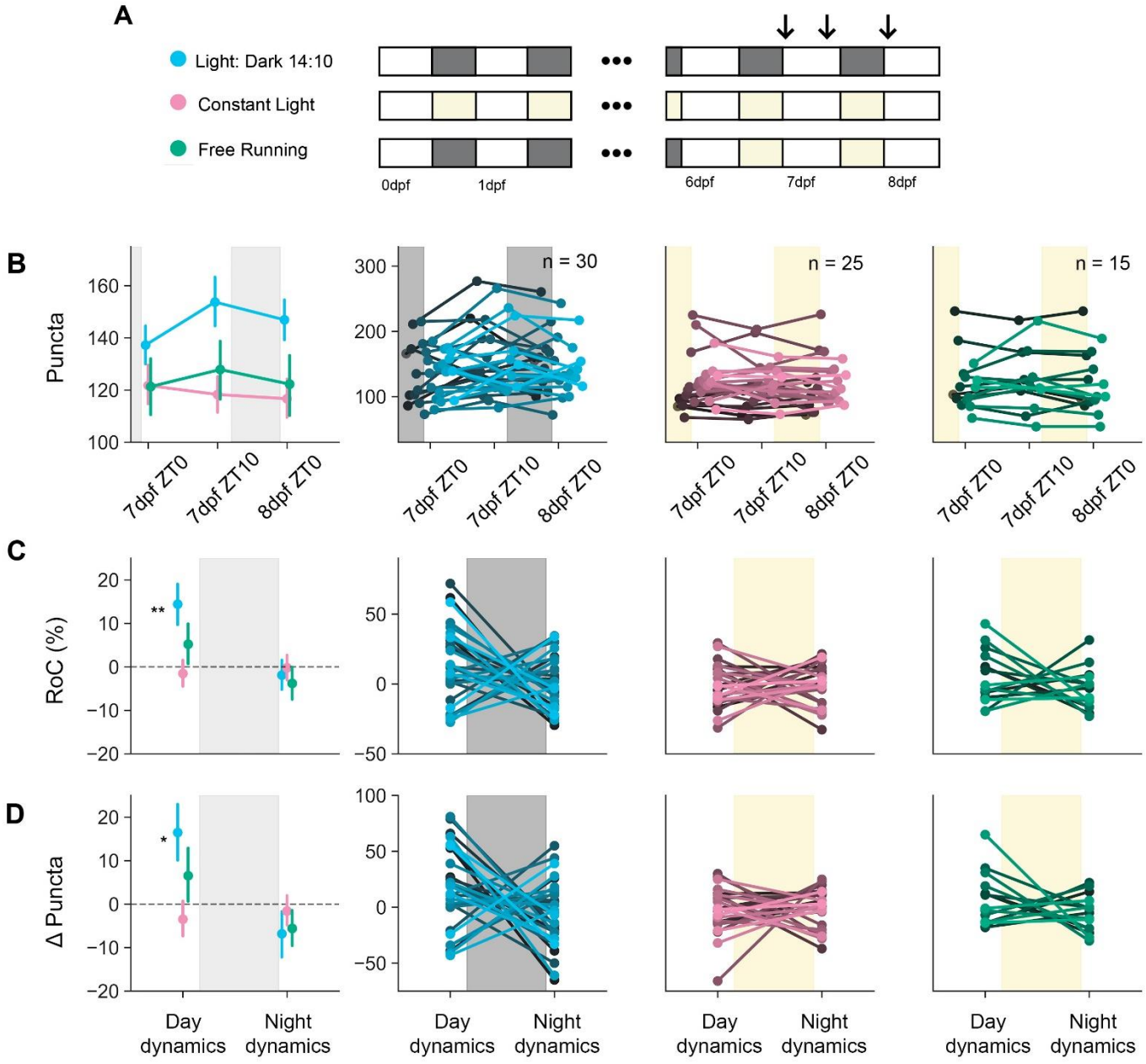

Figure 4.2: The LD cycle and circadian clock influence tectal neuron synapse number. A) Schematic of rearing condition and imaging paradigm. Normal light:dark reared larvae are shown in blue (LD). Larvae raised in constant light (LL) since fertilization are in pink. Free-running larvae (FR) that have been raised in normal LD then switched to LL from 6dpf are in green. White boxes indicate lights ON periods during daytime. Dark grey boxes indicate lights OFF period during nighttime. Yellow boxes indicate light ON during subjective night. Arrows indicate imaging time around ZT0 and ZT10 for each day. B-D) Left panel shows the average values corresponding to each row of FingR(PSD95) puncta per neuron through time. Subsequent panels show the raw values FingR(PSD95) corresponding to each row for each neuron through time for LD, LL, and FR, respectively. Each line represents a single neuron. B) Both the circadian clock and LD cycle influence synapse number. C) RoC of FingR(PSD95) puncta count through time. RoC day dynamics is the percentage change from ZT0 to ZT10 on 7dpf. RoC night dynamics is the percentage change from 7dpf ZT10 to 8dpf ZT0. D) Absolute puncta gain/loss during day and night over time. The average RoC and Δ puncta are higher in LD than LL raised larvae during the day phase. *p<0.05, **p<0.01, Mixed ANOVA with pairwise T-test.

4.3 EXTENDED TRACKING REVEALS THE INFLUENCE OF THE LD CYCLE ON SYNAPSE NUMBER

Repeated imaging of single FoxP2:FingR neurons over one day and one night showed that circadian signals are required for SHY-like synapse dynamics. We asked whether such synapse dynamics persists through multiple days and nights.

We extended our imaging paradigm over three days and two nights from 7-9dpf and imaged at approximately ZT0 and ZT10 on each day (Figure 4.3A). During 7-9dpf the total synapse number remains stable and is not confounded by development (Figure 4.3). This gave us an opportunity to further disentangle the influence of the internal circadian clock and light-driven influences on synaptic dynamics.

During extended tracking, tectal neurons of larvae reared under LD conditions have more synapses on average compared to both LL and FR entrained larvae at all six time points (Figure 4.3B). At the population level, the synapse dynamics of LD-reared larvae had similar dynamics as observed in the shorter tracking experiments. As seen by RoC analysis, synapse number increased during the day phase 5.0-12.7% and stabilized or decreased during the night phase across all the time points, with decreases ranging from 0.7-7.2%. As in the shorter tracking experiments, this population-level dynamics in synapses was not observed in all of the neurons when considered at a single cell level (Figure 4.3B-C, middle panel).

In contrast to the robust dynamics under LD conditions, and consistent with the shorter tracking experiment, synapses in LL larvae did not exhibit day to day changes in synapse number (Figure 4.3C). The RoC of synapse number in LL larvae was stable throughout the tracking (around 0%) except during the final 9dpf day phase where the net number of synapses increased at the rate of 9.4% (Figure 4.3C). This may reflect larvae reaching the late stage of neuronal maturation observed during developmental studies (Figure 4.1). However, when larvae are raised on an LD cycle and transitioned to free running conditions (FR), rhythmicity in the population level synapse dynamics was retained, although this rhythm dampened by the end of the experiment.

In the first day and night, FR tectal synapses increased during the day phase (+6.1%) and decreased during the night phase (-3.6%). However, from 8dpf onwards, FR synapse dynamics were not rhythmic like what was observed in LD condition. FR synapse dynamics decreased

throughout day and night on 8dpf and then increased during day phase on 9dpf (+3.3%). It must be noted that the FR group has lower samples (n=11) than in LD and LL (n= 22, 19, respectively) – since synapse dynamics differs at the single cell level, perhaps we have undersampled the rhythmic tectal neurons in this sample (and see below for the impact of tectal subtypes on dynamics). Nevertheless, after excluding the last timepoint, which appears to have an increase in all conditions that may reflect a second wave of synapse maturation, we found that synapse dynamics during the day phase of LD larvae were statistically different to LL but not FR conditions ($p=0.027$ and $p= 0.11$, respectively; mixed ANOVA with post hoc pairwise t-tests).

Our long-term tracking is consistent with the short-term tracking, showing that an endogenous circadian clock is required for synapse rhythmicity and without alternative light/dark cues to fully entrain the clock, the rhythmicity dampens. Moreover, long exposure to light decreases the overall number of synapses.

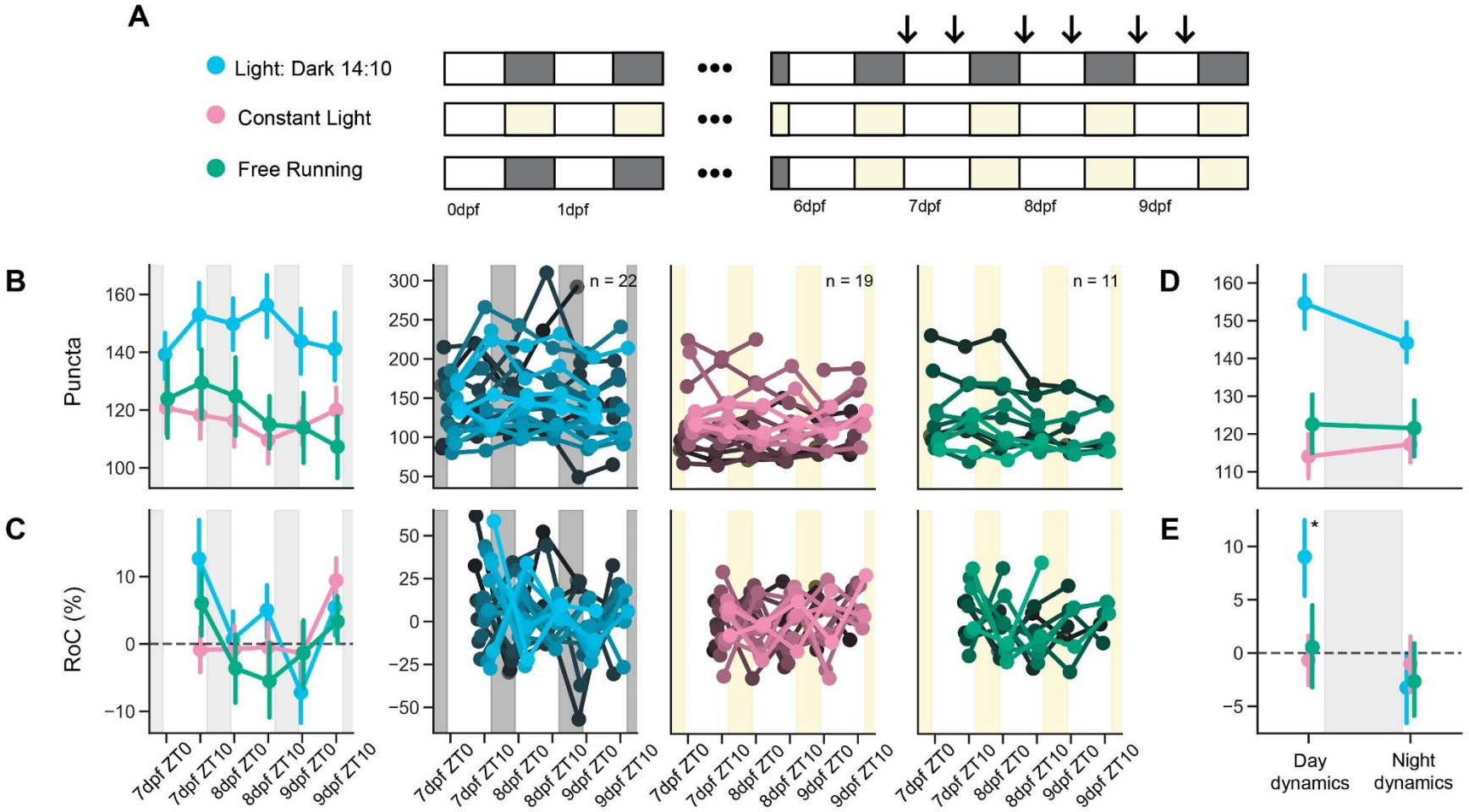
A
Light: Dark 14:10
Constant Light
Free Running
0dpf
1dpf
6dpf
7dpf
8dpf
9dpf
B
Puncta
n = 22
n = 19
n = 11
C
RoC (%)
7dpf ZT0
7dpf ZT10
8dpf ZT0
8dpf ZT10
9dpf ZT0
9dpf ZT10
D
E
*
Day dynamics
Night dynamics

Figure 4.3: Extended tracking reveals the influence of LD cycles and the circadian clock on tectal neuron synapse number. A) Schematic of rearing condition and extended imaging paradigm. Normal light:dark reared larvae are shown in blue (LD). Larvae raised in constant light (LL) since fertilization are in pink. Free-running larvae (FR) that have been raised in normal LD then switched to LL from 6dpf are in green. White boxes indicate lights ON periods during daytime. Dark grey boxes indicate lights OFF period during night time. Yellow boxes indicate light ON during subjective night. Arrows indicate imaging time around ZT0 and ZT10 for each day from 7-9dpf. B-C) Left panel shows the average values corresponding to each row of FingR(PSD95) puncta per neuron through time. Subsequent panels show the raw values of FingR(PSD95) corresponding to each row for each neuron through time for LD, LL, and FR, respectively. Each line represents a single neuron. B) Both the circadian clock and LD cycle influence synapse number. C) The Rate of Change (RoC) of FingR(PSD95) puncta counts through time. RoC day dynamics is the percentage change from ZT0 and ZT10 for each day. RoC night dynamics is the percentage change from ZT10 and ZT0 of the follow day timepoint. D-E) Average puncta count and RoC for ZT0 and ZT10 combined for all conditions LD, LL, and FR, respectively. We excluded 9dpf at ZT10 as synapse dynamics appeared to developmentally diverge. LD larvae average RoC and Δ puncta are higher than LL's during day phase. *p<0.05; mixed ANOVA with pairwise T-test.

4.4 REPEATED IMAGING DID NOT INTERFERE WITH FINGR(PSD95) PUNCTA NUMBER

To ensure that multiple repeated imaging does not interfere with synapse number dynamics, we performed imaging controls experiments in which FoxP2:FingR(PSD95)+ tectal neurons were imaged at the first time point (7dpf, ZT0) and again at the last time point (9dpf, ZT10). We then compared the puncta number between these controls to tectal neurons that were repeatedly imaged throughout the six time points (Figure 4.4). We found that the synapse number for tracked neurons is on average higher than those in controls. This might be due to the lower sample size of controls (n=6) than tracked neurons (n=14), which could lead to a lack of FoxP2.A neuronal subtypes with higher synapse count (see 4.5). Nonetheless, we found that the percentage change in synapse number between the first and last time points of controlled and tracked neurons are not statistically different (p=0.99, Student's t-test), suggesting that repeated imaging does not artefactually alter total synapse numbers.

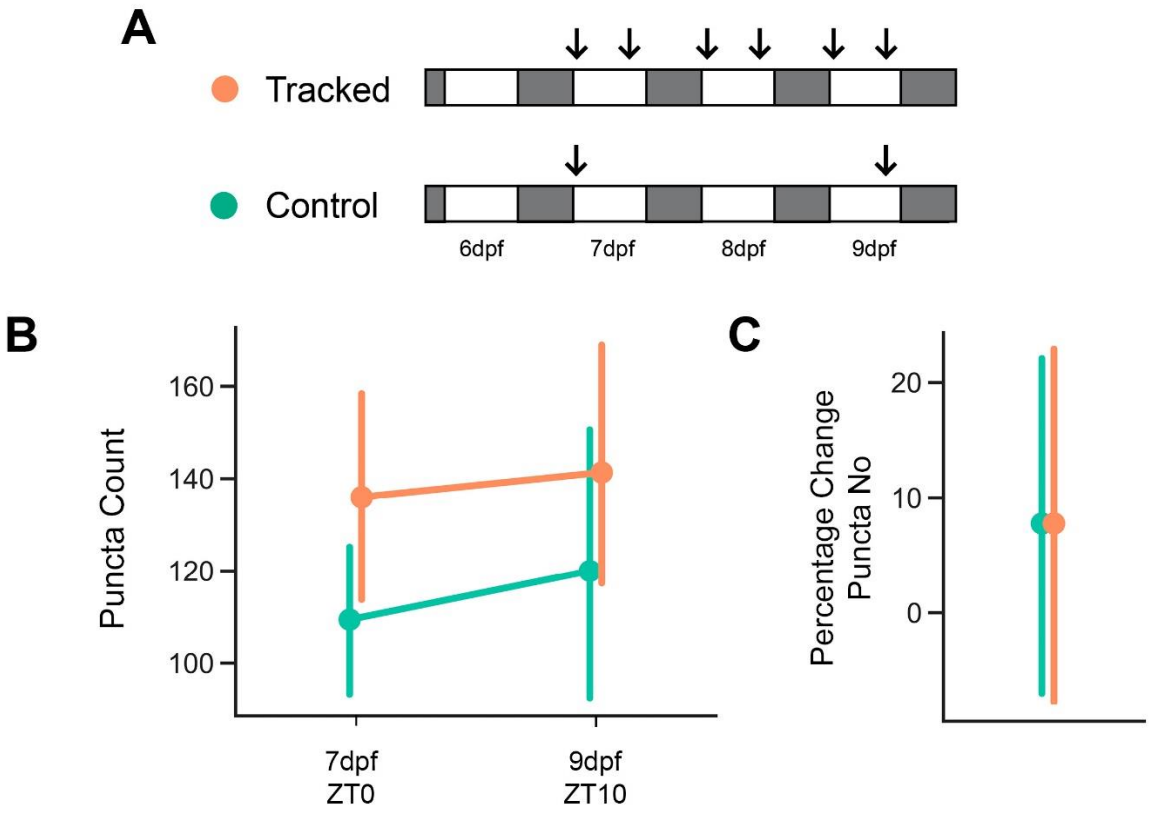

Figure 4.4: Repeated imaging did not affect total synapse number. A) Schematic of experimental set up. We reared larvae up in normal LD (indicated by white and black boxes) and imaged six times between 7-9dpf at ZT0 and ZT10 each day (Tracked, orange) or imaged at the first time point ZT0 on 7dpf and the last time point ZT10 on 9dpf (Control, green). B) Average FingR.PSD05 puncta at the first and last time point (7dpf ZT0 and 9dpf ZT10) of tracked and controls larvae. C) Percentage change in FingR(PSD95) number between tracked and controls larvae were not statistically different.

4.5 FOXP2.A NEURONS HAVE FOUR MORPHOLOGICAL SUBTYPES

The variability of synapse dynamics at the level of individual neurons and the correlation of morphology and functional identities of FoxP2.A interneurons (Nikolaou *et al.*, 2015) led us to ask whether subtypes of FoxP2.A neurons have specific synaptic dynamics. In order to test whether synapse dynamics correlates with morphological features, we extracted different morphological parameters from the FoxP2:FingR(PSD95)-GFP neurons at 7dpf. Six parameters were measured: 1) total filament sum, 2) distal arbour location, 3) proximal arbour location, 4) distal arbour thickness/extent, 5) anterior-posterior (AP) span of distal arbour, and 6) distance from skin (Figure 4.5A). Total filament sum, AP span, distal arbour laminar thickness, and distance from skin were features previously used to characterized the morphology of tectal cells (Robles *et al.*, 2011; Gabriel *et al.*, 2012; Nikolaou *et al.*, 2015). We included two more parameters as the four parameters previously described in Nikolaou et al. did not cluster morphological subtypes efficiently (see section 6.2.3). Each morphological feature was standardized by removing the mean and scaling to unit variance, transformed into PCA space, and clustered using k-means clustering based on the optimal PCA (see Methods 2.6.3). The optimal number of k clusters (4) was chosen by using the elbow method, Calinski-Harabasz index, and silhouette coefficient.

We found that FoxP2.A neurons have four morphological subtypes (Figure 4.5B). Type 1 neurons (green) lack proximal arbours and have overall a smaller filament length sum (Figure 4.5 B-H). Type 2 neurons (orange) have the highest total filament length on average compared to the other subtypes, suggesting that they are bigger neurons with extensive neurites. Type 3 neurons have the most laminar distal arbour and the smallest distal arbour thickness. Type 4 neurons (yellow) are much smaller than Type 2 but have a similar distal arbour thickness. Surprisingly, our clustering did not clearly separate distinct subtypes based on distance from the skin, even though it is known that tectal interneurons with distinct functional subtypes arborize into different laminae within the tectum (Gabriel *et al.*, 2012), suggesting that clustering based on morphology alone may not capture the full range of functional properties of these cells.

We decided to cluster all neurons from different lighting conditions (LD, LL, and FR) together as analyses based on clustering of all conditions did not alter the subtypes classification as compared to condition-specific clustering. For example, clustering using either all conditions

or only the LD condition gave the same optimal number of k-means cluster of 4. We then compared the outcomes of the two methods of clustering and found that most of the morphological subtypes using these two methods overlapped (Figure 4.6A). To confirm this further and to ensure that the addition of neurons in the combined group did not alter clustering boundaries, we also randomly selected 25 neurons from the LD condition and clustered these neurons by themselves. Their optimal number of k-means cluster was also 4. We then looked at these 25 randomly selected neurons and found that the distribution of cluster assignment of these 25 neurons are similar when clustered using only LD condition and using all conditions together (Figure 4.6).

It must be noted that when screening for positive FoxP2:FingR(PSD95) cells, we discarded any tectal neurons that had projection neurites outside of the tectum (discussed in Methods). This is because we could not track synapse dynamics of the neurites that project outside the tectum. One such neuron that was occasionally observed resembles the bistratification periventricular projection neurons discussed in Robles et al. (2011). Therefore, it must be noted that FoxP2.A neurons may have more than four morphological subtypes that are not included in our analysis of morphological types and synapse dynamics.

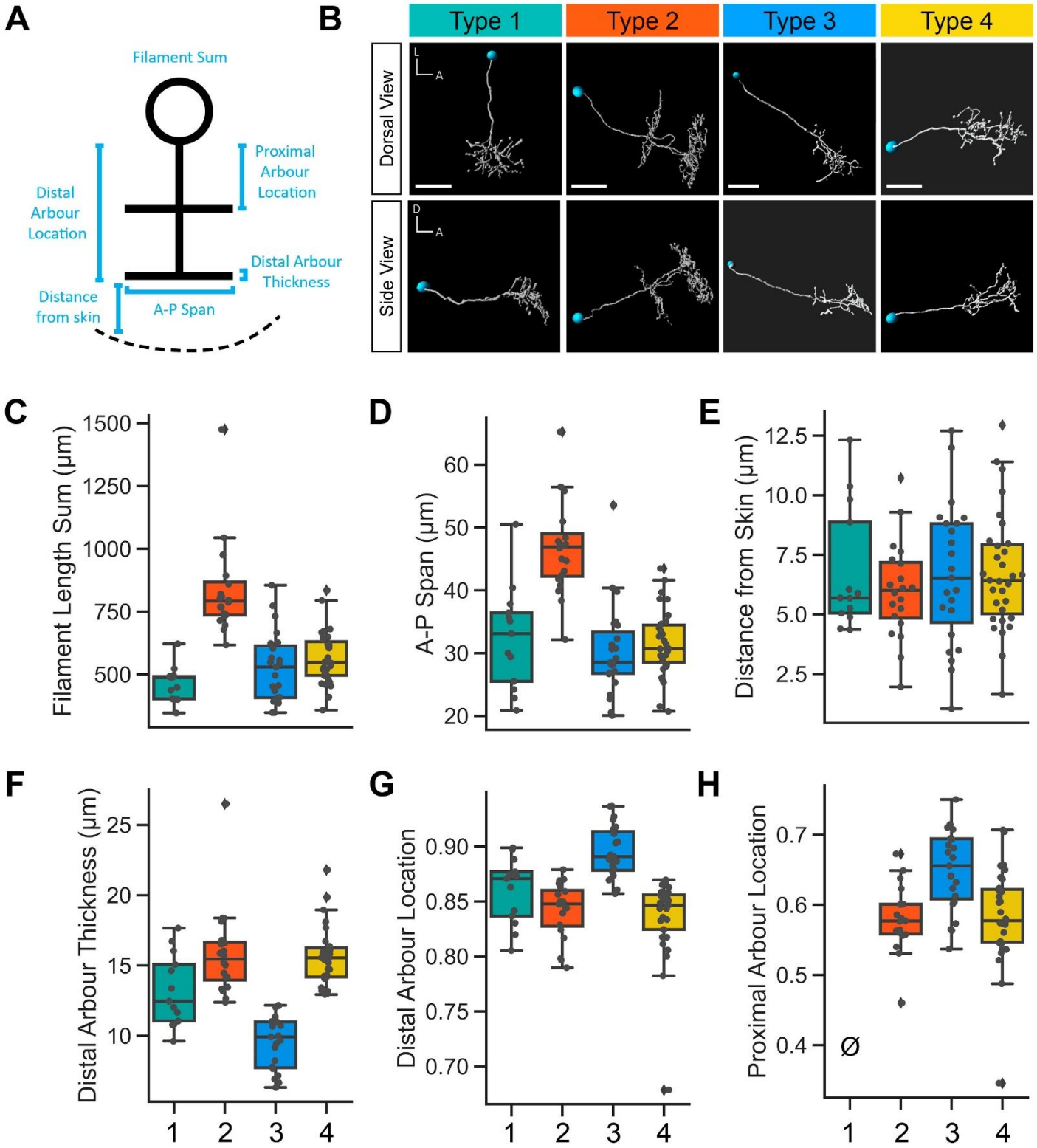

Figure 4.5: FoxP2.A neurons have 4 morphological subtypes. A) Morphological parameters used to characterize FoxP2.A tectal cells. B) Example neurons for each morphological subtype of FoxP2.A neurons. C-H) Box plot represents the median and interquartile range and the whiskers represent the distribution of different FoxP2.A subtypes for each morphological parameters: filament length sum (C), anterior-posterior span of distal arbour (D), distance from skin (E), distal arbour thickness (F), distal (G) and proximal (H) arbour location. Slashed zero represent absence of feature. Scale bar represents 10 µm. A, anterior; D, dorsal; L, lateral.

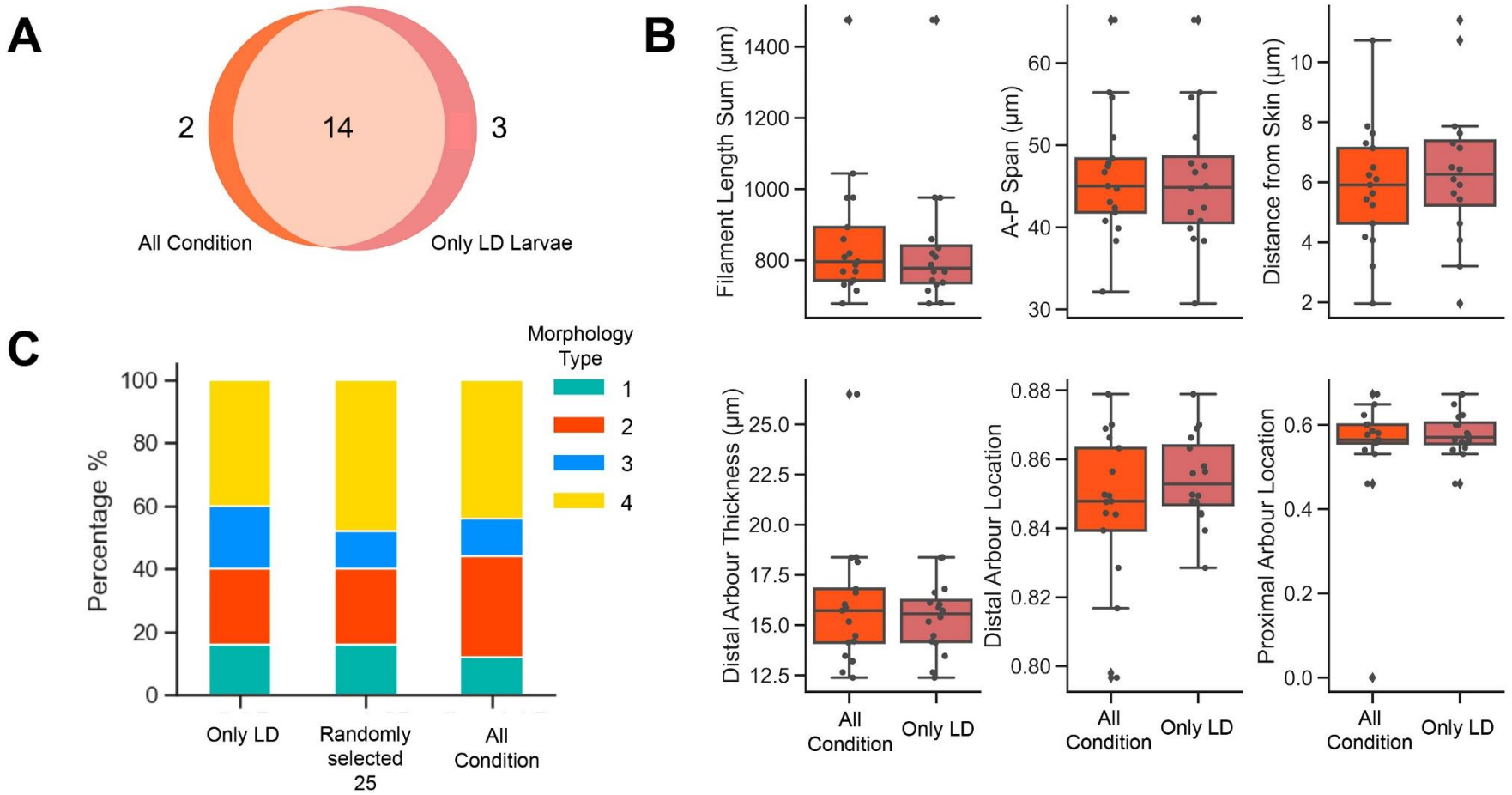

Figure 4.6: Neuronal morphology from different rearing conditions can be clustered together. A) Clustering using all conditions combined and clustering using only LD rearing larvae produced overlapping outcomes. Example of clustering methods outcomes for Type 2 neurons where 14 larvae overlapped. B) Type 2 neurons morphological parameters clustered using different animal conditions: all rearing conditions combined vs only LD rearing larvae. C) Clustering using all rearing conditions, only LD, and randomly selected 25 neurons from LD gave similar morphology subtypes distributions.

4.6 LACK OF A SYNCHRONIZED CIRCADIAN CLOCK ALTERS THE RATIO OF MORPHOLOGICAL TECTAL NEURONS SUBTYPES

Next, we examined how prevalent each of the morphological subtypes are. Under LD conditions, we found that Type 2 and 4 neurons are more common than Type 1 and 3. Type 2 and 4 occupied 34.7% (n=17/49) and 44.9% (n=22/49) of the total number of neurons, respectively. In contrast, Type 1 and 3 each accounted only for 10.2% (n=5/49) of the tectal cells (Figure 4.7A-B).

We asked whether the constant light 'circadian clock breaking' condition had any effect on the neuron subtypes observed. We found that the absence of synchronized clocks (or long exposure to light during development) biased the morphological subtypes of FoxP2.A neurons. Fish raised in LL conditions had statistically significant increases in the percentages of Type 1 and 3 neurons (25% and 54%) at the expense of Type 2 and 4 (4.2% and 16.7%) (Figure 4.7A-B; $p<0.00$, Chi-square with multiple comparison corrected using Benjamini-Hochberg). Inspection of the specific morphological parameters of tectal neurons under LL conditions revealed that these neurons overall had lower filament length sum and distal arbour thickness compared to tectal neurons of LD-raised larvae ($p=0.038$ and $p<0.000$, respectively, Kruskal-Wallis with post hoc Dunn's test). This is consistent with the observation that fish raised in LL have a higher proportion than LD raised fish of Type 3 neurons, which are characterized by a thinner distal arbour extent (Figure 4.8). We did not have enough tectal neurons from FR conditions to draw any conclusion on the distribution of neuronal subtypes (n=14).

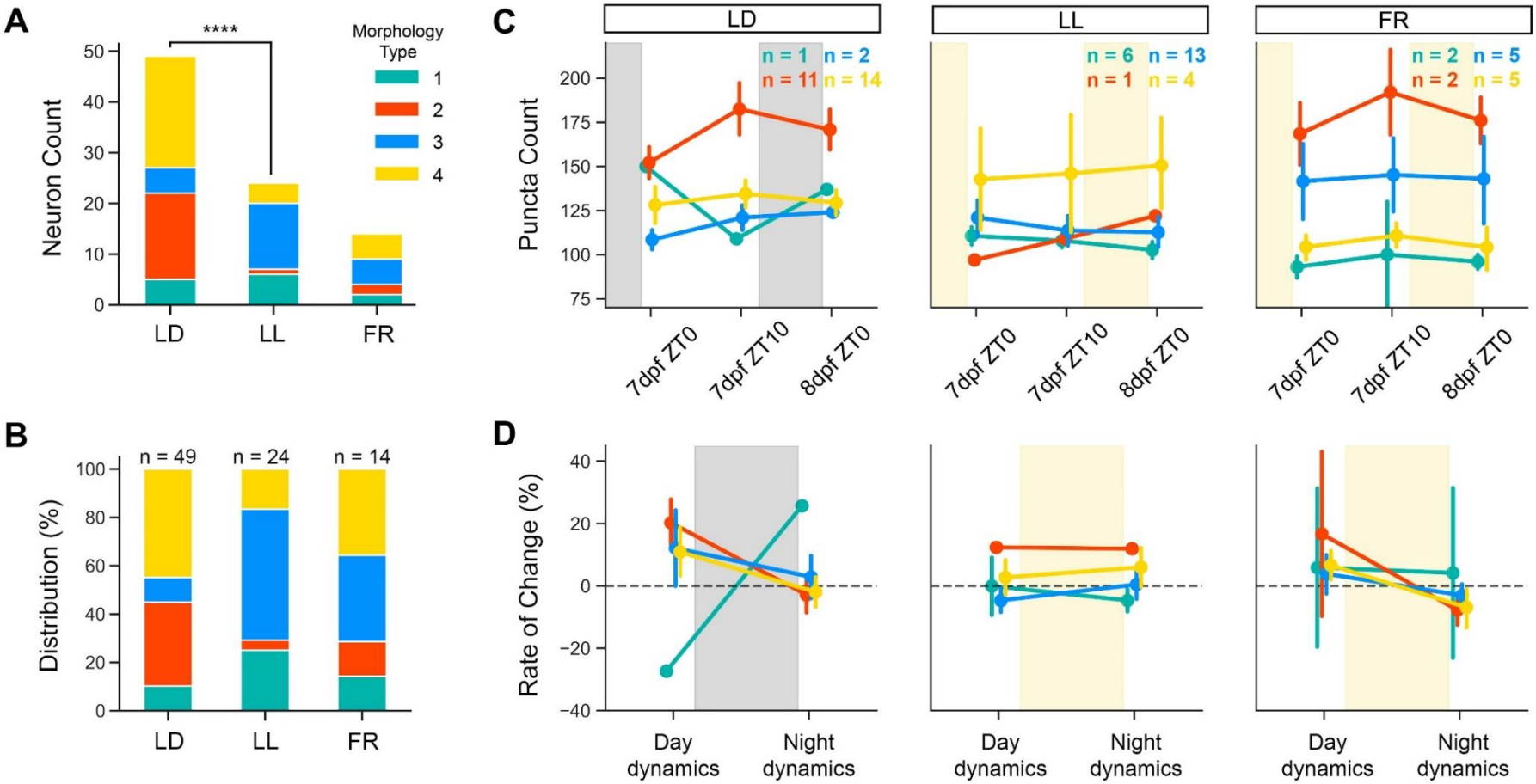

Figure 4.7: Raising larvae in constant light biased the ratio of FoxP2.A neuron subtypes. A) The count of subtypes observed in each rearing condition LD, LL, and FR. p<0.000, Chi-square adjusted with Benjamini Hochberg. B) Distribution of FoxP2.A neuronal subtypes (%) in each rearing condition LD, LL, and FR. C) The number of FingR(PSD95)-GFP puncta (synapses) per FoxP2.A neuronal across day-night tracking in each rearing condition. D) The Rate of Change (%) of synapse count for each FoxP2.A subtypes for fish reared in LD (left), LL (middle), and FR (right panel) conditions. White panels indicate light ON periods. Dark grey panels indicate lights OFF period. Yellow panels indicate light ON period during subjective night.

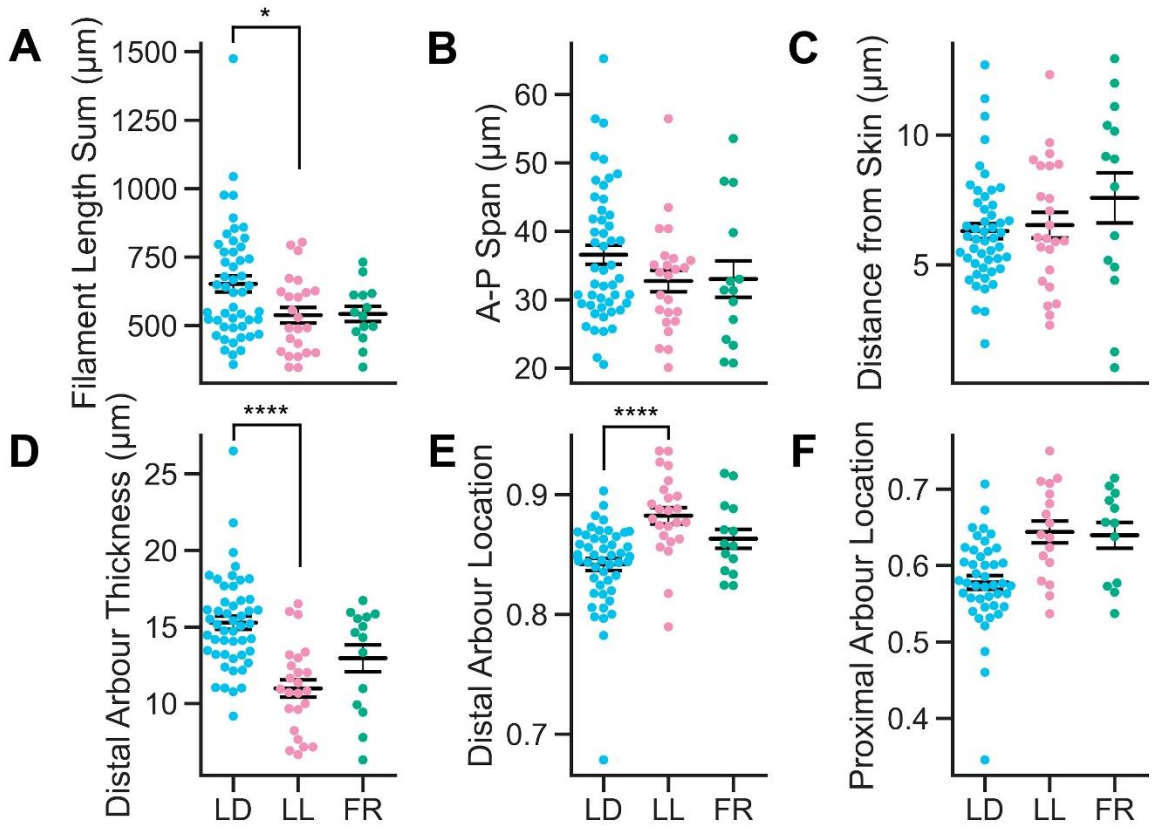

Figure 4.8: Constant light (LL) rearing larvae on average have smaller distal arbour thickness compared to LD-rearing larvae. A) Filament length sum, B) A-P span of distal arbour, C) Distance from skin, D) Distal arbour thickness, E) Distal arbour location, and F) Proximal arbour location for all three rearing conditions. *p<0.05, ****p< 0.0001, Kruskal Wallis with posthoc Dunn's test pairwise comparison. Black line indicates population average ± standard error of the mean.

4.7 POSSIBLE FOXP2.A NEURONAL SUBTYPE-DEPENDENT SYNAPSE DYNAMICS

The morphological heterogeneity of FoxP2.A neurons led us to ask whether the FoxP2.A subtypes have different synapse dynamics across a day-night cycle. We therefore looked at synapse number dynamics for each of the neuronal subtypes under different lighting conditions.

In normal LD conditions, each of the subtypes with a sufficient number of examples had increased synapse counts after the day phase and little or no change in the night phase (Figure 4.7C-D, 4.9-10). For example, Type 2 neurons, which had the largest number of synaptic puncta across all time points (consistent with also having the largest total filament lengths), have a robust day phase increase (average 14.8%) and night phase decrease (average 8.7%). Type 4 neurons in LD conditions did not exhibit robust day to day changes in synapse number (Figure 4.7, 4.9). The RoC of synapse number in Type 4 neurons was stable throughout tracking (around 0%) except for the increase after the first day phase, which were similar to Type 2 neurons day dynamics (Figure 4.8B). However, we do not have enough data from Type 1 and 3 to draw any conclusions on subtype-dependent synapse dynamics.

Analysis of tectal neurons subtypes under LL and FR conditions told a similar story. As observed in the population-wide analysis, the number of puncta in all tectal neuron subtypes in LL conditions did not change across the subjective day and night periods (Figure 4.7C-D and 4.10). Similarly, we did not observe subtype-specific synapse number dynamics in the FR larvae. Subtypes with sufficient n's increased in synapse count after the subjective day phase and stabilized or decreased after the subjective night phase (Figure4.7C-D and 4.10). Nonetheless, we do not have sufficient n's for all subtypes to draw any conclusions on subtype-specific synapse dynamics in LL and FR rearing conditions.

To shed light on the possible subtype-synapse dynamics, we need to increase the n number for each subtype. Power analysis based on LD conditions (alpha = 0.01 with 95% power) showed that we require n=6 for Type 1 neurons to be statistically different from Type 2 dynamics at the same time point. However, due to the unequal distribution of subtypes, where under LD condition Type 1 is labelled 10.2% (5/49) at a time, and we only have 1 out of 8 chances of successfully labelling a single tectal cell by electroporation, we would be required to electroporate 392 larvae to increase our Type 1 data to n=6. This high number of

animals electroporated would increase further when considering 'dropout' rates (e.g. bleaching after 2 imaging sessions) which is approximately 1/5 animals. Moreover, the number of animals electroporated is exacerbated in LL and FR conditions, where rare subtypes such as Type 2 under LL occurs only in 1 out of 24 neurons. Unfortunately, due to the high number of animals that would be required to achieve robust statistical power, we were not be able to draw any conclusions on potential subtype-specific synapse dynamics.

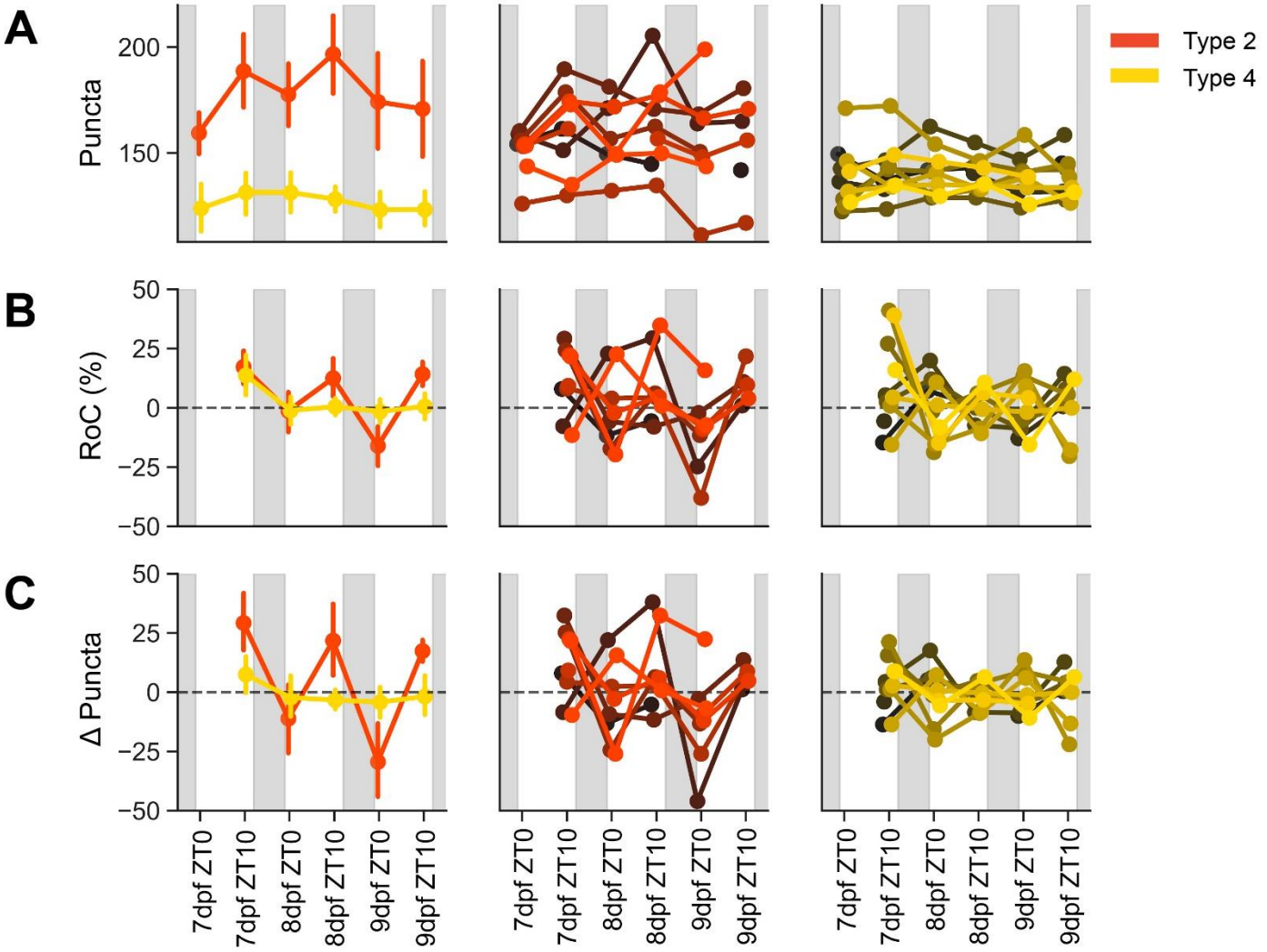

Figure 4.9: Possible synapse dynamics in different FoxP2.A tectal neuron subtypes of larvae raised in normal LD conditions. Examples of FoxP2.A subtypes exhibiting different synapse dynamics in extended tracking. A) Average FingR(PSD95) puncta count of Type 2 and 4 and their respective individual neurons puncta count. B) Average RoC of Type 2 and 4 and their respective individual neuron synapse number dynamics. C) Average absolute FingR(PSD95) puncta change of Type 2 and 4 and their respective individual neuron synapse dynamics

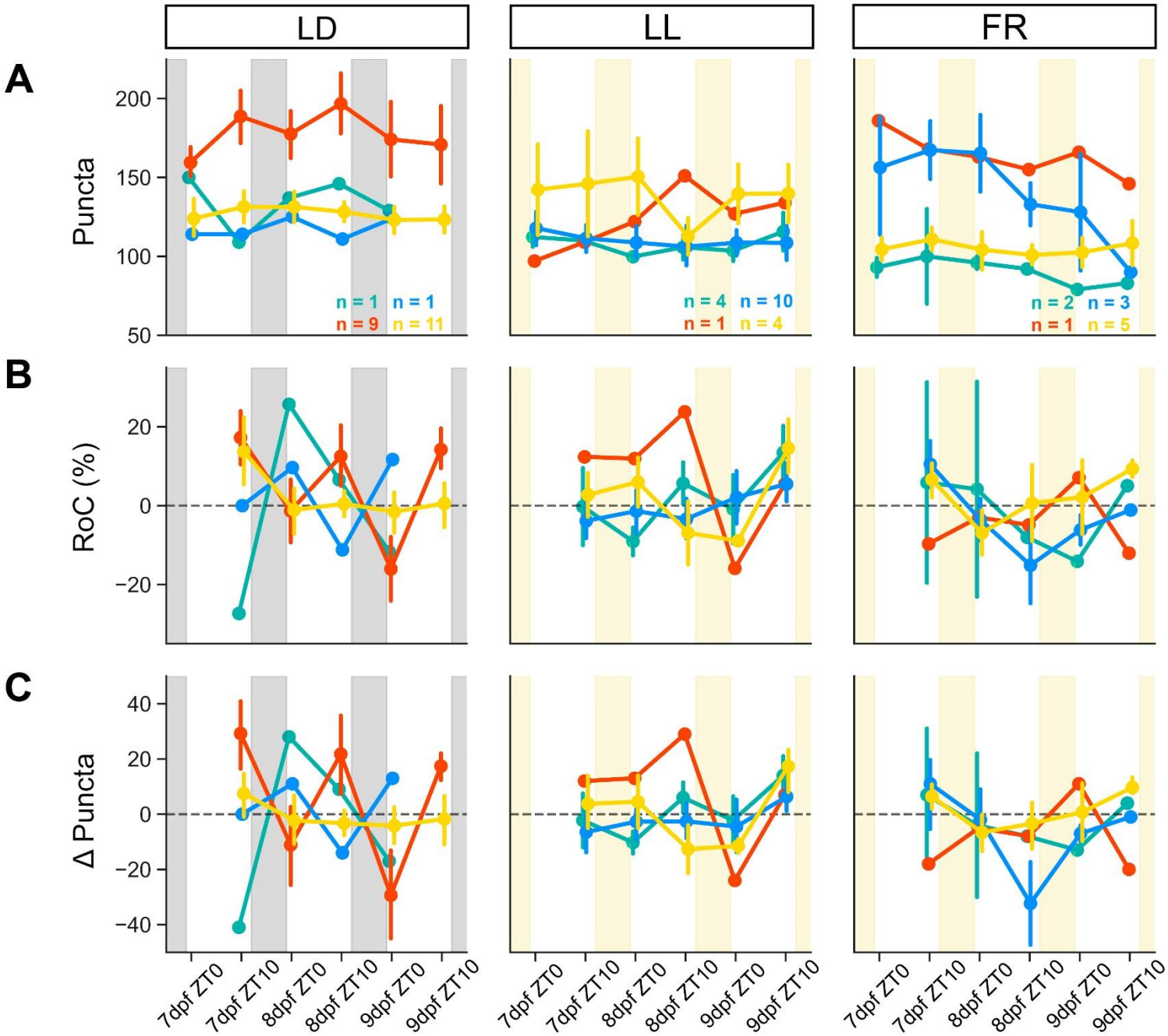
A
B
C
LD
LL
FR
Puncta
RoC (%)
Δ Puncta
200
150
100
50
20
0
−20
40
20
0
−20
−40
n = 1 n = 1
n = 9 n = 11
n = 4 n = 10
n = 1 n = 4
n = 2 n = 3
n = 1 n = 5
7dpf ZT0
7dpf ZT10
8dpf ZT0
8dpf ZT10
9dpf ZT0
9dpf ZT10

Figure 4.10: Extended morning/evening tracking of FoxP2.A subtypes synapse number dynamics. Left column) LD rearing animals. Middle column) constant light, LL, rearing animals. Right column) FR animals. A) Average FingR(PSD95) puncta number for each FoxP2.A subtypes in different rearing conditions from 7-9dpf at ZT0 and ZT10 on each day. FoxP2.A Type 1 (green), Type 2 (red), Type 3 (blue), and Type 4 (yellow). B) Average rate of change (RoC) in synapse number for each FoxP2.A subtypes in different rearing conditions from 7-9dpf at ZT0 and ZT10 on each day. C) Absolute puncta gain/loss for each FoxP2.A subtypes from 7-9dpf at ZT0 and ZT10 on each day.

4.8 SYNAPSE DYNAMICS DOES NOT CORRELATE WITH SLEEP AND WAKE BEHAVIOUR

One prediction of SHY is that increases in synaptic strength during the day are due to waking experience and decreases in strength at night are due to sleep. Some of the synapse dynamic observations on LD, LL, and FR are consistent with sleep/wake having an important role. For example, the diurnal zebrafish are more awake during the day, when synapses increased in number and sleep more at night, when synapse number is stable (Figure 4.2-3). Decreased sleep associated with FR conditions imposed by constant light (Prober et al., 2006) might also account for the elevated synapse number and dampened synapse dynamics observed under FR (Figure 4.2-3). Moreover, larvae have a high level of individuality in their sleep and wake profiles (Ghosh and Rihel, 2020), which could account for the individual variability in synapse dynamics we observed in our data. We therefore chose to simultaneously track sleep/wake behaviour and synapse dynamics in the same animal to see if the variability and diversity in synapse dynamics was dependent on the animal's waking and sleep experience.

Using behavioural tracking similar to (Rihel et al., 2010), we tracked individual larval sleep wake behaviour and repeatedly imaged tectal neuron synapse dynamics in the same animal. Larvae were screened for positive FoxP2:FingR(PSD95) cells at 6dpf and then placed into six-well plate for behavioural tracking from 6dpf-8dpf. After a day and night of baseline acclimatization, larvae were subsequently imaged around ZT0 (lights on) on 7dpf, ZT10 on 7dpf, and again at ZT0 on 8dpf, similar to previous experiments (Figure 4.11A). Larvae with irregular swimming behaviour during baseline day and night or with abnormal locomotor activity after imaging were excluded from the analysis.

The synapse dynamics of tectal neurons in tracked zebrafish larvae were consistent with what we observed in previous experiments: synapse number increased during the day phase and

decreased or stabilized overnight (Figure 4.11B). Although consistent, the changes are not as pronounced as we observed in previous experiments, possibly due to changes in lighting or temperature between the incubator used for initial experiments and the behavioural rig used in the current experiments.

In normal LD conditions, average activity during the day and night phase show no correlation with synapse dynamics of the same period (Figure 4.11B, r^2 = 0.026 and 0.054 for day and night, respectively). Total sleep time during the day showed a weak correlation with percentage change in number of synapses over the day phase (r^2 =0.29, Figure 4.11C), i.e. the more the fish sleeps during the day, the higher chance that tectal neurons will lose their synapses. However, visual inspection of the data revealed that this correlation is highly influenced by a few larvae that had high levels of sleep during the day time. Intriguingly, there is no correlation between total sleep time and synapse dynamics during the night. (r^2= 0.001, Figure 4.11C), suggesting that longer sleep does not translate to increases in downscaling.

Together these findings showed that the length of time larvae spent sleeping and their activity levels during wakefulness do not have a linear relationship with their synapse number in tectal neurons, suggesting that wakefulness and sleep effects on synapse dynamics are more complex than some simpler versions of SHY. For example, synapse changes may be non-linearly related to prior sleep/wake time, with sleep at the beginning or the end of the night having a differential effect on synapse dynamics, or periods of extended wakefulness having a stronger effect on synapse strengthening than a normal bout of waking.

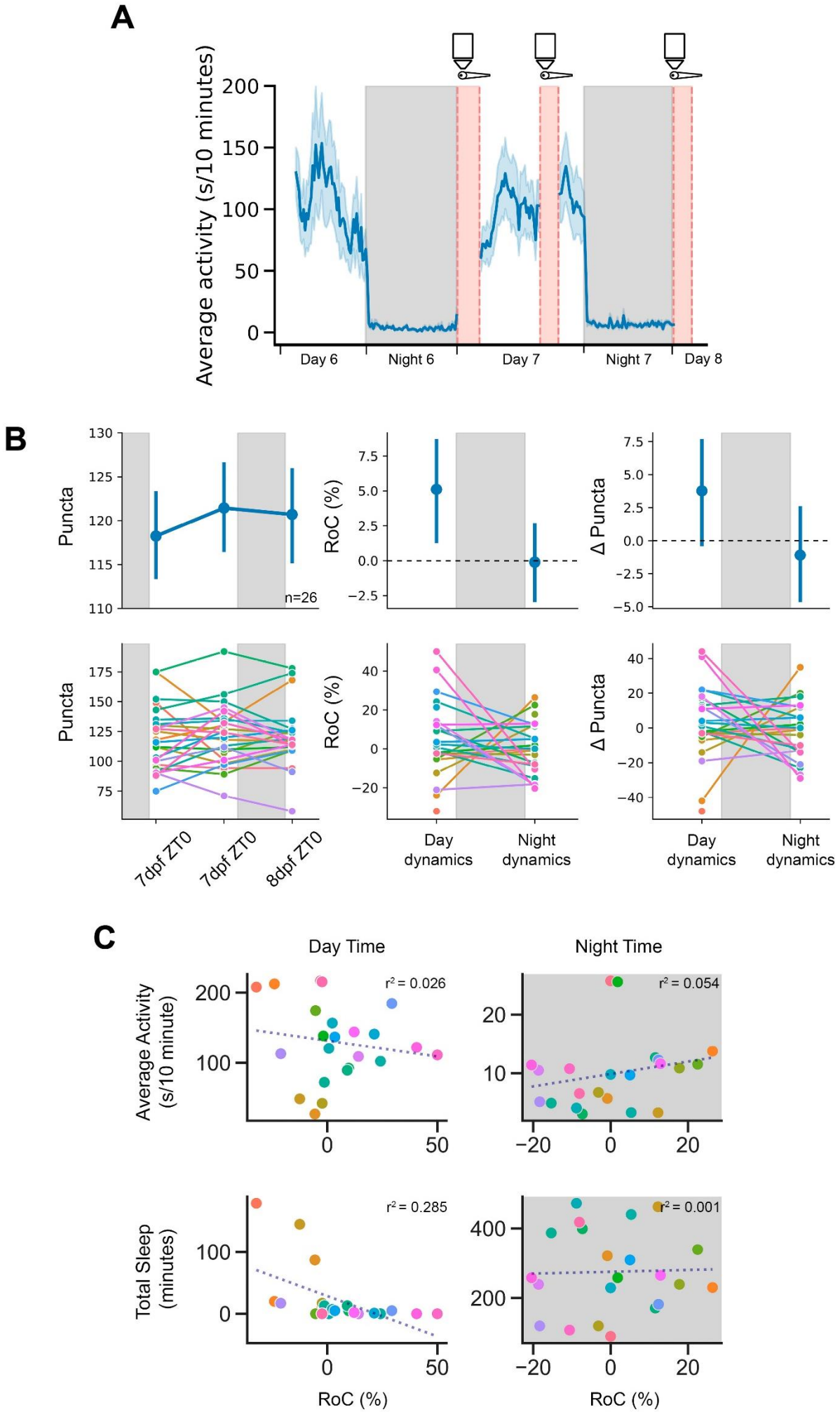
A
Average activity (s/10 minutes)
200
150
100
50
0
Day 6
Night 6
Day 7
Night 7
Day 8
B
Puncta
130
125
120
115
110
n=26
RoC (%)
7.5
5.0
2.5
0.0
−2.5
Δ Puncta
7.5
5.0
2.5
0.0
−2.5
−5.0
Puncta
175
150
125
100
75
7dpf ZT0
7dpf ZT0
8dpf ZT0
RoC (%)
40
20
0
−20
Day dynamics
Night dynamics
Δ Puncta
40
20
0
−20
−40
Day dynamics
Night dynamics
C
Day Time
Night Time
Average Activity (s/10 minute)
200
100
0
50
r² = 0.026
20
10
−20
0
20
r² = 0.054
Total Sleep (minutes)
100
0
0
50
r² = 0.285
400
200
−20
0
20
r² = 0.001
RoC (%)
RoC (%)

Figure 4.11: Synapse dynamics do not correlate with total sleep and wake experience. A) Schematic of behavioural and synapse tracking experimental set up. Larval locomotor behaviour was tracked on a 14hr:10hr LD cycle from 6-8dpf. The average activity (±68% confidence interval) of 10 example larvae are plotted. The red panels indicate the imaging period (ZT0 (lights on) and, ZT 10), when larvae were removed from sleep/wake tracking to image synapse dynamics. White and gray boxes indicate lights ON/OFF periods, respectively. B) Synapse number dynamics of behaviourally tracked LD larvae. The top row shows average dynamics across all imaged neurons while bottom row shows individual neurons. Each coloured line represents a single neuron in a single larva. Left column: Puncta count through 7-8dpf at ZT0 and ZT10. Middle column: Rate of change (RoC) of day and nights dynamics. Right column: absolute number of FingR(PSD95) puncta gained or lost over the day and night phase. C) Synapse dynamics have no correlation with sleep and waking activity. Top row: Scatter plot of average activity (s/10minutes) against synapse number RoC during the day (left) and night phase (right). Bottom row: Scatter plot of total sleep in minutes against synapse number RoC during the day (left) and night phase (right).

4.9 SLEEP DEPRIVATION INCREASE NUMBER OF SYNAPSES COMPARE TO CONTROLS

Under clock break conditions, the sleep-wake rhythm is also eliminated, while in free running conditions, the sleep-wake cycle will remain intact. Therefore, to distinguish whether sleep/wake states per se affect synapse number, we must compare synapse number dynamics in larvae that have been sleep deprived to control larvae that were allowed to have bone fide sleep. This experiment ensures that the circadian phase is relatively undisturbed between conditions but only the sleep/wake state will be altered. We sleep deprived (SD) larvae via a new gentle handling method under a red light for 4h at the beginning of the night (ZT14-18) (Figure 4.12A, see Methods 2.5.6). To confirm that this paintbrush method leads to changes in sleep homeostasis, we first examined the amount and structure of sleep immediately following the sleep deprivation paradigm. To control for larva to larva variation, we normalized for each larva the total sleep and average sleep bout length in the 6 hours following gentle handling (ZT18-24) to the prior, undisturbed, circadian-matched night. Larvae that experienced gentle handling on average had increased both total sleep and average sleep bout length compared to controls (Figure 4.12B-D; p =0.044 and 0.013 Student T-test, respectively). This is consistent with the observation that extended wakefulness is followed by longer and more intense rebound sleep (Borb and Achermann, 1999), suggesting that our gentle handling paradigm increased sleep pressure and is therefore a bona fide sleep deprivation technique that alters sleep homeostasis.

Next, we tracked FingR puncta throughout the night in 4hr-SD and control larvae, immediately after a full waking day but before the SD window (ZT13-14,7dpf), immediately after the SD (~ZT18,7dpf), and again in the morning (ZT0, 8dpf, Figure 4.13). In control larvae, we found that synapse number decreases from the beginning of the night to the end of the night. However, the bulk of synapse loss occurs in the first four hours of the night, when the average puncta loss is -4.94 puncta (average RoC of -4.49%), compared to the latter half of the night, when the average puncta change is 0.44 puncta (average RoC of 4.09%, Figure 4.13). In contrast, immediately after sleep deprivation, the neurons on average gained 11.73 more puncta with the average RoC of 12.42%. This increased RoC and delta synapses is significantly different from the decreased RoC in control larvae (Figure 4.13C, p=0.011 two-way mixed ANOVA with Greenhouse-Geisser corrections and post hoc pairwise-Student's t-tests find

statistical significance of p=0.007 at ZT18). However, during the six hours larvae were allowed to sleep post deprivation, the synapse number decreases, with a significant RoC of -7.22% and losing an average of -11.24 puncta (p=0.024 and 0.013, repeated-measures ANOVA with Greenhouse-Geisser correction, respectively). This decrease post sleep deprivation is more similar to the reduction in synapse number at the beginning of the control night than later in the evening, suggesting that the intensity of sleep pressure, which is high at the start of the night/immediately after SD, is influencing the rate of synapse loss.

These findings demonstrated that overall synapse number decrease at beginning of night and stabilize later in night, while extended waking alone (with the intact circadian clock and similar lighting condition) increases synapse number. Sleep rebound post-SD can reduce number of synapses regardless of circadian time. While consistent with SHY, our findings suggested that not all sleep is equally important for driving synapse dynamic but that sleep during high sleep pressure such as at sleep onset can drive overall reduction in synapse number.

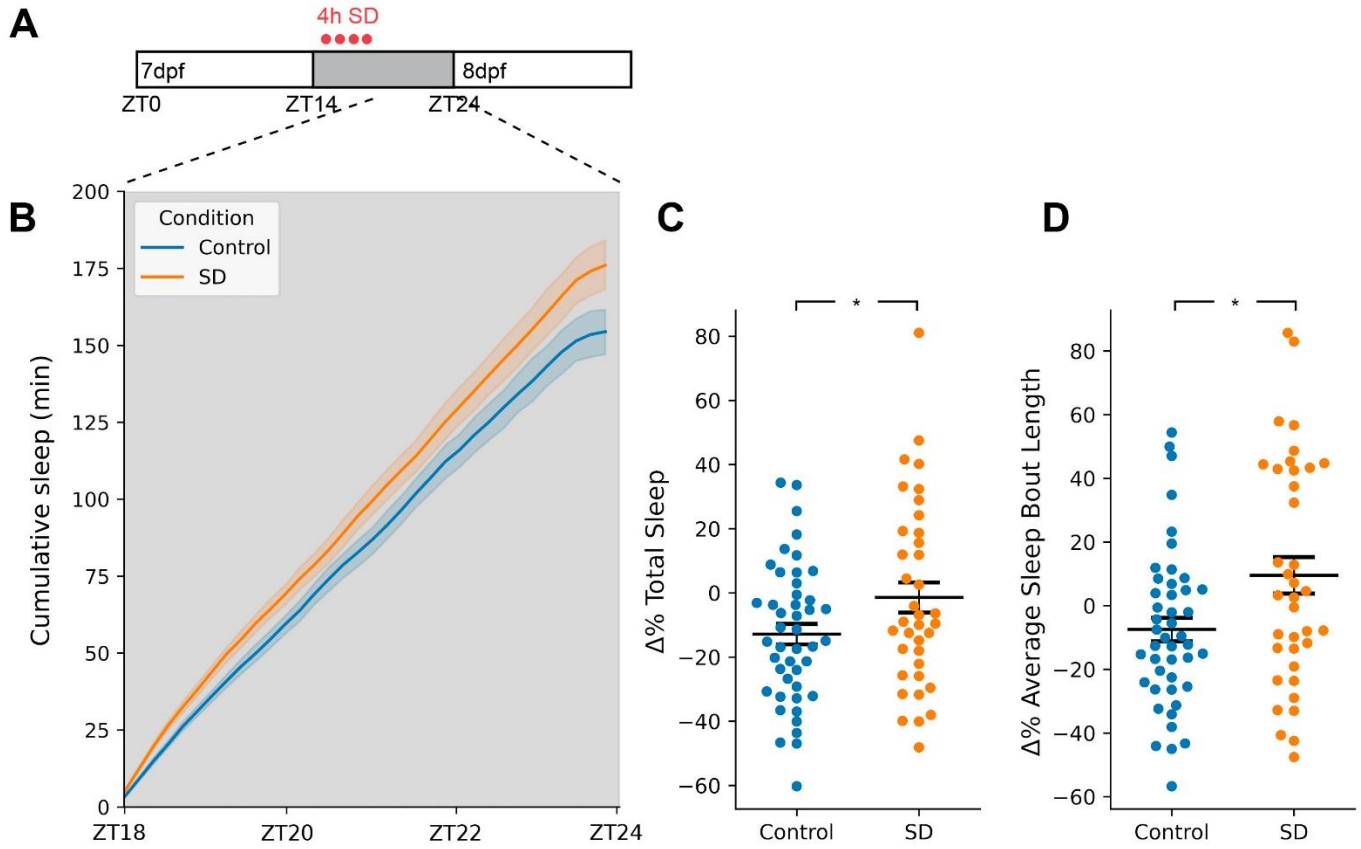

Figure 4.12: Gentle handling sleep deprivation paradigm increase average total sleep and sleep bout length. A) Schematic of sleep deprivation by gentle handling paradigm. Animals were subjected to gentle handling using paintbrush under red light for 4 hours from ZT14 (light off) to ZT18. B) Cumulative sleep during rebound phase following SD paradigm (±68% confidence interval). C) Percentage change of total sleep of each larva between ZT18-24 (post SD) and circadian-matched time on 6dpf. D) Percentage change of average sleep bout length of each larva between ZT18-24 (post SD) and circadian-matched time on 6dpf. Each dot represents a single larva. *$p<0.05$, Student T-test. Black line indicates population average ± standard error of the mean.

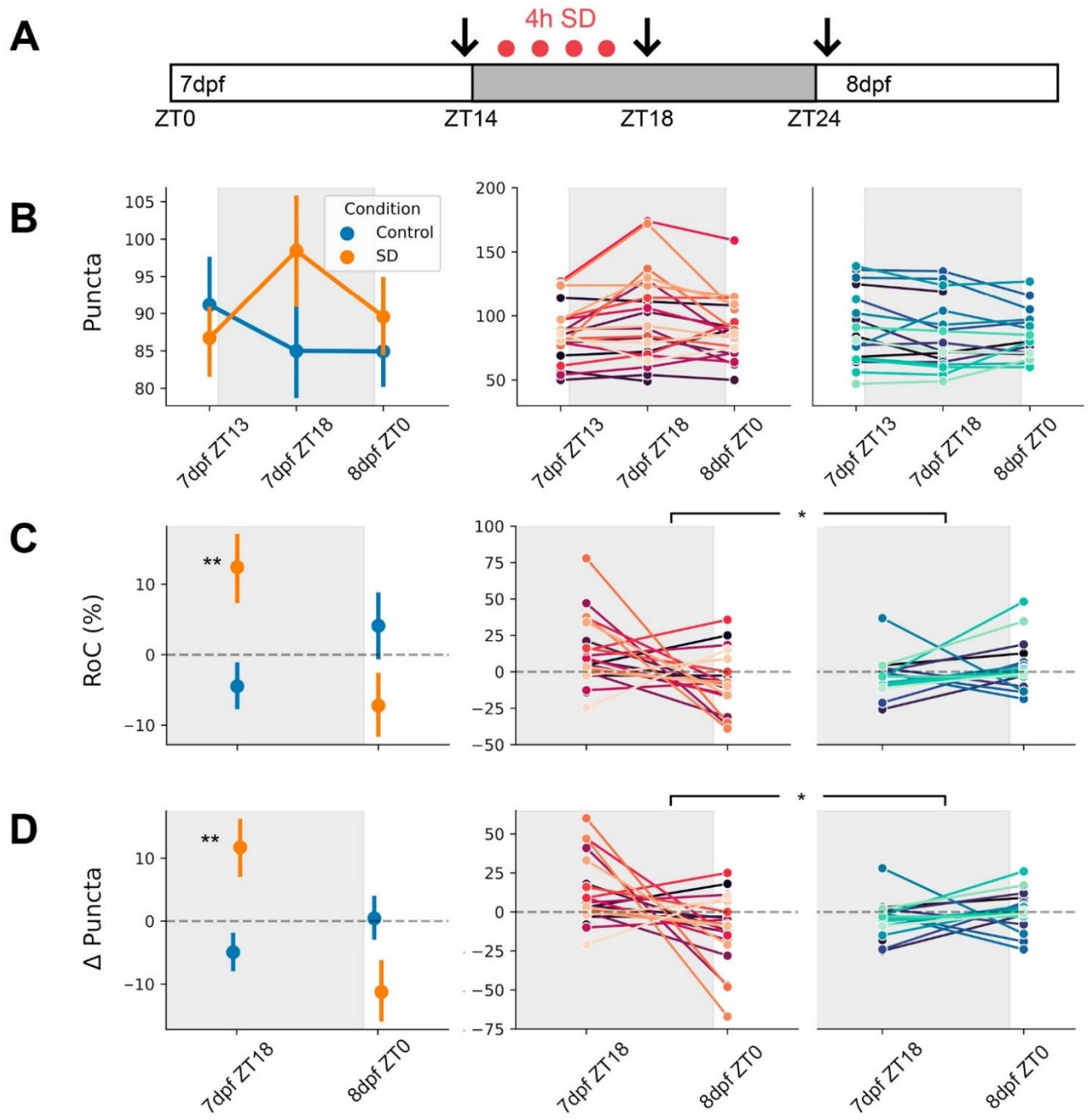

Figure 4.13: Sleep deprivation increase FingR puncta number compare to controls in FoxP2+ tectal neurons. A) Schematic of sleep deprivation and synapse tracking experimental set up. Larval locomotor behaviour was tracked on a 14hr:10hr LD cycle from 6-8dpf. The black arrows indicate the imaging periods (ZT14 (lights off), ZT 18on 7dpf, and ZT0 at 8dpf), when larvae were removed from sleep/wake tracking to image synapse dynamics. Red dots indicate sleep deprivation period (ZT14-18, 7dpf). White and gray boxes indicate lights ON/OFF periods, respectively. B) Puncta count of sleep deprived and control larvae (n=22 and 19, respectively). C) Rate of change (RoC %) during the night of sleep deprived and controls larvae. D) Absolute number of FingR(PSD95) puncta gained or lost over the night phase per neuron in sleep deprived and control larvae. Left panel: average dynamics across all imaged neurons. Middle and right panels: individual neurons of sleep deprived (orange) and control (blue) larvae. *p<0.05, **p<0.01; two-way mixed ANOVA with pairwise T-test.

Chapter 5 The Hypocretinergic system

5.1 CHARACTERIZATION OF THE HYPOCRETINERGIC SYSTEM

In the previous chapters, we demonstrated the utility of new synaptic tools to study synapse dynamics in visual neurons of zebrafish larvae. However, to fully realize the potential of zebrafish imaging to investigate the Synaptic Homeostasis Hypothesis (SHY), comprehensive studies of different types of neurons synapse dynamics during sleep and wake behaviour are needed. It would be interesting to see whether SHY applies to other types of neurons, such as those in the hypothalamus that have inputs from various brain regions, widespread efferent fibres throughout the brain, and roles in various behavioural regulation.

The majority of studies that address SHY have examined cortical neurons (Vyazovskiy *et al.*, 2008; Liu *et al.*, 2010; de Vivo *et al.*, 2017; Cary and Turrigiano, 2021). While a few studies have looked at brain-wide or subcortical-equivalent regions for evidence of SHY (Gilestro *et al.*, 2009; Appelbaum *et al.*, 2010; Elbaz *et al.*, 2016), these studies lacked spatial resolution or used methodologies with unwanted overexpression effects (see Chapter 1). Although we examined synapse dynamics of zebrafish tectal neurons, which is akin to the mammalian superior colliculi rather than the cortex, we would like to systematically image synapse dynamics on neurons much deeper in the brain such as in the hypothalamus. We also want to image synapse dynamics on neurons with different morphologies—the tetcal neurons send only modest projections within the tectum, while many other neuron types spread across the brain in great distances, adding to the imaging challenges.

One set of neurons that would be interesting to investigate are neurons of the sleep/wake regulatory circuits, where sleep pressure (i.e. effects of prior duration of wakefulness on sleep need) and circadian clock regulation are tightly linked to sleep effector neurons. One such neuronal type are the Hypocertin (Hcrt, also known as Orexins) neurons within the hypothalamus. To investigate whether SHY exists in these neurons, we need to better characterize the Hcrt circuit in larval zebrafish. The aim of this chapter is to provide a platform for synaptic investigation of Hcrt neurons by mapping their projections, both as a population and at the single-cell level.

5.2 A NOVEL HCRT:KALTA4 TRANSGENE LABELS HCRT NEURONS

A Tg(Hcrt:KalTA4) transgenic zebrafish line was generated (see Methods 4.2.1). This novel transgenic line allows the expression of various reporter genes in Hcrt neurons that the existing Tg(Hcrt:GFP) does not (Appelbaum, G. X. Wang, *et al.*, 2009). For example, it allows the expression of live synaptic markers such as the FingR systems (see Chapter 2). It also allows for single cell labelling.

To verify that the KalTA4 expression pattern of Hcrt:KalTA4 recapitulates that of Hcrt protein, we crossed Tg(Hcrt:KalTA4) with Tg(UAS:RFP;cry:GFP) to visualize Hcrt neurons in RFP. We then performed double immunohistochemistry using an Orexin A antibody (which labels Hcrt cells) and anti-RFP on dissected 6dpf larvae. Hcrt:KalTA4 driving RFP expression colocalized with all Orexin A antibody expression in all neurons (Figure 5.1).

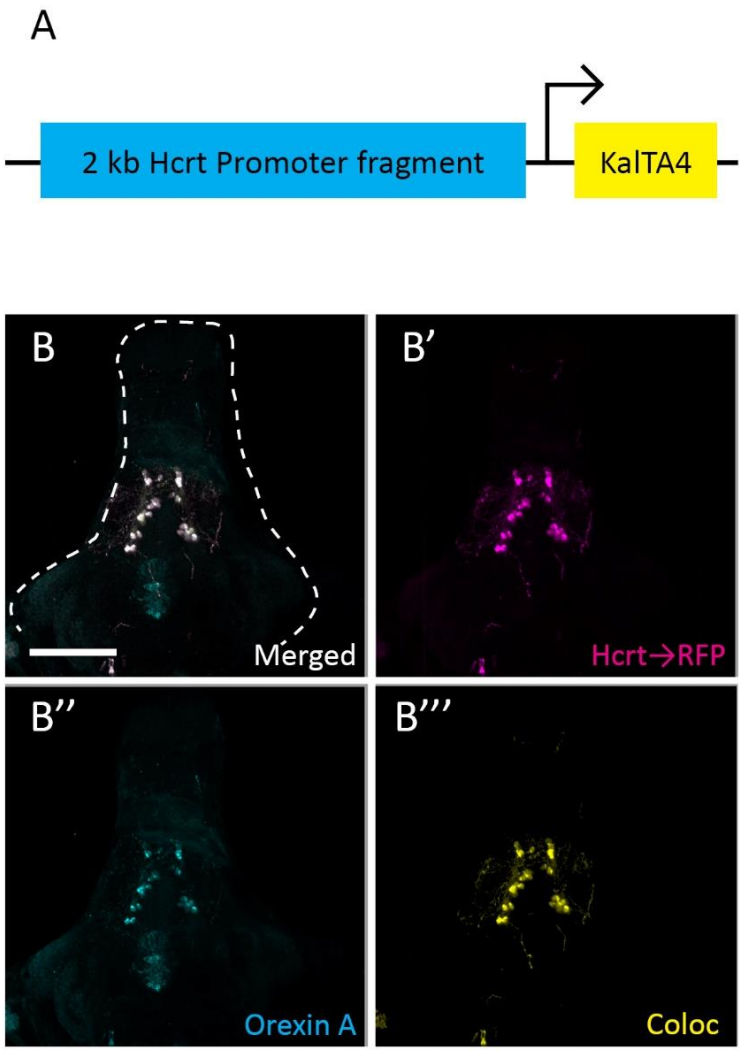

Figure 5.1: A new hypocretin transgenic line labels Hcrt/orexin cells. A) Diagram of pBR-Tol2-Hcrt:KalTA4 construct. B) Immunohistochemistry of RFP (magenta) and Orexin A/Hcrt (cyan)

expression in a dissected 6dpf larval zebrafish brain, ventral view. B'-B") All Orexin A expressing neurons also express RFP. The previously reported unspecific binding of Orexin A antibody posterior to Hcrt neuronal cell bodies (Kaslin, 2004; Prober et al., 2006) is not observed in the transgenic line. B"') The colocalization of RFP and Orexin A signal (yellow) shows complete overlap of both signals in Hcrt neurons. n=5/5. Scale bar 100µm. Hcrt →RFP denotes Hcrt:KalTA4; UAS:RFP.

5.3 COMPLEX HYPOCRETINERGIC PROJECTIONS ARE PRESENT DURING EARLY DEVELOPMENT IN LARVAL ZEBRAFISH

To establish the time window in which the projection patterns of Hcrt neurons become stabilised, we characterized Hcrt cell projections during development. Examination of RFP expression in transgenic fish at different ages revealed that Hcrt neurons form long and complex projections as early as 3 days post-fertilization (dpf). At 3dpf, Hcrt neurons form dense axon bundles that innervate the hypothalamus and send projections that travel dorsally to the optic tectum (OT), rostrally to the telencephalon (Tel), and caudally to the spinal cord (Figure 5.2). By 6dpf Hcrt neurons innervate the OT and have formed dense bundles at the locus coeruleus (LC). By 10dpf, Hcrt neurons also heavily innervate the hypothalamic neuropil and hindbrain.

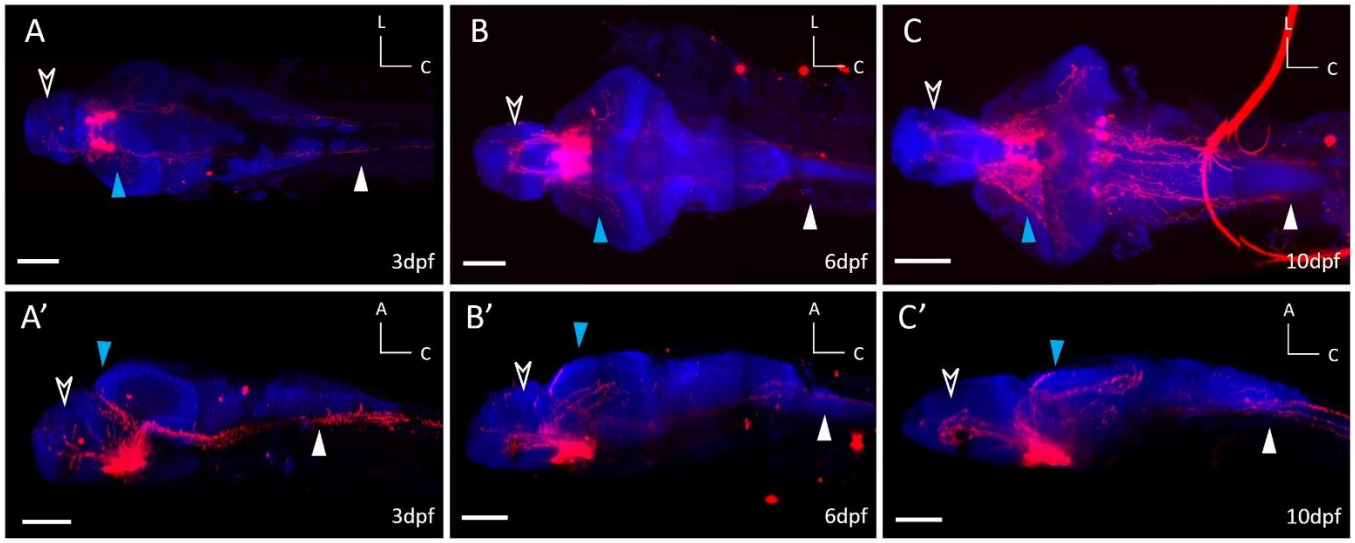

Figure 5.2: Brain-wide projections of Hcrt-positive cells in the developing zebrafish. Hcrt+ neurites expressing RFP are red; nuclei are counter-stained in blue. A-C) Dorsal and lateral view of 3, 6, and 10dpf larval brains. Growing neurites projecting towards the tectum (blue arrow). Dense projection towards spinal cord (white arrow). Projections innervating the telencephalon (white open arrow). A:anterior, C: caudal, L: lateral. Scale bar 100µm.

5.4 HCRT NEURON PROJECTIONS ARE STEREOTYPIC

To observe the inter-individual variability of Hcrt neuron projections, image stacks of immunostained Tg(Hcrt:KalTA4;UAS:RFP) 7dpf embryos were registered into one common reference stack (see 4.2.6 Methods). The positions of Hcrt neurons projections and cell bodies were found to be highly stereotypic, as evidenced by the tight colocalization in the registered sample. For example, the Hcrt positive somata are restricted to the lateral hypothalamus in v-shaped bilateral pairs (Figure 5.3C). However, it has been observed that age-matched larvae have different numbers of Hcrt-expressing cells, ranging from 7-8 on each side to 13-14 cells. The average total number of Hcrt+ cells per larvae is 19.1 ±1.5 cells (n=10 larvae, standard error, Figure 5.4). However, some larvae have 11 Hcrt+ neurons while others can have up to 25 neurons.

In the telencephalon, Hcrt+ neurites were found along the lateral forebrain bundles (LFBs) and crossing at the anterior commissure (AC) and medial olfactory track (Figure 5.3B), towards the ventral telencephalon/subpalium and olfactory bulb. In the diencephalon, Hcrt neurons had dense local projections within the hypothalamic neuropil and crossed the post-optic and horizonal commissures (Figure 5.3A-B). Only some larvae showed innervation of Hcrt+ projections towards the epithalamus (n=2/5 larvae) (Figure 5.2E). In the mesencephalon, all specimens had Hcrt+ neurites across project the anterior part of tectal commissures, along both sides of tectal neuropil border, and throughout the tegmentum (Figure 3.3A). In the hindbrain, Hcrt+ tracks were found throughout the medulla oblongata but not within the cerebellum. Dense fibres were found in the LC and in the spinal cord (Figure 5.3A-B and E). All the specimens examined projected Hcrt+ neurites across this same path; however, some also projected across the midline more rostrally and caudally in addition to the main tracks.

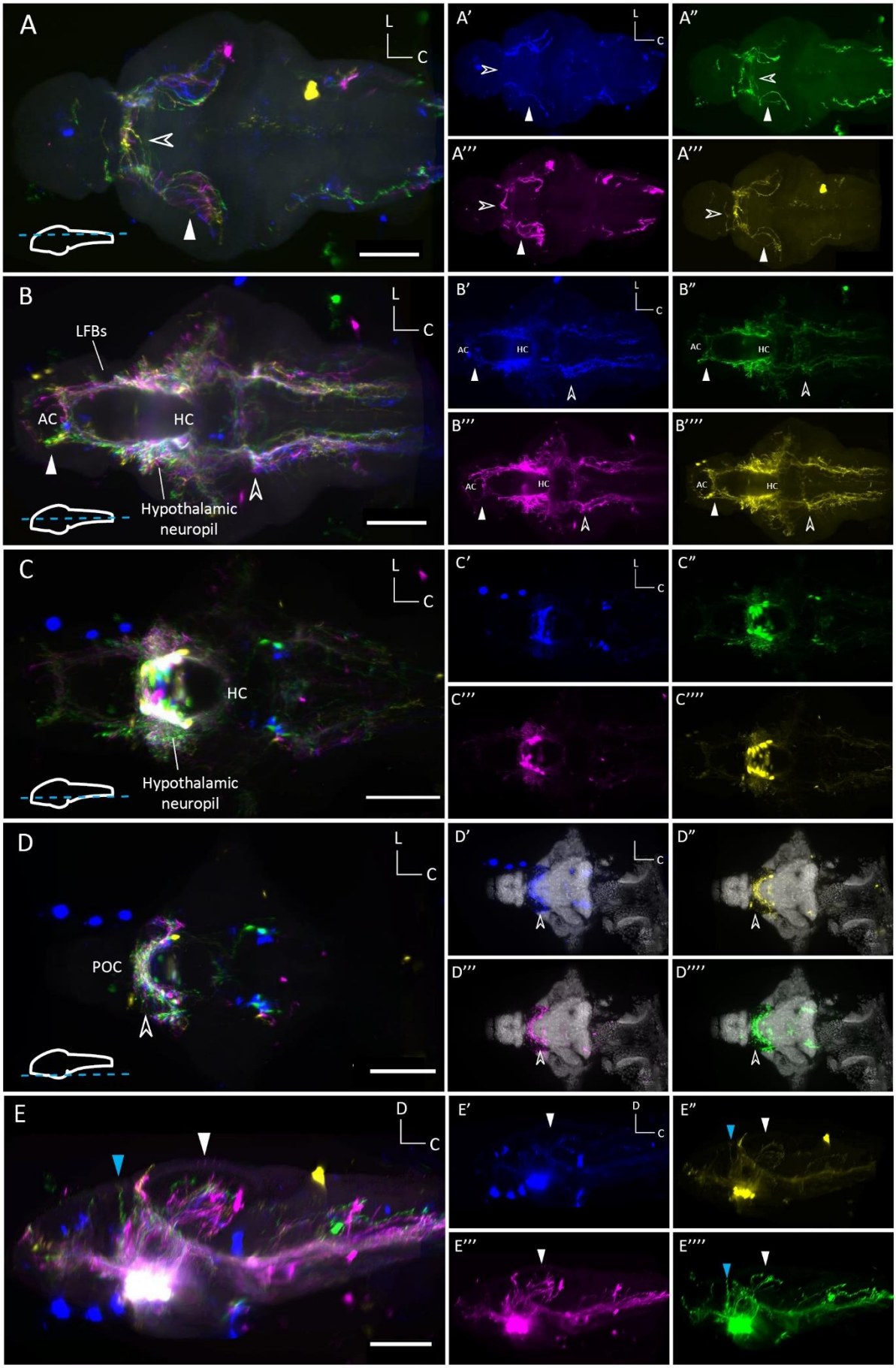
A
L
C
A'
A''
A'''
A''''
B
LFBs
AC
HC
Hypothalamic
neuropil
B'
B''
B'''
B''''
C
C'
C''
C'''
C''''
D
POC
D'
D''
D'''
D''''
E
D
E'
E''
E'''
E''''

Figure 5.3:The locations of Hcrt-positive cell somata, innervations, and tracks are highly stereotypical at 7dpf. A-D) Horizontal section of 3D registered common brain. Each panel depicts a section through the brain as indicated by the blue dotted line on the larval brain illustration from the most dorsal to most ventral. A) Horizontal section through the most dorsal part of the larval brain. 3D registration of all stacks into one common brain shows Hcrt neurites project to the OT and OT commissure in all animals observed. A'-A'''') Maximum projection at the level of the OT and Hcrt neurons innervation patterns shown by immunohistochemistry in four different 7dpf larvae represented by different colors. Hcrt neurons stereotypically project to both sides of the tectum (white arrow). All specimens show Hcrt neurites crossing the tectal commissure (open arrow), although some do so more caudally or rostrally than others. B) Horizontal section through the midbrain. 3D registration of all stacks into one common brain shows Hcrt positive fibres innervating stereotypical commissures and tracks. All specimens show stereotypic innervation at anterior commissure (AC), lateral forebrain bundles (LFBs), horizontal commissures, hypothalamic neuropil, locus coeruleus (LC, open arrow), and telencephalon (white arrow). B'-B'''') Maximum projection around hypothalamic neuropil showing Hcrt innervation patterns in four different larvae in the same view. C) Horizontal section through the brain at the level of the hypothalamus. 3D registration of all stacks into one common brain shows Hcrt-positive cell bodies in a stereotypic location and Hcrt+ cells in all specimen crosses at horizontal commissures (HC). C'-C''') Maximum projection around Hcrt cell bodies and their innervation patterns. D) Horizontal section through the most ventral part of the larval brain. 3D registration of all stacks into one common brain shows Hcrt neurites crossing post-optic commissure in all animal. D'-D'''') Maximum projection at the level of post-optic commissures and Hcrt innervation patterns (arrow) from four different larvae. E) Lateral view of registered larvae at 7dpf. E'-E''') Lateral view of Hcrt projections in four different larvae. Only some larvae show innervation of Hcrt towards the epithalamus (blue arrow). Scale bar 100µm.

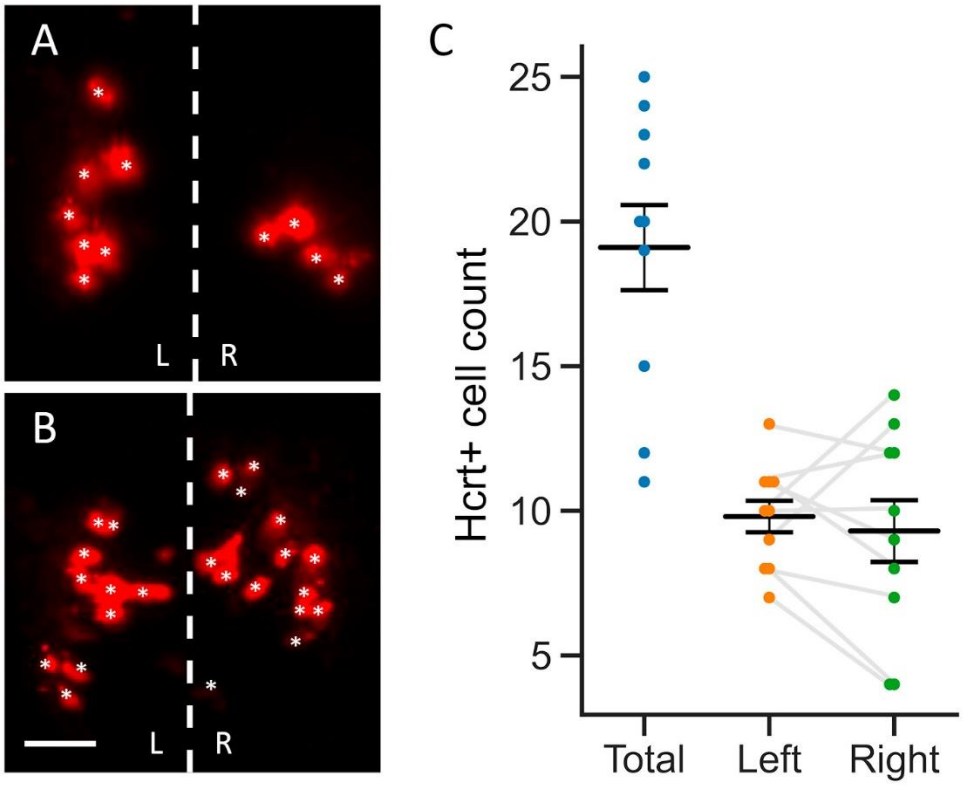

Figure 5.4: Variability of Hcrt cell counts in age-matched larvae. A) Example of Hcrt cells in 7dpf larvae showing 7 and 4 cells on the left and right side, respectively. B) Example of Hcrt cells in another 7dpf larvae showing 10 and 14 cells on the left and right side, respectively. Cell body marked by asterisks. C) Graph showing the number of Hcrt+ cells observed in total, the left, and the right side in different larvae at 7dpf. Light grey lines indicate left and right sides cell number of the same fish.

5.5 HCRT NEURITES PROJECT TO THE DEEPEST TECTAL NEUROPIL LAYER

Brain registration maps of Hcrt projections show extensive and consistent Hcrt innervation of the OT, the zebrafish homologue of the mammalian superior colliculus, at 7dpf (Figure 5.5A). As discussed in Chapter 3, the OT is a centre for visual processing. The OT has a highly laminar structure with inputs from the retina targeting precise sublayers of the neuropil in a retinotopic fashion across its rostrocaudal and mediolateral dimensions (Stuermer, 1988). We asked whether Hcrt innervation to the OT is layer specific. To investigate this, the Tg(Hcrt:KalTA4;UAS:RFP) fish that label the Hcrt neurons were crossed to Tg(Ath5:GFP) fish, in which the tectal neuropil are labelled with GFP. Atonal homolog 5 (Ath5 also known as Atoh7) is a basic helix-loop-helix transcription factor that is required for eye specification in zebrafish (Kay *et al.*, 2001). Ath5 projection patterns allow the demarcation of two tectal laminae: the stratum fibrosum et grisum superficialcentrale (SFGS) and the (SAC)/stratum griseum periventriculare (SPV). Figure 5.5 illustrates that Hcrt projections ramify within the deepest laminae of the tectal neuropil, the SAC/SPV. This is clearly shown in Figure 5.5C where Hcrt project along the border of tectal cell bodies or the SAC. This is quantified in Figure 5.5B where the strongest signal from the Hcrt:RFP channel coincides with the SAC/SPV laminae.

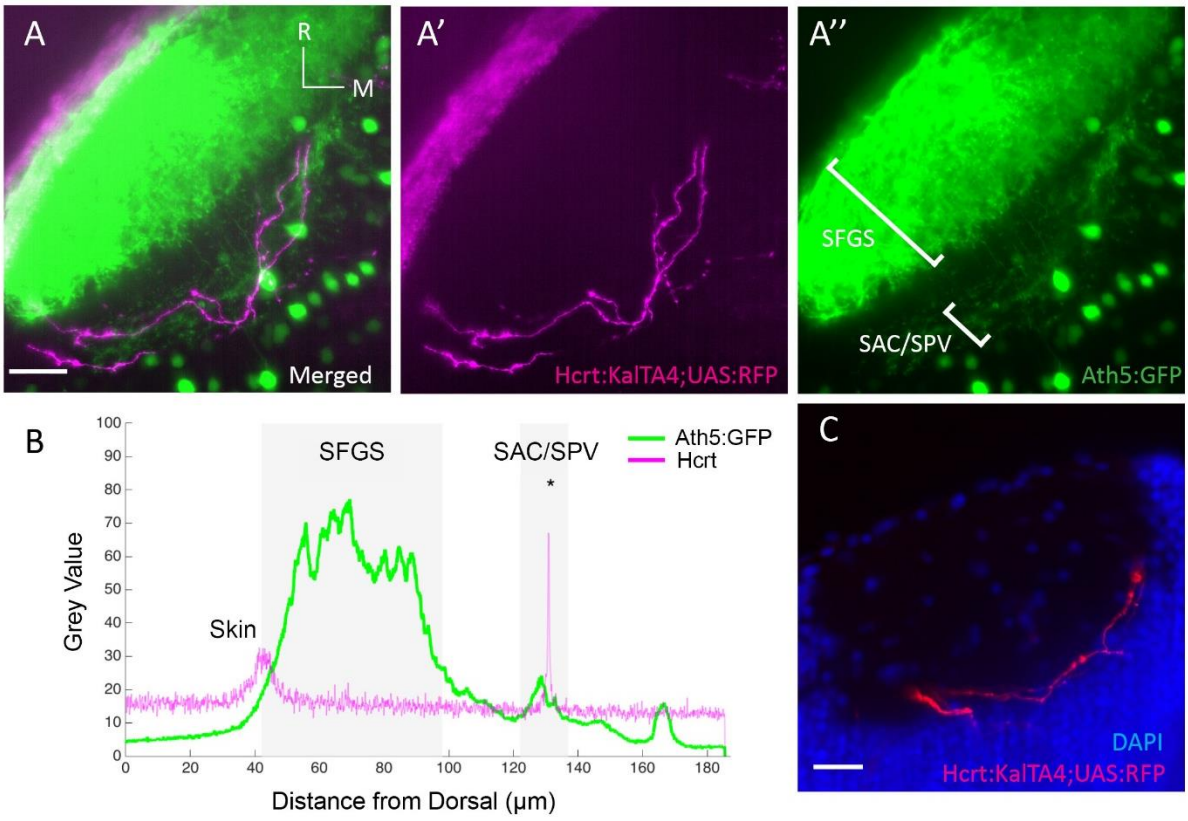

Figure 5.5: Hcrt neurites innervate the tectal layer SAC/SPV. A) Live imaging maximum projection of the left tectum of Hcrt:KalTA4; UAS:RFP; Ath5:GFP larvae at 7dpf. A') Hcrt neurite (magenta) and autofluorescence of the skin (top left). A") Ath5:GFP channel (green) showing SFGS and SAC/SPV layers. B) Quantification of the fluorescence signal from 3D stacks of RFP channel (magenta) and GFP channel (green) in panel A. The RFP signal peak coincides with the SPV/SAC layer peak in GFP. Note that the small peak at 40µm from the RFP channel represents autofluorescence signal from the skin. C) Single slice from immunostained Hcrt driving RFP larvae (red) with DAPI (blue) showing single neuron track along the SAC/SPV border, dorsal view. R: rostral, M: medial. Scale bar 20µm.

5.6 HCRT NEURITES PROJECT TO THE LC AND RAPHE NUCLEI

To verify that Hcrt neurites project to the locus coeruleus and the raphe nuclei, as previously described in zebrafish and mammals (Peyron *et al.*, 1998; Kaslin, 2004; Prober *et al.*, 2006), the Tg(Hcrt:KalTA4; UAS:RFP) fish were crossed with Tg(ETVmat2:GFP) fish, which labels both nuclei. Vmat2 is an integral membrane protein that transports monoamines from cellular cytosol into synaptic vesicles. It is vital for the function of neurotransmitters such as dopamine, norepinephrine, serotonin, and histamine (Wen *et al.*, 2008) and serves as a marker for these neuron populations. Figure 5.6 shows that Hcrt neurites project to and wrap around the both LC and raphe nuclei. Although this does not demonstrate functional connectivity, the tight anatomical association is strongly consistent with functional connection between the Hcrt and noradrenaline from the LC in rodents and zebrafish (Gompf and Aston-Jones, 2008; Carter *et al.*, 2012; Singh, Oikonomou and Prober, 2015).

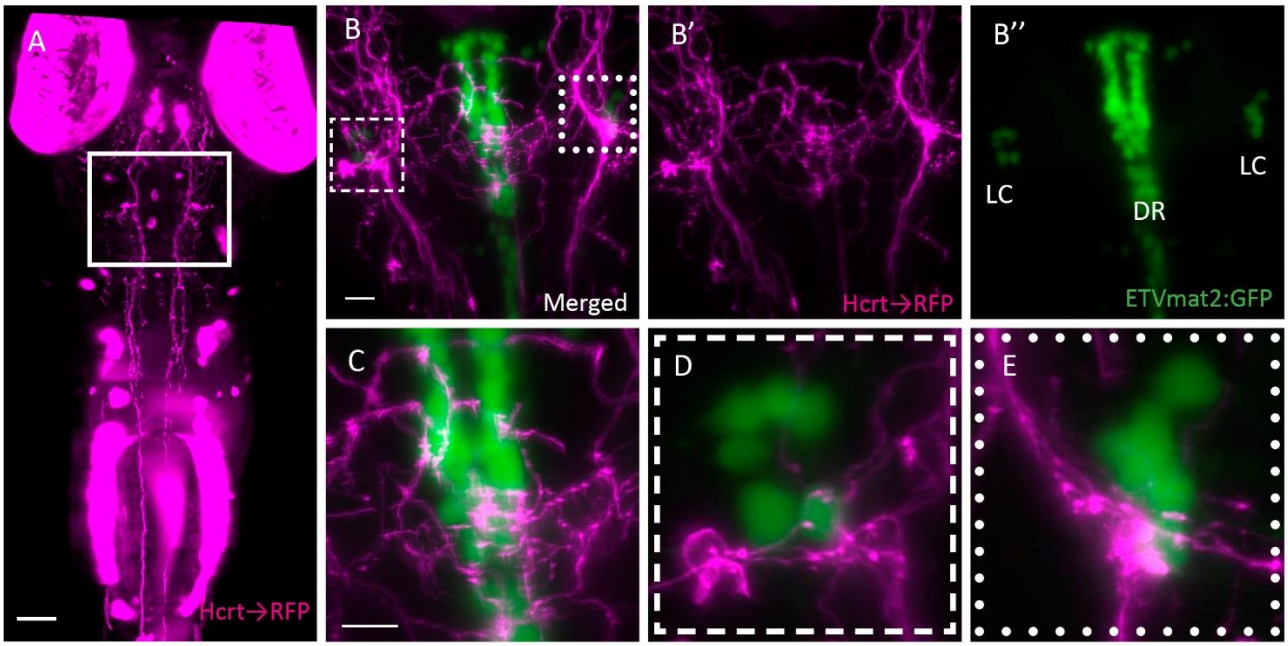

Figure 5.6:Hcrt neurites send extensive neurites to the raphe nuclei and both LCs in ETVmat2:GFP larval fish at 7dpf. A) Dorsal view of maximum projection of Hcrt cells morphology (magenta) of a different larva to illustrate where the panel B-E were taken are in relation to the fish. Scale bar = 100µm. B) Projection through the midbrain of ETVmat2:GFP; Hcrt:KalTA4; UAS:RFP fish from white box in panel A. The Hcrt neurites are in magenta, the locus coreleus (LC) and dorsal raphe (DR) in green. The RFP and GFP channels are separated in B' and B", respectively. C) A magnified image showing Hcrt processes (magenta) innervating the raphe nuclei (green). D-E) Hcrt neurites (magenta) wrapping around cells of the left and right LC (green). The areas of focus are shown as white dashed and dotted boxes in B. Hcrt →RFP denotes Hcrt:KalTA4; UAS:RFP. Scale bar = 20µm in B,C.

5.7 HCRT NEURONS DO NOT PROJECT TO THE HABENULAE BUT COLOCALIZE WITH ITS TRACKS AT THE VENTRAL INTERPEDUNCULAR NUCLEUS

We found that Hcrt neurons send projections to the raphe nuclei, but they also have extensive neurites in the mesencephalon. Therefore, we wanted to know what other areas of the midbrain received Hcrt neurites. To examine possible projections to the habenular nuclei, we crossed the Tg(Hcrt:KalTA4; UAS:RFP) fish with Tg(Gng8:GFP) fish, which express GFP in the dorsal habenula and along its axonal tracks that wrap around the interpeduncular nucleus (IPN) (Figure 5.7A) (Hong *et al.*, 2013). Figure 5.7B shows that the Hcrt neurons do not send projection to the habenulae at 5dpf (n=3/3). Hcrt fibres project antereo-dorsally towards the habenulae but cross the midline along the posterior commissure in the pretectum instead of continuing to the habenulae. Figure 5.7C shows that Hcrt neurites do however colocalize with the habenular tracks that wrap around the ventral IPN (n=3/3). As the colocalization is small and Tg(Gng8:GFP) only labels the habenular tracks and not the IPN proper, we cannot conclude that Hcrt neurons project into vIPN. The dorsal habenular – vIPN have been shown to be involved in food-seeking and food-induced social conflicts behaviour (Chen *et al.*, 2019; Nakajo *et al.*, 2020).

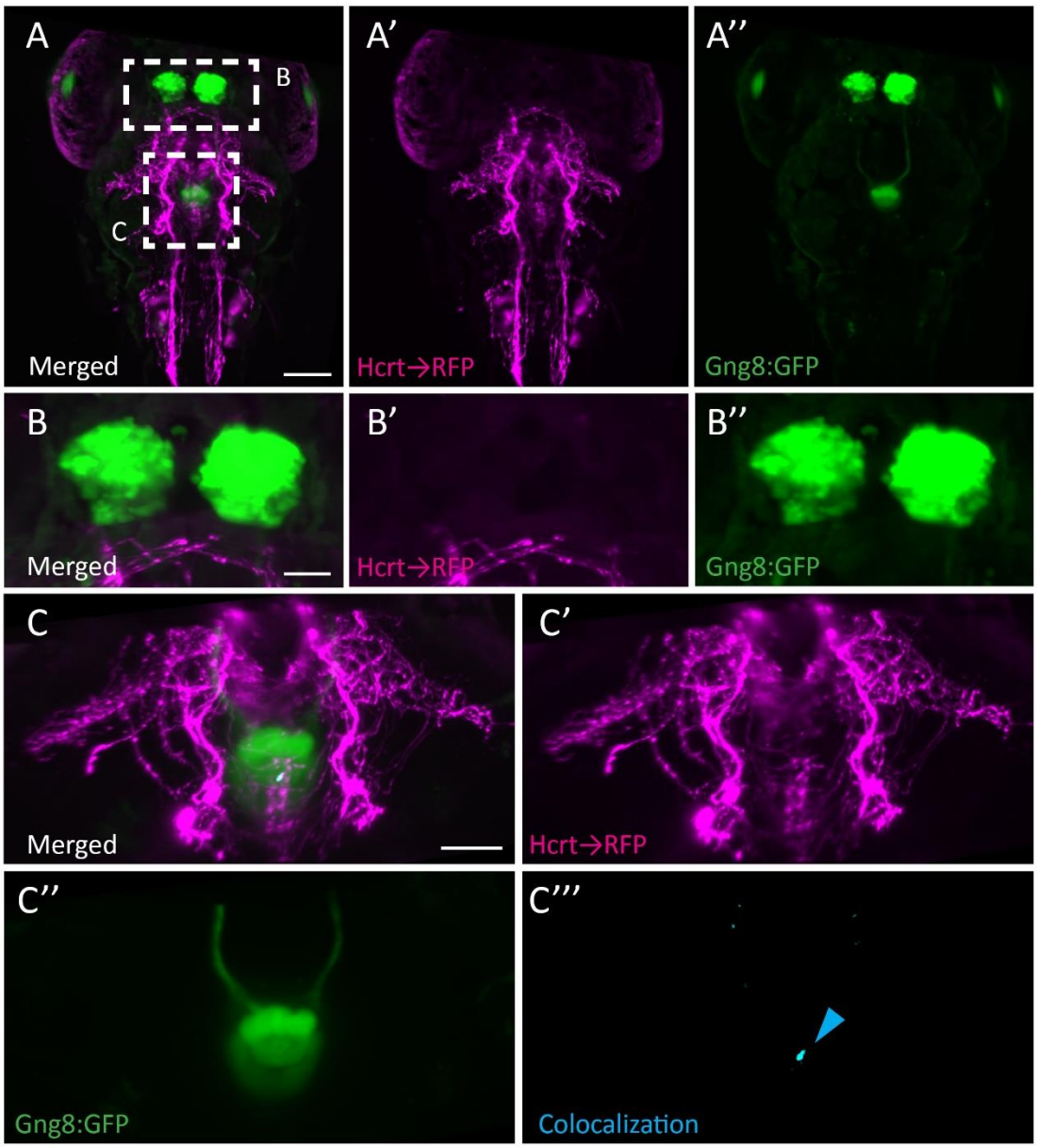

Figure 5.7: Hcrt neurites do not innervate the habenulae by 5dpf. A - A") Live imaging of Tg(Hcrt:KalTA4; UAS:RFP;Gng8:GFP) labels the dorsal habenular and its axons to the IPN (green), and Hcrt neurons and their projections (magenta). Dotted boxes denote the area in higher magnification in panel B and C. Scale bar = 100µm. B-B") Higher magnification of A showing Hcrt neurites (magenta) do not overlap with the habenulae (green). Scale bar = 30µm. C-C'') Higher magnification of A showing habenula axons (green) wrapping around the IPN. Hcrt neurites (magenta) colocalize with habenular axons that wrap around ventral IPN (cyan). Scale bar 50µm. Hcrt →RFP denotes Hcrt:KalTA4; UAS:RFP.

5.8 HCRT PROJECTIONS DO NOT INNERVATE THE PINEAL OR PARAPINEAL GLANDS

Although Hcrt-neurons projections to the pineal gland have been previously reported (Appelbaum *et al.*, 2009; Appelbaum *et al.*, 2010), we failed to detect any Hcrt projections to the pineal complex in our whole mount images (Figure 5.3). To test this more carefully, we crossed the Tg(Hcrt:KalTA4; UAS:RFP) with transgenic Tg(FoxD3:GFP) fish, which labels pre-migratory neural crest cells as well as the pineal and parapineal in zebrafish (Lekk *et al.*, 2019). We observed that Hcrt projections do not innervate the pineal or parapineal complex up to 8dpf (n=7/7, Figure 5.8). Hcrt+ neurites project along the posterior commissure and cross the midline ventral to the epiphysis proper without contacting the complex. It is possible that Hcrt neurites along the posterior commissure come into contact with the dorsoventral diencephalic tract, which originates from the epiphysis (Wilson and Easter, 1991). However, our FoxD3 transgene does not label these small cluster of pineal projection neurons. Labelling pineal projection neurons have been primarily achieved by using DiI stain or an *opn4xa* transgene, which do not label all pineal projection neurons (Yáñez *et al.*, 2009; Sapède *et al.*, 2020). Therefore, we can only conclude that Hcrt+ neurites do not innervate into the pineal or parapineal glands but the functional connections between these neuronal populations cannot be ruled out.

In some of the Tg(Hcrt:KalTA4;UAS:RFP) larvae, a cluster of RFP+ cells were observed within the pineal complex, in cells that are not expressing FoxD3:GFP. However, this ectopic cluster was not labelled by a Hcrt/Orexin antibody, demonstrating that these cells are not Hcrt positive cells (Figure 5.9).

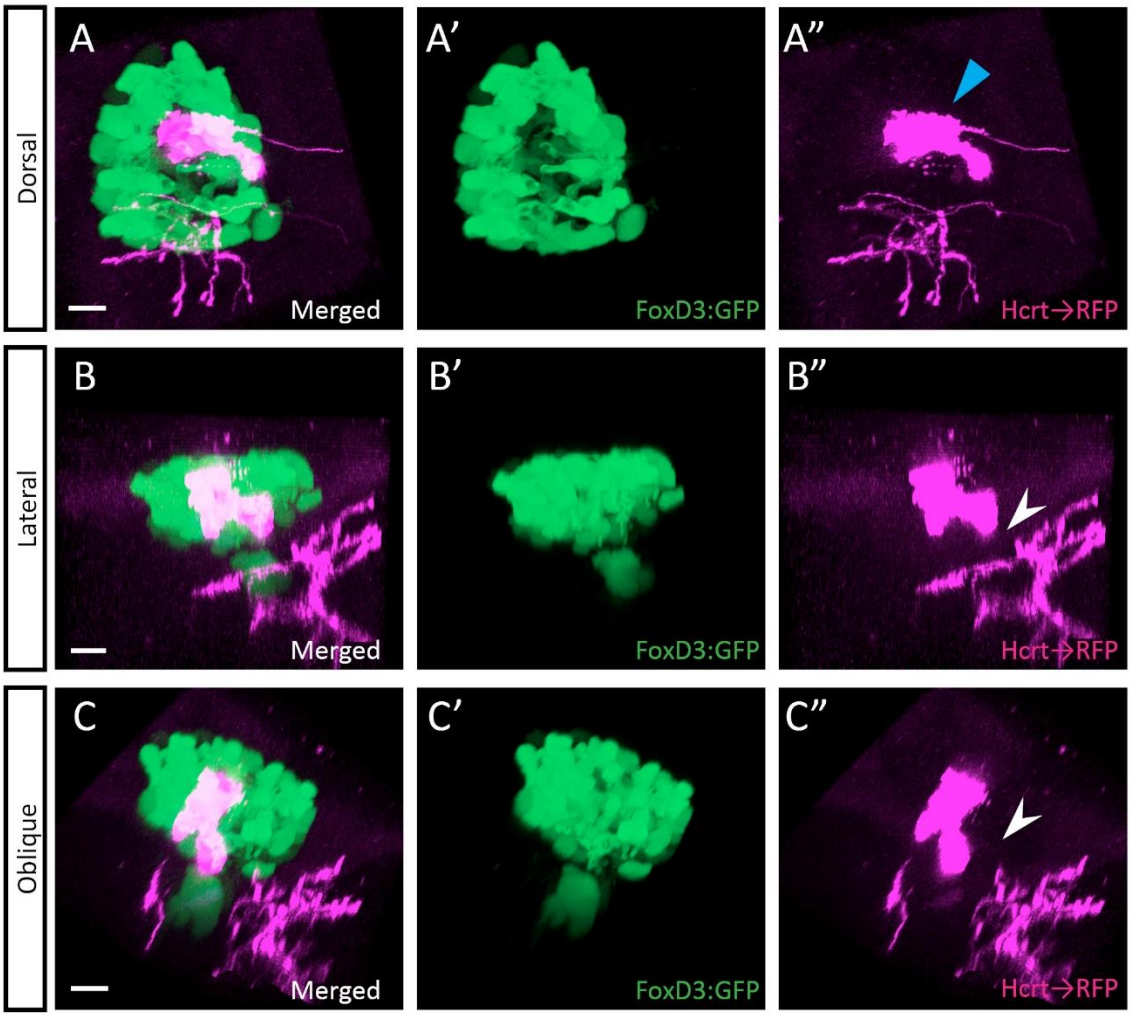

Figure 5.8: Hcrt projections do not innervate the pineal complex at 8dpf. A-C) Three views of the same 3D rendering of Hcrt neurons projections at the pineal complex. A-A") Dorsal view showing Hcrt neurites along the posterior commissure but not innervating the pineal complex. Ectopic expression of Tg(Hcrt:KalTA4) does not colocalize with the pineal complex (blue arrow, see Figure 5.9). B-B") Lateral view showing Hcrt neuron projections do not colocalize with the pineal complex (white arrow). C-C") Oblique view clearly showing Hcrt neurites do not contact the parapineal (n=7/7 fish). Hcrt →RFP denotes Hcrt:KalTA4; UAS:RFP. Scale bar = 10µm.

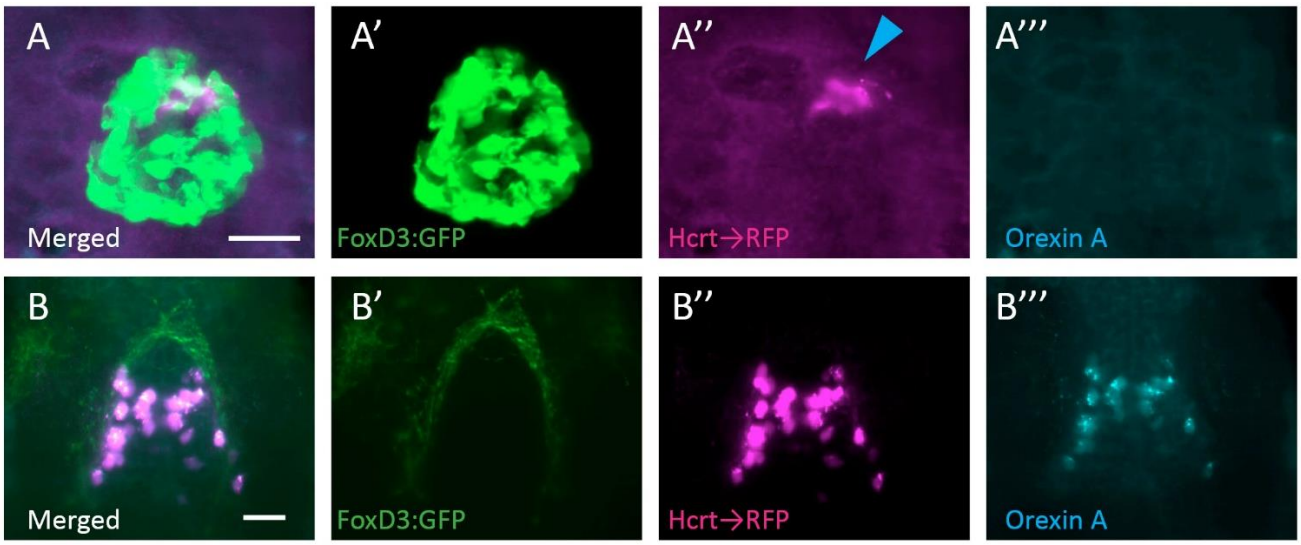

Figure 5.9: The Tg(Hcrt:KalTA4) has ectopic expression in the pineal complex in some larvae (n=2/5 fish). A-A''') Maximum projection at the pineal complex showing the Tg(Hcrt:KalTA4) ectopic expression (blue arrow) do not colocalize with anti-Orexin A/Hcrt antibody in 5dpf larvae. B-B''') The Tg(Hcrt:KalTA4) cell bodies still colocalize with anti-Orexin A from the same fish. Hcrt →RFP denotes Hcrt:KalTA4;UAS:RFP. Scale bar = 10µm.

5.9 HCRT RECEIVES INPUT FROM WITHIN HYPOTHALAMIC NEUROPIL AND THE LC

To establish whether we can visualize synapse dynamics in deeper areas of the brain, we expressed FingR(PSD95), a novel excitatory postsynaptic labelling tool as discussed in Chapter 2, under the control of the Hcrt:KalTA4 promoter. We have shown that Hcrt neurons consistently send innervations to sleep/wake areas of the brain such as the LC and dorsal raphe (Figure 5.3). We asked whether we can visualize synapses in these sleep/wake areas of the brain using our imaging set up. Live imaging of Tg(Hcrt:KalTA4; UAS:FingR(PSD95)-GFP-P2A-mKate2f) using the AiryScan at 6dpf showed that Hcrt neurons receive abundant excitatory input in the hypothalamic neuropil (Figure 5.10A, n=6/6 fish). We observed synaptic input into Hcrt neurons within the LC proper from both the left and right sides (Figure 5.10B-C) as well as en passant synapses within the spinal cord (data not shown). FingR(PSD95) puncta near the LC suggest that Hcrt neurons receive excitatory inputs within the area; however, as we did not co-label the LC with a pre-synaptic marker, we cannot conclude that there are bona fide excitatory synaptic inputs form the LC to Hcrt.

These findings demonstrate that we can detect excitatory synapses in deeper brain areas such as the hypothalamus and the midbrain using our synaptic tools and imaging set up. However, we had to use relatively high laser power to visualize FingR(PSD95) signal, suggesting that our current imaging set up with the AiryScan may cause photo-bleaching during repeated long term imaging of deeper areas of the brain. A possible way to improve this is to use multiphoton imaging using the AiryScan as this would allow us to use lower laser power.

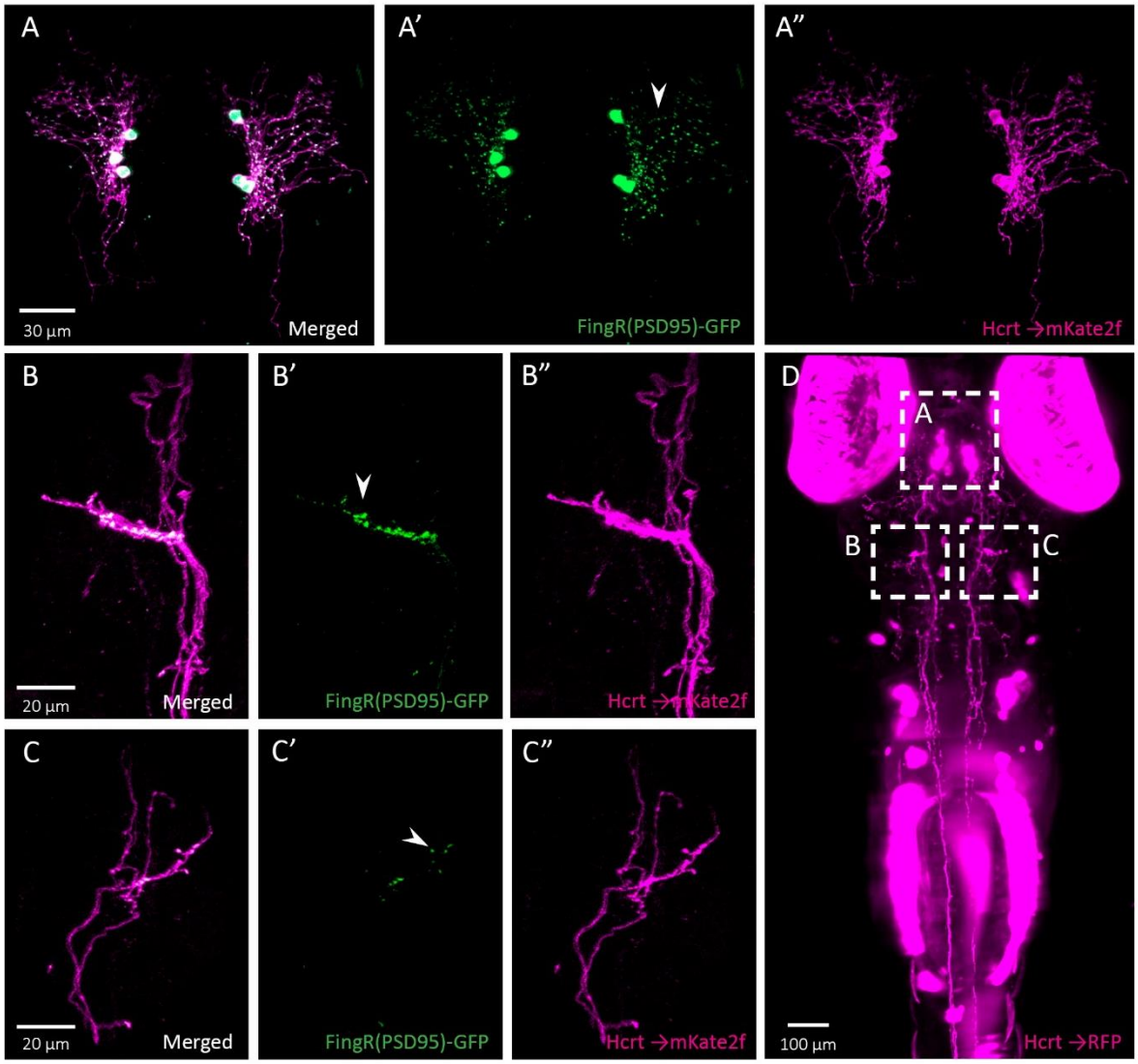

Figure 5.10: Excitatory synaptic input to Hcrt neurons observed in the hypothalamic neuropil and near the LC at 6dpf. Hcrt →RFP denotes Hcrt:KalTA4; UAS:RFP. A-C) Maximum projection of Tg(Hcrt:KalTA4; UAS:FingR(PSD95)-GFP-P2A-mKate2f) fish at the hypothalamic neuropil. A) Excitatory postsynaptic input to Hcrt neurons in the hypothalamic neuropil (n=6/6 fish). A') FingR puncta (white arrow annotating one punctum) and nuclei in green in the FingR(PSD95)-GFP channel. A'') Hcrt cell morphology in magenta in the Hcrt→mKate2f channel. B-C) Hcrt neurons receives excitatory synaptic input near both the left and right LC, respectively (n=6/6 fish). B',C') FingR(PSD95)-GFP puncta within the Hcrt neurite at the LC left and right, respectively. FingR puncta (white arrow annotating one punctum) in green in the FingR(PSD95)-GFP channel B",C") Hcrt→mKate2f showing extensive Hcrt innervation of the left and right LC, respectively. D) Maximum projection of Hcrt cells (magenta) of a different larva to illustrate where the panel A-C were taken in relation to the fish. Hcrt →mKate2f denotes Hcrt:KalTA4 driving mKate2f in UAS:FingR(PSD95)-GFP-P2A-mKate2f.

5.10 CHARACTERIZATION OF SINGLE HCRT NEURONS REVEALS DIVERSE PROJECTION TYPES

We found that Hcrt neurons send extensive processes to wide areas of the CNS, including areas of the forebrain, midbrain, hindbrain, and spinal cord. Does this mean that every Hcrt neuron projects to all of these areas, or do subsets of Hcrt neurons project to subsets of areas? If so, might the single cell map of projection diversity among Hcrt neurons reveal areas that are consistently innervated by single neurons, and might that reflect functionally distinct Hcrt neuron pool that are involved in different behaviours – arousal, feeding, reward and motivation – as has been proposed for other peptidergic neuron classes ? To address this, we characterized the projectomes of single Hcrt neurons.

To visualize and highlight single Hcrt cells to differentiate their projections within the background of the entire Hcrt population, we tried several approaches, including conversion of photoactivatable GFP (PaGFP), mosaic expression of a Hcrt:GFP construct, dextran single-cell electroporation, and Brainbow. We found that most approach could not reliably label single Hcrt cell. For example, due to the depth of Hcrt somata and their extensive projections, PaGFP could not fully convert to GFP and fill the entire Hcrt neuron without using higher laser power and/or longer exposure time, which often led to spillover and labelling of neighbouring Hcrt cells or damage to the live specimen. The advantages and disadvantages of these methods will be further highlighted in the discussion. The approach that reliably labelled single Hcrt cells was mosaic expression of a Hcrt:GFP transgene by injecting the construct into the Tg(Hcrt:KalTA4;UAS:RFP) larvae at the one-cell stage. This method created larvae with single Hcrt neurons labelled with GFP on the background of the whole population of Hcrt labelled with RFP. This allowed for single Hcrt neuron morphology tracking and mapping of its cell-body position within the whole Hcrt neuron population (Figure 5.11-13).

Preliminary data from this approach has identified distinct projectomes for individually labelled Hcrt cells, i.e. not all Hcrt neurons project to the same places. For example, only a subpopulation of single Hcrt neurons project to the tectum (Figure 5.11C) and only some project down the spinal cord (Figure 5.11A-B). Moreover, Hcrt neurons that project to the LC mostly do so ipsilaterally (Figure 5.12). We observed one Hcrt neuron that crosses the midline and projects contralaterally to the LC, indicating diversity of the projections to the LC (Ipsilaterally, n=17. Contralaterally, n=1).

Although the number of imaged neurons is currently small, as a preliminary examination of possible Hcrt subtypes, Sholl analysis and clustering was performed. Sholl analysis and k-means clustering of each single-cell Hcrt neuron revealed three distinct subtypes (Figure 5.13). Cluster 1 (n=10) has mainly neurons that travels midway down the spinal cord. Cluster 2 (n=7) contains neurons with neurites restricted within the brain. Cluster 3 (n=3) has neurons that project all the way down the spinal cord. It is possible that cluster 1 could represent a developmental wave of Hcrt that would later fully innervate the spinal cord as much as cluster 3. Our preliminary data showed that the three clusters are not dependent on the laterality of Hcrt somata location; that is, the Hcrt neuron subtypes do not have a specific topographic location within the hypothalamus. Currently, due to the low sample size, we can only conclude that single Hcrt neurons have diversity in their projection patterns. More single-cell data must be collected to improve the clustering and link morphological types of Hcrt projectome and their somata location.

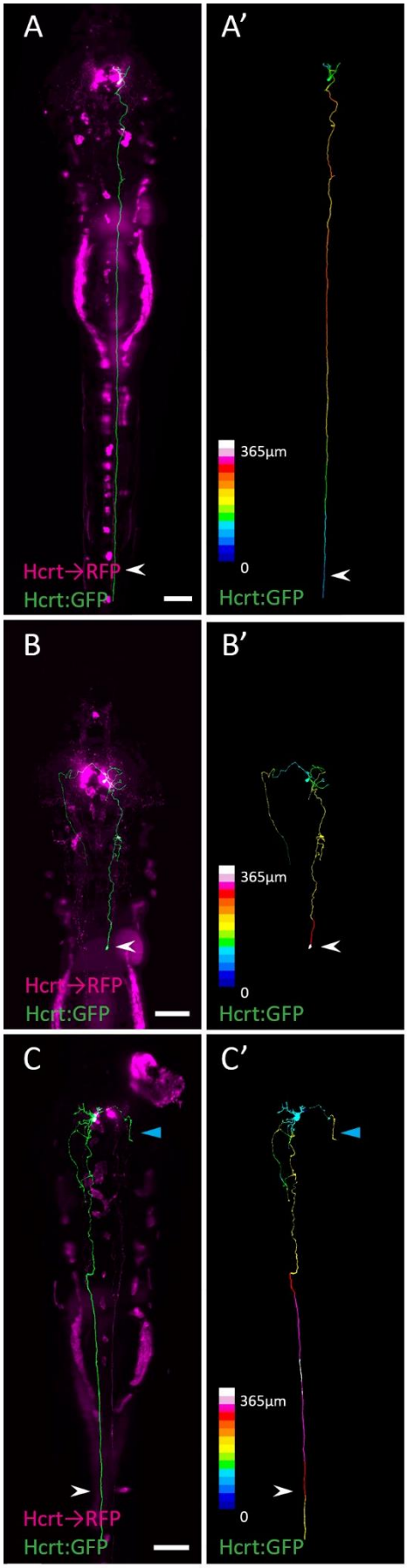

Figure 5.11: Examples of the heterogeneity of single Hcrt neurons. A) Maximum projection of single Hcrt:GFP+ (green) cell in the background of the whole Hcrt population expressing RFP (magenta) at 7dpf. Some Hcrt cells project down to the spinal cord (white arrow) at 7dpf, n= 9. B) Some Hcrt cells do not project all the way down to the spinal cord (white arrow), only to the hindbrain at 7dpf, n=3. C) Some Hcrt neurons project to the tectum (blue arrow), n=2. A',B',C') Maximum projection of depth color-coded single-cell Hcrt+ neuron. Depth scale bar shows white as most dorsal and blue as most ventral. Hcrt →RFP denotes Hcrt:KalTA4; UAS:RFP Scale bar = 100µm.

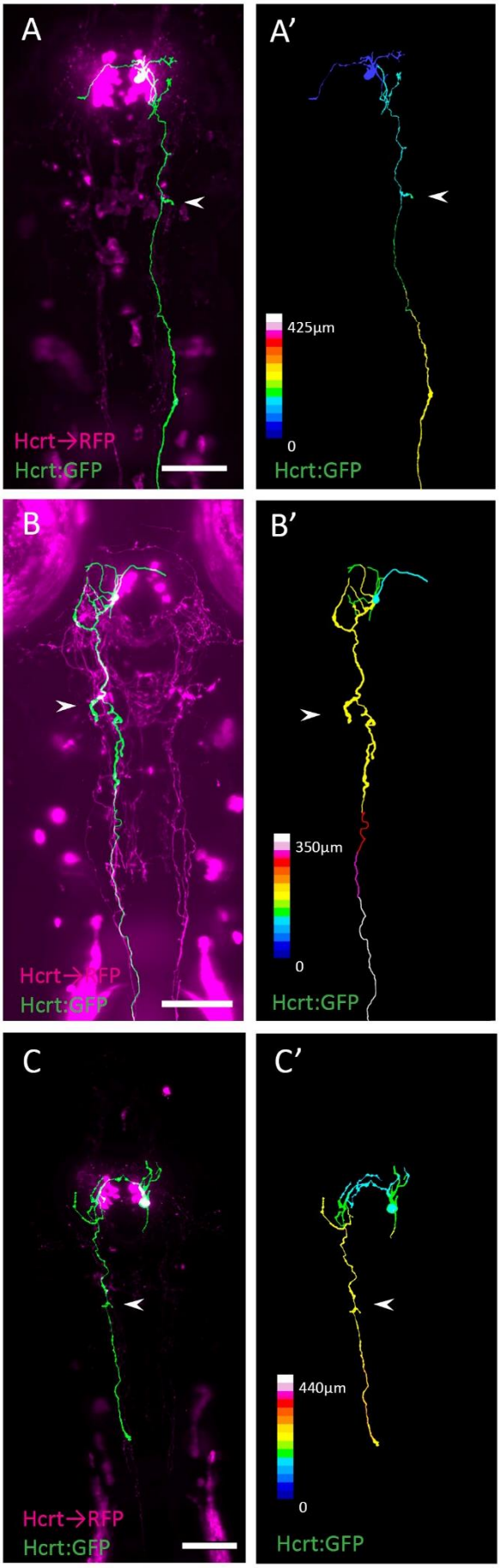

Figure 5.12: Most Hcrt cells project ipsilaterally to the LC. A-B) Examples of Hcrt cells projecting ipsilaterally to the LC (white arrow) at 7dpf, n= 10 (Left, A; Right, B). C) One Hcrt cell project contralaterally to the LC, n=1. A',B',C') Maximum projection of depth color-coded single-cell Hcrt+ neuron. Depth scale bar shows white as most dorsal and blue as the most ventral. Hcrt →RFP denotes Hcrt:KalTA4; UAS:RFP. Scale bar = 100µm.

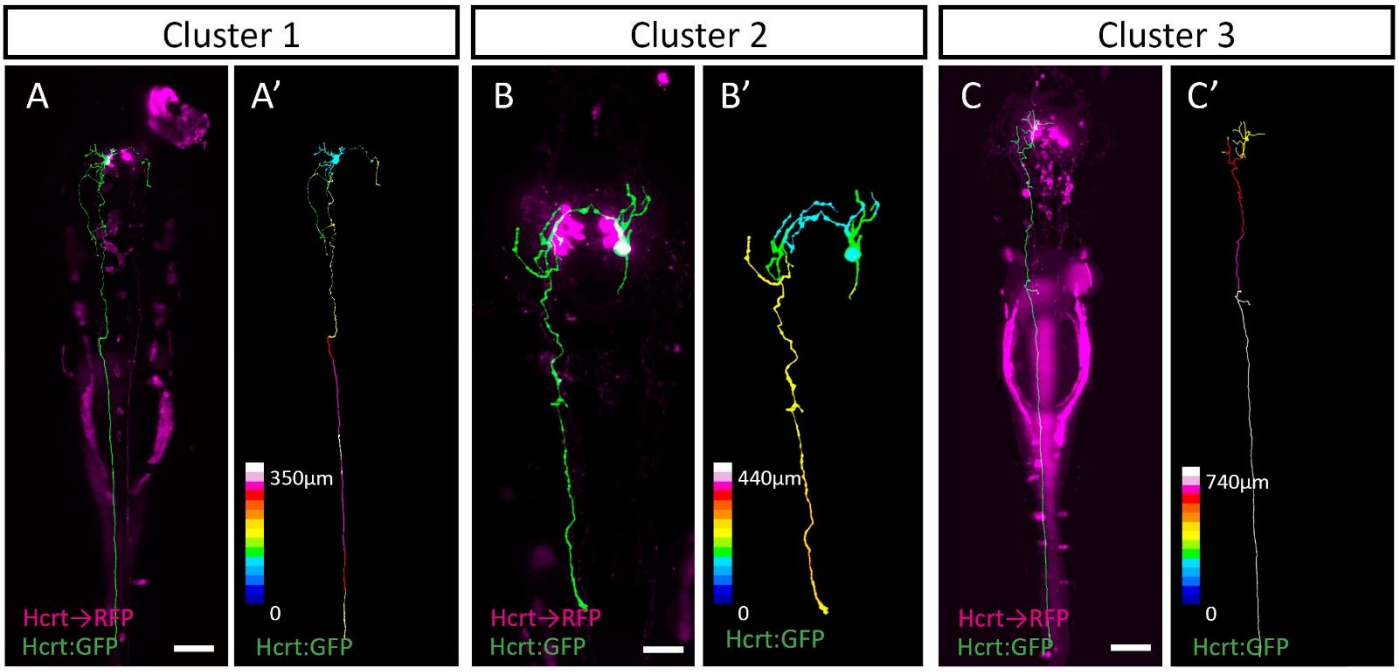

Figure 5.13: Clustering of single Hcrt cell at 7dpf reveals three types of neuronal clusters. Clustering was performed based on their morphology and somata location laterality (n = 20 cells in 20 larvae). A-A') Example neuron of from Cluster 1. A) single cell Hcrt (green) and populational Hcrt (magenta). Scale bar = 100µm. A') Maximum projection of depth color-coded single-cell Hcrt+ neuron. B-B') Example neuron of from Cluster 2. B) single cell Hcrt (green) and populational Hcrt (magenta). Scale bar = 50µm. B') Maximum projection of depth color-coded single-cell Hcrt+ neuron. C-C') Example neuron of from Cluster 3. C) single cell Hcrt (green) and populational Hcrt (magenta). Scale bar = 100µm. C') Maximum projection of depth color-coded single-cell Hcrt+ neuron. Depth scale bar shows white as most dorsal and blue as most ventral. Hcrt →RFP denotes Hcrt:KalTA4; UAS:RFP.

Chapter 6 Discussion

The work presented was set to provide a better understanding on factors that can influence synapse dynamics in the context of the Synaptic Homeostasis Hypothesis (SHY). To that end, we modified a live genetic marker for synapses, Fibronectin intrabodies generated with mRNA display (FingRs), to visualize both excitatory and inhibitory synapses in vivo. We also developed a novel tool that has the potential to simultaneously visualize calcium dynamics of the neuron and within their excitatory synapse. We verified that our modified FingR tools reliably label bona fide synapses in vivo and can respond to changes in synaptic formation and elimination dynamics.

Using these tools, we observed the dynamic changes in excitatory synaptic number across the sleep/wake cycle and circadian time for individual optic tectum neurons in the same animal. Several findings provide clues on the complex involvement of the circadian clock, physical external stimuli, and sleep/wake states in influencing synapse dynamics:

1. At the population level, synapse number exhibit diurnal fluctuations as predicted by SHY: net synapses increased during the day phase and decreased over the night.
2. A synchronized circadian clock is required for the diurnal fluctuations in synapse number. Larvae with abolished synchronized circadian clock exhibit arrhythmic synapse number dynamics, while free-running animals with intact circadian clock under constant conditions demonstrated 1-1.5 cycles of synapse number rhythmicity.
3. Physical light and dark cues can influence synapse dynamics. Free-running animals with intact circadian clock synapse rhythmicity was dampened and eventually abolished after 1-1.5 cycles in constant light. Moreover, prolonged light exposure can lower the baseline synapse number level.
4. Total sleep amount does not have a linear correlation with synapse dynamics. However, sleep immediately after lights OFF or following sleep deprivation (high sleep pressure) reduces the number synapses, while extended wakefulness increases synapse number.
5. Individual neurons have diverse synapse number and strength dynamics that is not reflective of the population dynamics. Furthermore, certain subtype of optic tectum neurons could potentially have different synapse dynamics.

Our findings, together with the wider literature, paint a more complex picture of sleep and synaptic plasticity than SHY envisioned. This highlights the need for a more comprehensive investigation of synapse dynamics in the context of sleep/wake and circadian clock at the single-cell level in various other types of neurons. Working towards this, Chapter 5 established a foundation to investigate synapse dynamics in hypothalamic neurons that have wide-ranging morphologies and functions. We mapped the projections of Hcrt neurons neurites in the zebrafish larvae, found that Hcrt single cell projectome are heterogenous, and identified potential regions to track Hcrt synapse dynamics through day and night using the FingR system.

6.1 GENERATION AND EVALUATION OF SYNAPTIC LABELLING TOOLS

To systematically investigate SHY, we asked whether there is a way to track the same synapses of the same neurons through sleep and wake and circadian time. In this chapter, we have established such synaptic tools. We enhanced the existing Fibronectin intrabodies generated with mRNA display (FingRs) system to allow for visualization of the synapse number and location as well as the cell morphology corresponding neuron of interest without the confounding effects of overexpression. Furthermore, we developed a novel tool that potentially allow the simultaneous visualize calcium dynamics of the neuron and within their excitatory synapse. We verified that our modified FingR tools reliably label bona fide synapses in vivo and can respond to changes in synaptic formation and elimination dynamics.

6.1.1 FingRs as tools to label synapses in vivo

To allow for the visualization of cell morphology, we inserted a self-cleavage peptide sequence with membrane-bound fluorescent protein into existing FingRs cassettes. With this modification, we found that our FingRs labelled synapses with high fidelity and at a similar rate to the previous versions (Son *et al.*, 2016; Cook *et al.*, 2019). Similar to previous findings using hippocampal cell culture and ex vivo zebrafish, our modified FingR systems, targeting both excitatory and inhibitory synapses, were found to colocalized more than 90% with endogenous synaptic proteins in vivo (Son *et al.*, 2016; Cook *et al.*, 2019). FingR targeting PSD95 have false negative rate of ~20% in hippocampal culture (Cook *et al.*, 2019), while our modified FingR showed 0% false negative rate in vivo zebrafish. Compare with in vitro and ex vivo studies, our modified FingRs were shown to have conserved labelling fidelity to their

respective synaptic targets. More importantly, we have shown that we can detect FingR labelling bona fide synapses in vivo.

Next, we showed that our modified FingR targeting PSD95 can detect changes in synapse number in response to pharmacological agents within the same timescale (multiple hours to days) we wish to observe across sleep/wake states. This suggested that FingRs targeting PSD95, as a tool, could be used to detect changes in synapse number during sleep/wake and circadian time and address SHY. We need to further verify the ability for the rest of our modified FingR systems (e.g. FingR targeting GPHN) for detecting changes in synapses. It has been reported that organophosphorus compounds, potent inhibitors of cholinesterases and widely used as chemical pesticides cause neuronal hyperexcitation and decreased gephyrin protein accumulation in zebrafish in vivo (Brenet *et al.*, 2020). We could utilize these known effects to further verify our modified FingRs systems ability to track synaptic changes. For instances, we could test whether FingR(GPHN)-GFP can detect organophosphorus compounds-induce increase in GPHN within the optic tectum, and whether FingR(PSD95)-GCaMP7b can reliably report seizure-like neuronal hyperexcitable induce by the compounds.

Overall, we generated new synaptic tools that label endogenous synaptic proteins and able to capture changes in synapse dynamics in vivo in zebrafish. We found that we can use our tools to reliably count synapses in vivo. These tools provide a platform for us to study sleep/wake-related synaptic plasticity and to address SHY in vivo.

6.1.2 Limitations and technical caveats

FingRs expressions

Despite labelling bona fide synapses, there were some limitations in our FingR systems and imaging methods. Firstly, we observed that, transient injections of FingR (i.e. non-genome integration) yielded variable expression and sometimes overexpression of FingRs. This is due to the FingR negative feedback mechanism, the FingR construct will work best when the whole of the FingR cassette is integrated into the genome. This could potentially explain the small discrepancies in our false negative labelling rate findings and Cook et al.'s (2019). We detected no false negative labelling for FingR targeting PSD95, contradictory to the 20% false negative rate found in hippocampal culture (Cook *et al.*, 2019). This might be due to several aspects of the different FingR expression methods used, such as the difference between cell culture transfection of previous studies and stable transgenic lines in our study. While cell

culture transfection could allow the DNA cassette to be integrated into the genome, the presence of unsuccessfully integrated leftover DNA cassettes within the cell cannot be ruled out. We found that generating a stable transgenic line in which the FingR cassettes were inserted within the genome exhibit reliable FingR expression. For our synaptic studies, we used stable transgenic lines that have been outbred through multiple generations, which eliminates the presences of unintegrated FingR cassettes as a source of overexpression.

One of the limitations is that we do not know the temporal efficiency of FingR to label their endogenous protein targets. PSD95 clusters have been observed at new axodendritic contact sites within 20-60 minutes of presynaptic contact labelled by the active synapse marker, FM 4-64 (Bresler *et al.*, 2001). As we currently do not know how long it takes for FingR (either those targeting PSD95 or GPHN) to express at a new synapse in vivo, this could result in the underestimation of number of puncta if new synapses are formed during the experiment. However, it has been shown that FingR targeting CaMKII can express at the synapse in dissociated hippocampal neurons upon chemically-induced LTP and LTD within 1 and 5 minutes, respectively (Cook *et al.*, 2019). Moreover, Gross et al. have observed GPHN.FingR-GFP trafficking at the velocity of 7 μm s^{-1} in the axons of cortical neuron cultures (2013). Since our experiment tracks the number of FingR synaptic puncta at a longer timescale (hours), we assume that FingR have a sufficient trafficking rate to newly created synapses. Moreover, it has been observed during synaptogenesis that other MAGUK proteins such as PSD93, SAP102, and SAP97 acts as a scaffold for NMDA and facilitate AMPAR recruitment to nascent synapses before PSD95 accumulate to provide long-term stability (Lambert *et al.*, 2017). Since FingR targeting PSD95 have been shown to also target SAP102 and SAP97 (Gross *et al.*, 2013), it is possible that our FingR-PSD95 label nascent synapses as well as mature ones.

Immunohistochemistry

We performed synaptic immunohistochemistry against respective FingR targets, PSD95 and GPHN, in motoneurons of 2dpf larvae because synapses are sparse at this age and location, making it possible to perform whole-mount synaptic immunohistochemistry as well as visualize and differentiate the punctate endogenous synapses in vivo. We could not perform colocalization experiments in the tectum (where we looked at synapse dynamics) at 7-9dpf because the densely packed endogenous synaptic proteins within the structure and the thickness of the tissue render it not practical to perform immunohistochemistry to measure

the level of colocalization between FingR puncta and endogenous proteins. Therefore, these FingR colocalization assumptions might not hold for other cell types such as tectal cells. A future experiment to test the reliability of our FingR in labelling tectal neurons synapses number is to do immunohistochemistry on brain sections of 7-9dpf larvae, which could potentially solve permeabilization issue of antibodies. Nevertheless, such a method would not allow us to examine FingRs reliability at labelling synapses at a whole-cell level.

Another limitation was that we were unable to verify in vivo anti-GPHN puncta labelled by FingR(GPHN) due to the high density of anti-GPHN puncta from nearby neurons present in the spinal cord of the larvae. To overcome this, more sparse labelling of FingR(GPHN) must be performed. As transient expression of FingR resulted in unwanted overexpression patterns, sparse labelling of FingR(GPHN) must be done with the FingR construct established in a stable transgenic line. For example, CRISPR-erosion techniques could be used in which CRISPR-Cas9 technology is used to target the Gal4 sequence, leaving very sparse expression of FingR labelling in the remaining Gal4 positive cells (personal communications, Wilson lab).

Imaging paradigm

Another limitation we faced was the imaging set up. We decided to use Zeiss Lightsheet because of the understandably low baseline signal of the FingR system. This is likely due to the negative feedback mechanism in the FingR system, which prevent runaway overexpression. By using lightsheet microscopy, we found that we could illuminate the sample with lower power than with a traditional confocal set up while obtaining higher sensitivity and reduced photo-bleaching. Nonetheless, this set up requires the submerging of live larvae in anaesthetic and could have undesired effects on synapse dynamics. Since glass capillary immobilization of fish is required to use the imaging system, which means that small movement from the larvae is exaggerated and can confound imaging of synapses. To prevent motion artefacts, larvae are anesthetized larvae using voltage-gated sodium channels blocker, MS-222, which prevents neural action potentials in zebrafish (Attili and Hughes, 2014). This means that synapse dynamics could be perturbed by the use of anaesthetics. Furthermore, lightsheet imaging reduces the resolution in the z-plane to 1.0µm, which could lead to an underestimate of FingR puncta counting, as puncta are approximately 0.4-0.6µm in diameter. To overcome these issues, we used LSM 980 with Airyscan 2 (Zeiss) to track synapse dynamics

across the sleep/wake cycle instead. With the Airyscan, we could image with Z-plane intervals as small as 0.34µm and without submerging in anaesthetic.

Another limitation to consider was that we were using genetically unidentified neuronal population during the drug exposure experiment. This meant that we did not know what types of neuron (inhibitory or excitatory) we were imaging. Different types of neurons can respond differently to the same pharmacological agents. For instance, NMDA receptor antagonist, such as MK801, can block excitatory glutamatergic neurotransmission via NMDAR inhibition as well as blocks NMDAR on GABAergic inhibitory neurons which leads to disinhibition and an enhancement of excitatory glutamatergic neurotransmission (Zanos and Gould, 2018). In this drug exposure experiment, we used sporadically expressed single tectal interneuron in a Tg(emx3:Gal4FF) line. Emx3 is a dorsal telencephalic marker and has not been reported to be express in tectal interneurons (Viktorin *et al.*, 2008). We suspect that this is a gene-trap artefact and the second generation of Tg(emx3:Gal4FF) lost this tectal expression. While the majority of tectal neurons are either GABAergic or glutamatergic interneurons, we could not pinpoint what types of neuron we were investigating (Robles *et al.*, 2011). This could potentially explain the non-uniform synapse dynamics in response to MK801 or DMSO. To improve this, we chose to label tectal neurons using genetically controlled FingR expression under zebrafish optic tectum promoter.

6.1.3 FingRs as a potential tool to measure calcium activity

We further enhanced the FingR system to potentially allow for the visualization of calcium transients at individual excitatory synapses and the whole-cell level. While more work has to be done to ensure that the calcium indicator within the FingR system can reliably detect subcellular calcium changes, if FingR can measure calcium transients at the synapses, this could have wide ranging applications. One way to test whether this modified FingR can reliably detect calcium transients at the synapse is to express FingR(PSD95)-GCaMP7b-P2A-mKate2f in tectal neurons such as under the control of FoxP2.A promoter. Using set up similar to (Nikolaou *et al.*, 2015), we can image these neurons whilst showing different visual stimuli such as moving bars that are known to evoke calcium transients.

In neurons, action potentials trigger a transient calcium influx though voltage-gated calcium channels that can occur at the soma, axon, and in the dendrites following backpropagation of the action potential (Jaffe *et al.*, 1992). This action potential-evoked calcium transient measured using genetically-encoded calcium indicators have been extensively used to study neuronal spiking activity in vivo (Ahrens *et al.*, 2013; Dana *et al.*, 2019). Moreover, in mammals, NMDA receptor-dependent calcium dynamics within dendritic spines have been used as a readout of inputs into individual synapses (Sabatini *et al*., 2002). With our FingR(PSD95)-GCaMP7b-P2A-mKate2f, we restrict calcium indicators to only at the synapses and the nucleus. This system could potentially allow visualization of cellular and compartmentalized calcium dynamics while avoiding the confounding readout of calcium changes caused by action potentials back-propagating into dendrites. Moreover, we can target the calcium indicator to excitatory synapses in animal models that do not have dendritic spines and to non-spine excitatory synapses.

Using our calcium indicator FingR system, we could potentially address SHY and examine whether the reduction in firing rate and/or synapse activity are dependent on UP/DOWN states during non-rapid eye movement sleep. While there has been some evidence linking non-rapid eye movement sleep after learning to reductions in the firing rates of task-unrelated neurons and synaptic strength (Gulati *et al.*, 2017; Norimoto *et al.*, 2018), it is unclear whether weakening of synapses causes reduction of firing rates of task-unrelated neurons or whether synaptic weakening occurs in task-unrelated synapses. Tracking the nuclear GCaMP7b signal would allow for the detection of ON/OFF firing epochs while FingR GCaMP7b signals at the synapses would allow us to monitor incoming synaptic activity and the strength of each synapse. Simultaneous monitoring of both neuronal and synaptic activity of task-related and -unrelated neurons after learning and sleep could pinpoint whether sleep-dependent weakening of task-irrelevant or 'noise' synapses is responsible for the effects of neuronal firing.

6.2 SYNAPTIC NUMBER DYNAMICS DURING SLEEP AND WAKE

In Chapter 4, we used our FingR(PSD95)-GFP synapse-imaging system to track the structural dynamics of excitatory synapses of individual tectal neurons through multiple days and nights. We found a developmental window where the net synapse number of tectal cells are relatively stable and used this period to investigate synapse dynamics through circadian time on various lighting regimes. We demonstrated that at the populational level, net synapse number increased during the day phase and decreased over the night, consistent with the predictions of SHY. However, the synapse trajectories of individual neurons showed that not all neurons follow this dynamic. Moreover, we demonstrated that a synchronized circadian clock is required for the synapse rhythmicity. Nonetheless, physical alternation of light/dark cycles can also influence synapse dynamics. We also found that sleep/wake behaviour does not have obvious linear correlation to synapse dynamics. However, sleep deprivation at beginning of the night phase increased number of FingR puncta compare to controls that were allowed to sleep, which is consistent with SHY and suggests a model by which the influences of circadian rhythmicity and light cues on synapse dynamics are consequence of how these processes alter sleep/wake states.

6.2.1 Development of tectal synapses

Our findings that excitatory postsynaptic input to tectal cells stabilized around 6-9dpf corroborate previous studies using different methodologies. These studies indicated that spatial receptive fields, arborization of neurites, and pre- and post-synaptic dynamics are stable around 6-10dpf (Niell, Meyer and Smith, 2004; Meyer and Smith, 2006; Zhang *et al.*, 2011).

Using whole-cell voltage-clamp recordings, Zhang et al. demonstrated that the receptive fields of tectal neurons undergo a growth phase from 4-6dpf and then refinement from 6-9dpf (2011). This is also reflected in studies using postsynaptic markers examining genetically unidentified tectal cells, where Niell et al. found that PSD95 puncta increased dramatically from 3-7dpf. They also found that the arbour and number of PSD95 puncta remained relatively stable from 7-10dpf, which is consistent with our findings. Such stabilization around 6-7dpf onwards is also reflected in the development of tectal presynaptic sites and RGC axons' innervation (Meyer and Smith, 2006; Gebhardt, Baier and Del Bene, 2013), suggesting that retinotectal circuits are stable during this developmental phase.

While there could still be some changes associated with development in this window that accounts for some of the synapse changes we observed, the circadian clock break experiment shows that synapse dynamics disappeared (Figure 4.3). This suggests that the developmental effect between 7-9dpf is unlikely to account for the synapse dynamics we observed. Moreover, we found that from 9-10dpf onwards, synapse dynamics have divergent trajectories (Figure 4.1). This is consistent with our findings in normal light:dark, clock break, and free running experiment that synapse number increased drastically at 10dpf, which may reflect a second wave of synapse maturation (Figure 4.3C). The synapse stability period was after swim bladder inflation (at 5dpf) , which is required for larva to swim, hunt, and (most importantly for this study) sleep (Winata *et al.*, 2009; Rihel, Prober and Schier, 2010; Bianco, Kampff and Engert, 2011).

Niell et al. found that PSD-95:GFP puncta were always excluded from branches arising from the proximal dendrite, which they concluded to be the local axonal arborization. We did not observe obvious areas in our neurons that lack FingR(PSD95) labelling. Nonetheless, we found that the distal arbours contain more FingR puncta compared to the proximal arbour (personal observation), suggesting that certain neurites within the proximal arbour (if present) could represent axons. The difference in cell type in our study and Niell et al. might explain such disparities. For example, while they selected cells by morphology to represent type-XIV tectal neurons, which have monopolar cell bodies in the deepest tectal layer and are bushy with non-stratisfied arbours, we genetically targeted FoxP2.A neurons, which have four morphologically distinct subtypes. By observation, type-XIV neurons studied in Niell et al. and our FoxP2.A neurons are distinct from each other.

6.2.2 Sleep/wake states and light/dark driven synapse dynamics

We showed that both sleep/wake states and physical light/dark cues can influence the number of synapses in tectal neurons. Specifically, a synchronized sleep/wake behaviour with an intact circadian clock and alternating light/dark cycles can drive synaptic rhythmicity, and prolonged light exposure also can alter the baseline synapse number. While these synaptic dynamics do not linearly correlate with prior sleep experience, extended waking via sleep deprivation can increase synapse number, while sleep post-deprivation reduces the number of synapses. Our findings are summarized in a model in Figure 6.1. While the influences of external light cues, sleep/wake states, and the internal circadian clock on synapse dynamics

of FoxP2.A tectal neurons have not been previously studied, these influences on synapse dynamics have been previously observed in other neuronal population and animal models (Frank and Cantera, 2014; Tononi and Cirelli, 2014; Pratt, Hiramoto and Cline, 2016).

Sleep/Wake

First, we showed that there are increased numbers of synapses during the day phase compared to overnight. This is consistent with several previous studies using molecular, electrophysiological, and morphological correlates of synaptic strength (Vyazovskiy *et al.*, 2008; de Vivo *et al.*, 2017; Diering *et al.*, 2017). Next, we showed that there is no linear correlation between synapse dynamics and prior total sleep and wake behaviour (Figure 4.9), suggesting total sleep amount does not drive synaptic downscaling in a one to one ratio in FoxP2.A neurons. This is also consistent with findings in rodents where mEPSCs properties did not correlate with prior sleep/wake experience (Cary and Turrigiano, 2021). However, our findings cannot rule out other possible relationships between sleep/wake and synapse dynamics such as the presence/absence of sleep.

To address whether the presence/absence of sleep affect synapses, we sleep deprived larvae at the beginning of the night (ZT14-18) and monitored their synapse dynamics. We found that SD larvae had increased synapse numbers compared to controls immediately after SD (Figure 4.10). This increase is reduced to similar levels to controls after larvae were allowed to sleep. This is consistent with the predictions of SHY and has been previously reported in other animal models such as in spine dynamics in mice, pre- and post-synaptic markers in Drosophila (Gilestro, Tononi and Cirelli, 2009; Maret *et al.*, 2011; Diering *et al.*, 2017; Weiss and Donlea, 2021).

While our observation that extended wakefulness increases the number of synapses independently of circadian rhythms is consistent with various studies (Gilestro, Tononi and Cirelli, 2009; de Vivo *et al.*, 2017; Khlghatyan *et al.*, 2020; Weiss and Donlea, 2021), it also contradicts studies such as (Matsumoto *et al.*, 2020; Cary and Turrigiano, 2021). For instance, Matsumoto used optogenetically evoked responses in mouse and found no effect of sleep deprivation on evoked transmission (2020). Using a similar approach, Cary and Turrigiano found that wake or sleep amount had no effect on evoked thalamocortical field excitatory postsynaptic potentials (2021). There are several methodological differences between our study and previous studies that might explain some of the differences. Like Cary and

Turrigiano, we also classify sleep history of every animal used. Unlike Cary and Turrigiano and Matsumoto et al., which use repeated optogenetically evoked populational recordings, which can itself affect synaptic responses and activity-regulated gene expression (Tyssowski and Gray, 2019), we follow the same cells undisturbed through circadian time and sleep/wake states. Moreover, we looked at whole-cell synapse dynamics of individual neurons, while they looked at changes at a population level of thalamocortical synapses and were unable to account for synapses connected to other areas of the brain.

Our data showed that the timing of synapse dynamics coincided with sleep pressure. Sleep pressure is highest at the onset of sleep and progressively decreases with time spent asleep and is increased after extended wakefulness (Dijk, 2009). This is also reflected in the amount and power of slow wave sleep (Dijk, 2009), the read out of sleep pressure. The timing of synapse number reduction observed in our study is consistent with the SHY prediction that the synchronized oscillations during slow-wave sleep drives sleep-dependent synaptic downselection (Tononi and Cirelli, 2014). However, as we cannot measure specific sleep stages in our paradigm, we cannot conclude that the synaptic reduction we observed is due to slow-wave sleep activity.

While there are ample studies that linked non-rapid eye movement (NREM) sleep to downregulation of neuronal activity and dendritic spines in the cortex and hippocampus in rodents (Gulati *et al.*, 2017; Norimoto *et al.*, 2018; Miyamoto *et al.*, 2021; Torrado Pacheco *et al.*, 2021), other sleep phases such as rapid eye movement sleep (REM) have also been implicated in reduction of neural activity and dendritic spine (Niethard *et al.*, 2016; Li *et al.*, 2017; Torrado Pacheco *et al.*, 2021). While recent findings suggested that different sleep stages akin to REM and NREM sleep exist in the zebrafish (Leung *et al.*, 2019), it is currently challenging to simultaneously image synapses and these neural signatures through multiple days and nights in living larval zebrafish.

It must be noted that while our extended wakefulness paradigm aimed to disentangle circadian processes and sleep/wake states, this sleep deprivation method is still introducing salient experience to the larvae. Even though we used red light for the experimenter to visualize the larvae as well as to minimize disruption to the larvae circadian rhythm (Emran *et al.*, 2010; Lin and Jesuthasan, 2017), it has been shown that zebrafish have photoreceptors

for, and are sensitive to, red light (Matsuo, Kamei and Fukamachi, 2021), and red light can shift their circadian rhythm (Steindal and Whitmore, 2020). Therefore, it is possible that our SD larvae see the paintbrush movement under red light, inducing not only wakefulness but activity-dependent synaptic changes in our visual neurons.

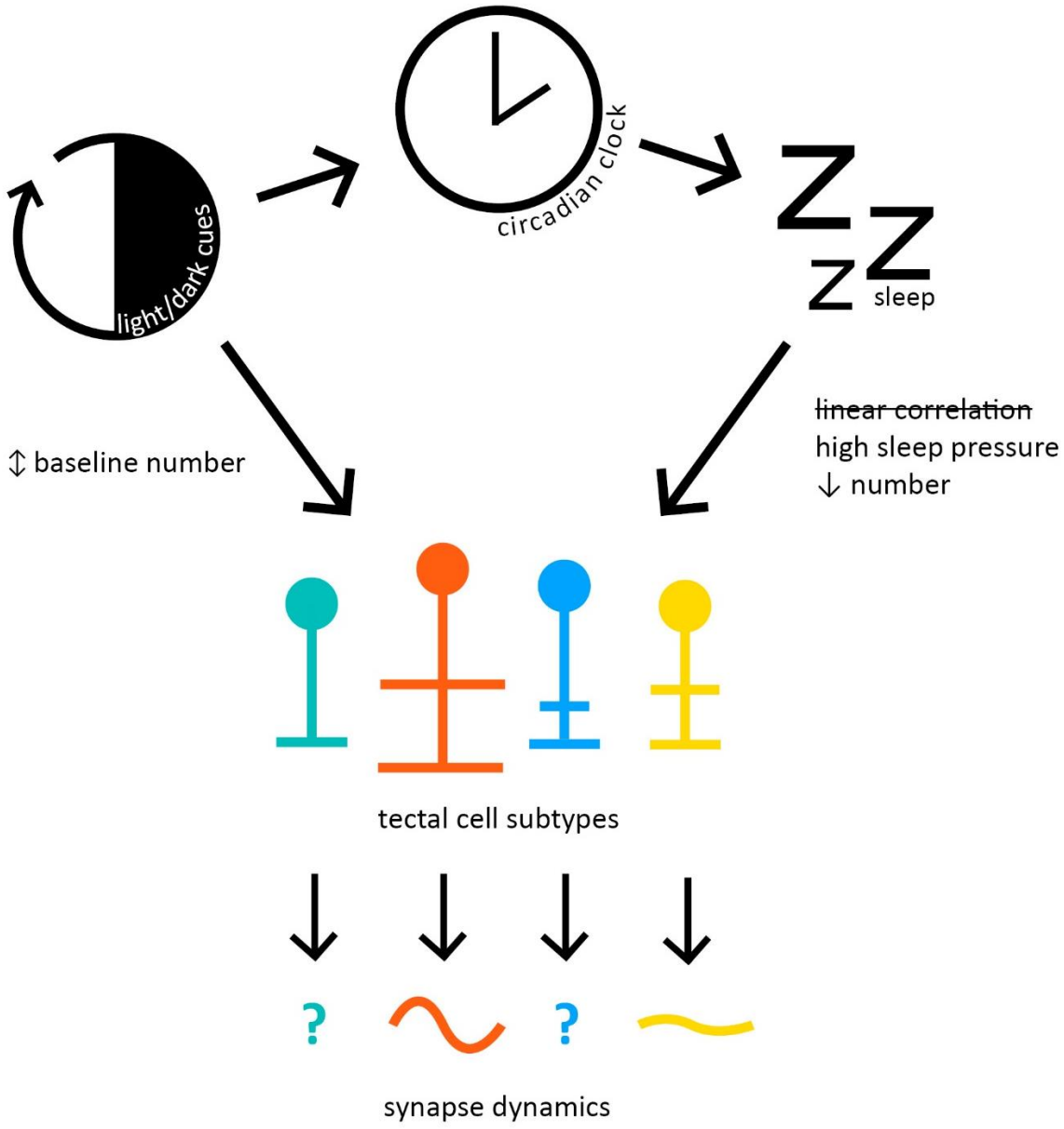

Figure 6.1: Working model of synapse dynamics in FoxP2.A neurons Synchronized circadian clock can influence the timing and consolidation of sleep/wake states. Alternating light/dark cues synchronize the circadian clock and also influence synapse number baseline. Long exposure to light can alter baseline synaptic number. Sleep amount do not have a linear correlation with synapse dynamics, but the presence/absence of sleep can alter synapse dynamics. Alternating light/dark cues, the circadian clock and subsequently sleep/wake cycle can influence subtypes of tectal cells differently. For example, Type 2 neurons (orange) have different synapse number dynamics compare to Type 4 neurons (yellow).

Light/dark and activity-driven influences

Our findings also showed that light/dark cues have effects on the dynamics of synapse number. We found that long exposure of light decreased the baseline number of excitatory synapses in tectal neurons (Figure 4.2-3, 6.1).

Previous studies have shown that activity-dependent mechanisms play a critical role in visual system development and can alter tectal synaptic properties. For example, Zhang et al. showed that changes in light stimuli such as a whole-field repetitive dimming light stimulus can induce LTP of retinotectal synapses of Xenopus larvae (2000). Moreover, visual experience such as moving bars can directly increase the strength of retinotectal glutamatergic synapses by increasing the abundance of AMPA receptors at synapses (Engert *et al.*, 2002; Haas, Li and Cline, 2006). These findings suggest that the light and visual dependent changes we observed in synapse dynamics might be due to visually evoked tectal activity. We are currently collecting data on activity driven changes in synapse number dynamics. To do this, we imaged FoxP2:FingR neurons in the fish to establish synapse dynamics baseline. We then showed larvae zebrafish different orientation and direction moving bars throughout the day phase and at the end of the day we image their synapse again. We also imaged the neurons and the synapses again the morning after (Table 6.1). We hypothesize that the prolonged neural activity induced by the visual stimuli would further increase the number of tectal synapses at end of the day phase. As observed previously, we expect that a decrease synapse number during the night phase; however, the rate of decrease would tell us how sleep and/or circadian night signals influence synapse dynamics in conjunction with preceding salient experience.

We found that synapse number dynamics are controlled by the sleep/wake cycle but can be manipulated with light cues. In the presence of an intact circadian clock and matching alternating light/dark cues, synapse number are rhythmic (Figure 4.2-3). However, in the absent of alternating light/dark cues with intact circadian clock, after a period of time, the light cue appears to have more weight over sleep/wake and/or circadian control of synapse number, rendering it arrhythmic. Our extended tracking data of FR larvae showed that synapse number rhythmicity persisted after two subjective nights and was abolished thereafter.

We assumed that circadian rhythms and consolidated sleep/wake patterns were present in constant conditions in FR larvae as it has been shown in age-matched FR zebrafish larvae for at least three cycles (Kaneko and Cahill, 2005; Gandhi *et al.*, 2015). Nonetheless, other studies have shown that in adult zebrafish maintained at 28.5°C under FR conditions, rhythmic locomotor activity became disrupted after several days (Hurd *et al.*, 1998), raising the possibility that our FR larvae may have altered sleep/wake patterns and/or circadian clocks. To further disentangle sleep/wake, circadian, and light/dark cues, we need to measure our FR zebrafish larvae sleep/wake behaviour as well as their circadian output (Table 6.1). To do this, we need to 1) track the sleep/wake behaviour of the same animal we use to image for synapses similar to what we have performed for normal LD rearing experiments (although this has its disadvantages due to pigmentation as discussed below in 6.2.5 Technical caveats section) and 2) measure clock gene output in these animals such as Period protein. Phosphorylation of Period proteins is involved in regulating the periodicity of the circadian clock. A Tg(per3:luc) reporter line allows for the measurement of zebrafish circadian molecular rhythms by recording bioluminescence of firefly luciferase driven by the rhythmic *per3* promoter (Kaneko and Cahill, 2005). However, as the bioluminescence clock output is animal-wide and will interfere with synapse imaging, we will not be able to directly measure the circadian molecular clock in the same animal that we track synapse rhythmicity. Nonetheless, these two approaches should give us an insight into circadian dynamics in free-running animals in our set up even without directly measuring clock output and synapse dynamics simultaneously from the same animals.

Circadian clock

While we found that extended waking period and subsequent sleep rebound can alter synapse dynamics, we cannot fully rule out the influence of circadian rhythms. The zebrafish retina displays robust circadian oscillations (Li *et al.*, 2005). For example, retinal neural sensitivity (measured by electrical physiological recordings from the cornea) and behavioural visual sensitivity (measured by the light threshold required to evoke visually-mediated escape responses) in larval zebrafish fluctuates between the day and night on normal LD cycles and persists in constant dark for 5-7 days, suggesting the involvement of circadian clock (Li and Dowling, 1998, 2000). However, prolonged light exposure at night restores visual responsiveness (Emran *et al.*, 2010). This is also reflected in the ribbon synapses at the

photoreceptors bipolar interface, which assemble during the day and disassemble during the night until exposed to light, when they reassemble (Emran *et al.*, 2010). Given that prolonged light exposure at night restores visual responsiveness and retains ribbon synapses, our observation that tectal cells synapse rhythmicity persisted for 1-1.5 cycles after transitioning into constant light suggests this process may be regulated by the internal circadian clock. To further distinguish between circadian influence and sleep/wake states-induce synaptic changes, we should sleep deprive the fish at different circadian times.

6.2.3 Circadian clock/constant light biases morphological subtypes development

We found that in the absence of an intact circadian clock, the relative proportion of tectal neurons was altered to include more Type 1 and 3 over Type 2 and 4 neurons. Setting aside the possibility of a technical artefact due to altered timing of/or sensitivity to electroporation, there are several intriguing possible mechanisms that warrant further exploration.

Circadian clock-gated cell division cycles and neurogenesis have been observed from cyanobacteria to mammals (Bouchard-Cannon *et al.*, 2013; Peyric, Moore and Whitmore, 2013; Hong *et al.*, 2014). It is possible that without circadian clock-gated cell division and synchronized developmental signals, FoxP2.A neurons were predisposed to becoming Type 1 and 3 neurons. For example, FoxP2.A expression is known to be regulated by Lef1, which is in turn activated by canonical Wnt signalling (Bonkowsky *et al.*, 2008). Wnt has been implicated in the mediation of coupling between cell cycle and the circadian clock (Matsu-ura *et al.*, 2016). Without a synchronized circadian clock, uncoordinated Wnt signalling could therefore lead to a bias of FoxP2.A neuronal subtypes if their differentiation is sensitive to the timing of the cell cycle.

There are also the possible effects of incoming RGC arbours, which could influence the development of the tectal cells (Culverwell and Karlstrom, 2002; Nikolaou *et al.*, 2015). Various circadian clock-controlled transcription factors have been shown to express in the developing retina. For example, *neurod*, a basic helix-loop-helix transcription factor that plays a role in cell cycle exit, cell fate determination, differentiation and cell survival, has rhythmic expression in the zebrafish retinal photoreceptors of developing zebrafish (Laranjeiro and Whitmore, 2014). Retinal photoreceptor genesis requires precise regulation of cell cycle exit and differentiation, which is aided by Neurod through the Notch signalling pathway.

Disruption of *neurod* rhythmic expression could alter RGC differentiation timing and retinotectal projection, which could then affect tectal subtype development.

Over-exposure of light stimuli could also cause neurons to change their morphology and functional identity. Sensory experience plays a major role in the formation and maturation of functional circuits, especially retinotopic mapping of RGC projections into the brain (Stuermer, 1988; Zhang *et al.*, 2016; Avitan *et al.*, 2017; Boulanger-Weill *et al.*, 2017). Recent findings have shown that the functional development of new-born neurons requires activity-dependent signalling (Boulanger-Weill and Sumbre, 2019). For instance, exposing Xenopus tadpoles to 4 hours of darkness triggered changes in morphology and excitability of tectal neurons (He *et al.*, 2016), and dark rearing zebrafish reduced functional connectivity between neuronal assemblies, impacting their ability to capture prey (Avitan *et al.*, 2017). Therefore, it is possible that prolonged light exposure in our assay led to functional and morphological changes in FoxP2.A neurons. To systematically test whether prolonged light exposure or circadian rhythm biased these cell subtypes, we need to look at the distribution of FoxP2.A subtypes in clock-break larvae raised in constant dark and circadian clock mutants reared under normal light/dark cycles.

6.2.4 FoxP2.A neuronal subtypes and their potential for synapse rhythmicity

We found that based on morphology FoxP2.A can be grouped into four subtypes. This is consistent with Nikolaou et al. where they also observed four subtypes in age-matched larvae to our study (2015).

It must be noted that while Nikolaou et al. used four morphological parameters (total filament sum, AP span, distal arbour laminar thickness, and distance from skin), we observed that using only these four parameters did not cluster morphological subtypes efficiently. For example, we often observed monostratified neurons (Nikolaou et al's Mt4/ our Type1) to be mixed with bistratified neurons. Therefore, we added two more morphological parameters (distal arbour location and proximal arbour location), which improved clustering subtypes. Additionally, some measuring method used to extract these parameters could differ between our studies. For example, we calculated AP span of the distal arbours in 3D, while Nikolaou et al measured in 2D. Clustering methods between our studies also differed. While we both standardized each data parameter, we found that transforming our parameters onto PCA space gives more definitive optimal k clusters using the elbow method, mean silhouette value, and Calinski

Harabasz coefficients. Moreover, Nikolaou et al cluster using 24 FoxP2.A neurons, whereas we used 87 neurons. While we believe that we were more methodical in categorizing FoxP2.A neuronal subtypes, these differences in parameter extraction and clustering methods makes it more difficult to compare Nikolaou et al. subtypes properties such as the subtype's functional identity probability to ours. This means that we have to identify and confirm our tectal neuron functional identities such as direction- and orientation-selectivity.

The UAS:FingR.PSD95(GCaMP7b) constructs/fish we have made will be most useful in linking the four subtypes to their functional properties. The replacement of GFP with a calcium indicator (which localizes at the synapses and the nucleus, see Chapter 3) will allow us to match FoxP2.A functional identity to synapse dynamics. Using the same short imaging paradigm, we could image the number of synapses through one-day and one-night, then show moving bars of different orientations and directions to identify the neuron's functional identity post hoc using the calcium indicator within the neuron's nucleus. Such experiments will not only allow us to compare our FoxP2.A subtypes to Nikolaou et al.'s but also elucidate the functional role of Type 2 neurons which have the potential to be rhythmic.

We found that Type 2 neurons' synapse number may be rhythmic in the presence of an intact circadian clock and alternating light/dark cues. By observation, Type 2 neurons are bistratified and resembles Mt1 in Nikolaou et al (2015). 65% of Mt1 population were vertically tuned. However, morphological details of each neuronal subtypes were not available in (Nikolaou *et al.*, 2015); therefore, we cannot conclusively determine whether our Type 2 is Nikolaou et al Mt1. Our Type 2 also appeared to be akin to GABAergic rostrocaudal-responsive type 1 neurons (Gabriel *et al.*, 2012). However, rostrocaudal-responsive Type 1 neuron have an average AP span of 38.7µm, while our Type 1 neuron is about ~47µm. Rostrocaudal-responsive type 1 neurons have average distal thickness of 10µm, while ours is ~15µm.

To give more insights into these neurons, we could more methodically look into what tectal laminae they target to, following the methodology of (Gabriel *et al.*, 2012). Briefly, we can sparsely express cell membrane markers such as mKate2f in FoxP2.A neurons in a Tg(pou4f3:GFP) line, in which the GFP expression reproducibly labels RGC fibres targeting stratum opticum and two sublayers of the stratum fibrosum et griseum superficiale ($SFGS_D$ and $SFGS_F$) (Gabriel *et al.*, 2012; Preuss *et al.*, 2014) . Using Tg(pou4f3:GFP) as an anatomical yardstick, we can determine more carefully the relative dendritic depth of our FoxP2.A

neurons. Then we could extract the same morphological parameters and cluster these neurons with our existing dataset. This will give a more precise understanding of the anatomy of our neurons that can be used to further infer functionality. Moreover, we should confirm our tracked FoxP2:FingR(PSD95) neurons' neurotransmitter identities by doing immunohistochemistry against GABAergic markers. In larval zebrafish, most tectal neurons are glutamatergic or GABAergic while a minority were found to be cholinergic (Robles *et al*., 2011). Distinguishing these would help infer the subtypes' functionality and may explain the subtype-specific synapse dynamics.

6.2.5 Technical caveats and future experiments

Using our modified FingR system, we were able to track synapse number of single cells in individual animals through different behavioural states. Our pipeline of labelling single-cells, repeated imaging, and behavioural tracking is highly technically challenging and comes with some caveats. Firstly, our genetically labelling single tectcal cell method is laborious and low throughput. Secondly, imaging animals multiple times a day resulted in a high level of animal handling which sometimes led to unhealthy animals and further reduced our sample size.

Thirdly, to acquire sleep/wake behaviour data, we were required to use pigmented animals as our automated video tracking system detects pixel changes. However, pigment molecules, such as melanin, absorb visible light and reduce the optical accessibility of tissues (Jacques, 2013). To image synapse dynamics and record their sleep/wake behaviour, we had to image pigmented larvae using a much higher laser power when compared to non-pigmented ones. This led to increased incidents of photo-bleaching and reduction in sample number. Skin pigmentation often occluded the FoxP2:FingR(PSD95)+ neuron resulting in reduced signal. To overcome this technical caveat, we can use F0 gene editing techniques to titrate pigmentation in individual larvae down but not completely removed, which would strike a balance between behavioural tracking and imaging (Kroll *et al.*, 2021). Nonetheless, less pigmentation on the larvae could also compromise the accuracy of behavioural tracking.

Table 6.1: On-going and future experiments. Details of proposed experiments and rationales discussed throughout 6.2 Discussion. Experiments are ranked by level of importance with the top representing most importance.

Question addressed	Future Experiment	Proposed Method
Do LL/FR still have intact circadian rhythm and sleep/wake behaviour?	Circadian/ locomotor tracking of LL and FR larvae	1) Track locomotor activity and synapse dynamics of LL and FR. 2) Track circadian output of LL and FR using Tg(per3:luc)
Is it light or tectal activity that drives synaptic change?	Activity-driven synaptic change	Visually-evoke tectal cells via moving bars and image synapse dynamics pre- and post-stimuli and sleep
What are FoxP2.A subtypes function?	FoxP2.A subtypes functional identity	Show FoxP2: FingR(PSD95)- GCaMP7b larvae moving bars of different orientation while imaging calcium response
What are FoxP2.A subtypes anatomical properties?	FoxP2.A subtypes anatomical identity	1) Posthoc immunohistochemistry of FoxP2:FingR(PSD95) cells for neurotransmitter type. 2) Tg(pou4f3:GFP) to confirm tectal layer abourization of subtypes
Are synapse dynamics neuron- or branch- or input-specific?	Location-specific synapse tracking	Segment neurons into obvious parts (proximal/distal arbour) and look at arbour-specific synapse dynamics
Can we balance reduced pigmentation for imaging while retain ability to track behaviour?	Improve synapse imaging in behaviourally tracked larvae	Titrate larvae pigmentation down but not completely removed them via F0 knockout methods

6.3 CHARACTERIZATION OF HYPOCRETIN SYSTEM

The main aim of Chapter 5 was to provide a platform for synaptic investigation of Hcrt neurons. To achieve this, we further characterized the hypocretinergic system in zebrafish larvae, investigated whether Hcrt neurons have distinct subtypes as defined by their projection sites, and identified potential regions to track Hcrt synapse dynamics.

We found that Hcrt projections were highly stereotypical and show little age-matched inter-fish differences and that projections were widespread throughout the brain. Our results are consistent with previous observations of Hcrt projections in zebrafish and mammals, with some potentially important differences discussed in more detail below. We also identified more diversity among single Hcrt neurons than has been widely appreciated. Finally, we identified several synapse-rich areas where Hcrt neurons receive input from other cell types; this will be important for future examination of the SHY hypothesis in subcortical neurons involved in sleep/wake regulation.

6.3.1 Mapping of the Hcrt system

Our results showed that Hcrt neurons project to the telencephalon, diencephalon, mesencephalon, and the spinal cord in the larval zebrafish, which is consistent with previous observations.

Telencephalon and Diencephalon

We found that Hcrt neurites project rostrally along the LFBs towards the ventral and dorsal telecephalic area in larval zebrafish. This is consistent with adult zebrafish sections showing Hcrt fibres innervating the dorsal telecephalic area (Appelbaum, *et al.*, 2009). Interestingly, adult zebrafish *hcrtr* mRNA expresses only in the ventral telencephalic area and not the dorsal counterpart. This suggests that Hcrt innervation of the pallium could have an afferent or glutamatergic target.

We found that Hcrt fibres cross the posterior commissure but do not innervate the habenulae in larval zebrafish. Adult zebrafish sections also show Hcrt:eGFP fibres cross the posterior commissure and habenula commissure. However, in adults, some Hcrt neurites innervate the ventral habenula, where HcrtR mRNA expression is also detected (Appelbaum *et al.*, 2009). This discrepancy in our findings at the larval stage to the adult sections suggests that Hcrt neurite innervate ventral habenulae at a later stage than 10dpf. The Hcrt-ventral habenular

circuit is also conserved in male mice, where it modulates aggressive behaviour by sending neuropeptide to inhibit lateral habenular cells, the mammalian equivalent of the ventral habenula (Flanigan *et al.*, 2020).

Our findings indicate that Hcrt neurites do not come into close contact with the epithalamus proper and therefore are unlikely to form glutamatergic synapses with the structure at the larval stage. The previously reported observation of circadian rhythmicity of the abundance of a Hcrt presynaptic marker that synapses onto the pineal gland (Appelbaum *et al.*, 2010), is more likely to be an en passant synapse along the posterior commissure. However, without co-labelling the pineal projection neurons, we and others cannot conclude that Hcrt neurons make bona fide synaptic connection with pineal projection neurons.

Our observations were contradictory to previous studies by Appelbuam et al (2009, 2010). This discrepancy is unlikely to be due to difference in our Hcrt:KalTA4 transgene, as we used the same promoter as the authors (obtained from Mourrain lab, Stanford). Both we and Appelbuam et al. observed Hcrt+ neurites along the posterior commissure; however, Appelbuam et al used both GFP as their marker for pineal (aanat2:EGFP) and Hcrt fibres, which could give rise to the misidentification of a physical innervation of Hcrt to the pineal complex. We confirmed that Hcrt fibers, at least up to 10dpf, do not innervate the pineal complex by labelling Hcrt neurons in RFP and the pineal complex in GFP. Moreover, the aanat2:EGFP transgene used in Appelbaum, similar to the FoxD3:GFP used in our study, does not label pineal projection neurons. Therefore, Appelbuam et al. could not observe connections between Hcrt+ neurites and pineal projection neurons. Nonetheless, using *in situ* hybridization, Appelbuam et al showed that Hcrt receptor was expressed in the pineal by 2dpf, indicating it is present at least at the mRNA level in larval stages. As Hcrt cells are glutamatergic and secrete Hcrt neuropeptide, our results indicate that Hcrt do not form bona fide glutamatergic synapses within the pineal complex, where close contact is needed. But long-range Hcrt signalling via the neuropeptide to the pineal complex cannot be ruled out.

In the ventral diencephalon, we found extensive Hcrt neurites in hypothalamic neuropil and dense connections within Hcrt neurons themselves with a high level of excitatory synapses onto Hcrt neurons. It is also known that Hcrt itself increases neuronal activity via HcrtR2, indicating a direct positive feedback regulation by Hcrt (Ono and Yamanaka, 2017).

Nonetheless, it is unknown whether the excitatory postsynaptic density that we observed are from Hcrt neurons themselves or from other cell types.

Mesencephalon

We found that Hcrt neurites project to the deepest tectal neuropil laminae: the SAC/SPV by 3dpf. Adult zebrafish brain sections also showed that Hcrt neurites project to and are restricted in the SAC of the tectum (Kaslin, 2004). 5% of the retinal ganglion cells (RGCs) project to the interface between the SAC/SPV (Nevin *et al.*, 2010). This deep tectal layer contains axonal inputs from other brain regions (including other sensory modalities), as well as the dendrites and axons of tectal neurons and is thought to play a role in secondary visual processing and coordination of the motor response (Scott and Baier, 2009; Nevin *et al.*, 2010; Baier, 2013). There are other examples of hypothalamic neurites arborizing in this tectal layer. Heap et al found that a genetically unidentified hypothalamic population, which does not appear to be Hcrt, projects to the same deep layer into the tectum (2018). These hypothalamic neurons were found to send inhibitory signals to tectal cells, suggesting hypothalamic neurons have a role in modulation of tectal output. Moreover, the nucleus isthmus, a cholinergic nucleus thought to modulate attention during hunting behaviour, also sends projections to the same layer (Henriques *et al.*, 2019). Hcrt neurites arborizing in this layer could play a role in the integration of generalized arousal states, sensory input, and motor output.

Elsewhere in the mesencephalon, Hcrt neurons send dense processes to the tegmentum, particularly at the LC and raphe nuclei, which is consistent with previous observations in zebrafish and mammals (Peyron *et al.*, 1998; Kaslin, 2004; Prober *et al.*, 2006). These anatomical connections to sleep/wake areas have also been confirmed functionally. The raphe nuclei, a serotoninergic hub, is thought to be downstream of Hcrt. This result is consistent with Kaslin et (2004) where Hcrt receptors were detected in the dorsal raphe of zebrafish. Recently, Chowdhury et al. showed that optogenetic activation of 5-HT in the LHA inhibits Hcrt neurons (2016).

The LC is an important wake-promoting nucleus. It has been shown in zebrafish and rodents that noradrenaline from the LC is a critical downstream effector of Hcrt neurons (Carter *et al.*, 2012; Singh *et al.*, 2015). For example, inactivation of LC neurons during Hcrt stimulation blocked Hcrt-mediated sleep-to-wake transition in rodents (Carter *et al.*, 2012). While the LC

is downstream of Hcrt neurons in the induction and maintenance of wakefulness, some evidence suggests that the LC also sends negative feedback signals onto Hcrt neurons in rodents (Gompf and Aston-Jones, 2008). Our live imaging experiments with FingR(PSD95) showed that Hcrt receive excitatory input near the LC proper, suggesting a potential positive feedback system back onto Hcrt from the LC. However, as we did not co-label the LC with a pre-synaptic marker, we cannot conclude that Hcrt neurons receive excitatory feedback from the LC in the zebrafish larvae. To verify the whether there are bona fide excitatory input into Hcrt neurons from the LC, we could use modified FingR(PSD95)-GCaMP7b to detect incoming excitatory inputs while simultaneously photoactivating LC neurons. Once this LC-Hcrt feedforward pathway is established, the LC is a good candidate for tracking synapse dynamics using the FingR system through sleep and wake behaviour, as the LC on both sides are easy to demarcate.

Due to the low level of expression of the FingR system (discussed in Chapter 2), it was very difficult to image Hcrt excitatory synapses in other neurites such as the tectum. One possible method to circumvent this problem is to do immunohistochemistry labelling with iterative expansion microscopy (iExM) (Wassie et al., 2019). Previously, amplifying FingR-GFP signal during immunohistochemistry was not possible (see Chapter 2), as unbound secondary antibody cannot be cleared out efficiently. iExM, where the specimen is expanded twice using a swellable gel in an isotropic fashion, would allow amplification of weak FingR fluorophore signals as well as clearing out unbound antibody labelling. Such experiments would allow for the investigation of anatomical connections between Hcrt neurites and the tectum; however, with our current imaging set up, potential Hcrt synapses within the tectum cannot be used to study long-term synaptic dynamics.

Spinal cord

Hcrt neurons projections to the spinal cord in larval zebrafish is consistent in the findings in mouse, rat, and human (van den Pol, 1999). That study found high densities of innervation in the dorsal horn, intermediolateral column, and lamina X of the spinal cord. Moreover, in rodents, Hcrt receptors were detected in all regions of spinal cord grey matter and on C-fibres within the dorsal root ganglion (Hervieu *et al.*, 2001), suggesting Hcrt involvement in the modulation of sensation, pain, and motor control. For example, Hcrt injections were found to have dose-dependent anti-nociceptive effects in mice and rats model of nociception and

hyperalgesia, which can be reversed by HcrtR antagonist (Bingham *et al.*, 2001). We also observed en passant excitatory synapses along Hcrt fibres in the spinal cord (data not shown), suggesting a potential positive feedback system back onto Hcrt from the spinal cord. It is interesting to speculate that Hcrt neurons directly communicate with these nociceptive neurons to ameliorate pain. To verify these connections, techniques such as GFP Reconstitution Across Synaptic Partners (GRASP) (Feinberg *et al.*, 2008) could be used. GRASP relies on the corresponding pre- and postsynaptic membranes at synapses to reconstitute a split GFP molecule. For example, one half of the split GFP can be express in Hcrt neurons and the other half of split GFP under somatosensory neurons promoter in the spinal cord such as neurogenin 1 (McGraw *et al.,* 2008). If these two neuronal population form putative synapses, functional GFP should form at the location of synapse.

6.3.2 Single cell Hcrt Characterization

The knowledge of the Hcrt projectome will give insight into the heterogeneity of the system. To visualize individual Hcrt neurons in their entirety, various approaches were attempted.

Single-cell visualization approaches

Firstly, we utilized PaGFP to label single Hcrt cells. PaGFP is a reporter that after photoactivated by 488 nanometer light, increases its fluorescence nearly two folds (Patterson and Lippincott-Schwartz, 2002). However, we found that PaGFP could not reliably label single Hcrt neurons due to the depth of Hcrt somata. It could not fully convert GFP to fill in the entire Hcrt neuron projections. Attempts at higher laser power and/or longer exposure time damaged the live specimen.

In a second approach, we utilized dextran electroporation to label single Hcrt cells. In this method, we electroporated a green dextran into single neurons in the transgenic line that labels the Hcrt population in RFP. However, dextran electroporation was not successful as the electroporation needle had to go through an entire brain to reach Hcrt somata.

Another approach taken was multicolor labelling of Hcrt neurons by Brainbow or cytobow. The Brainbow method is an elegant tool for morphological reconstruction of multiple cells in larval zebrafish (Robles et al., 2013), since it allows multicolor labelling in stable transgenic lines depending only on Cre recombinase, which can be added using drugs such as Tamoxifen. To attempt this UAS:cytobow line was generated in the background of Tg(Hcrt:KalTA4). In

theory, this approach should allow more efficient single-cell reconstruction, but its actual efficiency in Hcrt cells was overall very low due to the UAS:Cytobow line not fully expressing in all Hcrt neurons as well as being very leaky, with ectopic expression.

The method we found most successful was sparse single-color labelling by injecting a Hcrt:GFP plasmid into Tg(Hcrt:KalTA4;UAS:RFP) larvae. Although successful, the transient expression of Hcrt:GFP in only one Hcrt cell in the background of Hcrt:RFP population was difficult due to the low number of Hcrt neurons and their close proximity to each other. This often resulted in two Hcrt neurons being GFP+ or none at all. It was also low through-put as screening had to be done using laser microscopy such as lightsheet or confocal microscopy rather than widefield microscopy. Due to the low-throughput approach we took, we were not able to find a relationship between the single-cell Hcrt projectome and their soma location. Also of note, it is also possible that the Hcrt:GFP single-cell transient expression approach we took may favour certain subtypes of Hcrt expression. For instances, we only found one (out of 20) neuron that projects contralaterally towards the LC. Determining whether this is a common or rare subtype will require the imaging of many more single Hcrt neurons.

Another method that could be adopted in the future to improve our single-cell labelling experiment is to use the UAS:bloSwitch single-cell labelling technique (Marquart *et al.*, 2019). This method exploits the relatively inefficient yeast recombinase B3 under a heatshock promoter in zebrafish, where heat-shock conditions can be tritiated to achieve stochastic expression of RFP in only one neuron and not the rest, resulting in a single RFP+ neuron amongst GFP+ cell bodies. As bloSwitch is underneath the control of UAS (upstream activating site), it can be crossed to any existing Gal4 lines such as Hcrt:KalTA4 to activate expression. Moreover, Marquart et al (2019) also used a transgenic line with a different, non-overlapping fluorophore (Tg(elavl3:Cer)) as a brain-wide marker. This would allow brain registration into ZBB brain atlas (Marquart *et al.*, 2015), allowing for the easy comparison of different fish as well as to the database of other existing transgenic lines.

We could not register our single-cell labelling data, as a pan-neuronal transgenic line with non-overlapping fluorophore to RFP and GFP were not available. To circumvent this issue, we performed antibody labelling post Hcrt:GFP injection in order to use a pan-neuronal marker like DAPI. However, due to the transient nature of our injection, there are low non-genome integrated Hcrt:GFP signals in cells other than the single Hcrt cell, which were not detectable

during live imaging. These low GFP signals were amplified during the immunohistochemistry process causing more than one Hcrt GFP+ neuron to be visible, confounding our single-cell Hcrt labelling method.

Diversity in Hcrt neurons projections

Overall, the Hcrt neuron single-cell data collected so far have shown that there is a diversity in the Hcrt projectome. This is consistent with findings in rodents that Hcrt neurons can be at least subdivided into two functional and anatomical subpopulations (Estabrooke *et al.*, 2001; Fadel, Bubser and Deutch, 2002; Harris, Wimmer and Aston-Jones, 2005; Iyer *et al.*, 2018). Consistent with Iyer et al., our preliminary data found that not all individual Hcrt neurons project to the sleep/wake centres such as the LC, suggesting the possibility that different subpopulations of Hcrt neurons (depending on their projectome) are involved in discrete behavioural tasks. However, while Iyer et al. found that Hcrt neurons projecting to sleep/wake and reward centres are intermingled and do not have a topographic location, more single-cell data should be collected to uncover any relationship between Hcrt projectomes and their somata location in the larval zebrafish.

Other hypothalamic neuronal populations that have roles in diverse behaviors have been shown to have discrete subpopulations that are defined by their projection sites and functions. For example, in rodents, galanin-expressing neurons of the hypothalamus coordinate motor, motivational, hormonal, and social aspects of parenting in mice (Kohl *et al.*, 2018). Like Hcrt neurons, these neurons receive inputs from large number of brain areas and send neurites throughout the brain. Subsets of galanin neurons form discrete pools that are defined by their projection sites and function, regulating different aspect of parenting behaviors (Kohl *et al.*, 2018). Such projectome distinct subpopulations within the hypothalamus have also been observed in larval zebrafish. Oxytocin neurons regulate a diverse set of processes such as stress, metabolism, and social behavior. Oxytocin neurons were found to have two main subpopulations defined by their projections: a hypophysiotropic pool that projects primarily to the pineal and encephalotropic cells that have much more diverse morphologies, with each cell featuring a unique innervation pattern throughout the brain (Herget *et al.*, 2016). The hypophysiotropic population were found to reside in the rostral part of the neurosecretory pre- optic area, while encephalotropic cells were located more caudally (Herget *et al.*, 2016). Therefore, it is possible that other hypothalamic neurons

that have roles in diverse behaviors such as the Hcrt neurons also follow similar functional circuit architecture.

6.3.3 Hcrt synapse dynamics – future directions

Our characterization of Hcrt illustrated that excitatory postsynaptic densities were found near the LC, within the hypothalamic neuropil, as well as en passant synapses in the spinal cord. An interesting hypothesis to test is whether sleep/wake and sleep deprivation differentially alter distinct groups of Hcrt synapses within the same neuron. For example, the Hcrt-LC pathway are involved in wake promotion and maintenance, while Hcrt synapses within the hypothalamic neuropil may be involved in metabolic and energy regulation (Prober *et al.*, 2006; Gompf and Aston-Jones, 2008). We therefore predict that sleep/wake and sleep deprivation could alter synapse dynamics in these locations differentially within the same neuron. Recent studies have shown that homeostatic synaptic scaling in vivo is locally implemented rather than neuron-wide. For example, synaptic scaling was observed in a branch-specific manner in the mouse visual cortex (Barnes *et al.*, 2017). Target-specific synaptic changes have also been observed in Drosophila, where output from Kenyon cells to different synaptic partners showed varied changes with sleep loss (Weiss and Donlea, 2021). Although Weiss et al looked at the whole Kenyon cell population and not at a single-cell level, it would be interesting to see whether synapse dynamics in single Hcrt neurons, with widely projected neurite and involve in different behavior and circuits, have circuit-specific and behavioral-specific synapse dynamics. A possible experiment is to track FingR targeting PSD95 and GPHN within the LC, hypothalamic neuropil, and the spinal cord during day and night and during sleep deprivation (similar to experiments performed on tectal cells) as well as starvation.

Moreover, it has been found that the locomotor activity patterns of tethered larval zebrafish where the tails and eyes are free to move mimic normal sleep/wake patterns of freely swimming larvae (unpublished data, D Lyons, Rihel lab). For example, activity from the tails and eyes of tethered larvae are significantly higher during the day phase than the night phase. Moreover, Hcrt neuron activity, measured by genetically encoded calcium indicators, was tightly associated with tail and eye activity during the day , with considerably less activity at night (Naumann *et al.*, 2010). A possible experiment is to image Hcrt synapse dynamics at the LC using FingR with nuclear-restricted calcium indicator while simultaneously monitoring the

Hcrt nuclear calcium signal and tail movement as readouts of sleep/wake states. Although an attractive idea, to systematically address SHY within the Hcrt-LC pathway, we need to obtain more single-cell data to improve clustering and link morphological types of Hcrt projectome and their somata location.

6.4 IMPLICATIONS FOR SHY

SHY posits that sleep induces widespread downscaling of excitatory synaptic strength throughout the CNS, but evidence for this has been inconsistent. Here, we developed novel tools to visualize synapse numbers of the same neuron through sleep/wake states of freely behaving animals, asked whether sleep can drive widespread synapse number reduction in a group of easily accessible neurons, and provided a platform for similar studies in deeper and functionally-wide ranging hypothalamic neurons.

In optic tectal neurons, we found that population-level synapse rhythmicity is consistent with SHY, where synaptic increases coincided with periods wakefulness and synaptic depression coincided with sleep. While natural sleep and wake totals did not correlate with synapse dynamics, extended wakefulness increased the number of synapses and during subsequent sleep, synapses number was reduced. However, tracking of single neurons of freely behaving animals through multiple days and nights revealed highly diverse synapse dynamics, indicating that sleep/wake states and external light cues may differentially alter individual neurons. Together these findings provide evidence that while sleep may favour synaptic number depression at the populational level as SHY predicted, neurons have complex and diverse synapse dynamics that cannot be parsimoniously explained by SHY.

6.4.1 New Approach to Study SHY

Our approach to monitor synapses of individual cell at a whole-cell level have not been attempted previously. Our methodical dissection of circadian, light/dark cues, and sleep/wake states influences on synapses, were able to fill in the gap between molecular and structural 'snapshot' studies (Gilestro, Tononi and Cirelli, 2009; de Vivo *et al.*, 2017; Noya *et al.*, 2019) and branch or circuit specific synapse studies (Maret *et al.*, 2011; Matsumoto *et al.*, 2020; Cary and Turrigiano, 2021). For example, we were able to track synapse dynamics of the same neurons through different level of sleep pressure. To thoroughly examine SHY, comprehensive studies of different types of neurons synapse dynamics during sleep and wake

behaviour are needed. It would be interesting to see whether SHY applies to other types neurons, such as those in the hypothalamus that have inputs from various brain regions, widespread efferent fibres throughout the brain, and roles in various behavioural regulation. While synapse dynamics of such neuronal populations have been studied in isolated branches (Appelbaum *et al.*, 2010; Elbaz *et al.*, 2016), synapse visualization at a single-cell level with reliable tools had not been achieved. To that end, we have established a platform to thoroughly monitor synapse dynamics of single Hcrt cell. Moreover, with our modified FingR tools, we can study synapse dynamics of virtually any neuron in the zebrafish. Additionally, we can track inhibitory synapse dynamics during sleep and wake, an area that is understudied with regards to SHY (Tononi and Cirelli, 2014; Elbaz *et al.*, 2016; Bridi *et al.*, 2020).

One caveat is that our study only examined synapse number and not synapse strength. In terms of SHY, our readout of would only detect newly created synapses and weak ones that have been depressed resulting in their elimination. Our findings therefore are not sensitive to small changes in synaptic strength and could be underestimating sleep/wake-driven synapse dynamics and/or masking other influences on synapse dynamics such as the circadian clock. Nonetheless, from our approach we were be able to detect whole-cell synapse dynamics through time, which revealed highly diverse synapse dynamics that do not uniformly conform with SHY.

6.4.2 Individually, neurons do not SHY away

While at the population level, the synapse dynamics of tectal neurons coincided with day/night phases, we found such phenomena were not reflected at the individual neuron level. SHY proposes that sleep-dependent down-selection results in some synapses becoming less effective than others (Tononi and Cirelli, 2014). This could either be because stronger synapses undergo less depression in strength than weaker ones or stronger synapses are spared from depression all together. Both possibilities imply that there is a net synaptic depression in *individual* neurons after sleep. In contrast, we found that not every neuron undergoes net synaptic changes in line with the population dynamics. Moreover, preliminary findings of subtype dynamics suggest synaptic rhythmicity may be restricted to certain cell types, which casts doubt on the meaning of population level synaptic changes. As the group of neurons that exhibit SHY-like rhythmicity makes up a large proportion of cell studied, the average population synapse dynamics would appear to follow SHY even though the effect is

dominated by a single cell type. This also suggests that not all neurons need to undergo down-selection as predicted by SHY.

Although tracking of whole-cell individual neurons had not previously been done, diversity in sleep-dependent synapse dynamics of neurons of the same neuronal class have been observed in Drosophila. Using knock-in GFP-tagged Bruchpilot protein as a marker presynaptic strength, Weiss et al. found that presynaptic strength of terminals within the entire mushroom body lobes inversely correlated to recent sleep time (2021). However, cell-type specific examinations revealed that not all cell types that innervate the mushroom body follow this population-wide synapse dynamics. For example, Kenyon cells exhibit increases in pre-synaptic Bruchpilot protein abundance after sleep deprivation, but similar increases were not detected in other neurons that innervate the mushroom body. Similar to our observations on Type 2 neurons, these results indicate that within certain neuronal subpopulations synapse dynamics can drive the observed population level synaptic dynamics. Moreover, Weiss et al. also found that each class of Kenyon cell has diverse synapse dynamics after sleep deprivation. For example, Kenyon cells with output synapses onto mushroom body interneurons have different synapse dynamics to those with outputs onto mushroom body output neurons (2021), suggesting diversity in sleep-dependent synapse dynamics between neuronal class, which is consistent with our findings that individual FoxP2.A neurons have diverse synapse dynamics. Their results also suggest the possibility of compartment-specific synaptic changes within individual Kenyon cells; however, this was not confirmed by single-cell tracking of synapses. Our and Weiss et al. studies demonstrate diverse patterns of synapse dynamics and highlight the importance of observing synapse dynamics in cell-type or individual neuron manner in order to understand population wide dynamics. Our work in Chapter 5 provides a platform to extend the study of circuit specific synapse dynamics of single neurons.

Nonetheless, our findings could be interpreted as consistent with populational morphological studies that have been used to support SHY (Gilestro *et al.,* 2009; de Vivo *et al.*, 2017; Diering *et al.*, 2017), as the diversity in single neuron dynamics we observed may be masked by the population dynamics in studies that did not track single neurons through time. For example, using electron microscopy, De Vivo et al. compared the axon-spine interface of mice that were sleeping and mice that were awake at the time of sacrifice (2017). We both found that at the

populational level synapse number peaked during the phase that coincides with wakefulness and has a nadir with the phase that coincides with sleep. But due to the 'snapshot' nature of their studies, they could not look at this phenomenon at the individual neuron level.

Our findings are also consistent with studies that measure single neuron's synaptic properties such as Liu et al (2010) and Cary and Turrigiano (2021). Liu et al (2010) found that mEPSCs from frontal cortex slices of rodents are increased after waking and reduced after sleep, which corroborates our findings at the populational level. However, despite looking at the synaptic properties of neurons directly as a whole, ex vivo preparations are still 'snapshot' and could not determine single neuron dynamics through time. By tracking sleep/wake behaviour and synapses in the same animals, we found that sleep/ wake experience did not linearly correlate with synapse dynamics, similar to the conclusions of Cary and Turrigiano (2021). Liu et al did not look at sleep history of animal used for ex vivo recordings but used time-of-day as a proxy of prior sleep/wake experience. However, the inter-animal variability in the timing of consolidated sleep especially in rodents means that even when rodents are sacrificed at the exact same ZT, there are likely to have difference prior sleep/wake experience (Cary and Turrigiano, 2021).

6.4.3 Sleep driven synaptic number reduction

One of the unanswered questions about SHY is whether natural sleep state alone, without preceding salient experience, can drive synaptic depression. While we demonstrated that that natural sleep/wake amount do not correlate with synapse dynamics (Hengen *et al.*, 2016; Cary and Turrigiano, 2021; Torrado Pacheco *et al.*, 2021), like previous studies in favour of SHY we found that synapse number are reduced after the night phase (Gilestro, Tononi and Cirelli, 2009; Maret *et al.*, 2011; de Vivo *et al.*, 2017). This nighttime synapse number reduction in tectal neuron is specifically within the first period of sleep. Although we cannot rule out circadian influences from this finding, our extended wakefulness paradigm showed that synapse number reduction can occur during the latter part of the night independent of circadian time. Such periods coincides with high levels of slow wave sleep, which is highest at sleep onset, decreases with the time spent asleep, and progressively increases at sleep onset as the waking period is prolonged (Borb and Achermann, 1999; Vyazovskiy *et al.*, 2006).

Our findings are at least consistent with the SHY prediction that slow-wave sleep drives sleep-dependent synaptic downselection (Tononi and Cirelli, 2014). Indeed, morphological studies in favour of SHY that demonstrate the correlation between sleep (without the introduction of salient learning experiences) and synapse abundance and size were performed using sleep deprivation paradigms (Gilestro, Tononi and Cirelli, 2009; de Vivo *et al.*, 2017; Weiss and Donlea, 2021). It is possible that brain/region-wide reductions in synaptic strength of the animals that have slept compared to the sleep-deprived animals' found by these authors is due to the accumulation of slow wave-like and slow wave activity at sleep onset imposed by the sleep deprivation paradigm. Nonetheless, it is still unclear whether synaptic weakening correlates with sleep in animals that have not been sleep deprived or exposed to any salient learning experiences. This raises questions whether sleep rebound post extended wakefulness is 'natural sleep'.

The majority of studies that have linked sleep and synapse plasticity by tracking the same neurons/synapse over time have been conducted in the context of post-learning sleep (Gulati *et al.*, 2017; Norimoto *et al.*, 2018; Miyamoto *et al.*, 2021), leaving the role of sleep without prior learning experience ambiguous. Even in the context of learning, the role of sleep and synaptic plasticity have been complex. For instance, sleep plays a role in both strengthening and weakening synapses after specific learning tasks (Li and Gan, 2014; Durkin and Aton, 2016). Moreover, both REM and NREM stages of sleep have been linked to synaptic strengthening and weakening (Niethard *et al.*, 2016; Li *et al.*, 2017). For example, Li and Gan found that task-related neurons are activated during NREM sleep and that NREM sleep resulted in branch-specific spine formation (2014). There are also various evidences for sleep and wake states' role in numerous forms of plasticity (Aton *et al.*, 2013; Hengen *et al.*, 2016; Torrado Pacheco *et al.*, 2021). For instance, bidirectional changes in synaptic strength to baseline are gated by sleep and wake states after sensory deprivation and rebound (Torrado Pacheco *et al.*, 2021). This indicates that sleep/wake-dependent synaptic plasticity can occur after extreme perturbations such as monocular deprivation and eye reopening paradigm but not in natural sleep-wake periods. Together with the large body of literature, our findings are consistent with the view that sleep does not have a singular effect on synaptic strengths, but that sleep and wake states are able to gate various forms of synaptic plasticity.

6.4.4 Zebrafish tectal neurons compatibility with SHY

SHY proposes that sleep-dependent synaptic down-selection occurs in cortical neurons and are more reserved about ancient brain structures such as the brain stems or in invertebrates such as fruit flies (Tononi and Cirelli, 2014). Therefore, it could be argued that SHY is not applicable to non-cortical neurons such as our tectal neurons. However, we argue that zebrafish tectal neurons fulfil the neuronal plasticity criteria set by SHY.

SHY claims that neurons should follow certain criteria regarding plasticity. 1) Learning should happen mostly through synaptic potentiation. Hence, firing that denotes 'suspicious coincidences' – when inputs co-occur more frequently than chance – can percolate throughout the circuit (Barlow, 1989). Consequently, SHY argues that, in special cases, neurons that receive all its inputs from the same source or from strongly correlated sources could not foster competition among synapses, rendering down-selection ineffective. 2) Synaptic strengthening should primarily occur during wakefulness, when the animal learns and interacts with the environment. 3) Renormalization of synaptic strength should occur mostly during sleep when neurons can sample the circuit overall environment comprehensively and not be biased by signals occurring during wakefulness.

We argue that zebrafish tectal neurons fulfil these criteria set by SHY. 1) Despite being a part of the midbrain, tectal neurons detect 'suspicious coincidences' and undergo synaptic potentiation. Tectal neurons can undergo spike-timing-dependent plasticity. Zhang et al. (1998) found that activation of presynaptic RGCs input via electrode induce either LTP or LTD depending on timing of input and depolarization of postsynaptic tectal neurons. Moreover, despite being the main retinorecipient brain region, the OT is not only purely a sensory structure, it is an important sensorimotor integrator involved in orienting, avoidance, and visually-guided hunting (Gahtan, Tanger and Baier, 2005). In addition to receiving substantial retinal input, the OT is interconnected with numerous other brain regions such as pretectum, dorsal thalamus, dorsal tegmentum, nucleus isthmi, and reticular formation (Heap *et al.*, 2018; Bollmann, 2019; Henriques *et al.*, 2019). Tectal neurons receive inputs from a variety of sources and, therefore, have the potential to foster 'competition' amongst synapses, in line with expectations of SHY.

2) It has been shown that tectal cells can perform environmentally induced synaptic strengthening during wakefulness. Visual experience can directly strengthen tectal

glutamatergic synapses by increasing the abundance of AMPA receptors or the AMPA/NMDA ratio (Engert *et al.*, 2002; Haas, Li and Cline, 2006). Therefore, synaptic strengthening can occur in zebrafish tectal neurons when the animals interact with the environment as SHY suggested.

3) Zebrafish can 'sample the overall circuit environment' during sleep similar to higher vertebrates. SHY proposes that such mechanisms occur during higher vertebrate slow wave sleep (Tononi and Cirelli, 2006). Recent evidences have found sleep-dependent brain-wide neural signatures in larval zebrafish. One such neural signature, termed 'slow bursting sleep', shares commonalities with those of slow-wave sleep found in higher vertebrates where its occurrence is proportional to sleep pressure (Leung *et al.*, 2019). This demonstrates that zebrafish tectal neurons may be able to 'sample the circuit environment' during sleep as SHY hypothesized.

Based on these criteria, zebrafish tectal cells meet SHY's expectations for neurons to possess the ability for sleep-dependent synapse renormalization. However, we observed complex influences of the circadian clock, alternating light/dark cycle, and sleep in synapse dynamics in these tectal cells, that cannot be parsimoniously explained by SHY.

6.5 CONCLUDING REMARKS

In this past decade, SHY has been an influential and highly debatable hypothesis with many studies in support and many others that equally contradict it. This study has explored synapse dynamics in a small population of neurons in the zebrafish larvae and uncovered the complexity of synapse dynamics that are partially but not fully explained by SHY. Our study highlights the need for a comprehensive investigation of synapse dynamics in the context of sleep/wake and circadian clock at the single-cell level in various other types of neurons and animal models in order to address SHY.

References

Abel, T. *et al.* (2012) 'Genomic analysis of sleep deprivation reveals translational regulation in the hippocampus', *Physiological Genomics*.

Ahrens, M. B. *et al.* (2013) 'Whole-brain functional imaging at cellular resolution using light-sheet microscopy', *Nat Methods*, 10(5), pp. 413–420.

Antinucci, P. *et al.* (2020) 'A calibrated optogenetic toolbox of stable zebrafish opsin lines', *eLife*.

Appelbaum, L., Wang, G. X., *et al.* (2009) 'Sleep-wake regulation and hypocretin-melatonin interaction in zebrafish', *Proceedings of the National Academy of Sciences of the United States of America*, 106(51), pp. 21942–21947.

Appelbaum, L., Wang, G., *et al.* (2009) 'Sleep – wake regulation and hypocretin – melatonin interaction in zebrafish', pp. 1–6.

Appelbaum, L. *et al.* (2010) 'Circadian and homeostatic regulation of structural synaptic plasticity in hypocretin neurons', *Neuron*. Elsevier Inc., 68(1), pp. 87–98.

Aton, S. J. *et al.* (2013) 'Visual experience and subsequent sleep induce sequential plastic changes in putative inhibitory and excitatory cortical neurons', *Proceedings of the National Academy of Sciences of the United States of America*, 110(8), pp. 3101–3106.

Attili, S. and Hughes, S. M. (2014) 'Anaesthetic tricaine acts preferentially on neural voltage-gated sodium channels and fails to block directly evoked muscle contraction', *PLoS ONE*.

Avitan, L. *et al.* (2017) 'Spontaneous Activity in the Zebrafish Tectum Reorganizes over Development and Is Influenced by Visual Experience', *Current Biology*, 27(16), pp. 2407-2419.e4.

Baier, H. (2013) 'Synaptic Laminae in the Visual System: Molecular Mechanisms Forming Layers of Perception', *Annual Review of Cell and Developmental Biology*, 29(1), pp. 385–416.

Barker, A. J. and Baier, H. (2015) 'Sensorimotor decision making in the Zebrafish tectum', *Current Biology*. Elsevier Ltd, 25(21), pp. 2804–2814.

Barlow, H. B. (1989) 'Unsupervised Learning', *Neural Computation*..

Barlow, I. L. and Rihel, J. (2017) 'Zebrafish sleep: from geneZZZ to neuronZZZ', *Current Opinion in Neurobiology*. Elsevier Ltd, 44, pp. 65–71.

Barnes, S. J. *et al.* (2017) 'Deprivation-Induced Homeostatic Spine Scaling In Vivo Is Localized to Dendritic Branches that Have Undergone Recent Spine Loss Article Deprivation-Induced Homeostatic Spine Scaling In Vivo Is Localized to Dendritic Branches that Have Undergone Recent Spin', *Neuron*.

Bayés, À. *et al.* (2017) 'Evolution of complexity in the zebrafish synapse proteome', *Nature Communications*

Del Bene, F. *et al.* (2010) 'Filtering of visual information in the tectum by an identified neural circuit', *Science*.

Beuckmann, C. T. and Yanagisawa, M. (2002) 'Orexins: From neuropeptides to energy homeostasis and sleep/wake regulation', *Journal of Molecular Medicine*, 80(6)

Bianco, I. H. and Engert, F. (2015) 'Visuomotor transformations underlying hunting behavior in zebrafish', *Current Biology*, 25(7), pp. 831–846.

Bianco, I. H., Kampff, A. R. and Engert, F. (2011) 'Prey capture behavior evoked by simple visual stimuli in larval zebrafish', *Frontiers in Systems Neuroscience*.

Bingham, S. *et al.* (2001) 'Orexin-A, an hypothalamic peptide with analgesic properties', *Pain*.

Böhm, U. L. *et al.* (2016) 'CSF-contacting neurons regulate locomotion by relaying mechanical stimuli to spinal circuits', *Nature Communications*.

Bollmann, J. H. (2019) 'The Zebrafish Visual System: From Circuits to Behavior', *Annual Review of Vision Science*, 5(1), pp. 269–293.

Bonkowsky, J. L. *et al.* (2008) 'Domain-specific regulation of foxP2 CNS expression by lef1', *BMC Developmental Biology*, 8, pp. 1–15.

Borb, A. A. and Achermann, P. (1999) 'Sleep Homeostasis and Models of Sleep Regulation', *Journal of Biological Rhythms*.

Bouchard-Cannon, P. *et al.* (2013) 'The Circadian Molecular Clock Regulates Adult Hippocampal Neurogenesis by Controlling the Timing of Cell-Cycle Entry and Exit', *Cell Reports*.

Boulanger-Weill, J. *et al.* (2017) 'Functional Interactions between Newborn and Mature Neurons Leading to Integration into Established Neuronal Circuits', *Current Biology*, 27(12), pp. 1707-1720.e5.

Boulanger-Weill, J. and Sumbre, G. (2019) 'Functional integration of newborn neurons in the zebrafish optic tectum', *Frontiers in Cell and Developmental Biology*, 7(MAR), pp. 1–8.

Brenet, A. *et al.* (2020) 'Organophosphorus diisopropylfluorophosphate (DFP) intoxication in zebrafish larvae causes behavioral defects, neuronal hyperexcitation and neuronal death', *Scientific Reports*. d

Bresler, T. *et al.* (2001) 'The dynamics of SAP90/PSD-95 recruitment to new synaptic junctions', *Molecular and Cellular Neuroscience*, 18(2), pp. 149–167.

Bridi, M. C. D. *et al.* (2020) 'Daily Oscillation of the Excitation-Inhibition Balance in Visual Cortical Circuits', *Neuron*. Elsevier Inc., 105(4), pp. 621-629.e4.

Burket, C. T. *et al.* (2008) 'Generation and characterization of transgenic zebrafish lines using different ubiquitous promoters', *Transgenic Research*, 17(2), pp. 265–279.

Cai, D. *et al.* (2013) 'Improved tools for the Brainbow toolbox.', *Nature methods*, 10(6), pp. 540–7.

Carter, M. E. *et al.* (2012) 'Mechanism for Hypocretin-mediated sleep-to-wake transitions', *Proceedings of the National Academy of Sciences of the United States of America*, 109(39).

Cary, B. A. and Turrigiano, G. G. (2021) 'Stability of neocortical synapses across sleep and wake states during the critical period in rats', *eLife*, 10, pp. 1–28.

Chemelli, R. M. *et al.* (1999) 'Narcolepsy in orexin knockout mice: Molecular genetics of sleep regulation', *Cell*.

Chen, J. L. *et al.* (2012) 'Clustered Dynamics of Inhibitory Synapses and Dendritic Spines in the Adult Neocortex', *Neuron*. Elsevier Inc., 74(2), pp. 361–373.

Chen, S. *et al.* (2016) 'TRP channel mediated neuronal activation and ablation in freely behaving zebrafish', *Nature Methods*.

Chen, W. yu *et al.* (2019) 'Role of Olfactorily Responsive Neurons in the Right Dorsal Habenula–Ventral Interpeduncular Nucleus Pathway in Food-Seeking Behaviors of Larval Zebrafish', *Neuroscience*.

Chen, X. *et al.* (2015) 'PSD-95 family MAGUKs are essential for anchoring AMPA and NMDA receptor complexes at the postsynaptic density', *Proceedings of the National Academy of Sciences of the United States of America*, 112(50), pp. E6983–E6992.

Chowdhury, S. and Yamanaka, A. (2016) 'Optogenetic activation of serotonergic terminals facilitates GABAergic inhibitory input to orexin/hypocretin neurons', *Scientific Reports*.

Cirelli, C. (2017) 'Sleep, synaptic homeostasis and neuronal firing rates', *Current Opinion in Neurobiology*, pp. 72–79.

Colonnier, M. (1968) 'Synaptic patterns on different cell types in the different laminae of the cat visual cortex. An electron microscope study', *Brain Research*, 9(2), pp. 268–287.

Cook, S. G. *et al.* (2019) 'Simultaneous Live Imaging of Multiple Endogenous Proteins Reveals a Mechanism for Alzheimer's-Related Plasticity Impairment', *Cell Reports*.

Culverwell, J. and Karlstrom, R. O. (2002) 'Making the connection: Retinal axon guidance in the zebrafish', *Seminars in Cell and Developmental Biology*.

Dana, H. *et al.* (2019) 'High-performance calcium sensors for imaging activity in neuronal populations and microcompartments', *Nature Methods*.

Diering, G. H. *et al.* (2017) 'Homer1a drives homeostatic scaling-down of excitatory synapses during sleep', *Science*, 515(February), pp. 511–515.

Dijk, D. J. (2009) 'Regulation and functional correlates of slow wave sleep', *Journal of Clinical Sleep Medicine*.

Van Dongen, H. P. A. *et al.* (2003) 'The cumulative cost of additional wakefulness: Dose-response effects on neurobehavioral functions and sleep physiology from chronic sleep restriction and total sleep deprivation', *Sleep*.

Dreosti, E. *et al.* (2015) 'Development of social behaviour in young zebrafish.', *bioRxiv*, 9(August), p. 017863.

Durkin, J. and Aton, S. J. (2016) 'Sleep-dependent potentiation in the visual system is at odds with the synaptic homeostasis hypothesis', *Sleep*.

Easter, S. S. and Nicola, G. N. (1997) 'The Development of Eye Movements in the Zebrafish (Danio rerio)', *Developmental Psychobiology*.

El-Husseini, a E. *et al.* (2000) 'PSD-95 involvement in maturation of excitatory synapses.', *Science (New York, N.Y.)*, 290(5495), pp. 1364–1368.

Elbaz, I. *et al.* (2012) 'Genetic ablation of hypocretin neurons alters behavioral state transitions in zebrafish', *Journal of Neuroscience*, 32(37), pp. 12961–12972.

Elbaz, I. *et al.* (2016) 'Sleep-Dependent Structural Synaptic Plasticity of Inhibitory Synapses in the Dendrites of Hypocretin/Orexin Neurons', *Molecular Neurobiology*. Molecular Neurobiology, pp. 1–17.

Emran, F. *et al.* (2010) 'Zebrafish larvae lose vision at night', *Proceedings of the National Academy of Sciences of the United States of America*, 107(13), pp. 6034–6039.

Engert, F. *et al.* (2002) 'Moving visual stimuli rapidly induce direction sensitivity of developing tectal neurons', *Nature*, 419(6906), pp. 470–475.

Estabrooke, I. V. *et al.* (2001) 'Fos expression in orexin neurons varies with behavioral state', *Journal of Neuroscience*.

Fadel, J., Bubser, M. and Deutch, A. Y. (2002) 'Differential activation of orexin neurons by antipsychotic drugs associated with weight gain', *Journal of Neuroscience*, 22(15), pp. 6742–6746.

Faraco, J. H. *et al.* (2006) 'Regulation of hypocretin (orexin) expression in embryonic zebrafish', *Journal of Biological Chemistry*.

Feinberg, E. H. *et al.* (2008) 'GFP Reconstitution Across Synaptic Partners (GRASP) Defines Cell Contacts and Synapses in Living Nervous Systems', *Neuron*, 57(3), pp. 353–363.

Flanigan, M. E. *et al.* (2020) 'Orexin signaling in GABAergic lateral habenula neurons modulates aggressive behavior in male mice', *Nature Neuroscience*. Springer US, 23(5), pp. 638–650.

Frank, M. G. and Cantera, R. (2014) 'Sleep, clocks, and synaptic plasticity', *Trends in neurosciences*. Elsevier Ltd, 37(9), pp. 491–501.

Gabriel, J. P. *et al.* (2012) 'Layer-Specific Targeting of Direction-Selective Neurons in the Zebrafish Optic Tectum', *Neuron*. Elsevier Inc., 76(6), pp. 1147–1160.

Gahtan, E., Tanger, P. and Baier, H. (2005) 'Visual prey capture in larval zebrafish is controlled by identified reticulospinal neurons downstream of the tectum', *Journal of Neuroscience*.

Gandhi, A. V. *et al.* (2015) 'Melatonin Is required for the circadian regulation of sleep', *Neuron*. Elsevier Inc., 85(6), pp. 1193–1199.

Gebhardt, C., Baier, H. and Del Bene, F. (2013) 'Direction selectivity in the visual system of the zebrafish larva', *Frontiers in Neural Circuits*, 7(MAY), pp. 1–6.

Ghosh, M. and Rihel, J. (2020) 'Hierarchical compression reveals sub-second to day-long structure in larval zebrafish behavior', *eNeuro*.

Gilestro, G. F., Tononi, G. and Cirelli, C. (2009) 'Widespread Changes in Synaptic Markers as a Function of Sleep and Wakefulness in *Drosophila*', *Science*, 324(5923), pp. 109–112.

Godinho, L. (2011) 'Injecting zebrafish with DNA or RNA constructs encoding fluorescent protein reporters', *Cold Spring Harbor Protocols*, 6(7), pp. 871–874.

Gompf, H. S. and Aston-Jones, G. (2008) 'Role of orexin input in the diurnal rhythm of locus coeruleus impulse activity', *Brain Research*, 1224, pp. 43–52.

Gottmann, K., Mittmann, T. and Lessmann, V. (2009) 'BDNF signaling in the formation, maturation and plasticity of glutamatergic and GABAergic synapses', *Experimental Brain Research*.

Gross, G. *et al.* (2013) 'Recombinant Probes for Visualizing Endogenous Synaptic Proteins in Living Neurons', *Neuron*. Elsevier Inc., 78(6), pp. 971–985.

Gulati, T. *et al.* (2017) 'Neural reactivations during sleep determine network credit assignment', *Nature Neuroscience*, 20(9), pp. 1277–1284.

Haas, K., Li, J. and Cline, H. T. (2006) 'AMPA receptors regulate experience-dependent dendritic arbor growth in vivo', *Proceedings of the National Academy of Sciences of the United States of America*.

Hara, J. *et al.* (2001) 'Genetic ablation of orexin neurons in mice results in narcolepsy, hypophagia, and obesity', *Neuron*.

Harris, G. C., Wimmer, M. and Aston-Jones, G. (2005) 'A role for lateral hypothalamic orexin neurons in reward seeking', *Nature*, 437(7058), pp. 556–559.

He, H. Y. *et al.* (2016) 'Experience-Dependent Bimodal Plasticity of Inhibitory Neurons in Early Development', *Neuron*.

Heap, L. A. *et al.* (2018) 'Hypothalamic Projections to the Optic Tectum in Larval Zebrafish', *Frontiers in Neuroanatomy*, 11(January), p. 135. doi: 10.3389/fnana.2017.00135.

Hendricks, J. C. *et al.* (2000) 'Rest in Drosophila Is a Sleep-like State', *Neuron*, 25(1), pp. 129–138.

Hengen, K. B. *et al.* (2016) 'Neuronal Firing Rate Homeostasis Is Inhibited by Sleep and Promoted by Wake', *Cell*. Elsevier Inc., 165(1), pp. 180–191.

Henriques, P. M. *et al.* (2019) 'Nucleus Isthmi Is Required to Sustain Target Pursuit during Visually Guided Prey-Catching', *Current Biology*.

Herget, U. *et al.* (2016) 'Single-Cell Reconstruction of Oxytocinergic Neurons Reveals Separate Hypophysiotropic and Encephalotropic Subtypes in Larval Zebrafish', 4(February 2017), pp. 1–16.

Hervieu, G. J. *et al.* (2001) 'Gene expression and protein distribution of the orexin-1 receptor in the rat brain and spinal cord', *Neuroscience*.

Holler, S. *et al.* (2021) 'Structure and function of a neocortical synapse', *Nature*. Springer US, 591(March).

Hong, C. I. *et al.* (2014) 'Circadian rhythms synchronize mitosis in Neurospora crassa', *Proceedings of the National Academy of Sciences of the United States of America*.

Hong, E. *et al.* (2013) 'Cholinergic left-right asymmetry in the habenulo-interpeduncular pathway', *Proceedings of the National Academy of Sciences of the United States of America*.

Huang, Y. Bin *et al.* (2015) 'In vivo study of dynamics and stability of dendritic spines on olfactory Bulb interneurons in xenopus laevis tadpoles', *PLoS ONE*.

Hunter, P. R. *et al.* (2011) 'Localization of Cadm2a and Cadm3 proteins during development of the zebrafish nervous system', *Journal of Comparative Neurology*.

Hurd, M. W. *et al.* (1998) 'Circadian rhythms of locomotor activity in zebrafish', *Physiology and Behavior*, 65(3), pp. 465–472.

Inutsuka, A. and Yamanaka, A. (2013) 'The physiological role of orexin/hypocretin neurons in the regulation of sleep/wakefulness and neuroendocrine functions', *Frontiers in Endocrinology*, 4(MAR), pp. 1–10.

Iyer, M. *et al.* (2018) 'Identification of discrete, intermingled hypocretin neuronal populations', *Journal of Comparative Neurology*, 526(18), pp. 2937–2954.

Jacques, S. L. (2013) 'Optical properties of biological tissues: A review', *Physics in Medicine and Biology*.

Jaffe, D. B. *et al.* (1992) 'The spread of Na+ spikes determines the pattern of dendritic Ca2+ entry into hippocampal neurons', *Nature*.

Joiner, W. J. (2016) 'Unraveling the Evolutionary Determinants of Sleep', *Current Biology*, pp. R1073–R1087.

Jontes, J. D., Buchanan, J. A. and Smith, S. J. (2000) 'Growth cone and dendrite dynamics in zebrafish embryos: Early events in synaptogenesis imaged in vivo', *Nature Neuroscience*.

Kaneko, M. and Cahill, G. M. (2005) 'Light-dependent development of circadian gene expression in transgenic zebrafish', *PLoS Biology*.

Kaslin, J. (2004) 'The Orexin/Hypocretin System in Zebrafish Is Connected to the Aminergic and Cholinergic Systems', *Journal of Neuroscience*, 24(11), pp. 2678–2689.

Kawakami, K. *et al.* (2016) 'Gal4 Driver Transgenic Zebrafish: Powerful Tools to Study Developmental Biology, Organogenesis, and Neuroscience', *Advances in Genetics*, 95, pp. 65–87.

Kay, J. N. *et al.* (2001) 'Retinal ganglion cell genesis requires lakritz, a zebrafish atonal homolog', *Neuron*, 30(3), pp. 725–736.

Keck, T. *et al.* (2011) 'Loss of sensory input causes rapid structural changes of inhibitory neurons in adult mouse visual cortex', *Neuron*, 71(5), pp. 869–882.

Keck, T. *et al.* (2013) 'Synaptic scaling and homeostatic plasticity in the mouse visual cortex in vivo', *Neuron*, 80(2), pp. 327–334.

Khlghatyan, J. *et al.* (2020) 'Fxr1 regulates sleep and synaptic homeostasis', *The EMBO Journal*, 39(21), pp. 1–20.

Kim, J. H. *et al.* (2011) 'High cleavage efficiency of a 2A peptide derived from porcine teschovirus-1 in human cell lines, zebrafish and mice', *PLoS ONE*, 6(4), pp. 1–8.

Kimmel, C. B., Patterson, J. and Kimmel, R. O. (1974) 'The development and behavioral characteristics of the startle response in the zebra fish', *Developmental Psychobiology*, 7(1), pp. 47–60.

Kohl, J. *et al.* (2018) 'Functional circuit architecture underlying parental behaviour', *Nature*, 556(7701), pp. 326–331.

Kroll, F. *et al.* (2021) 'A simple and effective f0 knockout method for rapid screening of behaviour and other complex phenotypes', *eLife*.

Lambert, J. T. *et al.* (2017) 'Protracted and asynchronous accumulation of PSD95-family MAGUKs during maturation of nascent dendritic spines', *Developmental Neurobiology*, 77(10), pp. 1161–1174.

Laranjeiro, R. and Whitmore, D. (2014) 'Transcription factors involved in retinogenesis are co-opted by the circadian clock following photoreceptor differentiation', *Development (Cambridge)*, 141(13), pp. 2644–2656.

De Lecea, L. *et al.* (1998) 'The hypocretins: Hypothalamus-specific peptides with neuroexcitatory activity', in *Proceedings of the National Academy of Sciences of the United States of America*.

Lekk, I. *et al.* (2019) 'Sox1A mediates the ability of the parapineal to impart habenular left-right asymmetry', *eLife*.

Leung, L. C. *et al.* (2019) 'Neural signatures of sleep in zebrafish', *Nature*. Springer US, 571(7764), pp. 198–204.

Li, L. and Dowling, J. E. (1998) 'Zebrafish visual sensitivity is regulated by a circadian clock', *Visual Neuroscience*.

Li, L. and Dowling, J. E. (2000) 'Effects of dopamine depletion on visual sensitivity of zebrafish', *Journal of Neuroscience*.

Li, N. *et al.* (2010) 'mTOR-dependent synapse formation underlies the rapid antidepressant effects of NMDA antagonists', *Science*.

Li, P. *et al.* (2005) 'Circadian rhythms of behavioral cone sensitivity and long wavelength opsin mRNA expression: A correlation study in zebrafish', *Journal of Experimental Biology*.

Li, W. *et al.* (2017) 'REM sleep selectively prunes and maintains new synapses in development and learning', *Nature Neuroscience*, 20(3).

Li, W. and Gan, W. (2014) 'Sleep promotes branch-specific formation of dendritic spines after learning', *Science (New York, N.Y.)*, 344(6188), pp. 1173–1178.

Lin, Q. and Jesuthasan, S. (2017) 'Masking of a circadian behavior in larval zebrafish involves the thalamo-habenula pathway', *Scientific Reports*. Springer US, 7(1), pp. 1–11.

Liu, Z. W. *et al.* (2010) 'Direct evidence for wake-related increases and sleep-related decreases in synaptic strength in rodent cortex', *Journal of Neuroscience*, 30(25), pp. 8671–8675.

Mackiewicz, M. *et al.* (2007) 'Macromolecule biosynthesis: A key function of sleep', *Physiological Genomics*.

Maret, S. *et al.* (2011) 'Sleep and waking modulate spine turnover in the adolescent mouse cortex', *Nature Neuroscience*. Nature Publishing Group, 14(11), pp. 1418–1420.

Markram, H. *et al.* (2004) 'Interneurons of the neocortical inhibitory system', *Nature Reviews Neuroscience*.

Marquart, G. D. *et al.* (2015) 'A 3D searchable database of transgenic zebrafish gal4 and cre lines for functional neuroanatomy studies', *Frontiers in Neural Circuits*.

Marquart, G. D. *et al.* (2019) 'Prepontine non-giant neurons drive flexible escape behavior in zebrafish', *PLoS Biology*, pp. 1–19.

Marvin, J. S. *et al.* (2013) 'An optimized fluorescent probe for visualizing glutamate neurotransmission', *Nature Methods*.

Matsu-ura, T. *et al.* (2016) 'Intercellular Coupling of the Cell Cycle and Circadian Clock in Adult Stem Cell Culture', *Molecular Cell*.

Matsumoto, S. *et al.* (2020) 'Enhanced cortical responsiveness during natural sleep in freely behaving mice', *Scientific Reports*, 10(1), pp. 1–12.

Matsuo, M., Kamei, Y. and Fukamachi, S. (2021) 'Behavioural red-light sensitivity in fish according to

the optomotor response', *Royal Society Open Science*, 8(8).

Matsuzaki, M. *et al.* (2004) 'Structural basis of long-term potentiation in single dendritic spines', *Nature*.

McGraw, H. F., Nechiporuk, A. and Raible, D. W. (2008) 'Zebrafish dorsal root ganglia neural precursor cells adopt a glial fate in the absence of neurogenin1', *Journal of Neuroscience*.

McLean, D. L. and Fetcho, J. R. (2004) 'Ontogeny and innervation patterns of dopaminergic, noradrenergic, and serotonergic neurons in larval zebrafish', *Journal of Comparative Neurology*, 480(1), pp. 38–56.

Mehnert, K. I. *et al.* (2007) 'Circadian changes in Drosophila motor terminals', *Developmental Neurobiology*.

Meyer, M. P. and Smith, S. J. (2006) 'Evidence from in vivo imaging that synaptogenesis guides the growth and branching of axonal arbors by two distinct mechanisms', *Journal of Neuroscience*, 26(13), pp. 3604–3614.

Miyamoto, D. *et al.* (2021) 'Net decrease in spine-surface GluA1-containing AMPA receptors after post-learning sleep in the adult mouse cortex', *Nature Communications*. Springer US, 12(1), pp. 1–13.

Nakajo, H. *et al.* (2020) 'Hunger Potentiates the Habenular Winner Pathway for Social Conflict by Orexin-Promoted Biased Alternative Splicing of the AMPA Receptor Gene', *Cell Reports*, 31(12).

Nath, R. D. *et al.* (2017) 'The Jellyfish Cassiopea Exhibits a Sleep-like State', *Current Biology*, 27(19), pp. 2984-2990.e3.

Naumann, E. A. *et al.* (2010) 'Monitoring neural activity with bioluminescence during natural behavior', *Nature Neuroscience*.

Nevin, L. M. *et al.* (2010) 'Focusing on optic tectum circuitry through the lens of genetics', *BMC Biology*.

Niell, C. M., Meyer, M. P. and Smith, S. J. (2004) 'In vivo imaging of synapse formation on a growing dendritic arbor', *Nature Neuroscience*, 7(3), pp. 254–260.

Niethard, N. *et al.* (2016) 'Sleep-Stage-Specific Regulation of Cortical Excitation and Inhibition', *Current Biology*. Elsevier Ltd., 26(20), pp. 2739–2749.

Nikolaou, N. *et al.* (2012) 'Parametric Functional Maps of Visual Inputs to the Tectum', *Neuron*. Elsevier Inc., 76(2), pp. 317–324.

Nikolaou, N. *et al.* (2015) 'Lamination Speeds the Functional Development of Visual Circuits', *Neuron*. The Authors, 88(5), pp. 999–1013.

Nishino, S. *et al.* (2000) 'Hypocretin (orexin) deficiency in human narcolepsy', *Lancet*.

Norimoto, H. *et al.* (2018) 'Hippocampal ripples down-regulate synapses', *Science*, 359(6383), pp. 1524–1527.

Noya, S. B. *et al.* (2019) 'The forebrain synaptic transcriptome is organized by clocks but its proteome is driven by sleep', *Science*, 366(6462).

Ognjanovski, N. *et al.* (2014) 'CA1 hippocampal network activity changes during sleep-dependent memory consolidation', *Frontiers in Systems Neuroscience*.

Ono, D. and Yamanaka, A. (2017) 'Hypothalamic regulation of the sleep/wake cycle', *Neuroscience Research*. Elsevier Ireland Ltd and Japan Neuroscience Society, 118, pp. 74–81.

Panula, P. (2010) 'Hypocretin/orexin in fish physiology with emphasis on zebrafish', *Acta Physiologica*, 198(3), pp. 381–386.

Paquet, D. *et al.* (2009) 'A zebrafish model of tauopathy allows in vivo imaging of neuronal cell death

and drug evaluation', *Journal of Clinical Investigation*..

Patterson, G. H. and Lippincott-Schwartz, J. (2002) 'A photoactivatable GFP for selective photolabeling of proteins and cells', *Science*.

Peters, A. (2002) 'Examining neocortical circuits: Some background and facts', *Journal of Neurocytology*.

Petersen, J. D. *et al.* (2003) 'Distribution of Postsynaptic Density (PSD)-95 and Ca 2+/Calmodulin-Dependent Protein Kinase II at the PSD', *Journal of Neuroscience*.

Peyric, E., Moore, H. A. and Whitmore, D. (2013) 'Circadian Clock Regulation of the Cell Cycle in the Zebrafish Intestine', *PLoS ONE*.

Peyron, C. *et al.* (1998) 'Neurons containing hypocretin (orexin) project to multiple neuronal systems.', *The Journal of neuroscience : the official journal of the Society for Neuroscience*, 18(23), pp. 9996–10015.

Peyron, C. and Kilduff, T. S. (2017) 'Mapping the Hypocretin/Orexin Neuronal System: An Unexpectedly Productive Journey', *The Journal of Neuroscience*, 37(9), pp. 2268–2272.

van den Pol, a N. (1999) 'Hypothalamic hypocretin (orexin): robust innervation of the spinal cord.', *The Journal of neuroscience : the official journal of the Society for Neuroscience*, 19(8), pp. 3171–3182.

Pratt, K. G., Hiramoto, M. and Cline, H. T. (2016) 'An evolutionarily conserved mechanism for activity-dependent visual circuit development', *Frontiers in Neural Circuits*, 10(OCT), pp. 1–12.

Preuss, S. J. *et al.* (2014) 'Classification of object size in retinotectal microcircuits', *Current Biology*. Elsevier Ltd, 24(20), pp. 2376–2385.

Prober, D. A. *et al.* (2006) 'Hypocretin/Orexin Overexpression Induces An Insomnia-Like Phenotype in Zebrafish', *Journal of Neuroscience*, 26(51), pp. 13400–13410.

Rantamäki, T. and Kohtala, S. (2020) 'Encoding, consolidation, and renormalization in depression: Synaptic homeostasis, plasticity, and sleep integrate rapid antidepressant effects', *Pharmacological Reviews*, 72(2), pp. 439–465.

Rihel, J. *et al.* (2010) 'Zebrafish Behavioral Profiling Links Drugs to Biological Targets and Rest/Wake Regulation', *Science*, 327(5963), pp. 348–351.

Rihel, J., Prober, D. A. and Schier, A. F. (2010) *Monitoring Sleep and Arousal in Zebrafish*. Third Edit, *Methods in Cell Biology - Volume 100*. Third Edit. Elsevier Inc.

Rizzoli, S. O. and Betz, W. J. (2005) 'Synaptic vesicle pools', *Nature Reviews Neuroscience*.

Robles, E., Smith, S. J. and Baier, H. (2011) 'Characterization of genetically targeted neuron types in the zebrafish optic tectum', *Frontiers in Neural Circuits*, 5(FEB), pp. 1–14.

Sabatini, B. L., Oertner, T. G. and Svoboda, K. (2002) 'The life cycle of Ca2+ ions in dendritic spines', *Neuron*.

Sakurai, T. *et al.* (1998) 'Orexins and orexin receptors: A family of hypothalamic neuropeptides and G protein-coupled receptors that regulate feeding behavior', *Cell*.

Sapède, D. *et al.* (2020) 'Functional heterogeneity in the pineal projection neurons of zebrafish', *Molecular and Cellular Neuroscience*. Elsevier, 103(February), p. 103468.

Scott, E. K. and Baier, H. (2009) 'The cellular architecture of the larval zebrafish tectum, as revealed by Gal4 enhancer trap lines', *Frontiers in Neural Circuits*, 3(OCT).

Sheets, L. *et al.* (2011) 'Ribeye is required for presynaptic CaV1.3a channel localization and afferent innervation of sensory hair cells', *Development*.

Shepherd, J. D. and Bear, M. F. (2011) 'New views of Arc, a master regulator of synaptic plasticity',

Nature Neuroscience.

Siegel, J. M. *et al.* (2001) 'A brief history of hypocretin/orexin and narcolepsy', *Neuropsychopharmacology*, 25(5), pp. S14–S20.

Singh, C., Oikonomou, G. and Prober, D. A. (2015) 'Norepinephrine is required to promote wakefulness and for hypocretin-induced arousal in zebrafish', *eLife*, 4(September), pp. 1–22.

Son, J.-H. *et al.* (2016) 'Transgenic FingRs for Live Mapping of Synaptic Dynamics in Genetically-Defined Neurons.', *Scientific reports*. Nature Publishing Group, 6, p. 18734.

Steindal, I. A. F. and Whitmore, D. (2020) 'Zebrafish Circadian Clock Entrainment and the Importance of Broad Spectral Light Sensitivity', *Frontiers in Physiology*, 11(August), pp. 1–9.

Stuermer, C. A. O. (1988) 'Retinotopic organization of the developing retinotectal projection in the zebrafish embryo', *Journal of Neuroscience*.

Taft, C. E. and Turrigiano, G. G. (2014) 'PSD-95 promotes the stabilization of young synaptic contacts', *Philosophical Transactions of the Royal Society B: Biological Sciences*, 369(1633).

Tononi, G. and Cirelli, C. (2003) 'Sleep and synaptic homeostasis : a hypothesis', 62(August), pp. 143–150.

Tononi, G. and Cirelli, C. (2006) 'Sleep function and synaptic homeostasis', *Sleep Medicine Reviews*, pp. 49–62.

Tononi, G. and Cirelli, C. (2014) 'Sleep and the Price of Plasticity: From Synaptic and Cellular Homeostasis to Memory Consolidation and Integration', *Neuron*, 81(1), pp. 12–34.

Tononi, G. and Cirelli, C. (2016) 'Sleep and Synaptic Down-Selection', 6(95), pp. 453–456.

Torrado Pacheco, A. *et al.* (2021) 'Sleep Promotes Downward Firing Rate Homeostasis', *Neuron*. Elsevier Inc., 109(3), pp. 530-544.e6.

Trojanowski, N. F. and Raizen, D. M. (2016) 'Call it Worm Sleep', *Trends in Neurosciences*, pp. 54–62.

Tsujino, N. and Sakurai, T. (2009) 'Orexin/hypocretin: a neuropeptide at the interface of sleep, energy homeostasis, and reward system', *Pharmacol Rev*, 61(2), pp. 162–176.

Turrigiano, G. G. and Nelson, S. B. (2004) 'Homeostatic Plasticity in the Developing Nervious System'.

Tyagarajan, S. K. and Fritschy, J.-M. (2014) 'Gephyrin: a master regulator of neuronal function?', *Nature Reviews Neuroscience*. Nature Publishing Group, 15(3), pp. 141–156.

Tyssowski, K. M. and Gray, J. M. (2019) 'Blue light induces neuronal-activity-regulated gene expression in the absence of optogenetic proteins', *bioRxiv*, 6(October), pp. 1–10.

Vecsey, C. G. *et al.* (2009) 'Sleep deprivation impairs cAMP signalling in the hippocampus', *Nature*.

van Versendaal, D. *et al.* (2012) 'Elimination of Inhibitory Synapses Is a Major Component of Adult Ocular Dominance Plasticity', *Neuron*, 74(2), pp. 374–383.

Viktorin, G. *et al.* (2008) 'Emx3 is required for the differentiation of dorsal telencephalic neurons', *Developmental Dynamics*.

de Vivo, L. *et al.* (2017) 'Ultrastructural evidence for synaptic scaling across the wake/sleep cycle', *Science*, 355(6324), pp. 507–510..

Vyazovskiy, V. V. *et al.* (2006) 'Running wheel accessibility affects the regional electroencephalogram during sleep in mice', *Cerebral Cortex*.

Vyazovskiy, V. V. *et al.* (2008) 'Molecular and electrophysiological evidence for net synaptic potentiation in wake and depression in sleep', *Nature Neuroscience*, 11(2), pp. 200–208.

Vyazovskiy, V. V. *et al.* (2009) 'Cortical Firing and Sleep Homeostasis', *Neuron*. Elsevier Ltd, 63(6), pp. 865–878.

Walling, S. G. and Harley, C. W. (2004) 'Locus Ceruleus Activation Initiates Delayed Synaptic Potentiation of Perforant Path Input to the Dentate Gyrus in Awake Rats: A Novel β-Adrenergic- and Protein Synthesis-Dependent Mammalian Plasticity Mechanism', *Journal of Neuroscience*, 24(3), pp. 598–604.

Wang, G. and Smith, S. J. (2012) 'Sub-diffraction Limit Localization of Proteins in Volumetric Space Using Bayesian Restoration of Fluorescence Images from Ultrathin Specimens', *PLoS Computational Biology*.

Wassie, A. T., Zhao, Y. and Boyden, E. S. (2019) 'Expansion microscopy: principles and uses in biological research', *Nature Methods*.

Weiss, J. T. and Donlea, J. M. (2021) 'Sleep deprivation results in diverse patterns of synaptic scaling across the Drosophila mushroom bodies', *Current Biology*. Elsevier Ltd., pp. 1–14.

Wen, L. *et al.* (2008) 'Visualization of monoaminergic neurons and neurotoxicity of MPTP in live transgenic zebrafish', *Developmental Biology*, 314(1), pp. 84–92.

Whitmore, D., Foulkes, N. S. and Sassone-Corsi, P. (2000) 'Light acts directly on organs and cells in culture to set the vertebrate circadian clock', *Nature*.

Willie, J. T. *et al.* (2003) 'Distinct narcolepsy syndromes in orexin receptor-2 and orexin null mice: Molecular genetic dissection of non-REM and REM sleep regulatory processes', *Neuron*.

Wilson, S. W. and Easter, S. S. (1991) 'A pioneering growth cone in the embryonic zebrafish brain', *Proceedings of the National Academy of Sciences of the United States of America*.

Winata, C. L. *et al.* (2009) 'Development of zebrafish swimbladder: The requirement of Hedgehog signaling in specification and organization of the three tissue layers', *Developmental Biology*.

Xiao, T. and Baier, H. (2007) 'Lamina-specific axonal projections in the zebrafish tectum require the type IV collagen Dragnet', *Nature Neuroscience*.

Yáñez, J. *et al.* (2009) 'Pineal projections in the zebrafish (Danio rerio): overlap with retinal and cerebellar projections', *Neuroscience*. Elsevier Inc., 164(4), pp. 1712–1720.

Yang, G. and Gan, W. B. (2012) 'Sleep contributes to dendritic spine formation and elimination in the developing mouse somatosensory cortex', *Developmental Neurobiology*.

Yokogawa, T. *et al.* (2007) 'Characterization of sleep in zebrafish and insomnia in hypocretin receptor mutants', *PLoS Biology*, 5(10), pp. 2379–2397.

Zanos, P. and Gould, T. D. (2018) 'Mechanisms of ketamine action as an antidepressant', *Molecular Psychiatry*.

Zhang, L. I. *et al.* (1998) 'A critical window for cooperation and competition among developing retinotectal synapses', *Nature*.

Zhang, L. I., Tao, H. Z. W. and Poo, M. M. (2000) 'Visual input induces long-term potentiation of developing retinotectal synapses', *Nature Neuroscience*.

Zhang, P. and Lisman, J. E. (2012) 'Activity-dependent regulation of synaptic strength by PSD-95 in CA1 neurons', *Journal of Neurophysiology*, 107(4), pp. 1058–1066.

Zhang, R. W. *et al.* (2016) 'Stereotyped initiation of retinal waves by bipolar cells via presynaptic NMDA autoreceptors', *Nature Communications*.

Zhdanova, I. V. *et al.* (2001) 'Melatonin promotes sleep-like state in zebrafish', *Brain Research*, 903(1–2), pp. 263–268.

Zhu, J., Shang, Y. and Zhang, M. (2016) 'Mechanistic basis of MAGUK-organized complexes in synaptic development and signalling', *Nature Reviews Neuroscience*. Nature Publishing Group, 17(4), pp. 209–223.